Glycerol reforming and methanol synthesis for the production of renewable methanol

van Bennekom, Joost Gerardus

Glycerol reforming and methanol synthesis for the production of renewable methanol

Glycerol reforming and methanol synthesis for the production of renewable methanol
J.G. van Bennekom, PhD dissertation, University of Groningen, Groningen, The Netherlands

Cover: Methanol synthesis in a view cell with *in situ* condensation

RIJKSUNIVERSITEIT GRONINGEN

Glycerol reforming and methanol synthesis for the production of renewable methanol

Proefschrift

ter verkrijging van het doctoraat in de

Wiskunde en Natuurwetenschappen

aan de Rijksuniversiteit Groningen

op gezag van de

Rector Magnificus, dr. E. Sterken,

in het openbaar te verdedigen op

vrijdag 15 maart 2013

om 16.15 uur

door

Joost Gerardus van Bennekom

geboren op 18 januari 1981

te Hengelo

Promotor: Prof. dr. ir. H.J. Heeres

Copromotor: Dr. ir. R.H. Venderbosch

Beoordelingscommissie: Prof. dr. A.A. Broekhuis

                          Prof. dr. ir. J.A.M. Kuipers

                          Prof. dr. F. Vogel

Table of contents

1 Introduction

Part of this chapter is published in a modified form as: A. Kruse, F. Vogel, J.G. van Bennekom, R.H. Venderbosch, Biomass gasification in supercritical water, in: Handbook Biomass Gasification, H.A.M. Knoef (Ed.), 2012.

1.1 Environmental issues

Depletion of fossil fuel reserves and environmental issues urge for clean and renewable chemicals and fuels. Biomass has great potential for the production of carbon neutral chemicals and fuels. Methanol is an important platform chemical for the chemical industry and it also has potential as a clean and renewable fuel. In this perspective, the production of methanol from a renewable feed is very interesting.

1.2 Supermethanol project

The use of biofuels and other types of renewable energy in the transportation sector is promoted by the European Commission (EC). The share of transportation fuel derived from renewable resources is targeted at a minimum of 10% in 2020 [1]. It is expected that biodiesel and ethanol will make up the lion's share of the renewable transportation fuel as a result of the EC directives. The European biodiesel production capacity has increased significantly in the 2000s [2]. As the production of every ton biodiesel roughly requires 100 kg methanol and yields the same amount of crude glycerin, both the methanol demand and the glycerol production increased. The economics of biodiesel production in the EU deteriorated, as among others the income from the sales of the byproduct glycerol decreased.

An interesting option addressing the surplus of glycerol and the demand for methanol is to produce methanol from glycerol by the biodiesel producer itself. In this way the biodiesel producer becomes less dependent on the methanol spot price, establishes partial security of methanol supply, and uses its own byproduct as a green and sustainable feed. However, the scale of traditional methanol synthesis (> 2000 t/d) is much larger than the scale of methanol synthesis required for a biodiesel plant. Conventional methanol synthesis is operated at large scale due to:

➢ Large scale requirements for reforming reactors
➢ Extensive gas cleaning
➢ Recycling of unconverted syngas
➢ The need for methanol purification

The Supermethanol project was initiated to develop a cost-effective process for small and medium scale methanol synthesis which can be integrated with an existing biodiesel producing facility [3]. The production of glycerol, as resource for syngas, in the biodiesel plant is in the range of 3000 to 10,000 t/y. The process for glycerol conversion to methanol is from here on referred to as the Glycerol-to-Methanol (GtM) concept or process.

The scope of the GtM-concept is schematically outlined in Fig. 1.1. In a biodiesel plant, vegetable oil reacts with methanol in the presence of a catalyst to produce biodiesel and byproduct glycerol. The glycerol is then converted into methanol using the GtM-process. This process is an integration of two separate processes, viz. glycerol reforming in supercritical water (RSCW) to syngas followed by the conversion of this syngas into methanol. In the conversion of glycerol into syngas some fuel gas is produced as byproduct, which can be used to produce heat for the biodiesel production or the GtM-process itself.
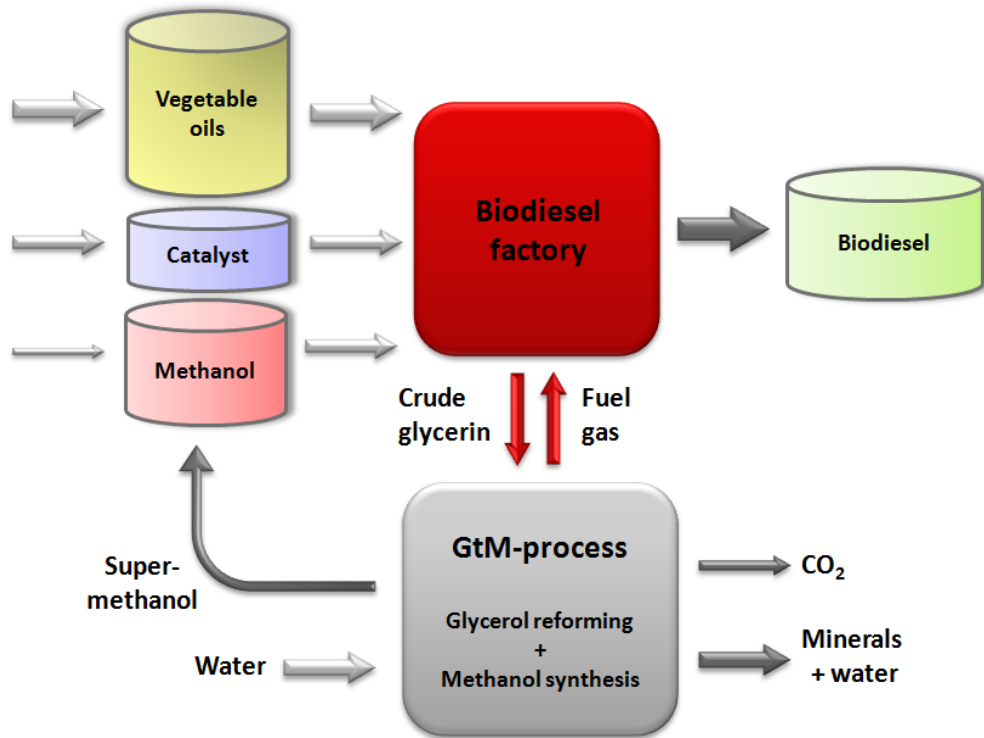
Fig. 1.1 Outline of the Supermethanol concept. The GtM-process is the process under investigation in the Supermethanol project.

In this chapter an introduction to the two processes that are part of the GtM-concept is given. Some background of the individual processes will be given, before attention is paid to the integration of the two processes.

1.3 Reforming in supercritical water

1.3.1 Supercritical water

Water becomes supercritical at conditions above its critical temperature (T_c = 647 K) and critical pressure (P_c = 22.1 MPa). In the phase diagram in Fig. 1.2 the square area in the upper right corner represents the supercritical area of water [4]. Supercritical water (SCW) is very reactive.

Various processes to convert biomass into solids, liquids, or gases are under development [5-9]. In so-called hydrothermal liquefaction biomass is degraded to mainly bio-crude, a viscous water-insoluble oil, at subcritical temperatures and pressures above the saturated vapor pressure of water [8]. Byproducts are char, water-soluble substances, and gas. Hydrothermal carbonization aims at the production of solid charcoal with water soluble components as byproducts [8]. Finally, reforming in supercritical water is aimed at gas production. Typical process conditions for liquefaction, catalytic reforming and high temperature reforming are indicated in Fig. 1.2.
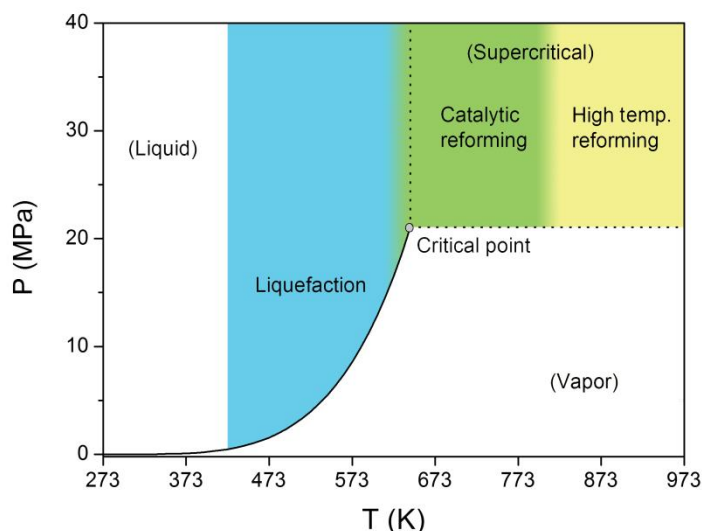
Fig. 1.2 Phase diagram of water. Phases are indicated in parenthesis. Hydrothermal processes with their typical conditions are indicated in the colored areas. This figure was originally published in ref. [4] and is reproduced by permission of The Royal Society of Chemistry.

In this dissertation the focus is on the RSCW of biomass which takes place usually at temperatures in the range of 650 – 1000 K and pressures exceeding the critical pressure. The temperature range can be roughly subdivided into catalytic and noncatalytic reforming. Catalytic reforming aims at the lower temperature while noncatalytic or high temperature

reforming usually requires higher temperature to ensure high/complete conversions. Furthermore, SCW can be used as reaction medium for the destruction of hazardous organic waste in water (often in combination with external oxygen) and for organic synthesis reactions.

At supercritical conditions water has some distinct other properties than water at ambient conditions. Some properties of water at a pressure of 30 MPa are illustrated in Fig. 1.3 [4, 10, 11]. The density (ρ), dielectric constant (ε), ionic product (K_w), and viscosity (not shown in Fig. 1.3) of water are important properties that determine the applicability of water for different processes. When the critical point of water is exceeded, the density drops significantly. The density of SCW, however, is relatively high compared to the density of a gas. The dielectric constant of water depends on the temperature as well and decreases with increasing temperature. Just as the density, the dielectric constant is one of the parameters that influences the solubility of (nonpolar) organics in water [12].

Water changes from a polar solvent at ambient conditions to a nonpolar solvent in the supercritical region. Organic compounds such as benzene and n-pentene become soluble in SCW, while the solubility of inorganic salts such as KCl, NaCl, and Na_2CO_3 decreases strongly [13]. Furthermore, SCW is miscible with permanent gases as N_2, H_2, CO, CO_2, and O_2 [14-16]. The ionic product of sub- and supercritical water can be 2 to 3 orders of magnitude higher than that of water at ambient conditions. The higher values of the ionic product around the critical temperature may play a role in acid or base catalyzed reactions due to the higher concentration of H_3O^+ and OH^- [15]. The viscosity of SCW is close to the viscosity of a normal gas and the diffusion coefficients are at least an order of magnitude higher than the diffusion coefficient of a liquid, enhancing the mass transfer characteristics of SCW [14]. Due to these properties of SCW, water is believed to act as catalyst, reaction medium, and reactant [4].
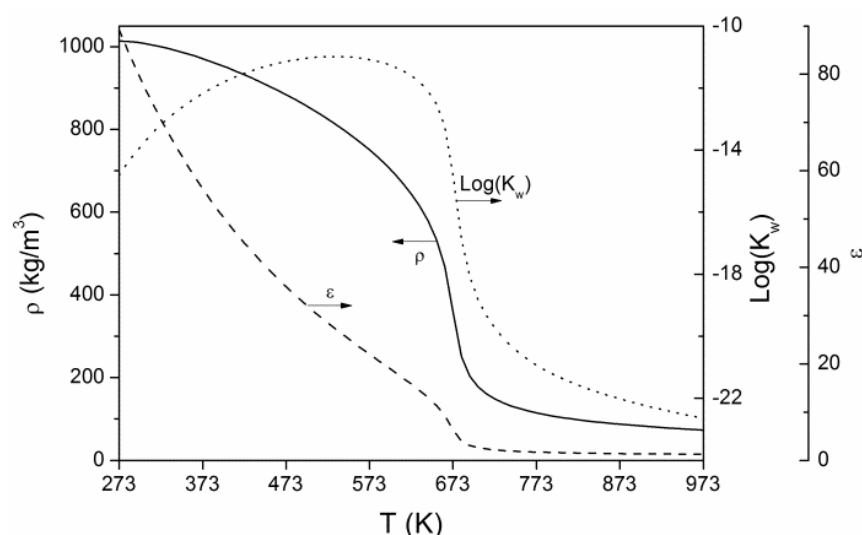
Fig. 1.3 Relevant properties of water at 30 MPa. Ionic product (K_w), density (ρ), and dielectric constant (ε) [4, 10, 11].

1.3.2 Advantages of reforming in supercritical water

The first literature on RSCW was published in the 1980s, when Modell *et al*. described experiments involving the quick immersion of maple wood sawdust in SCW [17]. Later work showed that at temperatures exceeding 1000 K most biomass is effectively converted into gas. Since the pioneering work by Modell, research to RSCW has increased tremendously. The feedstocks under investigation ranged from model compounds, such as methanol, glycerol, glucose, and lignin to real biomass, such as agricultural residues, bagasse, wood, algae, sewage sludge, and chicken manure [18, 19]. Research was on the one hand dedicated to gaining insight into the decomposition mechanism of organic (model) compounds or biomass and on the other hand to maximizing the production of H_2, CH_4, or a syngas like gas [20, 21]. The current state of the art of RSCW has been reviewed extensively in several publications in the 2000s [4, 14, 16, 18, 22-25]. The main advantages of RSCW technology are:

- Counter current heat exchange can be used over the complete temperature range of the process with high efficiencies.
- Wet biomass and liquid streams can be converted without prior drying.
- Complete biomass conversions can be obtained.
- The gas produced is clean due to the high solubility of H_2S and NH_3 in pressurized water and free of tar.
- The gas produced is not diluted with N_2 or other inert gases.
- The gas composition can be steered depending on the process conditions.
- A gas is produced at high pressure which can be beneficial for follow-up processes.

RSCW can be an environmentally friendly process and this has been confirmed by two life cycle assessments and a comparison with other biomass conversion technologies [26, 27]. Overall, the assessment of the RSCW process in terms of consumption of resources, acidification, and particle emission is very positive.

Without considering the low-temperature heat of the products, energy efficiencies of the different approaches and process designs varied between 44 and 65% and exergy efficiencies were in the range of 41 – 52% [28-32]. A comparison with fermentation appears favorable from an energy efficiency point of view, but at significantly higher costs [30]. Importantly, heat recovery is crucial, as this will have a major effect on energy efficiency.

1.3.3 Influence of reaction conditions and type of biomass

In reforming at temperatures below 573 K and without the addition of a catalyst, the gas yield is low, as liquid production is usually favored [22, 33]. Higher temperatures lead to (increased) gas formation, higher conversions, and reduced charring and re-polymerization. In some systems, the gas composition is substantially dependent on the temperature as higher temperatures also promote gas phase reaction rates [34, 35].

Residence times required to achieve sufficient conversion are a function of the operating temperature and the presence of a catalyst. At low temperatures, around 773 K, residence

times in the order of several minutes are typically necessary to allow complete conversion of the feedstock in noncatalytic reforming, while seconds are sufficient at temperatures > 923 K [36, 37].

The more complex the biomass structure (for example defined by the number of carbon atoms) and the higher its concentration, the more coke is usually produced (which can lead to reactor plugging), and the higher the CH_4 concentration in the product gas. For some components the gas yield decreases with increasing feed concentration. The conversion of glucose and lignin decreases significantly at higher feed loadings [35, 38]. Repolymerization of feed molecules and intermediates, instead of cracking and further reforming, then seems to be a reaction pathway of major importance which is not the case for dilute feedstocks [23]. The decreasing yield for larger organic molecules may also be due to a dramatic change in solubility of the feedstock or intermediate products in SCW, leading to deposition of the feedstock (and subsequent repolymerization and charring), even before any reforming reaction has taken place. Such significantly lower gas yields at higher feed loading are observed mainly for more complex molecules such as cellulosic biomass, lignin, and glucose, but this phenomenon may not be true for all components. For example, for smaller molecules such as methanol or glycerol less dramatic changes in the relative yields as a function of the feed loading have been reported [37, 39]. This can be explained by the reaction pathways leading to gas formation. Intermediates showing significant polymerization are furfurals formed from pentoses, hexoses, and phenols [40]. Compounds which are not able to form furfurals like glycerol or methanol should therefore show a lower tendency for re-polymerization than glucose or lignocelluloses.

1.3.4 Dedicated catalysts

Catalysts can significantly promote decomposition and influence the gas composition. Several sources can be catalytically active, such as the reactor wall itself, homogeneous catalysts (salts present in the feed), or dedicated heterogeneous catalysts [22, 34]. For example, the presence of small amounts of dissolved Na^+-ions promotes the water-gas shift (WGS) reaction [24, 34]. In quartz tubes an increased conversion was observed after addition of Inconel 625 powder, a commonly applied reactor material. In the presence of a heterogeneous Pt/Al_2O_3 catalyst, high H_2 and CO_2 yields were obtained from model compounds, while metals such as Ru, Ni, and Pd promote methanation [22].

Such catalysts are usually very active in RSCW, but also influence the overall reforming process in different ways: (i) affecting the carbon-to-gas efficiency (C_{GE}), and/or (ii) influencing the gas phase composition and/or (iii) changing the reaction mechanism. Even more complicating, catalysts are hardly stable for long operating times under the harsh conditions of RSCW and appropriate support materials are required [22]. Also nonmetallic catalysts have been found to be active, such as activated carbon [41].

Catalysis can thus play a key role in further development of RSCW as it may significantly reduce required operation temperatures and enables steering of the gas yields and conversions.

Another important aspect of RSCW is the catalytic effect of salts. These salts are usually part of the biomass fed to the reactor. Their effects are discussed in the next section.

1.3.5 Presence of salts

Salts can be present in biomass as ash or as catalyst residue in for example crude glycerin. The most important role of salts, in particular alkali salts, is the catalysis of the WGS reaction [22]. In fact, only in the presence of salts the high H_2 yields predicted by thermodynamic calculations are reached. Natural biomass usually contains such alkali salts, therefore the gas composition in experiments using natural biomass will generally be closer to equilibrium than in case of e.g. pure glucose reforming [24, 42].

Preventing reactors from plugging by salt precipitation appears a major challenge in biomass reforming. The salt concentration, the nature of the salts and understanding the seed crystal formation and crystal growth are important parameters for salt behavior in SCW [43, 44].

1.3.6 Main challenges

Corrosion: Universal challenges in RSCW are corrosion and problems with salt deposition. In RSCW, H_2 is formed, which is known to be able to change the mechanical stability of metals. In the RSCW of methanol, corrosion of the reactor tube (Ni based alloy) was observed after more than 1000 h of operation [45]. Corrosion behavior depends among others on reactor material, process conditions, and type of biomass. For protein-containing biomass, severe corrosion was found, likely because of the sulfur in the biomass [46].

Pumping: The biomass has to be pumped to enter the setup and to reach the desired pressure. The type of pump (membrane, piston, etc.) and in particular the pump valves have to be selected carefully. Liquid streams are preferred. Solid biomass must be conditioned to a pumpable slurry, dispersion, or aqueous solution.

Salt and ash deposits: Reduced solubility of salts in SCW leads to plugging. This is problematic especially if the tube diameters are small and the flow velocity is low. When using heterogeneous catalysts, plugging is even more critical, as the free diameter is even smaller, but also because catalyst poisoning by the salts fed in with the biomass is expected [47]. For both, plugging and catalyst poisoning, it is required to conceive a process that separates the salts before they get into contact with the heterogeneous catalyst. A reverse-flow vessel was shown to be able to separate a large fraction of the salts present in the feed stream and to yield a concentrated brine [43].

Energy efficiency: A crucial point is the efficiency of heat exchange in the process. Without efficient heat exchange, the RSCW process would not make sense from an energetic point of view. The heating rate of the feedstock should be higher than achieved by a heat exchanger, as for some reactants low heating rates may lead to unwanted reaction products like tars thereby reducing the gas yield [24]. As a solution, pure water can be heated by the heat exchanger, which is then mixed with the biomass [24].

Cost and acceptance: Although research and development has started in the 1980s, the interest for a technical application in industry is low. The main reasons are the high investment costs and the risk of using such a new technology [48]. In particular, the combination of a process temperature up to or above 873 K and a pressure of 30 MPa is regarded as a negative aspect of the technology.

1.4 Methanol synthesis

1.4.1 Synthesis reactions

Containing only one carbon atom, methanol is the simplest of all alcohols, but in spite of its structural simplicity methanol has a wide variety of applications. Methanol is among others used to produce: formaldehyde, acetic acid, dimethylether, methyl-tert-butyl-ether, and gasoline (methanol-to-gasoline-process). Furthermore it is used in biodiesel production and can be used directly as fuel additive or fuel in an internal combustion engine. Methanol is mostly produced from syngas which consists of predominantly H_2, CO, CO_2, and CH_4 and is mainly derived from natural gas or coal. In 2007, the global methanol production amounted 38 Mt and is forecasted to grow to 60 Mt in 2015 according to the Methanol Institute [49]. Methanol synthesis is dominated by three main reactions: (i) the hydrogenation of CO (Eq. 1.1), (ii) the (reverse) WGS reaction, and (iii) the hydrogenation of CO_2 (Eq. 1.3):

$$CO + 2\ H_2 \ \rightleftharpoons \ CH_3OH \qquad \Delta_r H^0_{298} = -90.64\ kJ/mol \qquad (Eq.\ 1.1)$$

$$CO_2 + H_2 \ \rightleftharpoons \ CO + H_2O \qquad \Delta_r H^0_{298} = +41.17\ kJ/mol \qquad (Eq.\ 1.2)$$

$$CO_2 + 3\ H_2 \ \rightleftharpoons \ CH_3OH + H_2O \qquad \Delta_r H^0_{298} = -49.47\ kJ/mol \qquad (Eq.\ 1.3)$$

The reactions are equilibrium reactions and their progress is restricted by thermodynamic equilibrium. Only two of the reactions are independent and suffice to determine the equilibrium composition. Both methanol synthesis reactions are exothermic and proceed under volume contraction. To reach full conversion of reactants, the ratio between CO, CO_2, and H_2 is very stringent. An important parameter describing the quality of the syngas for methanol synthesis is the stoichiometric number (S_N) defined as [50]:

$$S_N = \frac{(H_2 - CO_2)}{(CO + CO_2)} \qquad (Eq.\ 1.4)$$

With S_N equal to 2, all reactants can be converted into methanol. For $S_N > 2$, CO+CO_2 are the limiting components, while for $S_N < 2$, H_2 is limiting. In Fig. 1.4 the equilibrium conversion of CO+CO_2 is shown as a function of the temperature at different pressures for a gas composed of H_2/CO/CO_2/CH_4 = 67/24/4/5 vol% (S_N = 2.25). As can be seen in the figure the equilibrium conversion increases with increasing pressure and decreasing temperature. Therefore, high

pressure and relatively low temperatures are the most favorable reaction conditions from a thermodynamic point of view. Reaction rates, however, increase with increasing temperature and the optimal operating conditions are a subtle balance between the positive and negative effects of temperature on kinetics and thermodynamics respectively.
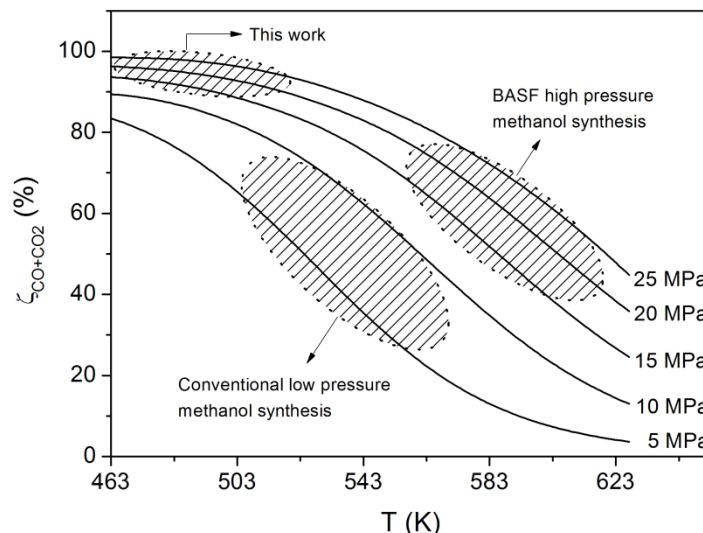
Fig. 1.4 Equilibrium conversion of CO+CO$_2$ as a function of the temperature for different pressures. The condition ranges of the various processes are roughly indicated. Gas composition: H$_2$/CO/CO$_2$/CH$_4$ = 67/24/4/5 vol%.

1.4.2   Industrial methanol synthesis

The first commercial methanol synthesis plant was erected in 1923 in Ludwigshafen by BASF. Operating pressures were between 10 and 25 MPa and operating temperatures between 573 and 673 K [51]. This process is generally referred to as 'high pressure methanol synthesis.' High temperature and high pressure were required because of low catalyst activity. Since then, a lot of research has been dedicated to enhance catalytic activity. Cu containing catalysts were found to be more active than the conventional high pressure catalysts (ZnO/Cr$_2$O$_3$), but these catalyst were (too) sensitive to sulphur and metal carbonyl poisoning. With the availability of improved syngas purification techniques and better process control (particularly preventing hot spots) Cu based catalysts came into industrial use by Imperial Chemical Industries Ltd. (ICI) in the 1960s. The use of the new catalyst allowed the operating pressure and temperature to be reduced to 5 – 10 MPa and 500 – 563 K [51]. In this 'low pressure process' the conversion of syngas into methanol is restricted to approximately 30 – 70% per pass through the reactor. Recycling of unconverted syngas is thus required. In a typical ICI plant the recycle ratio between make-up gas and recycle gas varies between 1 : 3 to 1 : 4 depending on the operating conditions and the composition of the syngas [51]. The operating conditions of BASF's high pressure process, conventional methanol synthesis (for example the ICI process), and the conditions envisaged for the Supermethanol project are shown in Fig. 1.4.

The trend in (gas phase) methanol synthesis is to lower temperatures and pressures, as gas compression is costly. In this work, however, high pressure methanol synthesis is under investigation again. In RSCW of glycerol a syngas comes available at high pressure. This syngas at high pressure can be used directly in methanol synthesis avoiding the energy intensive compression step. Advantageously, high pressure methanol synthesis can be operated in a once-through mode, avoiding recycles and purge streams to prevent the build-up of inert or less reactive components.

From a kinetic point of view there is also an advantage, as with increasing pressure the fugacities (or partial pressures) increase, leading to higher reaction rates. Due to the exothermicity of the reaction the formation of hot spots should be prevented by sufficient cooling. High pressure and high reaction rates lead to a reduction of the volume of the methanol synthesis reactor, though they will require larger wall thicknesses of the equipment.

1.4.3 Literature on methanol synthesis

The first publications (1920s) in the open literature on methanol synthesis deal predominantly with equilibria for methanol synthesis from CO (Eq. 1.1). Different approaches in the determination of these equilibria were undertaken. The equilibria were calculated theoretically by minimization of the Gibbs free energy [52, 53] or determined experimentally [53-62]. The majority of these experimental equilibrium constants are collected in Fig. 1.5. The equilibrium constants measured at elevated pressure were corrected with fugacities obtained using the Lewis & Randall rule. Discrepancies between different publications are relatively large as not all investigators measured exit gas compositions and considered relevant side reactions which are likely to proceed at such conditions [63]. The theoretical calculation performed by Graaf *et al.* [64] represents approximately the average value of the equilibrium constants for all the 'earlier' measurements performed. Detailed investigations of experimental high pressure equilibria do not exist at the (favorable) combination of high pressure (> 15 MPa) and low temperatures (< 523 K).

Although methanol synthesis is a mature process, there is still some controversy about the mechanism and primary carbon source of the methanol synthesized over Cu based catalysts and the influence of CO_2 on the reaction rate. Literature can be divided in three groups, viz. CO as the primary carbon source [65], CO_2 as the primary carbon source [51, 66, 67], or both [68-70]. Currently the prevailing view is that CO_2 is the primary carbon source which is also confirmed by isotopic labeling of the C and O in CO and CO_2 [66].
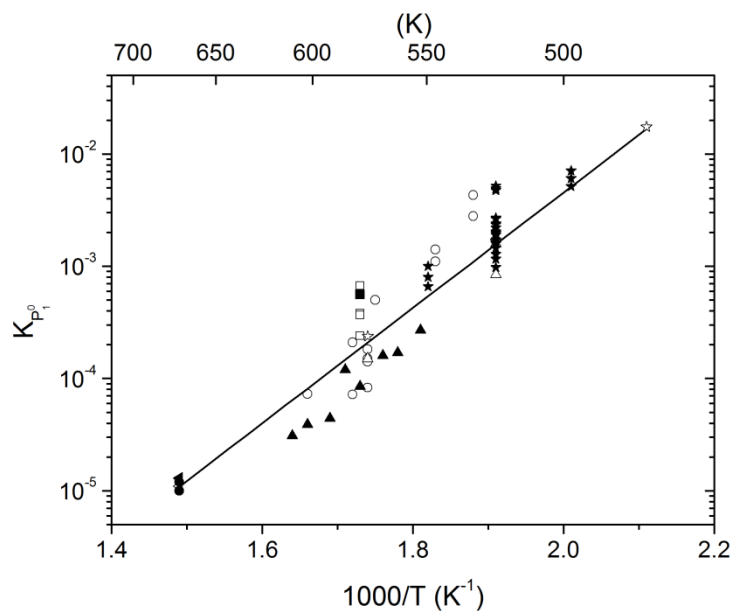
Fig. 1.5 Literature data on the chemical equilibrium of methanol synthesis from Eq. 1.1.
○, Von Wettberg and Dodge [62]; ◄, Audibert and Raineau [54]; ◁, Lewis and Frolich [57]; ●, Brown and Galloway [53]; □, Smith and Hirst [61]; ■, Smith and Branting [60]; △, Lacy et al. [56]; ▲, Newitt et al. [58]; ☆, Ewell [55]; ★, Newton and Dodge [59]; the line is the theoretical equilibrium calculated by Graaf et al. [64]. Equilibrium constants were measured at pressures between 0.1 – 20.0 MPa and corrected for the pressure if necessary.

The influence of CO_2 on methanol synthesis kinetics remains a topic of debate. Contradictory results were obtained by several researchers, such as promoting effects [66, 71, 72] or deactivating effects with increasing CO_2 concentration [65]. A similar discussion exists for the promoting or inhibiting effects of H_2O [65, 70].

The activity of the catalyst is determined by the composition of the catalyst (even though the main active element is Cu in all publications dealt with in this section), the ratio between the active components and support, and the preparation procedure [73]. In general, proper catalysts for methanol synthesis possess high metal dispersion, large surface area, and ultrafine or nanostructured active metal sites to prevent agglomeration of active sites [74].

1.4.4 Influence of process conditions on methanol synthesis

Higher process temperatures result in decreasing methanol yields at equilibrium. The reaction rates increase with increasing temperature [68]. In several reactor systems, reaction rates up to 523 K are too low to achieve equilibrium [75, 76]. Lower space velocities result in high methanol yields which can reach the equilibrium yields. Increasing the space velocity appears to have different effects on the CO and CO_2 conversion [51]. CO conversion decreases more rapidly with increasing space velocities, while the CO_2 conversion remains relatively constant. Increasing space velocity thus, changes the consumption ratio of CO and CO_2, over $Cu/ZnO/Al_2O_3$ or Cu/ZrO_2 [51, 77].

Industrially, strict limitations are imposed on the syngas composition, to prevent the build-up of inert components in the recycle loops. The ideal S_N is $2.10 < S_N < 2.15$, with a CO_2 content of 2-10% which is necessary to increase the reaction rate [78]. Syngas derived from biomass has a composition deviating from the ideal S_N value of 2. Generally, glycerol derived syngas is deficient in H_2, has a relatively high CO_2 content, and contains CH_4 [20]. Such a gas, thus, requires additional treatment to obtain a S_N around 2 and to prevent build-up of components in the recycle loop. Treatments can, for example, be the addition of supplementary H_2 or the removal of excess CO_2. A consequence of the hydrogenation of CO_2 is the formation of water as a byproduct and the suppression of the formation of higher alcohols [63].

1.5 GtM-concept and perspective

The combination of syngas production in an RSCW process followed by syngas conversion in methanol synthesis is the core of the Supermethanol process. In the RSCW of glycerol a high pressure syngas is produced by feeding a liquid and the use of this high pressure syngas has distinct consequences for methanol synthesis. However, before successful integration can be carried out both processes need to be optimized separately. A setup was available to investigate both processes separately and integrated, and the majority of the experimental work was conducted with this setup.

The relevance of the project described in this dissertation, however, is beyond the production of methanol from glycerol for the re-use in biodiesel production only. The feedstock for the reforming process in this dissertation is glycerol, but several types of biomass (preferably liquid) including aqueous phase fractions from pyrolysis oil upgrading, black liquor, etc. can be used for the reforming process. When these types of feedstocks are 'green', renewable methanol can be produced, which is a promising process for the (near) future.

1.6 Thesis outline

The work described in this dissertation focuses on reforming in supercritical water, methanol synthesis and the GtM-concept, which is the common theme throughout the dissertation. Finally, the GtM-concept will be demonstrated experimentally. To realize this objective an extensive dataset including glycerol conversions, gas compositions, syngas conversions, equilibria in methanol synthesis, methanol synthesis kinetics, etc. is required. First the individual processes, glycerol reforming and methanol synthesis, were studied, before these processes were integrated for the experimental demonstration of the GtM-concept. In the future the dataset provided in this dissertation can be used as the basis for a detailed design of a GtM-plant.

Several aspects of the reforming process and the methanol synthesis are addressed. **Chapter 2** deals with an extensive study to the reforming of glycerol and methanol (as model component) focusing on gas compositions/yields that can be obtained from these components.

In **Chapter 3** the catalytic reforming of glycerol is described. In this chapter the influence of several catalysts on the conversion and gas composition/yield is addressed. The focus lies on improving the gas composition derived in noncatalytic glycerol reforming.

In experiments in a view cell reactor (**Chapter 4**) methanol condensation was observed which has huge consequences for the equilibria in methanol synthesis. In **Chapter 5** a solution method is described to calculate the equilibria in methanol synthesis taking the formation of a liquid phase into account. A modified Soave-Redlich-Kwong equation of state fitted to phase equilibria of binary mixtures is used to correct for nonideality.

The focus of **Chapter 6** is on high pressure methanol synthesis. Methanol synthesis aiming for high conversions was investigated experimentally. The consequences of the formation of the liquid phase are further elucidated with the results obtained in this chapter.

Finally, in **Chapter 7** the GtM-concept is validated experimentally by the integration of RSCW of glycerol and high pressure methanol synthesis. In **Appendix C** and **D** two preliminary studies to production rates of methanol and water are presented.

1.7 References

1   Directive 2009/28/EC of the European Parliament and of the Council of 23 April 2009 on the promotion of the use of energy from renewable sources and amending and subsequently repealing Directives 2001/77/EC and 2003/30/EC, in: Official Journal of the European Union, Strasbourg, (2009) 47.

2   European Biodiesel Board, Statistics, the EU biodiesel industry, www.ebb-eu.org/stats.php (accessed 07 March 2012)

3   J.G. van Bennekom, J. Vos, R.H. Venderbosch, M.A.P. Torres, V.A. Kirilov, H.J. Heeres, Z. Knez, M. Bork, J.M.L. Penninger, Supermethanol: Reforming of crude glycerine in supercritical water to produce methanol for re-use in biodiesel plants, in: 17th European Biomass Conference and Exhibition, Hamburg, (2009) 899-902.

4   A.A. Peterson, F. Vogel, R.P. Lachance, M. Fröling, M.J. Antal Jr., J.W. Tester, Thermochemical biofuel production in hydrothermal media: A review of sub- and supercritical water technologies, Energy Environ. Sci., 1 (2008) 32-65.

5   N. Boukis, U. Galla, H. Müller, E. Dinjus, Biomass gasification in supercritical water. Experimental progress achieved with the Verena pilot plant, in: 15th European biomass conference & exhibition, Berlin, Germany, (2007).

6   A. Kruse, F. Vogel, J.G. van Bennekom, R.H. Venderbosch, Biomass gasification in supercritical water, in: H.A.M. Knoef (Ed.) Handbook of biomass gasification, (2012).

7   J.A. Libra, K.S. Ro, C. Kammann, A. Funke, N.D. Berge, Y. Neubauer, M.M. Titiric, C. Fühner, O. Bens, J. Kern, K.H. Emmerich, Hydrothermal carbonization of biomass residuals: A comparative review of the chemistry, processes and applications of wet and dry hydrolysis, Biofuels, 2 (2011) 89-124.

8   S.S. Toor, L. Rosendahl, A. Rudolf, Hydrothermal liquefaction of biomass: A review of subcritical water technologies, Energy, 36 (2011) 2328-2342.

9   F.W. Vogel, M. H.; Rouff, A. A.; Rabe, S. Synthetic natural gas from biomass by catalytic conversion in supercritical water. Green Chem. 9 (2007) 616-619.

10   W.L. Marshall, Dielectric constant of water discovered to be simple function of density over extreme ranges from – 35 to + 600 ^{o}C and to 1200 MPa (12000 Atm.), Believed Universal., Nature Precedings, Available from Nature Precedings (precedings.nature.com) (2008).

11   W.L. Marshall, E.U. Franck, Ion product of water substance, 0-1000 ^{o}C, 1-10,000 bars. New international formulation and its background., J. Phys. Chem. ref. Data, 10 (1981) 295-304.

12   S. Yesodharan, Supercritical water oxidation: An environmentally safe method for the disposal of organic wastes, Curr. Sci., 82 (2002) 1112-1122.

13   F.J. Armellini, J.W. Tester, Solubility of sodium chloride and sulfate in sub- and supercritical water vapor from 450-550°C and 100-250 bar, Fluid Phase Equilib., 84 (1993) 123-142.

14   G. Brunner, Near critical and supercritical water. Part I. Hydrolytic and hydrothermal processes, J. Supercrit. Fluids, 47 (2009) 373-381.

15   A. Kruse, E. Dinjus, Hot compressed water as reaction medium and reactant. Properties and synthesis reactions, J. Supercrit. Fluids, 39 (2007) 362-380.

16   H. Weingärtner, E.U. Franck, Supercritical water as a solvent, Angew. Chem. Int. Ed., 44 (2005) 2672-2692.

17   M. Modell, Gasification and liquefaction of forest products in supercritical water, in: R.P. Overend (Ed.) Fundamentals of thermochemical biomass conversion Elsevier, London, (1985).

18   Y. Matsumura, T. Minowa, B. Potic, S.R.A. Kersten, W. Prins, W.P.M. van Swaaij, B. van de Beld, D.C. Elliot, G.G. Neuenschwander, A. Kruse, M.J. Antal Jr., Biomass gasification in near- and supercritical water: Status and prospects, Biomass Bioenergy, 29 (2005) 269-292.

19   A. Nakamura, E. Kiyonaga, Y. Yamamura, Y. Shimizu, T. Minowa, Y. Noda, Y. Matsumura, Detailed analysis of heat and mass balance for supercritical water gasifications, J. Chem. Eng. Jpn., 41 (2008) 1-12.

20   A.J. Byrd, K.K. Pant, R.B. Gupta, Hydrogen production from glycerol by reforming in supercritical water over Ru/Al$_2$O$_3$ catalyst, Fuel, 87 (2008) 2956-2960.

21   M.H. Waldner, F. Vogel, Renewable production of methane from woody biomass by catalytic hydrothermal gasification, Ind. Eng. Chem. Res., 44 (2005) 4543-4551.

22   D.C. Elliot, Catalytic hydrothermal gasification of biomass, Biofuels, Bioprod. Biorefin., 2 (2008) 254-265.

23   A. Kruse, Supercritical water gasification, Biofuels, Bioprod. Biorefin., 2 (2008) 415-437.

24   A. Kruse, Hydrothermal biomass gasification, J. Supercrit. Fluids, 47 (2009) 391-399.

25   P. Basu, V. Mettanant, Biomass gasification in supercritical water - A review, Int. J. Chem. Reactor Eng., 7 (2009) 1-61.

26   E. Gasafi, L. Meyer, L. Schebek, Using life-cycle assessment in process design: Supercritical water gasification of organic feedstocks J. Ind. Ecol., 7 (2003) 75-91.

27   J.S. Luterbacher, M. Froling, F. Vogel, F. Marechal, J.W. Tester, Hydrothermal gasification of waste biomass: Process design and life cycle asessment, Environ. Sci. Technol., 43 (2009) 1578-1583.

28   E. Gasafi, L. Meyer, L. Schebek, Exergetic efficiency and options for improving sewage sludge gasification in supercritical water, Int. J. Energy Res., 31 (2007) 343-363.

29   W. Feng, H.J.v.d. Kooi, J.d.S. Arons, Biomass conversions in subcritical and supercritical water: Driving force, phase equilibria, and thermodynamic analysis, Chem. Eng. Process., 43 (2004) 1459-1467.

30   Y. Matsumura, Evaluation of supercritical water gasification and biomethanation for wet biomass utilization in Japan, Energy Convers. Manage., 43 (2002) 1301-1310.

31   Y. Lu, L. Guo, X. Zhang, Q. Yan, Thermodynamic modeling and analysis of biomass gasification for hydrogen production in supercritical water, Chem. Eng. J., 131 (2007) 233-244.

32   Y. Calzavara, C. Joussot-Dubien, G. Boissonnet, S. Sarrade, Evaluation of biomass gasification in supercritical water process for hydrogen production, Energy Convers. Manage., 46 (2005) 615-631.

33   W. Bühler, E. Dinjus, H.J. Ederer, A. Kruse, C. Mas, Ionic reactions and pyrolysis of glycerol as competing reaction pathways in near- and supercritical water, J. Supercrit. Fluids, 22 (2002) 37-53.

34   S.R.A. Kersten, B. Potic, W. Prins, W.P.M. van Swaaij, Gasification of model compounds and wood in hot compressed water, Ind. Eng. Chem. Res., 45 (2006) 4169-4177.

35   D. Yu, M. Aihara, M.J. Antal Jr., Hydrogen production by steam reforming glucose in supercritical water, Energy Fuels, 7 (1993) 574-577.

36   H. Schmieder, J. Abeln, N. Boukis, E. Dinjus, A. Kruse, M. Kluth, G. Petrich, E. Sadri, M. Schacht, Hydrothermal gasification of biomass and organic wastes, J. Supercrit. Fluids, 17 (2000) 145-153.

37   J.D. Taylor, C.M. Herdman, B.C. Wu, K. Wally, S.F. Rice, Hydrogen production in a compact supercritical water reformer, Int. J. Hydrogen Energy, 28 (2003) 1171-1178.

38   F.L.P. Resende, S.A. Fraley, M.J. Berger, P.E. Savage, Noncatalytic gasification of lignin in supercritical water, Energy Fuels, 22 (2008) 1328-1334.

39   N. Boukis, V. Diem, W. Habicht, E. Dinjus, Methanol reforming in supercritical water, Ind. Eng. Chem. Res., 42 (2003) 728-735.

40   A. Kruse, A. Gawlik, Biomass conversion in water at 330 - 410 ºC and 30 - 50 MPa. Identification of key compounds for indicating different chemical reaction pathways, Ind. Eng. Chem. Res., 42 (2003) 267-279.

41   X. Xu, Y. Matsumura, J. Stenberg, M.J. Antal Jr., Carbon-catalyzed gasification of organic feedstocks in supercritical water, Ind. Eng. Chem. Res., 35 (1996) 2522-2530.

42   J. Yanik, S. Ebale, A. Kruse, M. Saglam, M. Yüksel, Biomass gassification in supercritical water: Part 1. Effect of the nature of biomass, Fuel, 86 (2007) 2410-2415.

43   M. Schubert, Catalytic hydrothermal gasification of biomass - Salt recovery and continuous gasification of glycerol solutions, ETH, Zürich, (2010).

44   M. Schubert, J.W. Regler, F. Vogel, Continuous salt precipitation and separation from supercritical water. Part 2: Type 2 salts and mixtures of two salts, J. Supercrit. Fluids, 52 (2010) 113-124.

45   N. Boukis, W. Habicht, G. Franz, E. Dinjus, Behavior of Ni-base alloy 625 in methanol-supercritical water systems, Mater. Corros., 54 (2003) 326-330.

46   A. Kruse, A. Krupka, V. Schwarzkopf, C. Gamard, T. Henningsen, Influence of proteins on the hydrothermal gasification and liquefaction of biomass. 1. Comparison of different feedstocks, Ind. Eng. Chem. Res., 44 (2005) 3013-3020.

47   M.H. Waldner, F. Krumeich, F. Vogel, Synthetic natural gas by hydrothermal gasification of biomass: Selection procedure towards a stable catalyst and its sodium sulfate tolerance, J. Supercrit. Fluids, 43 (2007) 91-105.

48   E. Gasafi, M.Y. Reinecke, A. Kruse, L. Schebek, Economic analysis of sewage sludge gasification in supercritical water for hydrogen production, Biomass Bioenergy, 32 (2008) 1085-1096.

49   M. Berggren, Methanol industry in focus, milestones, www.methanol.org (accessed 19 January 2012)

50   E. Supp, How to produce methanol from coal, Springer-Verlag, Berlin, (1990).

51   S. Lee, Methanol synthesis technology, CRC Press Inc., Boca Raton, Florida, (1990).

52   K.K. Kelley, A thermodynamic consideration of the synthetic methanol process, Ind. Eng. Chem., 18 (1926) 78.

53   R.L. Brown, A.E. Galloway, Methanol from hydrogen and carbon monoxide, Ind. Eng. Chem., 20 (1928) 960-966.

54   E. Audibert, A. Raineau, A Study of the synthesis of methanol, Ind. Eng. Chem., 20 (1928) 1105-1110.

55   R.H. Ewell, Calculation of chemical equilibrium at high pressures, Ind. Eng. Chem., 32 (1940) 147-153.

56   B.S. Lacy, R.G. Dunning, H.H. Storch, Equilibrium in the synthesis and decomposition of methanol, J. Am. Chem. Soc., 52 (1930) 926-938.

57   W.K. Lewis, P.K. Frolich, Synthesis of methanol from carbon monoxide and hydrogen, Ind. Eng. Chem., 20 (1928) 285-290.

58   D.M. Newitt, B.J. Byrne, H.W. Strong, Equilibrium in the system methyl alcohol-hydrogen-carbonic oxide, Proc. R. Soc. London, Ser. A, A123 (1928) 236-252.

59   R.H. Newton, B.F. Dodge, The equilibrium between carbon monoxide, hydrogen, formaldehyde and methanol. II. The reaction $CO + 2H_2 <=> CH_3OH$, J. Am. Chem. Soc., 56 (1934) 1287-1291.

60   D.F. Smith, B.F. Branting, The equilibrium between methanol, carbon monoxide and hydrogen, J. Am. Chem. Soc., 51 (1929) 129-139.

61   D.F. Smith, L.L. Hirst, Reactions that occur on a methanol catalyst, Ind. Eng. Chem., 22 (1930) 1037-1043.

62   E.F. von Wettberg, B.F. Dodge, The methanol equilibrium, Ind. Eng. Chem., 22 (1930) 1040-1046

63   P. Forzatti, E. Tronconi, I. Pasquin, Higher alcohol synthesis, Catal. Rev. Sci. Eng., 33 (1991) 109-168.

64   G.H. Graaf, P.J.J.M. Sijtsema, E.J. Stamhuis, G.E.H. Joosten, Chemical equilibria in methanol synthesis, Chem. Eng. Sci, 41 (1986) 2883-2890.

65   K. Klier, V. Chatikavanij, R.G. Herman, G.W. Simmons, Catalytic synthesis of methanol from CO/H_2. IV. The effects of carbon dioxide J. Catal., 74 (1982) 343-360.

66   G.C. Chinchen, P.J. Denny, J.R. Jennings, M.S. Spencer, K.C. Waugh, Synthesis of methanol. Part 1. Catalysts and kinetics, Appl. Catal., 36 (1988) 1-65.

67   I.B. Dybkjaer, Design of ammonia and methanol synthesis reactions, in: NATO conference on chemical reactor design and technology, Canada, (1985) 795-819.

68   G.H. Graaf, E.J. Stamhuis, A.A.C.M. Beenackers, Kinetics of low-pressure methanol synthesis, Chem. Eng. Sci., 43 (1988) 3185-3195.

69   C. Kuechen, U. Hoffmann, Investigation of simultaneous reaction of carbon monoxide and carbon dioxide with hydrogen on a commercial copper/zinc oxide catalyst, Chem. Eng. Sci, 48 (1993) 3767-3776.

70   H.H. Kung, G. Liu, D. Wilcox, The effect of CO_2 and H_2O in the methanol synthesis reaction on Cu-Zn-O, in: ACS fuels fall meeting, Philadelphia, (1984) 194-195.

71   X.M. Liu, G.Q. Lu, Z.F. Yan, J. Beltramini, Recent advances in catalysts for methanol synthesis via hydrogenation of CO and CO_2, Ind. Eng. Chem. Res., 25 (2003) 6518.

72   Y. Zhang, Q. Sun, J. Deng, D. Wu, S. Chen, A high activity $Cu/ZnO/Al_2O_3$ catalyst for methanol synthesis: Preparation and catalytic properties Appl. Catal., A, 158 (1997) 105-120.

73   G. Natta, Synthesis of methanol, in: P.H. Emmett (Ed.) Catalysis: Hydrogenation and dehydrogenation, Rheinhold, New York, (1955) 349-411.

74   J. Liu, J. Shi, D. He, Q. Zhang, X. Wu, Y. Liang, Q. Zhu, Surface active structure of ultra-fine Cu/ZrO_2 catalysts used for the $CO_2 + H_2$ to methanol reaction, Appl. Catal., A, 218 (2001) 113-119.

75   A. Bill, A. Wokaun, B. Eliasson, E. Killer, U. Kogelschatz, Greenhouse gas chemistry, Energy Convers. Manage., 38 (1997) 415-422.

76   Q. Sun, C.W. Liu, W. Pan, Q.M. Zhu, J.F. Deng, In situ IR studies on the mechanism of methanol synthesis over an ultrafine $Cu/ZnO/Al_2O_3$ catalyst, Appl. Catal., A, 171 (1998) 301-308.

77   R.A. Koeppel, A. Baiker, A. Wokaun, Copper/zirconia catalysts for the synthesis of methanol from carbon dioxide: Influence of preparation variables on structural and catalytic properties of catalysts, Appl. Catal., A, 84 (1992) 77-102.

78   J.B. Hansen, P.E.H. Nielsen, Methanol Synthesis, in: G. Ertl, H. Knözinger, F. Schüth, J. Weitkamp (Eds.) Handbook of heterogeneous catalysis, Wiley-VCH Verlag, Weinheim, (2008) 2920-2949.

2 Reforming of methanol and glycerol in supercritical water

Abstract

Reforming of pure glycerol, crude glycerin, and methanol (pure and in the presence of Na_2CO_3) in supercritical water was investigated. Continuous experiments were carried out at temperatures ranging from 723 – 923 K, residence times between 6 – 173 s, and feed concentrations of 3 – 20 wt%. For methanol the gas products were mainly H_2, CO_2, and CO. The carbon-to-gas efficiency and the observed activation energy for pure methanol were higher than for methanol with Na_2CO_3. This can be explained by assuming different decomposition mechanisms for pure methanol and methanol with Na_2CO_3. For glycerol, H_2, CO, CO_2, CH_4, and higher hydrocarbons were produced. The carbon-to-gas efficiencies of crude glycerin and pure glycerol were comparable. Overall at complete conversion, 2 of the 3 carbon atoms present in glycerol end up as carbon oxides, while 1 carbon atom becomes C_xH_y. Then, the mechanism of glycerol decomposition involves the dehydration of 1 mol of H_2O/mol glycerol. For both, methanol and glycerol at carbon-to-gas efficiencies below 70%, the gas yields (mol/mol feed) and carbon-to-gas efficiency correlate well.

2.1 Introduction

Research on renewable and sustainable energy resources is receiving a high interest currently due to environmental concerns and depletion of fossil fuel reserves. A wide range of alternatives is actively explored to produce green and versatile energy carriers from biomass. Reforming of biomass in supercritical water, denoted RSCW here, is such a versatile technique. The objective of this technique is to convert preferably liquid biomass into H_2-rich gas, CH_4-rich gas, or syngas. Supercritical water (SCW) has unique properties, making it an excellent reaction medium for such reforming reactions. Water at or above the critical point is used to dissolve the biomass and acts as the reaction medium. Degradation of the biomass resource in SCW is very rapid and since most reaction intermediates are soluble in SCW, coke formation can be suppressed [1]. RSCW has some other distinct advantages, highlighted in several comprehensive reviews [2-11]. The most striking ones are:

➢ Wet biomass streams can be converted to gas without prior drying.
➢ Counter current heat exchange between feed stream and reactor effluent can be used for efficient heat integration.
➢ The gas is clean and tar formation is suppressed.
➢ The product gas becomes available at high pressure.

An attractive feedstock for RSCW is glycerol, a byproduct in biodiesel production. Glycerol can, for example, be converted through syngas into methanol that can be re-used in the biodiesel process [12]. The economic value of the product gas from the RSCW of glycerol for subsequent methanol synthesis strongly depends on its composition and syngas rich in H_2 containing a significant amount of CO is preferred from a kinetic point of view [13]. RSCW of crude glycerin, containing insoluble catalyst residues (e.g. Na^+ and K^+) entails operational challenges because of a low solubility of the inorganic catalyst residues in SCW [14]. Additionally, the gas mixtures produced in the RSCW process are rich in H_2 and CO_2 instead of the preferential syngas-like composition [15, 16]. Insight in the factors that determine the gas composition for RSCW of glycerol is lacking due to the complex decomposition pathways at molecular level [17].

In this chapter, an experimental research study is conducted to gain more insight in the RSCW of glycerol and to investigate options to steer the gas composition. Due to the complexity of RSCW of glycerol, RSCW of methanol with and without inorganic salts is investigated as well. Methanol can be considered a less complex model compound for glycerol. The results of the experimental work on RSCW of methanol (with and without Na_2CO_3), pure glycerol and crude glycerin will be provided and the effect of process conditions and feed concentration on the carbon-to-gas efficiency (C_{GE}) and gas yield will be discussed. The influence of the C_{GE} on the gas yield and indirectly the gas composition is addressed to enable steering of the RSCW process towards an 'optimized syngas composition' for the subsequent methanol synthesis process. Finally, insights in decomposition pathways to gas phase products are provided. Before the

experimental work is discussed in more detail, a short literature review is presented on the state of the art of RSCW in general, followed by details on the RSCW of methanol and glycerol.

2.2 Literature review

2.2.1 General aspects of RSCW

RSCW is characterized by the occurrence of various reactions, proceeding both in series and in parallel. The overall reaction of an actual feed to liquid and gas phase products is shown in Eq. 2.1.

$$C_xH_yO_z + a\ H_2O \longrightarrow \alpha\ CO + \beta\ H_2 + \chi\ CO_2 + \delta\ H_2O + \varepsilon\ CH_4 + \eta\ C_{x'}H_{y'}O_{z'} \qquad \text{(Eq. 2.1)}$$
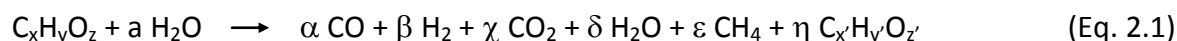
Byproducts ($C_{x'}H_{y'}O_{z'}$) are low molecular weight organic compounds, polymerized products, higher hydrocarbons ($x' \geq 2$, $z' = 0$), or elemental carbon ($y' = z' = 0$). Some of the low molecular weight organics can react further to gas phase components. Subsequent reactions of the gas phase components may also occur. The following (reversible) gas phase reactions may occur, depending on process conditions [18]:

$CO_2 + H_2 \rightleftharpoons CO + H_2O$	(reverse water-gas shift reaction)	(Eq. 1.2)
$CO + 3H_2 \rightleftharpoons CH_4 + H_2O$	(CO methanation)	(Eq. 2.2)
$CO_2 + 4H_2 \rightleftharpoons CH_4 + 2\ H_2O$	(CO_2 methanation)	(Eq. 2.3)
$2\ CO \rightleftharpoons CO_2 + C\ (s)$	(Boudouard reaction)	(Eq. 2.4)
$CH_4 \rightleftharpoons C(s) + 2H_2$	(CH_4 cracking)	(Eq. 2.5)
$CO + H_2 \rightleftharpoons C\ (s) + H_2O$	(CO coking)	(Eq. 2.6)
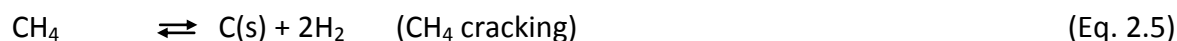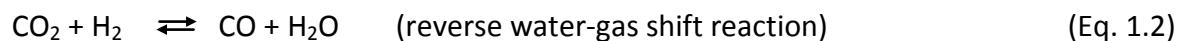
Obviously, the individual reaction rates depend on operating conditions and the presence of catalysts. A number of parameters affect the C_{GE} in RSCW, such as feedstock type, feed concentration, operating conditions, presence of catalysts or catalytic surfaces, and interaction between different components.

In the literature on RSCW two different definitions of conversion are used. The conversion can either be based on the amount of carbon in the gas phase after reaction (C_{GE}), or the residual amount of carbon in the liquid effluent (conversion, ζ). When coke formation or char deposition is absent, both approaches will yield similar values.

Biomass feed concentration

The biomass concentration is a critical process parameter in RSCW. It appears that the C_{GE} for glucose, wood saw dust, or lignin decreases significantly at higher feed concentrations [10, 19-22]. Char formation or polymerization seems to become an important reaction pathway at higher feed concentrations and finally leads to reactor plugging [23-25]. This effect can be reduced by substantial (gas) back-mixing inside the reactor, allowing for *in situ* hydrogenation of

the feed before polymerization occurs [25]. The decreasing gas yield for glucose at high concentration may be due to changes in solubility of the feed or the formation of intermediate products in SCW. Another explanation is that polymerization reactions are higher order reactions and promoted at higher feed concentrations. Both explanations lead to deposition of the feed even before any gasification reaction takes place. Interestingly, associated problems related to plugging due to high feed concentrations are reported to reduce by increasing the operating temperature, indicating that that polymerization and char formation can be suppressed [24]. The phenomenon of decreasing gas yields at higher feed concentrations may not be generic for RSCW, for example, small molecules such as methanol or glycerol give much less dramatic or even no changes in relative yields at higher feed concentrations [15, 26-28]. A conversion of 94% for a 64 wt% methanol solution has been obtained and complete conversion for a 40 wt% glycerol solution over a Ru/Al_2O_3 catalyst has been reported, with gas compositions coinciding nicely with equilibrium values [15, 26, 29].

Process conditions
The conversion of any type of biomass is a strong function of <u>temperature</u>. Higher temperatures lead to higher conversions and a reduced tendency for charring and polymerization. The gas composition will vary as well, due to the effect of temperature on the reaction rates of gas phase reactions and the temperature dependency of the equilibrium constants [19, 30].

At higher <u>operating pressures</u>, CH_4 production at the expense of H_2 is thermodynamically favored [27]. This is indeed observed for methanol and glucose [18, 31, 32]. However, at most conditions the reactions are kinetically driven, chemical equilibria are not always reached, and pressure has no great effects on the gas composition [33, 34]. <u>Residence times</u> required to achieve sufficient conversion are a strong function of the operating temperature and the presence of a catalyst. At lower temperatures around 773 K, typically residence times in the order of minutes are required to achieve complete conversion of the feed [32]. At 973 – 1073 K in the presence of catalysts such as Ru/Al_2O_3, complete conversion can be obtained in seconds [15]. The definition of residence time here should be treated with care, since in most publications the residence time is calculated using the average process temperature, pressure as well as the assumption that the whole feed consists of water without considering the gas production. This is an acceptable assumption as the 'real' residence time is very difficult to determine and strongly related to the local conditions in the reactor.

Catalysts
Reactions in RSCW can be catalyzed by heterogeneous catalysts, ash, and even reactor walls. These catalysts can be very active in promoting the C_{GE}, the water-gas shift (WGS) reaction, or methanation [15, 22, 23, 35, 36]. An extensive review on catalytic reforming is provided elsewhere [4]. Various components present in the ash of biomass, particularly alkali salts are reported to be active [4, 6, 35-37]. The rate of the WGS reaction has been shown to increase by the presence of Na^+-ions, while the C_{GE} was not enhanced [19]. Literature results are

contradictory though, as lower gas yields are reported for glycerol in the presence of Na_2CO_3 compared to pure glycerol [38]. Apart from heterogeneous catalysts and ash, inner reactor parts like reactor walls are also shown to be catalytically active [19, 22, 23, 26]. The use of different reactor materials by different researchers complicates the understanding and comparison of literature data.

Plugging

Reactor plugging can occur due to char formation or polymerization of reforming products, as already discussed in the section on biomass loading. Precipitation of inorganic salts is another likely source of reactor plugging and it is a major challenge in the development of RSCW to prevent this. At higher temperatures, salts become less soluble in SCW and precipitate causing plugging of reactor tubes [14]. Salt concentration, salt type, the rate of seed crystal formation, and crystal growth are important parameters for salt behavior in SCW [7, 35, 39, 40].

2.2.2   Methanol reforming in supercritical water

A possible reaction pathway for methanol decomposition and follow-up reactions is shown in Fig. 2.1 [41]. In this hypothesis, methanol either decomposes directly into H_2 and CO or reacts with water to produce H_2 and CO_2. CO reacts with water to produce CO_2 and H_2 in the WGS reaction, while CH_4 is produced by hydrogenation of CO or CO_2. Theoretically 3 mol of H_2 can be produced from 1 mol of methanol at complete conversion, when methanation is neglected and there is no CO in the final product.

$$CH_3OH \longrightarrow CO + 2H_2 \underset{- H_2O}{\overset{+ H_2O}{\rightleftarrows}} CO_2 + 3\,H_2$$

$$CH_4 + H_2O$$
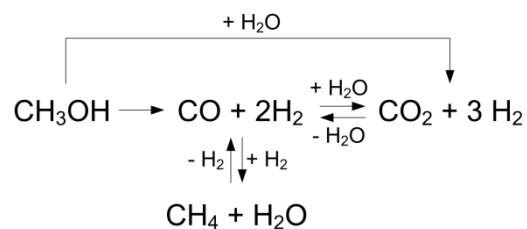
Fig. 2.1 Methanol decomposition pathways in supercritical water and possible follow-up reactions [28].

In inert quartz capillaries, a typical methanol conversion of 25% can be reached at 823 K and a residence time of 140 min. The addition of Ni wire to the quartz capillaries increased the conversion notably to nearly 95%, at a much lower residence time of 12 min [42]. The effect of metals remains rather unclear. For instance, the CH_4 production is reduced from 0.25 mol CH_4/mol feed to almost zero after replacing an Inconel reactor with a Ni-Cu alloy reactor [18]. The fact that the reactor material can have a significant influence is important, as most research studies for methanol are performed in reactors constructed from Inconel 625. At temperatures of 773 K or lower and in the absence of catalysts, methanol appears rather stable and limited gas yields are reported [27, 42]. Using Inconel as reactor material for temperatures exceeding 873 K, complete conversion can be obtained for feed concentrations up to 50 wt% [26-28]. The

product gas consists mainly of H_2, CO_2, and CO, while CH_4 is only observed at longer residence times and for higher feed concentrations. At a short residence time the yield for the different gas products ranges from 2-3 mol H_2/mol feed, 0.1-1 mol CO/mol feed, and 0.1-1 mol CO_2/mol feed. Decreasing CO/CO_2 ratios are observed for higher temperature and lower feed concentrations. The H_2 yield increases with increasing CO_2 formation due to the WGS reaction. The addition of K_2CO_3 or KOH also promotes the WGS reaction, but it reduces methanation [18].

2.2.3 Glycerol reforming in supercritical water

Methanol, a rather simple molecule, has a rather complex decomposition mechanism, but the decomposition mechanism of glycerol is even more complex. Several reactions can take place leading to different intermediate products. Decomposition reactions of glycerol are described in the literature [17, 23, 43, 44]. At temperatures below 773 K, glycerol decomposes into many products (among others acetic acid, hydroxyacetone, acetaldehyde, propionaldehyde, allyl alcohol, methanol, formaldehyde, acrolein) and a gaseous mixture of H_2, CO, CO_2, CH_4, C_2H_4, and C_2H_6. At temperatures around the critical point, ionic reaction pathways can explain the product composition. Free radical pathways are favored at higher temperatures, eventually leading to the formation of gaseous products [17].

RSCW aims at high gas yields instead of valuable soluble organic compounds. In quartz capillaries, only at temperatures exceeding 973 K, sufficiently high C_{GE}'s are obtained [19]. Complete conversion is already reported at 873 K, using Inconel reactors [16]. The residence time is decisive in obtaining a gas rich in CO_2 or rich in CO. A gas containing almost 30 vol% CO_2 and 2 vol% CO has been obtained at a residence time of 44 s, while at a residence time of 4 s a gas with 12 vol% CO_2 and 30 vol% CO has been produced [16, 45].

Catalytic effects are also important for glycerol. Again, the precise effect of catalysts is not entirely known and understood. Complete conversion has been obtained with Ru/Al_2O_3 in an Inconel reactor at temperatures around 1073 K, with a residence time less than 1 s [15]. In these experiments the H_2, CO, CO_2, and CH_4 yields are very close to equilibrium. Effects of alkali are significant as well, these are known to increase the H_2 yield, due to the WGS reaction [4, 6, 35-37]. However, these salts may reduce the conversion at lower temperatures [38].

Conversion and gas composition considerably depend on the process conditions and a wide variety of gas compositions can be obtained. Glycerol reforming is more complex than methanol reforming, because of the involvement of a large variety of liquid soluble intermediates. Each of these intermediates has its own reaction rate and mechanism to arrive at the various gaseous components and this further complicates the picture. The C_{GE} is definitely strongly promoted by temperature, residence time and presence of any catalyst.

2.3 Experimental section

2.3.1 Materials

Methanol (purity 99+%) was supplied by Acros, Belgium. Glycerol was supplied by Chemproha, The Netherlands. $Na_2CO_3 \cdot 10H_2O$ was provided by Sara Lee Household, The Netherlands. Crude glycerin was supplied by Acciona, Spain. The composition of the crude glycerin is shown in Table 2.1. The main components are glycerol, water, and NaCl. Small amounts of other cat-ions are present as well. Artificial gas ($H_2/CO/CO_2/CH_4$ = 55.9/14.7/25.5/3.9 vol%) for the WGS reaction experiments was supplied by Linde Gas Benelux, The Netherlands.

Table 2.1 Composition of crude glycerin.

Component	Concentration
Glycerol	> 88 wt%
Water	6.5 wt%
NaCl	4.5 wt%
Other cat-ions	< 60 ppm
Fatty acids methyl esters + monoglycerids	< 0.1 wt%

2.3.2 Description of the experimental setups

The RSCW of methanol, glycerol, and crude glycerin was investigated in two continuously operated setups, here referred to as 'bench scale unit' and 'pilot plant'.

Bench scale unit

The bench scale unit is schematically depicted in Fig. 2.2. The system, with a capacity of approximately 1 L aqueous feed/h, comprises two high pressure pumps (Haskel, model: CIP-71). One to introduce the premixed feed or water and the other for injecting the pure feed in SCW when the setup is operated in 'injection mode'. The feed streams can be monitored by weighing the feed reservoir(s) from which the water and feed are pumped. The reactors are constructed from Incoloy 825 and the connections from stainless steel. The reactor consists of 4 insulated electrically heated reactor tubes (R1-R4, *ID* = 5.4 mm, *L* = 0.5 m) and optionally an additional 'residence time reactor' (R5, *ID* = 5.4 mm, *L* = 5 m) placed in an electrically heated furnace to enable variation of the residence time.

The reactor effluent is cooled in a double-walled heat exchanger (C1) using tap water. In premixing and injection mode, a back-pressure regulator is used to reduce the process pressure to atmospheric pressure (see Fig. 2.2A). In premixing mode with *in situ* gas separation, the gas is separated from the liquid in a high pressure separator (HPS), before the pressure is reduced to atmospheric pressure (see Fig. 2.2B). The water phase collected in the HPS is depressurized and collected in a low pressure separator (LPS), using a conventional sluice system. During depressurization the gases dissolved are released from the water in the LPS and subsequently quantified and analyzed. The gas flow is quantified using a wet gas meter (Gallus 2000 G1.6).

The total gas yield and composition are obtained by the summation of gas flows from the HPS and the LPS.
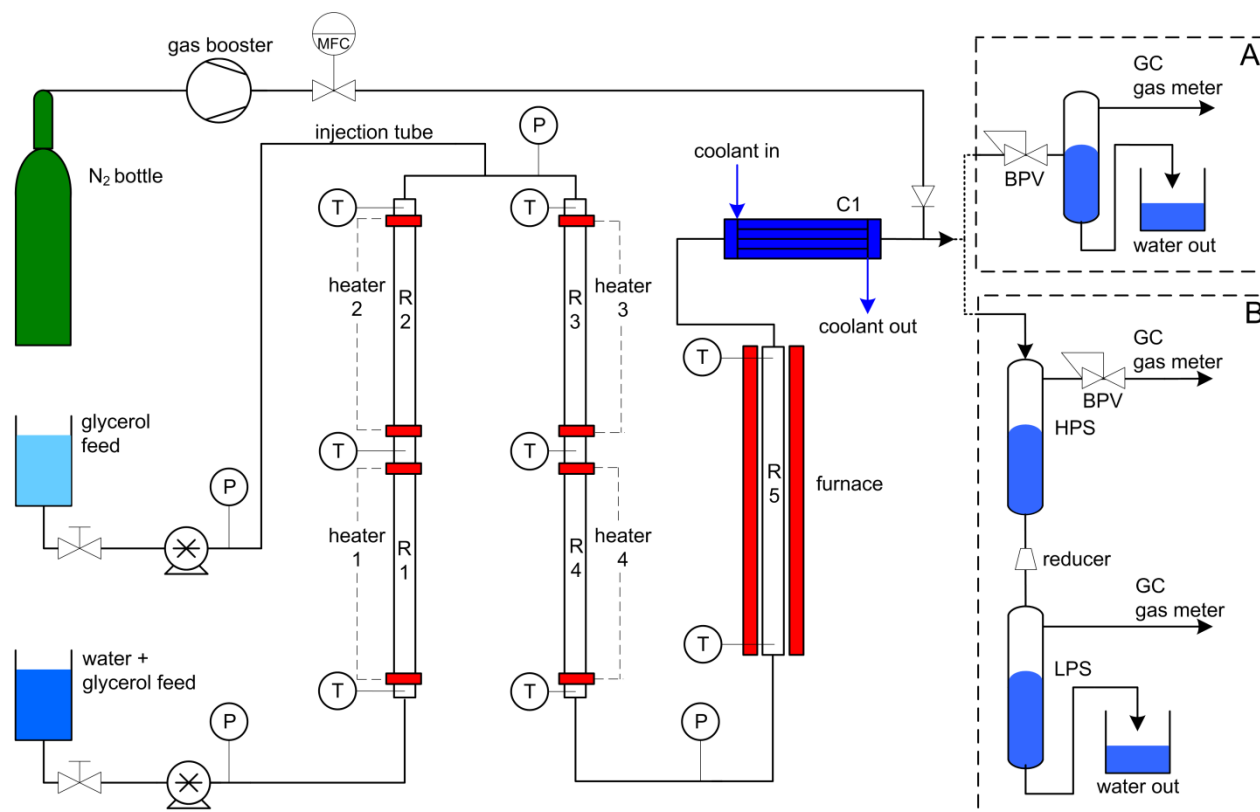
Fig. 2.2 Schematic representation of the continuous bench scale unit. Gas-liquid separation after pressure reduction (A). *In situ* gas-liquid separation (B).

Type K thermocouples are located at the outer walls of the reactors, in the liquid flow after the heat exchanger, and in the liquid/supercritical flows at the in- and outlets of the reactors. Pressure meters are located at the reactor in- and outlets. Setup control and data logging are carried out using a computer equipped with the Adam view software package.

Before and after each experiment, the system was flushed with water at sub- and supercritical conditions for at least 1 h. The following process parameters were varied: temperature (723 K – 923 K), residence time (6 – 47 s), and feed concentration (3 – 20 wt%). The residence time is set by variation of the reactor length from 2 to 7 m and variation of the throughput between 0.8 and 1.2 kg/h, while the pressure was maintained in the region of 25.5 – 27.0 MPa.

The bench scale unit was operated in three different modes:
  ➢ The 'premixing mode', where reactant and water are premixed and the mixture is fed to the setup.
  ➢ The 'injection mode', in which reactant is injected in the water at supercritical conditions via an injection tube.
  ➢ The 'premixing mode + *in situ* gas separation', where reactant and water are premixed and the mixture is fed to the setup, the water phase and the gas phase are separated at high pressure.

A huge advantage of the premixing mode with *in situ* gas separation is the production of gas at high pressure which can be used in a downstream process.

Some experiments were performed to determine the extent and progress of the WGS reaction as a function of the operating conditions. For these experiments; model gas was mixed with water before entering the first reactor. The inlet and the outlet gas were analyzed and quantified. The experiments were carried out at 787 K and 890 K with a total gas flow rate of 85 NL/h.

Pilot plant (PP)

The pilot plant is depicted in Fig. 2.3 and is constructed from Incoloy 825. Premixed feed is fed to the setup using a high pressure pump (Haskel, model: CIP-71). Subsequently heat is exchanged between the feed and the reactor effluent in a counter current heat exchanger before the feed enters the reactor (ID = 14 mm, L = 17 m). The reactor is placed in a furnace and heated by burning propane or natural gas. After cooling down the reactor effluent in the heat exchanger, the effluent is cooled to room temperature in a double-walled cooler using tap water. The water phase and gas phase are separated *in situ* in a high pressure separator (HPS). The pressure of the HPS gas is reduced to atmospheric pressure through a back-pressure valve. The gas flow is measured using a Brooks mass flow meter and corrected for the gas composition. The water phase is fed to a low-pressure separator (LPS) after being further depressurized. Gases dissolved in the water are released and quantified using a second Brooks mass flow meter. The total gas yield is the sum of both gas flows, HPS gas and LPS gas.
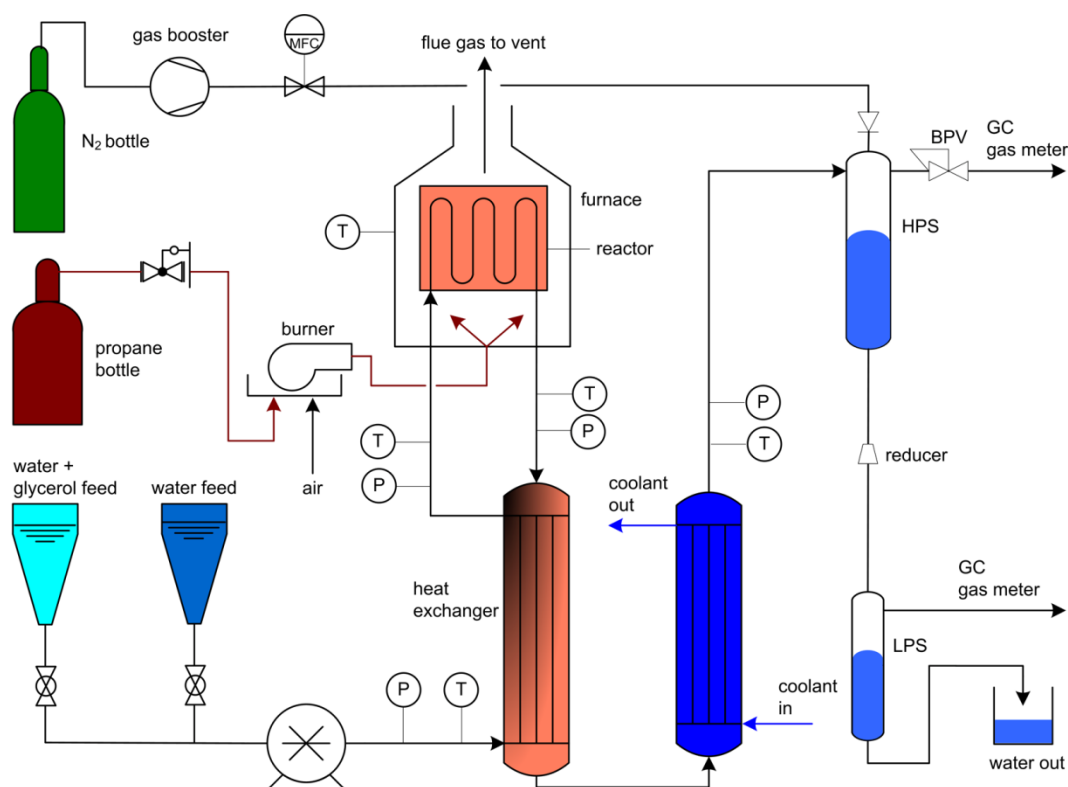
Fig. 2.3 Schematic representation of the pilot plant.

Temperature and pressure can be monitored at various locations; viz. before and after the heat exchanger, at the entrance and exit of the reactor, and after the cooler. Before and after each experiment, the system was flushed with water at sub- and supercritical conditions for at least 1 hour. The process parameters varied include: temperature (843 – 893 K), residence time (74 – 173 s), and feed concentration (4.8 – 16.7 wt%). The throughput of the experiments was between 4.1 – 13.3 kg/h, while the pressure was maintained in the region of 25.5 – 27.0 MPa. An overview of the experiments carried out in the setups is listed in Table 2.2.

Table 2.2 Operating modes of the experiments.

Feedstock	Mode	Setup	Fig.
Gas (WGS experiment)	Premixing + *in situ* gas separation	Bench scale unit	2.2B
Methanol (pure)	Premixing + *in situ* gas separation	Bench scale unit	2.2B
Methanol + Na_2CO_3	Premixing + *in situ* gas separation	Bench scale unit	2.2B
Glycerol	Premixing	Bench scale unit	2.2A
Glycerol	Premixing + *in situ* gas separation	Bench scale unit	2.2B
Glycerol	Injection	Bench scale unit	2.2A
Crude glycerin	Premixing	Bench scale unit	2.2A
Crude glycerin	Premixing + *in situ* gas separation	Bench scale unit	2.2B
Crude glycerin	Injection	Bench scale unit	2.2A
Glycerol + Na_2CO_3	Premixing + *in situ* gas separation	Pilot plant	2.3

2.3.3 Analyses

The gas derived in the bench scale unit was analyzed using an online dual-column gas chromatograph (GC 955, Syntech Spectras) equipped with thermal conductivity detectors. CH_4 and CO were analyzed over a molecular sieves 5 Å column (L = 1.6 m) with helium as carrier gas. CO_2 and C_{2+} were analyzed on a Chromosorb 102 column (L = 1.6 m) with helium as carrier gas. H_2 was analyzed on the molecular sieves column using argon or nitrogen as carrier gas. The gases from the pilot plant experiments were analyzed with the same GC as mentioned before, but using He as carrier gas for all analyses.

In addition, the total organic carbon (TOC) content of the effluent water from the bench scale unit was analyzed using a dedicated TOC analyzer (TOC-V$_{CSN}$, Shimadzu). Before the TOC measurement, the effluent sample was diluted appropriately to obtain values within the measuring range of the apparatus. In some experiments the composition of the effluent water was determined by high pressure liquid chromatography, using an HPLC equipped with a Hewlett Packard 1050 pump, a Biorad Aminex HPX-87H organic acid column and a Waters 410 refractive index detector. The mobile phase was an aqueous solution of sulfuric acid (5 mM) at a flow rate of 0.55 mL/min. The column temperature was 333 K.

The water content of the crude glycerin was measured using Karl-Fischer titration and the sodium content using Atomic Absorption Spectrometry (AAnalyst 200, Perkin-Elmer). The content of other metals was determined with Inductively Coupled Plasma Mass Spectrometry (Optima 4300 DV, Perkin-Elmer), while the chloride content was measured by a titration method using silver nitrate with potassium chromate as indicator. Finally, the fatty acid methyl esters were extracted from the crude glycerin with chloroform, and analyzed using a gas chromatograph (HP 5890 SII Plus) equipped with a mass selective detector (HP 5972).

2.3.4 Definitions

The temperatures of the reactors in the bench scale setup are measured at the outer surface of the reactor tubes. Each reactor segment contains two thermocouples. The reactor temperature is taken as the average of the temperatures measured at the reactor walls. The reactor temperature in the pilot plant is taken as the temperature of the liquid effluent from the reactor. The carbon-to-gas efficiency (C_{GE}) is defined as the ratio between the molar carbon flow in the gas ($\sum_i \phi_{C,i}$) and the molar carbon flow of the feed ($\phi_{C,feed}$). The molar carbon flow of the feed is calculated from the glycerol concentration and feed flow, while the molar carbon flow in the gas is derived from the gas flow and gas composition:

$$C_{GE} = \frac{\sum_i \phi_{C,i}}{\phi_{C,feed}} \cdot 100\%$$

(Eq. 2.7)

The hydrogen-to-gas efficiency (H_{GE}) and oxygen-to-gas efficiency (O_{GE}) are determined in a similar way.

$$H_{GE} = \frac{\sum_i \phi_{H,i}}{\phi_{H,feed}} \cdot 100\%$$ (Eq. 2.8)

$$O_{GE} = \frac{\sum_i \phi_{O,i}}{\phi_{O,feed}} \cdot 100\%$$ (Eq. 2.9)

The carbon conversion (ζ) is calculated from the molar carbon flow of the feed and the effluent.

$$\zeta = \frac{\phi_{C,feed} - \phi_{C,effluent}}{\phi_{C,feed}} \cdot 100\%$$ (Eq. 2.10)

The residence time (τ) was calculated as follows

$$\tau = \frac{V_r \cdot \rho_{T,P}}{\phi_{m,STP}}$$ (Eq. 2.11)

with V_r as the geometric reactor volume, $\rho_{T,P}$ as the water density at (average) process temperature and pressure and $\phi_{m,STP}$ as the mass flow at standard conditions. For all residence time calculations the feed is assumed to consist of pure water.

2.4 Results

This section starts with a description of the equilibrium gas compositions as a function of the temperature. Subsequently, experimental data on the WGS reaction are provided to gain insight into the progress and relative rate of this reaction at process conditions. These results are useful for the interpretation of the results for RSCW of methanol and glycerol, which are presented subsequently.

2.4.1 Estimation of the gas phase equilibrium for methanol and glycerol

At the conditions relevant for RSCW, thermodynamics may play a significant role. In many publications equilibrium data are given considering the complete set of H_2, CO, CO_2, CH_4, and C_xH_y. The experimental results, however, demonstrate that in many cases the thermodynamic equilibrium is not reached. Therefore, another approach will be presented here, viz. the equilibrium composition in the case that all reactions are at equilibrium and in the case that only the WGS is at equilibrium, the latter is likely the case for most RSCW data. The equilibrium gas yields at complete conversion are calculated using an in-house-developed Matlab program, using equilibrium correlations for the WGS reaction and methanation taken from literature [46].

The Soave-Redlich-Kwong equation of state is used to correct for nonideality [47]. Critical properties and acentric factors are taken from literature [48].

In Fig. 2.4 the equilibrium yield at 25 MPa as a function of the temperature is shown for methanol feed concentrations of 6.3 and 12.5 wt.%, taking into account the WGS reaction and methanation (Figs. 2.4A and 2.4B) or solely the WGS reaction (Fig. 2.4C). These feed concentrations are the limits of the concentration range of the majority of the experimental work, which will be discussed later.

The equilibrium yield, taking into account the WGS reaction and methanation (case A and B) differs considerably from the equilibrium yields based on solely the WGS reaction (case C). The equilibrium yield is a strong function of the methanol feed concentration. The yield of H_2 and CO_2 is considerably higher at a lower feed concentration, while the opposite is true for CH_4. The CO yields are low in both cases. For case C, the yields hardly depend on the two feed concentrations. The H_2 and CO_2 yields only decrease slightly with increasing temperature, while the CO yield compensates for the CO_2 decrease.
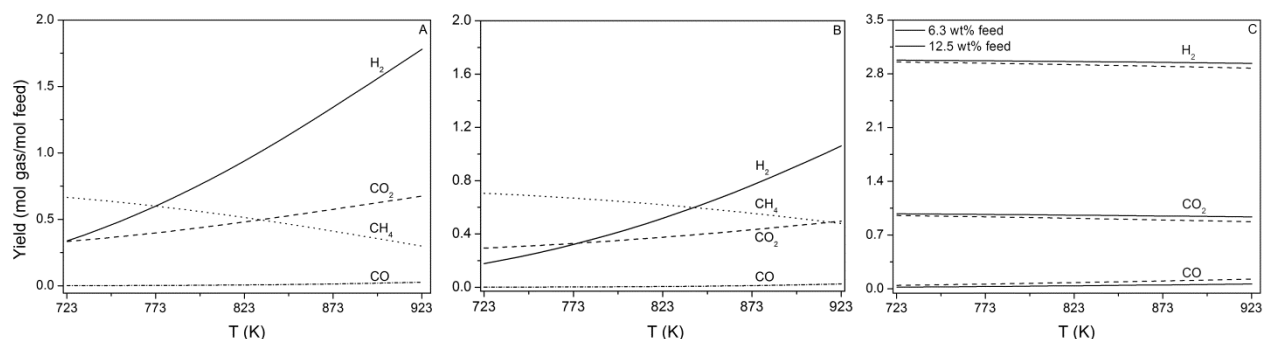
Fig. 2.4 Equilibrium yields for methanol reforming taking into account the WGS reaction and methanation for a 6.3 wt% feed solution (A) and a 12.5 wt% feed solution (B). In (C) only the WGS reaction is taken into account for both concentrations.

Equilibrium yields for glycerol are shown in Fig. 2.5, for feed concentrations of 5 and 20 wt% respectively and a pressure of 25.0 MPa. In Figs. 2.5A and 2.5B, methanation and the WGS reaction (case A and B) are taken into account and in Fig. 2.5C, solely the WGS reaction (case C) is taken into account with the assumption that per mol of glycerol 1 mol of CH_4 is produced. In the results section will be shown that at complete conversion 1 out of 3 carbon atoms from a glycerol molecule ends up in a hydrocarbon. Similarly with methanol, equilibrium yields in case A and B strongly depend on temperature and feed concentration. H_2 and CO_2 yields are significantly higher for a 5 wt% feed solution than for a 20 wt% feed solution, while the CH_4 yield is substantially lower for the lower feed concentration. In case C, gas yields are nearly independent of temperature and feed concentration. In both cases, CO is almost absent.
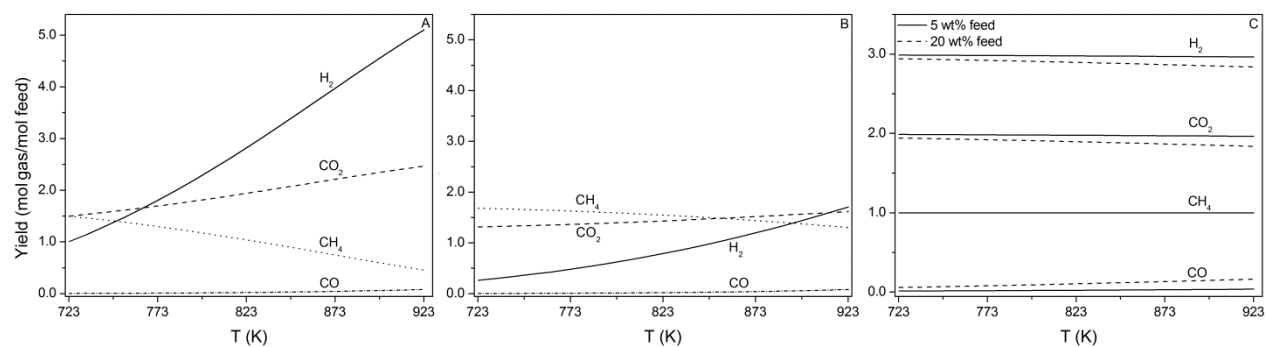
Fig. 2.5 Equilibrium yields for glycerol reforming taking into account the WGS reaction and methanation for a 5 wt% feed solution (A) and a 20 wt% feed solution (B). In (C) only the WGS reaction is taken into account for both concentrations.

2.4.2 Experimental studies on the WGS reaction

The extent to which the WGS reaction and methanation proceed can be demonstrated by feeding an artificial gas with known composition to the reactors and measuring the change in the gas composition. The results for two temperatures, 787 K and 890 K, and residence times of respectively 15 s and 12 s are shown in Table 2.3. The product gas composition is compared with the equilibrium composition considering only the WGS reaction and neglecting methanation. This comparison leads to the conclusion that the WGS reaction hardly proceeds at the lower temperature, since the product gas composition is far from equilibrium and similar to the feed gas composition. At the higher temperature, a slight reduction in the CO concentration was observed. This indicates a minor effect of the WGS reaction, nevertheless, also here the WGS reaction is far from equilibrium and methanation is fully absent. Only after adding Na_2CO_3, a slightly higher activity was observed for the WGS reaction, but again, the gas composition remained far from equilibrium.

Table 2.3 Overview of experiments on the WGS reaction in the bench scale unit.

	T	τ	H_2	CO	CO_2	CH_4
	(K)	(s)	(vol%)	(vol%)	(vol%)	(vol%)
Feed	-	-	55.9	14.7	25.5	3.9
Off gas	787	15	56.1	14.4	25.5	4.0
Off gas (+ Na_2CO_3)	787	15	57.3	11.7	27.0	4.0
Equilibrium[a]	787	-	61.4	0.4	34.8	3.4
Off gas	890	12	57.0	12.7	26.2	4.1
Off gas (+ Na_2CO_3)	890	12	58.1	9.8	28.2	3.9
Equilibrium[a]	890	-	61.3	0.7	34.6	3.4

[a]The equilibrium composition was calculated using the model described in Section 2.4.1.

2.4.3 RSCW of methanol

Experiments were performed using pure methanol and methanol containing 0.1 wt% Na_2CO_3 (from here on referred to as soda methanol) as feed. First, an experiment with pure methanol was performed three times to demonstrate the reproducibility of the experiments. The relative deviation in the C_{GE} between the experiments was below 6%. The closure of the carbon balance was at least 90% for all experiments. The results obtained in the premixing mode with *in situ* gas separation are shown in Fig. 2.6 and Fig. 2.7. C_{GE} and ζ are plotted as a function of the temperature in Fig. 2.6 and as a function of the feed concentration in Fig. 2.7. In all figures, closed symbols represent experiments with pure methanol, while the open symbols are the results for soda methanol.

In Fig. 2.6 the influence of the temperature on the C_{GE} is shown for a feed concentration of 12.5 wt% and a residence time of 39 − 47 s. For both, pure methanol and soda methanol, the C_{GE} increases with temperature, confirming the results published in the literature [26-28]. Eventually the C_{GE} reaches 82% and 93% for soda methanol and pure methanol respectively at 915 K. Except for the lowest temperature, the C_{GE} for pure methanol is significantly higher than for soda methanol.
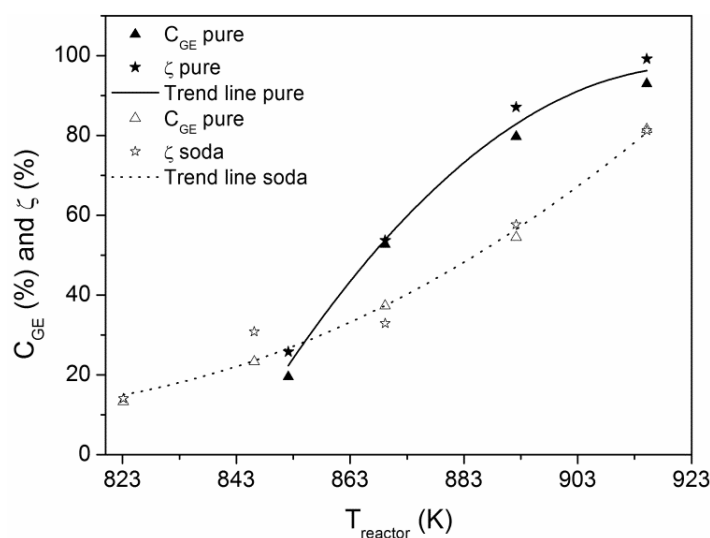
Fig. 2.6 C_{GE} and ζ for methanol reforming as a function of the temperature. Experimental conditions: τ = 39 − 47 s, [49] = 12.5 wt%, Na_2CO_3 concentration = 0.1 wt%. The solid line and the dotted line are trend lines for respectively pure and soda methanol.

The dependence of the C_{GE} and the ζ on the feed concentration is shown in Fig. 2.7. The C_{GE} for pure methanol has a constant value of approximately 52% for feed concentrations of 3 − 12.5 wt%, but decreases slightly at higher concentrations. Such a trend has been reported before in the literature for combinations of short residence times and high feed concentrations [27, 28]. For soda methanol, the conversion is again significantly lower than for pure methanol, over the

complete range of feed concentration. The decrease in C_{GE} as a function of the feed concentration is more pronounced for soda methanol than for pure methanol.

The C_{GE} for (soda) methanol was measured for two different residence times of 9 s and 44 s at 869 K and a feed concentration of 12.5 wt%. At a residence time of 9 s, the C_{GE} for both types of feed has a similar value of 8%. The C_{GE} increases with residence time, but again, at higher residence times, the C_{GE} for soda methanol with a value of 32% is lower than the C_{GE} value of 53% for pure methanol. During the experiments, no tar formation or carbon deposition was observed. The effluent was clear and the interior of the reactor remained clean after several runs. The latter was observed visually. The deviation between the C_{GE} and the ζ can thus only be attributed to measurement errors, which, for a typical experiment is less than 8%.
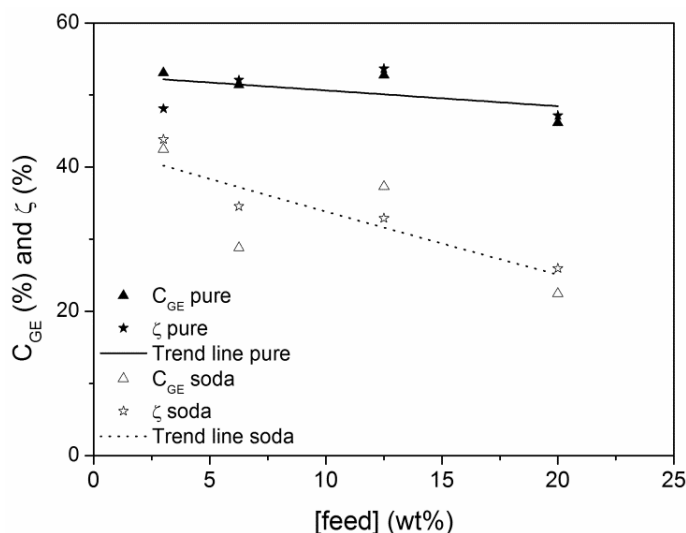
Fig. 2.7 C_{GE} and ζ for methanol reforming as a function of the feed concentration. Experimental conditions: T = 869 K, τ = 42 − 43 s, Na$_2$CO$_3$ concentration = 0.1 wt%. The solid line and the dotted line are trend lines for respectively pure and soda methanol.

In Fig. 2.8 a compilation for the H_{GE} and O_{GE} versus the C_{GE} is shown for all experiments performed with methanol. The solid and the dotted line represent the trend lines for pure and soda methanol respectively, while the dashed line represents the parity with the C_{GE}. The parity line is defined as the H_{GE} (Fig. 2.8A) or O_{GE} (Fig. 2.8B) theoretically derived for the case that methanol decomposes stoichiometrically to gas products (CH$_3$OH $\longrightarrow$ CO + 2H$_2$). In that situation no water is consumed in the reaction, no coke is formed, and no liquid products are formed.

For all conditions and for both pure and soda methanol, the H_{GE} and O_{GE} are higher than the C_{GE} and consequently more hydrogen and oxygen end up in the gas phase than based on the carbon in the methanol. This is more apparent for soda methanol than for pure methanol.

Some intermediate products were traced back with HPLC analysis of the effluent water. The concentration of intermediate products was smaller than 0.01 wt% of the TOC content of the effluent. The main organic component in the effluent water was unconverted methanol.
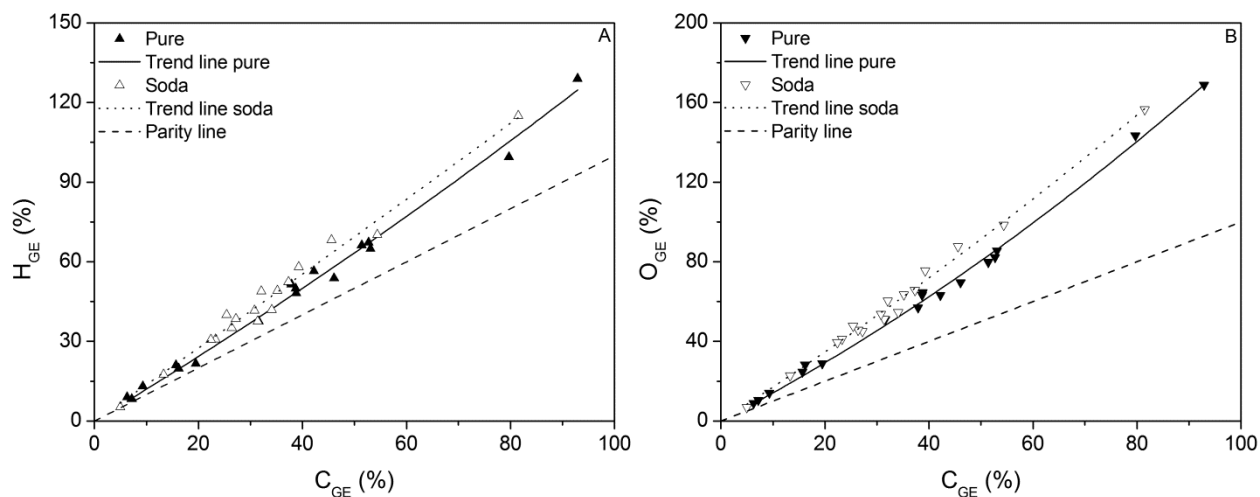
Fig. 2.8 H_{GE} (A) and O_{GE} (B) as a function of the C_{GE}. The dashed line is the parity with the C_{GE}. Conditions: T = 823 – 915 K, [feed] = 6.3 – 12.5 wt%, τ = 9 – 47 s. The solid lines and the dotted lines are trend lines for respectively pure and soda methanol.

As coke formation is negligible, it can only be concluded that water is consumed to produce extra hydrogen and oxygen in the gas phase. Water consumption is indeed likely, because of the WGS reaction or the reaction of methanol with water to CO_2 and H_2. The amount of water consumed can be calculated from the element balances and the result is shown in Fig. 2.9. Although both the hydrogen balance and the oxygen balance can be used here, the present calculation is based on the oxygen balance, because the CO and CO_2 concentration can be measured the most accurate. Water is consumed over the complete C_{GE} range. Extrapolating the trend line for soda methanol, the water consumption approaches 1 mol H_2O/mol feed, which is the theoretical maximum in case of full conversion of CO to CO_2 via the WGS reaction. Alternatively, it may suggest that overall 1 mol of H_2O then reacts with 1 mol of methanol. The water consumption for pure methanol is slightly lower than for soda methanol, though the consumption increases exponentially at C_{GE} values exceeding 50%.
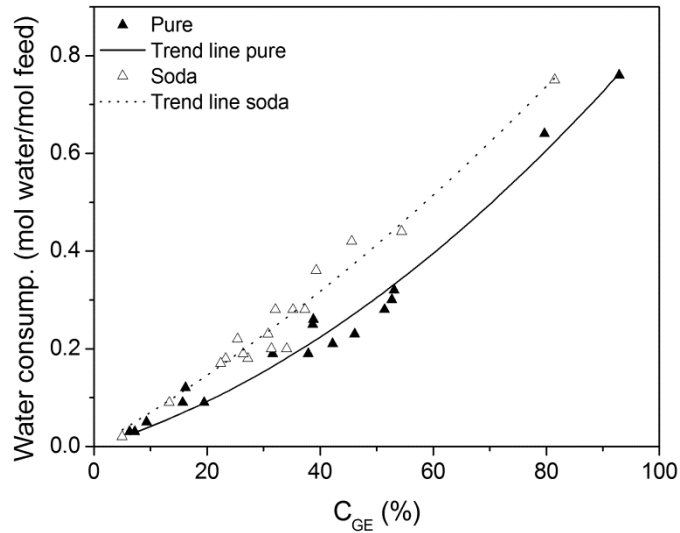
Fig. 2.9 Water consumption for methanol reforming as a function of the C_{GE}. Conditions: $T = 823 - 915$ K, [feed] = 6.3 − 12.5 wt%, $\tau = 9 - 47$ s. The solid line and the dotted line are trend lines for respectively pure and soda methanol.

The gas yields are presented as a function of the C_{GE} in Fig. 2.10. It appears that the H_2 yield increases almost linearly with the C_{GE}. The H_2 yield for soda methanol is slightly higher than for pure methanol. At complete conversion, the H_2 yield approaches the theoretical maximum of 3 mol H_2/mol feed. For CO, the yield goes up almost linearly till a C_{GE} of 50%, then it reaches a maximum, and decreases subsequently. The trend line in case of pure methanol is quite straightforward, but for soda methanol, the CO yield shows more scattering. The yield is, however, significantly lower than for pure methanol.

The CO_2 yield in turn increases significantly and almost linearly. It can be concluded from Fig. 2.10 that the CO/CO_2 ratio decreases with increasing C_{GE}. That means that the CO/CO_2 ratio decreases with increasing temperature and increasing residence time, or a combination of the two. This observation is in agreement with literature [27, 28]. Finally, the CH_4 yields are below 0.033 mol CH_4/mol feed for pure methanol and increase slightly with C_{GE}. This suggests that methanation indeed hardly occurs at these conditions. In the case of soda methanol, the CH_4 yields are even lower and the presence of alkalis seems to inhibit the methanation reaction almost completely as reported in the literature before [18].
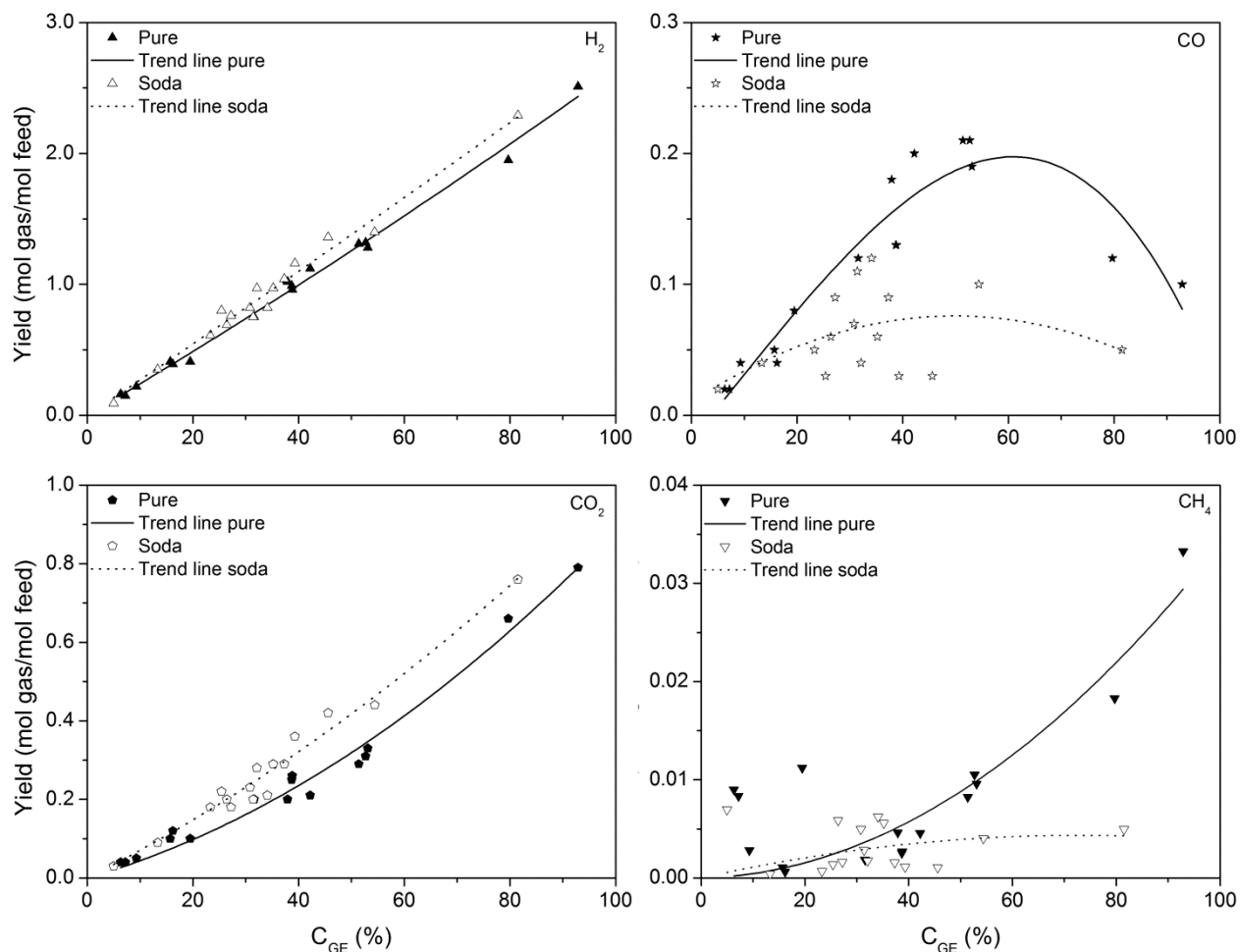
Fig. 2.10 Gas yields for methanol reforming as a function of the C_{GE} for different components (H_2, CO, CO_2, and CH_4). Experimental conditions: $T = 823 - 915$ K, [feed] $= 6.3 - 12.5$ wt%, $\tau = 9 - 47$ s. The solid lines and the dotted lines are trend lines for respectively pure and soda methanol.

2.4.4 RSCW of Glycerol

Similar experiments as for methanol were also performed for glycerol, at temperatures between $733 - 923$ K, feed concentrations of $5 - 20$ wt%, and residence times of $6 - 173$ s. In all experiments the pressure was maintained at $25.5 - 27.0$ MPa and the carbon balance closure was greater than 90%. Some experiments were performed in duplicate or three times. The absolute deviation in the C_{GE}, ζ, and gas yield was below 7%.

The C_{GE} for glycerol as a function of various parameters is shown in Fig. 2.11-13. In all these figures, closed symbols represent experiments with pure glycerol, while the open symbols are the results for crude glycerin or glycerol with Na_2CO_3. It can be seen in Fig. 2.11 that the C_{GE} increases with temperature, with the highest values of 87% and 91% for pure glycerol and crude glycerin respectively at 886 K. In the literature similar temperature dependencies have been observed [45]. The presence of alkali in the feed enhances the C_{GE} at low temperatures, while

the effect is hardly visible at higher temperatures, coinciding with the results obtained in quartz capillaries [19].
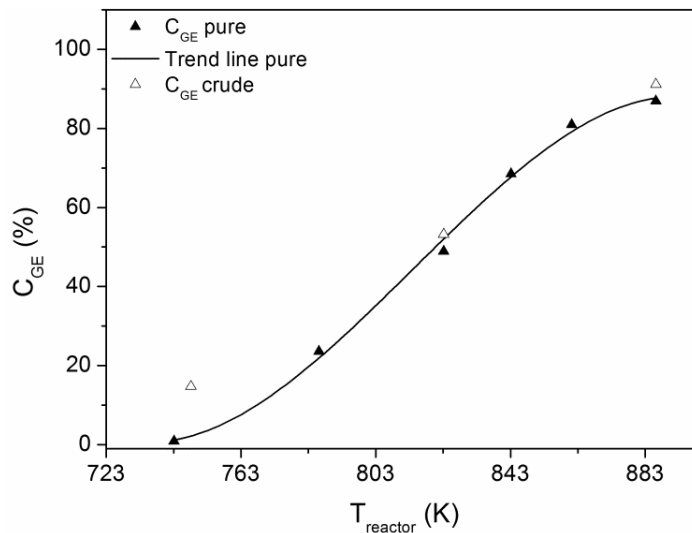
Fig. 2.11 C_{GE} for pure glycerol and crude glycerin reforming as a function of the temperature. Experimental conditions: τ = 17 – 24 s, [feed] = 10 wt%. The experiments were performed in the premixing mode. The solid line is a trend line for pure glycerol.

For pure glycerol, the C_{GE} is relatively constant with a value of 87% for the glycerol concentration range of 10 – 20 wt% (see Fig. 2.12). Only the C_{GE} for a 5 wt% solution is slightly higher. For crude glycerin, the C_{GE} is slightly higher than for pure glycerol at feed concentrations from 5 – 10 wt%, but at the higher feed concentration the C_{GE} value is lower than for pure glycerol. For the experiment with a feed concentration of 15 wt%, the gas yield decreased continuously with operating time. It is known from literature that the reactor wall has catalytic effects [7, 22, 23, 40]. Therefore, decreasing gas yields can be due to salt deposition at the reactor wall resulting in loss of active metal surface area. Furthermore, decreasing gas yields can be due to a reduction in heat transfer from the reactor wall to the reaction medium due to salt deposition [23].
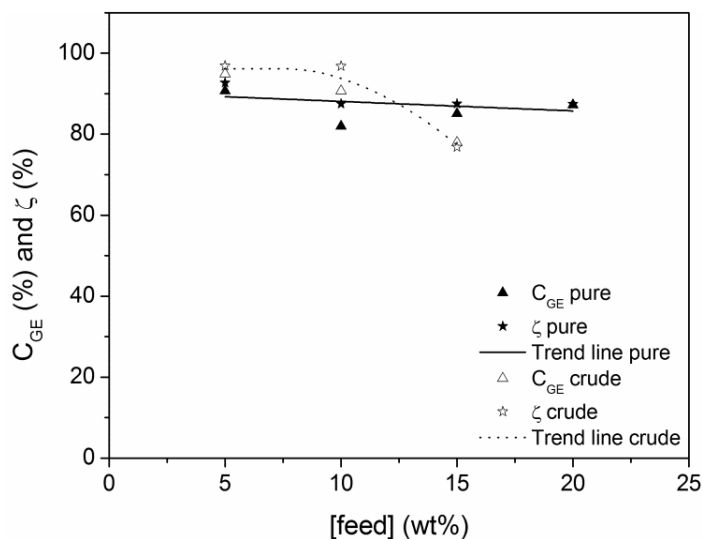
Fig. 2.12 C_{GE} and ζ for pure glycerol and crude glycerin reforming as a function of the feed concentration. Experimental conditions: T = 892 K, τ = 39 s. The experiments were performed in the premixing mode with *in situ* gas separation. The solid line and the dotted line are trend lines for respectively pure glycerol and crude glycerin.

The C_{GE} as a function of the residence time is shown in Fig. 2.13. The C_{GE} increases with residence time for both types of glycerol. The increase is significant up to approximately 20 s, then it levels off. The difference between the values for pure glycerol and crude glycerin is small and is within the measurement error range.
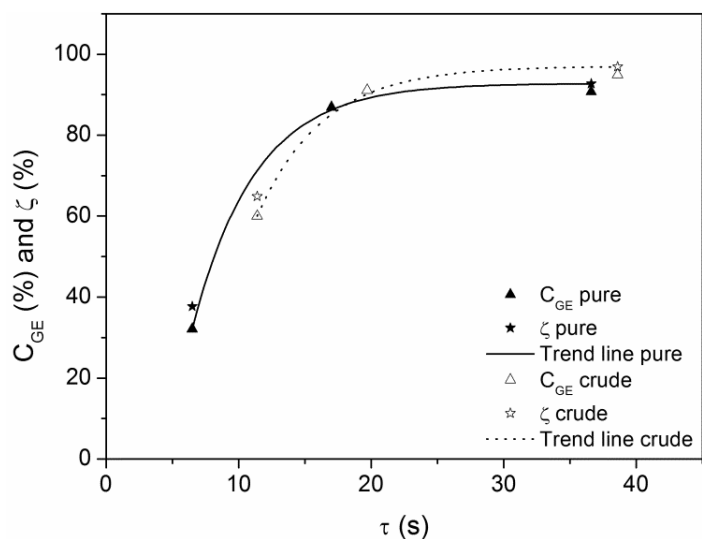
Fig. 2.13 C_{GE} and ζ for pure glycerol and crude glycerin reforming as a function of the residence time. Experimental conditions: T = 892 K, [feed] = 5 wt%. The experiments were performed in the premixing mode with *in situ* gas separation. The solid line and the dotted line are trend lines for respectively pure glycerol and crude glycerin.

As mentioned in the literature, salts in the feed can cause reactor plugging through precipitation [35, 39, 40]. This is also the case for the experiments with crude glycerin. Reactor plugging occurs after several hours of operation. The operating time before plugging depends on the feed concentration.

The C_{GE} values for all the experiments are compared with their accompanying H_{GE} and O_{GE} values in Fig. 2.14. The results of all the experiments are presented here; independent of process parameters, conditions, and the setup in which they were performed. The solid and the dotted line represent trends for pure glycerol and crude glycerin, respectively, while the dashed line represents the parity with the C_{GE}. The parity line is defined as the H_{GE} (Fig. 2.14A) or O_{GE} (Fig. 2.14B) theoretically derived for the case that glycerol decomposes stoichiometrically to gas products.

Though some scattering is present, clear trends can be noted. Theoretically, C_{GE}, H_{GE}, and O_{GE} should be equal if glycerol is directly converted to the gas phase without interaction of water, intermediate product formation, coke formation, and any gas phase follow up reactions. Coke formation can be neglected in these experiments, because the effluent water was clear and the interior of the reactor was clean upon opening.
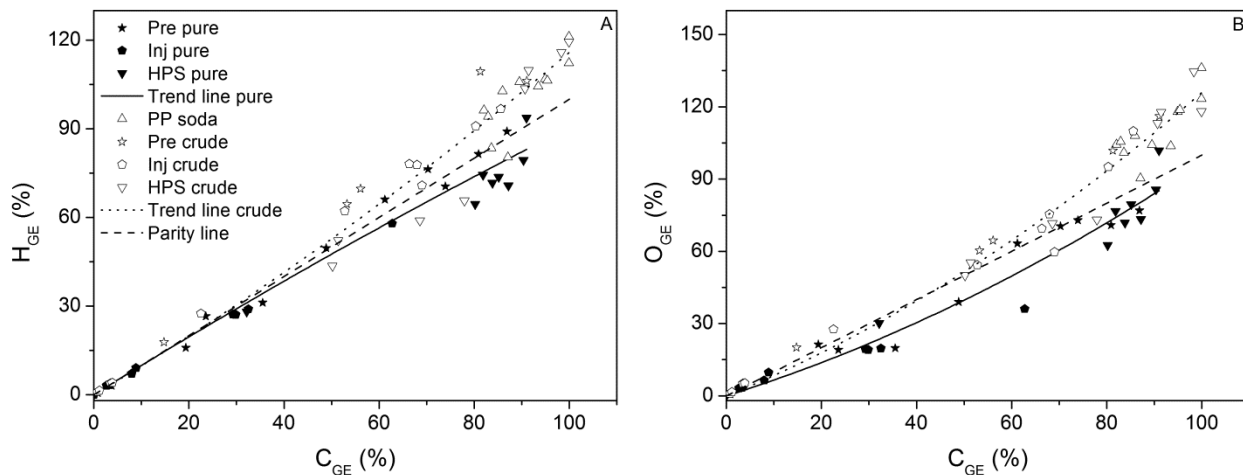
Fig. 2.14 H_{GE} (A) and O_{GE} (B) as a function of the C_{GE} for pure glycerol and crude glycerin reforming. The dashed line is the C_{GE}. Conditions: T = 733 − 923 K, [feed] = 5 − 20 wt%, τ = 6 − 173 s. The solid lines and the dotted lines are trend lines for respectively pure glycerol and crude glycerin.

For crude glycerin more hydrogen and oxygen end up in the gas phase relative to carbon indicating water consumption. On the contrary, for pure glycerol less hydrogen and oxygen are present in the gas phase than expected on basis of the carbon balance. Only minor quantities of among others propionic acid, acetaldehyde, acetic acid, formaldehyde, methanol, and ethanol were detected in the effluent with HPLC. The formation of the water-soluble products can only partly explain the differences between C_{GE} on the one hand and H_{GE} and O_{GE} on the other hand. These differences strongly indicate water production instead of water consumption. Assuming that the differences in the hydrogen and oxygen balance compared to the carbon balance are

due to reactions involving water, the 'overall' water consumption can be calculated from the oxygen balance. The results are shown in Fig. 2.15.

For reforming of pure glycerol, the water consumption is negative indicating that water is produced. The production increases until the C_{GE} reaches approximately 50%, after which the production reduces. The latter is again likely due to the WGS reaction. A theoretical approach can now be undertaken assuming that for C_{GE}'s below 40% the WGS reaction can be neglected. The dashed line in Fig. 2.15A is a linear trend line for these specific data points including the intercept with the origin. Extrapolation of this line to point A in Fig. 2.15 then leads to a net water consumption in the range of 1 mol H_2O/mol feed. It suggests that the overall primary mechanism for pure glycerol decomposition is the dehydration of 1 mol H_2O/mol glycerol. Dehydration reactions in SCW are free radical reactions [17]. According to the literature, free radical reactions are likely to proceed at the process conditions used in this research study.

For crude glycerin, water is consumed if the C_{GE} exceeds 50%, while the overall water consumption reaches 1 mol H_2O/mol glycerol when the crude glycerin is completely converted. Thus, higher water consumptions are observed for reactions in the presence of alkali catalysts, an indication that the presence of alkali increases the rate of the WGS reaction. This phenomenon has been observed by several researchers [4, 6, 35-37].
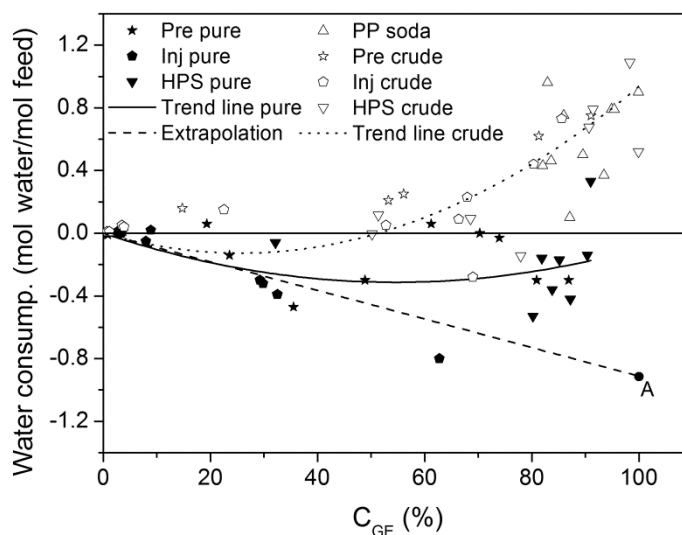
Fig. 2.15 Water consumption for pure glycerol and crude glycerin reforming as a function of the C_{GE}. Conditions: $T = 733 - 923$ K, [feed] $= 5 - 20$ wt%, $\tau = 6 - 173$ s. The solid line and the dotted line are trend lines for respectively pure glycerol and crude glycerin. The dashed line is an extrapolation of the trend line for pure glycerol data points with a C_{GE} below 40%.

As for methanol, the various gas yields are plotted as a function of the C_{GE}. Eight gas components were detected, viz. H_2, CO_2, CO, CH_4, C_2H_4, C_2H_6, C_3H_6, and C_3H_8. The yields are plotted in Fig. 2.16 as a function of the C_{GE} except for the C_3H_6 and C_3H_8 yields, because of their low values. This figure represents all experiments carried out in the different setups and

operating modes at different process conditions. The scattering in the data can be caused by: (i) measurement errors, (ii) small differences in the velocity of the WGS reaction, (iii) effect of equilibria, and (iv) the use of different setups and operating modes. Despite these complexities, the trend lines in Fig. 2.16 are clear for both pure glycerol and crude glycerin. The H_2, CO_2, CH_4, and C_2H_6 yields increase with C_{GE}. For pure glycerol the CO yield increases with C_{GE}, while for crude glycerin the yield goes through a maximum at a C_{GE} of 50 – 60%. The yield of C_2H_4 is very low in all experiments, which partly explains the relative large scattering. However, the data should be considered with some care, as they are not always measured accurately in the experiments in the premixing mode with *in situ* gas separation (HPS). Nevertheless, a trend can be observed. The yield of C_2H_4 as a function of the C_{GE} goes through a maximum and the component is essentially absent at a C_{GE} of 100%. The yield of C_3H_6 which is not plotted shows a similar trend, while C_3H_8 starts to appear when the C_{GE} exceeds 30%. The H_2, CO_2, and CH_4 yields for crude glycerin at a C_{GE} of approximately 20% are slightly higher than expected based on these trend lines. Detailed inspection revealed that the low C_{GE}'s measured are likely due to small gas leakages in the reactor system.

Some differences between the results for pure and crude glycerin are apparent as well. For instance, the increase in the H_2 and CO_2 yields is more significant for crude glycerin than for pure glycerol. Over the complete conversion range, the CO yield increases for pure glycerol, however, a maximum is reached for crude glycerin at a C_{GE} of around 50 – 60%. The CO_2 yield for both feeds is close to zero in the C_{GE} range of 0 – 30%, but increases at higher C_{GE}'s. At low C_{GE}'s the H_2, CO, and CO_2 yield are more or less comparable for both feeds, however they start to deviate at C_{GE}'s exceeding 50%. It is expected that this is caused by the WGS reaction. For C_{GE}'s below 50% the WGS reaction hardly proceeds, but for higher C_{GE}'s the WGS reaction becomes noticeable. The rate increase of the WGS reaction for crude glycerin is more pronounced due to the presence of alkali. Also in case of pure glycerol the WGS reaction proceeds at the higher C_{GE}'s, as the yield for CO levels off and CO_2 appears. The reaction rate of the WGS reaction is, however, lower. As the CO yield at equilibrium which is depicted in Fig. 2.5 is close to zero, the gas composition is far from equilibrium and only approaches equilibrium for crude glycerin at C_{GE}'s exceeding 80%.

In the case of pure methanol, it was already shown that the CH_4 yield is very low, also in the presence of alkalis. Conversely, for both pure glycerol and crude glycerin, up to 0.6 mol CH_4/mol feed can be obtained as shown in Fig. 2.16. Consequently, and in line with results obtained from methanol reforming, it can be assumed that CH_4 is a primary gas product and not formed or only to a little extent by methanation. Further proof that CH_4 is a primary product is the dependency of the CH_4 yield on the C_{GE}. Already at low C_{GE}'s CH_4 is present, increasing linearly with C_{GE}. This trend is in contrast with the trend of a component such as CO_2, which only appears from C_{GE}'s exceeding 30%. CO_2 is probably not produced in a primary reforming reaction, but in a secondary reaction which is most probably the WGS reaction. The trend for C_3H_8 is similar as the trend for CO_2, although the yields are much lower. C_3H_8 is therefore considered as a secondary product.
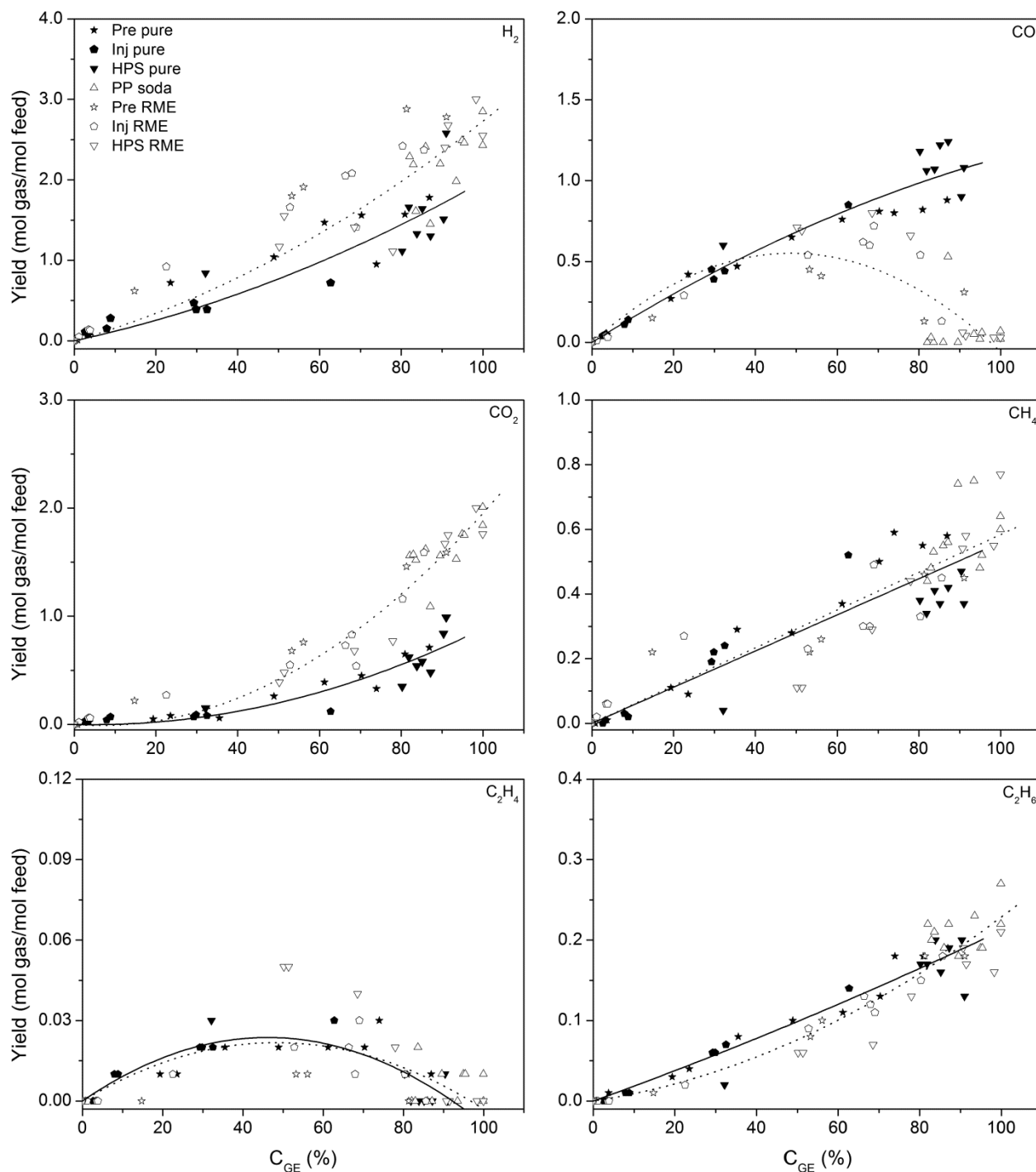
Fig. 2.16 Gas yields for pure glycerol and crude glycerin reforming as a function of the C_{GE} for different components. The solid symbols represent the data for pure glycerol and the open symbols for crude glycerin. Experimental conditions: T = 733 – 923 K, [feed] = 5 – 20 wt%, τ = 6 – 173 s. The solid lines and the dotted lines are trend lines for respectively pure glycerol and crude glycerin.

The trend for the C_2H_6 yield seems to be linear, however, it is not clear whether C_2H_6 is a primary gas product. It could be a primary gas phase product, the result of 'instant' hydrogenation of C_2H_4, or a combination of both. It is reasonable to assume that C_2H_4 is a primary gas product, because it is already present at low C_{GE} and like CH_4 it is known to be formed as a primary gas product in the steam reforming of acrolein and acetaldehyde [50].

Another important observation is that at complete conversion, two out of three carbon atoms originally present in the glycerol end up in either CO or CO_2. The total number of gas molecules produced per mol glycerol in the feed as a function of the C_{GE} can be calculated using the trend lines from Fig. 2.16. The maximum number of moles gas for pure glycerol is 4.8 mol gas/mol glycerol and 5.5 mol gas/mol glycerol for crude glycerin. A plausible explanation for this difference is the WGS reaction, promoted by the presence of alkali [4, 6, 35-37].

The quality of the syngas, if it were to be used in subsequent methanol synthesis, can be expressed with the stoichiometric number (S_N, see Eq. 1.4). Values for S_N close to 2 are preferred, but a S_N of 1.33 is the maximum value for gas obtained in RSCW of glycerol, see Eq. 7.2 in Chapter 7. By means of the trend lines based on the experimental data given in Fig. 2.16, the S_N can be calculated as a function of the C_{GE} and is depicted in Fig. 2.17.
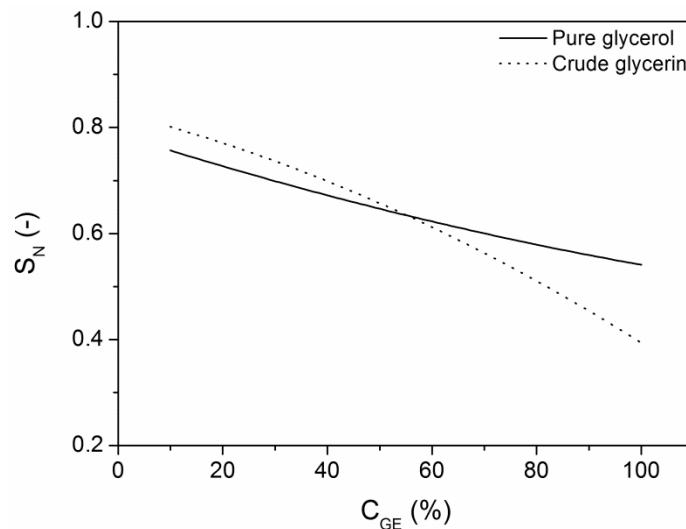
Fig. 2.17 S_N for pure glycerol and crude glycerin as a function of the C_{GE}.

For both types of glycerol the S_N decreases with increasing conversion and this effect is the most pronounced for crude glycerin. The more attractive S_N's for methanol synthesis are obtained at the lower C_{GE}'s although they remain below 1.

2.5 Discussion

2.5.1 Comparing methanol and glycerol reforming

A qualitative comparison of the RSCW of glycerol and methanol as a function of three process parameters is given in Table 2.4. Similar trends were observed for the dependency on temperature, feed concentration, and residence time for methanol and glycerol. Although the

experiments were not performed at exactly the same conditions, the C_{GE} for glycerol is higher than for methanol at similar conditions. This indicates that methanol appears to be more stable than glycerol at such conditions. The decreasing C_{GE} trend as a function of the feed concentration is less pronounced for methanol than for crude glycerin, while such a trend is not visible for pure glycerol. The decreasing trend for crude glycerin can most likely be attributed to salt precipitation in the reactor.

Table 2.4 Qualitative comparison of the influence of the increase of the process parameters on the C_{GE} of methanol and glycerol.

Process parameter	Methanol	Soda methanol	Glycerol	Crude glycerin
T (K)	++	++	++	++
[feed] (wt%)	+/- or -	-	+/-	-
τ (s)	++	++	++	++

++ = increase, + slight increase, +/- constant, -- = decrease, - slight decrease

Conditions for methanol reforming: $T = 823 - 915$ K, [feed] $= 3 - 20$ wt%, $\tau = 9 - 47$ s.

Conditions for glycerol reforming: $T = 733 - 923$ K, [feed] $= 5 - 20$ wt%, $\tau = 6 - 173$ s.

2.5.2 Mechanistic aspects for methanol reforming

Correlations for the gas yields versus the C_{GE} of methanol are shown in Fig. 2.10, irrespective of whether the higher value for C_{GE} is obtained by increasing the temperature, prolonging the residence time or by lowering the feed concentration. Apparently, the process severity which is a combination of temperature and residence time influences the gas yield significantly. To arrive at an overall reaction scheme for methanol decomposition the effluent water was analyzed by HPLC. Besides unconverted methanol only traces of formic acid and formaldehyde were identified. Probably these products are intermediate products in the decomposition of methanol, however, they are not very stable, considering their very low concentrations. Therefore, the reaction scheme of methanol decomposition and follow up gas phase reactions as depicted in Fig. 2.18 is proposed.

$$CH_3OH \longrightarrow CH_2O + H_2 \longrightarrow CO + 2H_2$$

$$\begin{array}{c} -H_2O \diagdown \nearrow +H_2O \\ CH_3OH + H_2O \longrightarrow CH_2O_2 + 2H_2 \longrightarrow CO_2 + 3H_2 \\ \diagdown \qquad \nearrow \\ CO + 2H_2 + H_2O \end{array}$$

Fig. 2.18 Decomposition pathways for methanol in SCW supposedly through formaldehyde and formic acid.

It is assumed that methanol either decomposes via formaldehyde or formic acid after the reaction with water. Formaldehyde and formic acid are known to decompose rapidly in supercritical water [11, 51]. For the decomposition of formic acid, two competing pathways

have been proposed [51]. The dominant reaction pathway is the decarboxylation of formic acid producing H_2 and CO_2, while the dehydration pathway producing H_2 and CO is reported to be the minor pathway. Subsequently, the WGS reaction can take place. The methanation reaction appears absent and no CH_4 is produced. This reaction scheme is an extension of Fig. 2.1 with the addition of hypothetical intermediate products.

In the present study the maximum CH_4 yield was 0.033 mol CH_4/mol feed as shown in Fig. 2.10. For these conditions (915 K, 25.5 MPa) and a feed concentration of 12.5 wt%, however, a CH_4 equilibrium yield close to 0.5 mol gas/mol feed is predicted by thermodynamic calculations shown in Fig. 2.4B. The experimental data are far from equilibrium. Low CH_4 yields were also observed in several other studies, showing that the WGS reaction is the only relevant gas phase reaction for these kind of systems [26-28, 42]. The CO yield at C_{GE}'s around 50% for pure methanol is higher than predicted by equilibrium calculations indicating that the WGS reaction is not at equilibrium for these C_{GE}'s. At higher C_{GE}'s the CO yield decreases, approaching equilibrium. The WGS reaction appears to be relatively slow. This was confirmed by separate WGS reaction experiments (see Section 2.4.2) and by literature data as well. Several researchers noted that the rate of the WGS reaction depends on the concentration of CO and that the reaction is enhanced at water concentrations exceeding 10 mol/L [52, 53]. In the experiments done in this study, the CO concentration in the supercritical mixture was very low and the water concentration remained far below 10 mol/L. The water concentration is 6.0 mol/L at 723 K and 25.0 MPa and 3.6 mol/L at 923 K and 25.0 MPa.

The value for C_{GE} as a function of the residence time can be used to calculate the reaction rate constant, assuming a first order decomposition reaction in methanol and plug flow behavior of the liquid phase. The kinetic rate constants are plotted in an Arrhenius diagram in Fig. 2.19 for the experiments with pure methanol and soda methanol. As expected on basis of the lower conversions, the kinetic rate constants for soda methanol are lower than for pure methanol, but strikingly the observed activation energy is lower as well. Activation energies of 191 kJ/mol and 144 kJ/mol are calculated for pure methanol and soda methanol, respectively. The value of the activation energy for pure methanol is slightly higher than the 164 kJ/mol reported by Hack *et al*. [54].

The activation energy for reforming soda methanol is lower than for pure methanol although the C_{GE} at similar conditions is lower. This phenomenon can be explained by assuming a different decomposition mechanism for pure methanol versus soda methanol which will be discussed later, or by an inhibiting effect of soda salt. In the literature is reported that the decrease in gas yield after addition of alkali salts (KOH or K_2CO_3) can be caused by precipitation of the salts on the reactor wall [18]. It is unclear though, whether the activity loss can be attributed to passivation of the active reactor wall. Another hypothesis deals with competing reaction pathways. The competing pathways for pure methanol and soda methanol decomposition are shown in Fig. 2.18 and can be direct decomposition to H_2 and CO or the reaction of methanol with water to produce H_2 and CO_2. Possibly the direct decomposition for pure methanol dominates. For soda methanol, the reaction with water may prevail, while the

decomposition route to H_2 and CO is inhibited. This also explains why the C_{GE} for soda methanol decreases more significantly with increasing feed concentration and thus decreasing water concentration as shown in Fig. 2.7.
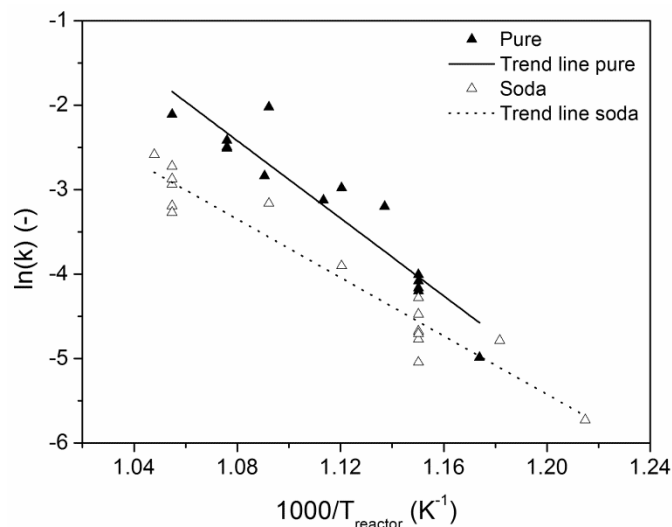
Fig. 2.19 Arrhenius diagram for methanol reforming.

The two different reaction pathways are summarized in the energy diagram depicted in Fig. 2.20. Starting with the heat of formation (at standard conditions) of methanol as the baseline, the reaction proceeds via possible intermediate products. The heat of formation of the end-products is presented relative to methanol (and water). If the competing reaction pathway mechanism is correct, the observed activation energy for decomposition of pure methanol into H_2 and CO is lower than the observed activation energy for the decomposition reaction with water. For soda methanol, it should be the other way around. Decomposition of pure methanol proceeds predominantly to CO at lower temperatures and to CO_2 (plus additional H_2) at higher temperatures [11], indicating that the reaction of methanol with water is enhanced at higher temperatures, or the rate of the WGS reaction increases at higher temperatures, or both phenomena occur.
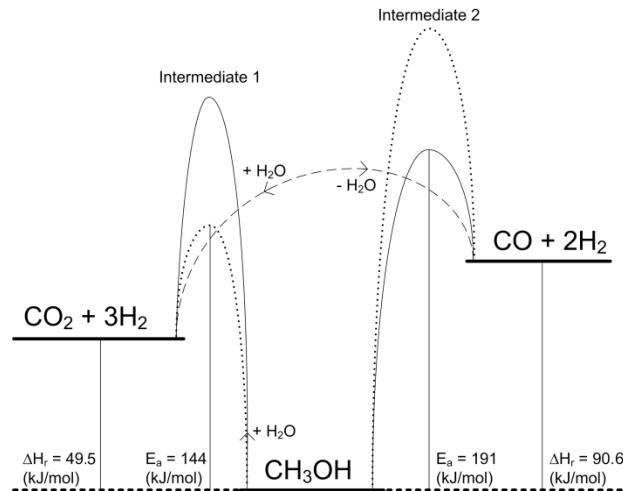
Fig. 2.20 Reaction energy diagram for methanol reforming. The solid lines are possible reaction pathways for pure methanol. The dotted line represents possible reaction pathways for methanol containing Na_2CO_3. The dashed line represents the WGS reaction for both methanol types. Reaction enthalpies are determined at 0.1 MPa and 298 K.

2.5.3   Mechanistic aspects for glycerol reforming

Just as for methanol, unique correlations for the gas yields versus the C_{GE}, irrespective of the process conditions and feed concentration are obtained for glycerol and shown in Fig. 2.16. These correlations hold for experiments carried out in the bench scale setup in one of the three operating modes and the experiments performed in the much larger pilot plant. It is thus reasonable to conclude that glycerol decomposition proceeds more or less through the same mechanism for the process conditions investigated. A simplified reaction scheme without stoichiometry for the decomposition of glycerol with a focus on gas production is given in Fig. 2.21. The choice of primary and secondary products is based on the analysis in Section 2.4.4. In this scheme, CH_4 is shown as a primary product, but can also be formed as a secondary product by methanation. However, this reaction was not observed or only to a small extent for glycerol. Furthermore, water is produced and the WGS reaction and alkene hydrogenation are included.

It is suggested that glycerol can either decompose into liquid soluble products that react further to gas products or that glycerol can directly decompose into gas products. In practice probably both reaction pathways occur. From Fig. 2.15 it is concluded that the decomposition of pure glycerol proceeds roughly through the dehydration of 1 mol H_2O/mol feed. For crude glycerin at a C_{GE} of 100% the water consumption is 1 mol H_2O/mol feed. From Fig. 2.16 it is clear that at this C_{GE} 2 mol of CO_2 are produced from crude glycerin, which initially originate from CO. That means that in the WGS reaction 2 mol of H_2O is consumed, indicating that the primary decomposition of crude glycerin proceeds, as for pure glycerol, through the dehydration of 1 mol H_2O/mol feed.
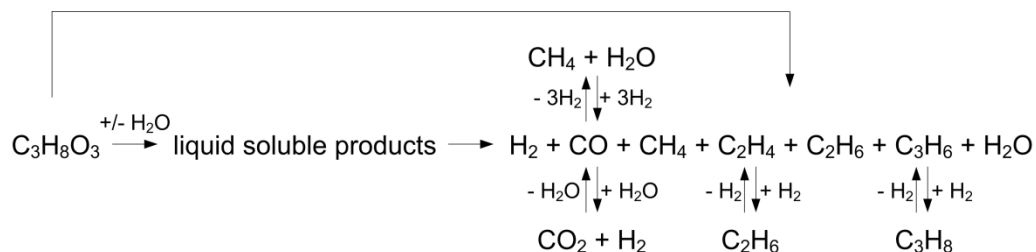
Fig. 2.21 Decomposition pathways for glycerol in SCW to gaseous products including possible follow-up reactions.

The results for glycerol are plotted in an Arrhenius diagram in Fig. 2.22 assuming pseudo first-order kinetics in glycerol. The observed activation energies for pure glycerol and crude glycerin were E_a = 196 kJ/mol and 183 kJ/mol respectively, which is somewhat higher than the literature values for pure glycerol of E_a = 150 kJ/mol [17] and 110 kJ/mol [45]. For glycerol the presence of alkali reduces the activation energy slightly.
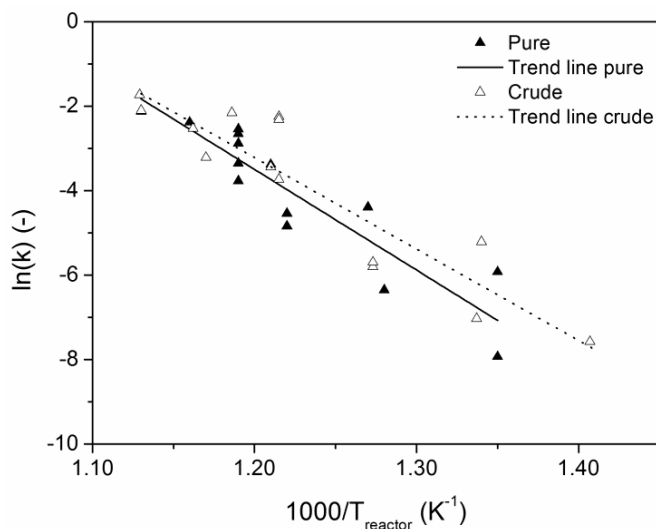
Fig. 2.22 Arrhenius diagram for pure glycerol and crude glycerin reforming. The experiments were conducted in premixing and injection mode.

2.6 Conclusion

Methanol (pure and with soda) and glycerol (pure and crude) were reformed in supercritical water. Glycerol reforming was carried out in two different continuous setups made of Incoloy 825 and methanol reforming was carried out in one setup. The influence of the process conditions, feed concentration, and alkali on the conversion and gas yields was investigated. For both, methanol and glycerol, clear trends in gas yields are observed as a function of the C_{GE}.

2.6.1 Methanol reforming

The C_{GE} for methanol increases with temperature and residence time, while increasing feed concentration has an adverse effect on the C_{GE}. The latter effect is more pronounced for soda methanol than pure methanol. The presence of alkali in the feed decreases the C_{GE} of methanol. The activation energy for pure methanol turns out to be higher than for soda methanol which can be an indication of different decomposition pathways. Primary methanol decomposition may proceed through two reaction pathways, either by reacting with water yielding CO_2 and H_2, or by direct decomposition to CO and H_2. The primary reaction mechanism can be affected by the presence of Na^+. The main gas products in methanol reforming are H_2, CO, and CO_2. The yield of CH_4 is very low indicating that the methanation reaction hardly proceeds.

2.6.2 Glycerol reforming

The C_{GE} for pure glycerol and crude glycerin increases with temperature and residence time, while the C_{GE} for pure glycerol is nearly independent of concentration and the C_{GE} for crude glycerin decreases at higher concentration. The main gas products in glycerol reforming are H_2, CO, CO_2, CH_4, and C_2H_6 with smaller quantities of C_2H_4, C_3H_6, and C_3H_8. From these gas products; H_2, CO, CH_4, C_2H_4, and C_3H_6 are the primary gas products. CO_2 and C_3H_8 are formed due to secondary gas phase reactions, while it remains unclear whether C_2H_6 is a primary or a secondary gas product. The carbon present in the glycerol ends up in carbon oxides and hydrocarbons with a ratio of carbon in CO_x : carbon in C_yH_z of roughly 2. The ratios of $CO:CO_2:H_2$ can be steered by the operating conditions. The overall mechanism of glycerol decomposition seems to proceed through the dehydration of 1 mol H_2O/mol glycerol and is independent of the presence of Na^+ in the glycerol. Thus, the reaction pathway is not a function of the presence of alkali metals in the feed.

2.7 References

1   M. Modell, Gasification and liquefaction of forest products in supercritical water, in: R.P. Overend (Ed.) Fundamentals of thermochemical biomass conversion Elsevier, London, (1985).

2   P. Basu, V. Mettanant, Biomass gasification in supercritical water - A review, Int. J. Chem. Reactor Eng., 7 (2009) 1-61.

3   G. Brunner, Near critical and supercritical water. Part I. Hydrolytic and hydrothermal processes, J. Supercrit. Fluids, 47 (2009) 373-381.

4   D.C. Elliot, Catalytic hydrothermal gasification of biomass, Biofuels, Bioprod. Biorefin., 2 (2008) 254-265.

5   Y. Guo, S.Z. Whang, D.H. Xu, Y.M. Gong, H.H. Ma, X.Y. Tang, Review of catalytic supercritical water gasification for hydrogen production from biomass, Renewable Sustainable Energy Rev., 14 (2010) 334-343.

6   A. Kruse, Supercritical water gasification, Biofuels, Bioprod. Biorefin., 2 (2008) 415-437.

7   A. Kruse, Hydrothermal biomass gasification, J. Supercrit. Fluids, 47 (2009) 391-399.

8   A. Kruse, E. Dinjus, Hot compressed water as reaction medium and reactant. 2. Degradataion reactions, J. Supercrit. Fluids, 41 (2007) 361-379.

9   Y. Matsumura, T. Minowa, B. Potic, S.R.A. Kersten, W. Prins, W.P.M. van Swaaij, B. van de Beld, D.C. Elliot, G.G. Neuenschwander, A. Kruse, M.J. Antal Jr., Biomass gasification in near- and supercritical water: Status and prospects, Biomass Bioenergy, 29 (2005) 269-292.

10   G. van Rossum, B. Potic, S.R.A. Kersten, W.P.M. van Swaaij, Catalytic gasification of dry and wet biomass, Catal. Today, 145 (2009) 10-18.

11   M. Watanabe, T. Sato, H. Inomata, R.L. Smith_Jr, K. Arai, A. Kruse, E. Dinjus, Chemical reactions of C_1 compounds in near-critical and supercritical water, Chem. Rev., 104 (2004) 5803-5821.

12   J.G. van Bennekom, J. Vos, R.H. Venderbosch, M.A.P. Torres, V.A. Kirilov, H.J. Heeres, Z. Knez, M. Bork, J.M.L. Penninger, Supermethanol: Reforming of crude glycerine in supercritical water to produce methanol for re-use in biodiesel plants, in: 17th European Biomass Conference and Exhibition, Hamburg, (2009) 899-902.

13   K. Klier, V. Chatikavanij, R.G. Herman, G.W. Simmons, Catalytic synthesis of methanol from CO/H_2. IV. The effects of carbon dioxide J. Catal., 74 (1982) 343-360.

14   F.J. Armellini, J.W. Tester, Solubility of sodium chloride and sulfate in sub- and supercritical water vapor from 450-550°C and 100-250 bar, Fluid Phase Equilib., 84 (1993) 123-142.

15   A.J. Byrd, K.K. Pant, R.B. Gupta, Hydrogen production from glycerol by reforming in supercritical water over Ru/Al_2O_3 catalyst, Fuel, 87 (2008) 2956-2960.

16   X. Xu, Y. Matsumura, J. Stenberg, M.J. Antal Jr., Carbon-catalyzed gasification of organic feedstocks in supercritical water, Ind. Eng. Chem. Res., 35 (1996) 2522-2530.

17   W. Bühler, E. Dinjus, H.J. Ederer, A. Kruse, C. Mas, Ionic reactions and pyrolysis of glycerol as competing reaction pathways in near- and supercritical water, J. Supercrit. Fluids, 22 (2002) 37-53.

18   J.B. Gadhe, R.B. Gupta, Hydrogen production by methanol reforming in supercritical water: Suppression of methane formation, Ind. Eng. Chem. Res., 44 (2005) 4577-4584.

19   S.R.A. Kersten, B. Potic, W. Prins, W.P.M. van Swaaij, Gasification of model compounds and wood in hot compressed water, Ind. Eng. Chem. Res., 45 (2006) 4169-4177.

20   Y.J. Lu, L.J. Guo, C.M. Ji, X.M. Zhang, X.H. Hao, Q.H. Yan, Hydrogen production by biomass gasification in supercritical water: A parametric study, Int. J. Hydrogen Energy, 31 (2006) 822-831.

21   F.L.P. Resende, S.A. Fraley, M.J. Berger, P.E. Savage, Noncatalytic gasification of lignin in supercritical water, Energy Fuels, 22 (2008) 1328-1334.

22   D. Yu, M. Aihara, M.J. Antal Jr., Hydrogen production by steam reforming glucose in supercritical water, Energy Fuels, 7 (1993) 574-577.

23   M.J. Antal Jr., S.G. Allen, D. Schulman, X. Xu, R.J. Divilio, Biomass gasification in supercritical water, Ind. Eng. Chem. Res., 39 (2000) 4040-4053.

24   A.J. Byrd, K.K. Pant, R.B. Gupta, Hydrogen production from glucose using Ru/Al_2O_3 catalysts in supercritical water, Ind. Eng. Chem. Res., 46 (2007) 3574-3579.

25   A. Kruse, M. Faquir, Hydrothermal biomass gasification - effects of salts backmixing and their interaction, Chem. Eng. Technol., 30 (2007) 749-754.

26   N. Boukis, V. Diem, U. Galla, E. Dinjus, Methanol reforming in supercritical water for hydrogen production, Combust. Sci. Technol., 178 (2006) 467-485.

27   N. Boukis, V. Diem, W. Habicht, E. Dinjus, Methanol reforming in supercritical water, Ind. Eng. Chem. Res., 42 (2003) 728-735.

28   J.D. Taylor, C.M. Herdman, B.C. Wu, K. Wally, S.F. Rice, Hydrogen production in a compact supercritical water reformer, Int. J. Hydrogen Energy, 28 (2003) 1171-1178.

29   F.A.P. Voll, C.C.R.S. Rossi, C. Silva, R. Guirardello, R.O.M.A. Souza, V.F. Cabral, L. Cardozo-Filho, Thermodynamic analysis of supercritical water gasification of methanol, ethanol, glycerol, glucose and cellulose, Int. J. Hydrogen Energy, (2009).

30   I. Lee, M. Kim, S. Ihm, Gasification of glucose in supercritical water, Ind. Eng. Chem. Res., 41 (2002) 1182-1188.

31   T. Sato, M. Osada, M. Watanabe, M. Shirai, K. Arai, Gasification of alkylphenols with supported noble metal catalysts in supercritical water, Ind. Eng. Chem. Res., 42 (2003) 4277-4282.

32   H. Schmieder, J. Abeln, N. Boukis, E. Dinjus, A. Kruse, M. Kluth, G. Petrich, E. Sadri, M. Schacht, Hydrothermal gasification of biomass and organic wastes, J. Supercrit. Fluids, 17 (2000) 145-153.

33   P. D'Jesus, N. Boukis, B. Kraushaar-Czarnetzki, E. Dinjus, Influence of process variables on gasification of corn silage in supercritical water, Ind. Eng. Chem. Res., 45 (2006) 1622-1630.

34   X.H. Hao, L.J. Guo, X. Mao, X.M. Zhang, X.J. Chen, Hydrogen production from glucose used as a model compound of biomass gasified in supercritical water, Int. J. Hydrogen Energy, 28 (2003) 55-64.

35   A. Kruse, E. Dinjus, Influence of salts during hydrothermal biomass gasification: The role of the catalysed water–gas shift reaction, Z. Phys. Chem., 219 (2005) 341-366.

36   J. Yanik, S. Ebale, A. Kruse, M. Saglam, M. Yüksel, Biomass gasification in supercritical water: II. Effect of catalyst, Int. J. Hydrogen Energy, 33 (2008) 4520-4526.

37   J.M.L. Penninger, M. Rep, Reforming of aqueous wood pyrolysis condensate in supercritical water, Int. J. Hydrogen Energy, 31 (2006) 1597-1606.

38   D. Xu, S. Wang, X. Hu, C. Chen, Q. Zhang, Catalytic gasification of glycine and glycerol in supercritical water, Int. J. Hydrogen Energy, 34 (2009) 5357-5364.

39   M. Schubert, J.W. Regler, F. Vogel, Continuous salt precipitation and separation from supercritical water. Part 2: Type 2 salts and mixtures of two salts, J. Supercrit. Fluids, 52 (2010) 113-124.

40   M. Schubert, J.W. Regler, F. Vogel, Continuous salt precipitation and separation from supercritical water. Part 1: Type 1 salts, J. Supercrit. Fluids, 52 (2010) 99-112.

41   J.D. Taylor, C.M. Herdman, B.C. Wu, K. Wally, S.F. Rice, Hydrogen production in a compact supercritical water reformer, International J. Hydrogen Energy, 28 (2003) 1171-1178.

42   G.J. DiLeo, P.E. Savage, Catalysis during methanol gasification in supercritical water, J. Supercrit. Fluids, 39 (2006) 228-232.

43   M.J. Antal Jr., W.S.I. Mok, J.C. Roy, A. T-Raissi, Pyrolitic sources of hydrocarbons from biomass, J. Anal. Appl. Pyrolysis, 8 (1985) 291-303.

44   A. May, J. Salvedo, C. Torras, D. Montane, Catalytic gasification of glycerol in supercritical water, Chem. Eng. J., (2010) 751-759.

45   A.G. Chakinala, D.W.F. Brilman, W.P.M. van Swaaij, S.R.A. Kersten, Catalytic and non-catalytic supercritical water gasification of microalgae and glycerol, Ind. Eng. Chem. Res., 49 (2010) 1113-1122.

46   M.V. Twigg, Catalyst Handbook, second edition ed., Wolfe Publishing Ltd., (1989).

47   G. Soave, Equilibrium constants from a modified Redlich-Kwong equation of state, Chem. Eng. Sci., 27 (1972) 1197-1203.

48   R.C. Reid, J.M. Prausnitz, B.E. Poling, The properties of gases and liquids, Fourth Edition ed., McGraw-Hill, Inc., New york, (1987).

49   E. Gasafi, L. Meyer, L. Schebek, Using life-cycle assessment in process design: Supercritical water gasification of organic feedstocks J. Ind. Ecol., 7 (2003) 75-91.

50   Y.S. Stein, M.J. Antal Jr., A study of the gas-phase pyrolysis of glycerol, J. Anal. Appl. Pyrolysis, 4 (1983) 283-296.

51   Y. Zhang, J. Zhang, L. Zhao, C. Sheng, Decomposition of formic acid in supercritical water, Energy Fuels, 24 (2010) 95-99.

52   H.R. Holgate, P.A. Webley, J.W. Tester, R.K. Helling, Carbon monoxide oxidation in supercritical water: The effects of heat transfer and the water-gas shift reaction on observed kinetics., Energy Fuels, 6 (1992) 586-597.

53   S.F. Rice, R.R. Steeper, J.D. Aiken, Water density effects on homogeneous water-gas shift reaction kinetics, J. Phys. Chem. A, 102 (1998) 2673-2678.

54   W. Hack, D.A. Masten, S.J. Buelow, Methanol and ethanol decomposition in supercritical water, Z. Phys. Chem., 219 (2005) 367-378.

3   Explorative catalyst screening studies on reforming of glycerol in supercritical water

Abstract

An explorative screening study for glycerol reforming in supercritical water with $Pt/CeZrO_2$, Ni/ZrO_2, $Ni/CaO-6Al_2O_3$, $NiCu/CeZrO_2$, and a CuZn alloy was carried out to investigate the influence of different catalysts on the carbon-to-gas efficiency and gas composition. Experiments were conducted at 25.5 − 27.0 MPa in a continuous setup, with temperatures ranging from 648 to 973 K, a feed concentration of 10 wt%, and a residence time of 8 to 87 s. The catalysts promoted the decomposition of glycerol significantly. At 947 K the conversion of glycerol without catalyst was approximately 40%, while in the presence of catalysts (almost) complete conversion was obtained. All catalysts promoted the water-gas shift reaction, while the ones based on Ni also promoted methanation. Visual coke formation was significant for Ni/ZrO_2 and $Pt/CeZrO_2$, which might be responsible for the observed reduction in activity at longer runtimes for these two catalysts. The specific surface area of all catalysts, except for CuZn, decreased after contact with water at supercritical conditions. Except for $NiCu/CeZrO_2$, XRD analysis indicated only minor changes in crystal structure of the supports, confirming the stability and suitability of these supports in supercritical water.

3.1 Introduction

Biomass is an attractive renewable feedstock for the production of energy and chemicals. For relatively dry feeds, technologies such as pyrolysis, gasification, or combustion, may be used to produce liquid fuels, fuel gas/syngas, or heat/electricity. For wet biomass streams, hydrothermal conversion processes are promising process routes as energy intensive drying steps can be avoided. Hydrothermal processes can be divided in those producing solids (hydrothermal carbonization), liquids (hydrothermal liquefaction), or gases (hydrothermal gasification). An extensive overview on these processes is presented elsewhere [1-6]. Hydrothermal gasification can be carried out at sub- and supercritical water conditions. The latter process is also referred to as reforming in supercritical water (RSCW).

In the RSCW of biomass, the product gas can be steered towards a gas rich in H_2 and CO_2, CH_4 and CO_2, or a mixture of H_2, CO and CO_2 (syngas) [7-10]. The exact composition of the product gas is a strong function of process conditions and biomass feed. RSCW has some distinct advantages over other gasification processes, such as higher energy efficiencies for wet biomass and improved product gas qualities [3, 11, 12]. Furthermore, a gas at high pressure is produced which is advantageous for use in downstream synthesis processes [13].

Aqueous glycerol is a very promising feedstock for RSCW, as it decomposes rapidly in supercritical water (SCW) and coke formation is negligible in the absence of catalysts [7, 14]. On the contrary, coke formation was observed in the presence of catalysts [8]. The RSCW of glycerol is briefly reviewed Chapter 2. The conversion of glycerol and the gas composition strongly depend on the process conditions, feed concentration, reactor material, and the presence of any type of catalyst. In Table 3.1 the gas compositions are summarized for noncatalytic and catalytic glycerol reforming experiments. In all cases, the gas comprises H_2, CO_2, and CH_4, but the concentrations differ substantially. The concentration of the different components in the product gas varies over a broad range, viz. CO_2 (6 − 44 vol%), H_2 (0 − 67 vol%), CO (0 − 51 vol%) and CH_4 (4 − 58 vol%). It is known that the reactor wall has catalytic activity and promotes glycerol decomposition, the water-gas shift reaction (WGS), and methanation. The activity for these reactions depends on the reactor material used [15-18]. In experiments using inert quartz capillaries, the conversion of glycerol increased from below 65% to above 85% by the addition of Inconel powder, a common reactor material for this type of processes [17].

Table 3.1 Overview of literature data on RSCW of glycerol.

Cat.	Reactor material		Feed (wt%)	T (K)	P (MPa)	τ (s)	H_2 (vol%)	CO	CO_2	CH_4	C_xH_y	Ref.
-	Incoloy 825	Cont.	5-20	743-923	25.0	6-45	26-51	20-37	6-22	6-23	3-7	[7]
-	Inconel	Cont.	10	873	30.0	?	28	7	37	16	12	[19]
-	Hasteloy 276	Cont.	1	653-773	25.0	65-300	48-64	0-1	27-44	4-8	0-4	[20]
-	Inconel 625	Cont.	18	873	34.5	44	52	2	31	14	1	[21]
-	Inconel 600	Cont.	10	823-923	25.0	3-7	50-54	30-32	9-13	2-6	0-3	[14]
-	Quartz	Batch	19	823-973	30.0	60	14-33	30-51	8-15	14-22	6-9[a]	[17]
Na_2CO_3	Incoloy 825	Cont.	5-17	853-893	25.0	50-173	37-50	0-14	28-40	9-16	3-7	[7]
K_2CO_3	Inconel 600	Cont.	10	873	25.0	5	55	1	30	5	9	[14]
Inc. 625	Quartz	Batch	5	873	30.0	60	25-38	34-40	13-14	10-11	4-11[b]	[17]
C	Inconel 625	Cont.	18	873	34.5	44	54	2	29	13	1	[21]
Ru/TiO_2	Inconel	Cont.	10	873	30.0	?	40	1	37	22	0	[19]
Ru/Al_2O_3	Inconel 600	Cont.	2.5-40	973-1073	24.1	1-4	42-67	0-5	25-35	3-19	0	[8]
Ru/C	Steel 316L	Cont.	20	673	30.0	?	0-2	0	40-42	56-58	0	[9]

[a]In this publication only H_2, CO, CO_2, and CH_4 are mentioned. These components add up to values between 91 and 96%. It is assumed that the remaining part is composed of higher hydrocarbons.

[b]Data is taken for Inconel powder loadings of approximately 2 – 6 g Inconel/g solution.

The number of publications on the catalytic RSCW of glycerol is rather limited, but both homogeneous (alkali salts) and heterogeneous catalysts were investigated, the latter mainly focusing on Ru as active metal. Alkali salts promote the WGS reaction and enhance the H_2 yield [16, 17, 22, 23]. The use of heterogeneous catalysts promotes the WGS reaction in most cases, whereas supported Ru catalysts promote methanation as well [9, 24]. In Chapter 2, it is shown that the product gas composition is very well correlated with the conversion. The relations between the gas yields and the conversion are combined and shown in Fig. 3.1 for respectively pure glycerol (A) and crude glycerin (B). H_2, CO, and CH_4 have been shown to be primary gas phase products in glycerol decomposition, while CO_2 is formed in a secondary follow-up reaction. Methanation hardly proceeds at the conditions investigated [5, 7].

One of the attractive outlets for high pressure product gas from RSCW processes is syngas for the production of methanol (see Chapter 1). A syngas with a stoichiometric number (S_N) of 2 is preferred, with the S_N defined as [25]:

$$S_N = \frac{(H_2 - CO_2)}{(CO + CO_2)}$$

(Eq. 1.4)
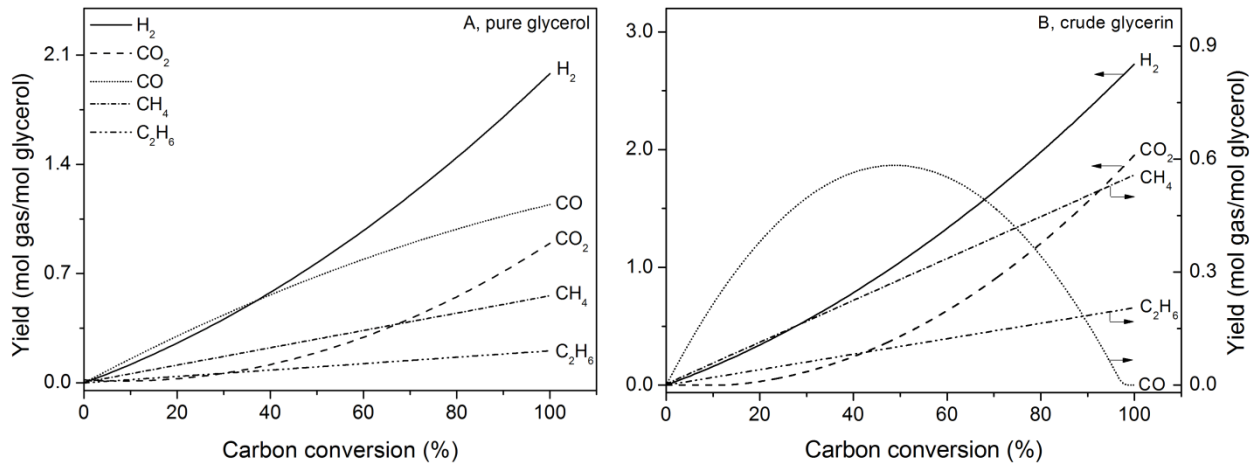
Fig. 3.1 Relations between the conversion and the gas yield for pure glycerol (A) and crude glycerin (B).

The highest theoretical S_N that can be obtained in glycerol reforming is 1.33. This is the case when glycerol is completely converted to H_2, CO, and CO_2 without any CH_4 and/or higher hydrocarbons. The WGS reaction does not influence the S_N, as for every disappearing CO molecule a H_2 and a CO_2 molecule are formed (see Eq. 3.1).

$$C_3H_8O_3 \quad \begin{array}{c} \nearrow \quad 3\ CO + 4\ H_2 \\ \\ \searrow \quad 3\ CO_2 + 7\ H_2 \end{array}$$

(Eq. 3.1)

The syngas composition from glycerol RSCW without catalysts or with alkali catalysts is not ideal for methanol synthesis as the yield of H_2 is low compared to the yield of carbon oxides resulting in an S_N smaller than 1. The gas composition needs to be improved to obtain a higher S_N, which can possibly be accomplished by using heterogeneous catalysts in the RSCW of glycerol.

Catalyst selection is based on the literature on RSCW of various feedstocks. The selected catalysts are: Pt/CeZrO$_2$, Ni/ZrO$_2$, Ni/CaO-6Al$_2$O$_3$, NiCu/CeZrO$_2$, and a CuZn alloy. Ni is known to promote C-C scission, methanation, and to a smaller extent the WGS reaction [10, 24, 26]. Cu can be used to reduce the methanation activity of Ni. When an Inconel 600 reactor (an alloy of Ni, Cr, and Fe) was replaced by a reactor made of a Cu-Ni alloy, CH_4 production rates decreased significantly when methanol was used as a feedstock [16]. Pt is selected based on studies on C_2H_6 hydrogenolysis, where it was shown to have low activities for both the methanation and the WGS reaction [27]. Catalysts based on CuZnO are well known for methanol synthesis and methanol steam reforming and as such are expected to be active for glycerol reforming as well [28]. Metal alloys are more simple to prepare and cheaper. Therefore, a CuZn alloy is tested as well. As a support for these catalysts, α-Al$_2$O$_3$ modified with CaO and (Ce modified) ZrO$_2$ are selected as ZrO$_2$ and α-Al$_2$O$_3$ are reported to be relatively stable supports in SCW [18, 24, 26].

In this chapter, screening studies of catalytic glycerol RSCW are presented, to investigate whether a syngas with an improved composition for methanol synthesis can be produced. This research study is explorative in nature and involves the investigation of the effect of catalysts on (i) the carbon conversion and (ii) the composition of the product gas over a broad range of reactor temperatures.

3.2 Experimental section

3.2.1 Catalyst preparation

Pt/CeZrO$_2$ (1.83 wt% Pt, Ce$_{0.08}$Zr$_{0.92}$O$_2$)

A CeZrO$_2$ support was prepared by co-precipitation of an aqueous solution of Ce(NO$_3$)$_3$·6H$_2$O and ZrO(NO$_3$)$_2$·2H$_2$O. The pH was increased from 2.7 to 8 by the addition of NH$_4$OH (2.2 mol/L, 10 mL/min). The precipitate obtained was aged at 353 K for 6 h, filtered and dried for 5 h at 383 K. The solid was calcined in an electric furnace at 993 K for 5 h in air atmosphere. After calcination, the product was finely dispersed and was then pressed into tablets, crushed, and sieved to achieve the desired particles size (0.5 − 1 mm). The support was impregnated with an aqueous H$_2$PtCl$_6$ solution by incipient wetness impregnation. The catalyst precursor was dried for 5 h at 383 K and calcined for 2 h at 973 K.

Ni/ZrO$_2$ (15 wt% Ni)

A ZrO$_2$ support was prepared by thermal decomposition of ZrO(NO$_3$)$_2$·2H$_2$O powder at 973 K for 12 h. The finely dispersed ZrO$_2$ obtained was pressed into tablets, crushed, and sieved. A sieve fraction of 0.5 − 1 mm was collected. The catalyst was prepared using incipient wetness impregnation with an aqueous solution of Ni(NO$_3$)$_2$·6H$_2$O. The resulting solid was dried at 383 K for 5 h and calcined at 973 K for 2 h.

Ni/CaO-6Al$_2$O$_3$ (10.5 wt% Ni)

A CaO-6Al$_2$O$_3$ support was prepared by precipitation of an aqueous solution of Al(NO$_3$)$_3$·9H$_2$O and addition of CaCO$_3$ after drying. The pH was increased from 2.2 to 8 by drop wise addition of NH$_4$OH (2.2 mol/L, 10 mL/min). The precipitate obtained was filtered, dried for 5 h at 383 K, and subsequently blended with CaCO$_3$ powder. Calcination was performed in an electric furnace for 10 h at 1173 K in air. The powder was finely dispersed and subsequently pressed into tablets, crushed, and sieved to achieve the desired particle size distribution (0.5 − 1 mm). The CaO-6Al$_2$O$_3$ support was impregnated with an aqueous solution of Ni(NO$_3$)$_2$·6H$_2$O by incipient wetness impregnation. The catalyst precursor was dried for 5 h at 383 K and calcined for 2 h at 973 K.

NiCu/CeZrO$_2$ (25.5 wt% Ni, 8.5 wt% Cu, Ce$_{0.46}$Zr$_{0.54}$O$_2$)

The catalyst was prepared by co-precipitation of the metal salts (Ce(NO$_3$)$_3$·6H$_2$O, ZrO(NO$_3$)$_2$·2H$_2$O, Ni(NO$_3$)$_2$ ·6H$_2$O, and Cu(NO$_3$)$_2$ ·3H$_2$O). A detailed preparation procedure can be found in the literature [29].

CuZn alloy (80% Cu, 20% Zn)

The representative alloys with a size of 5 x 5 mm and thickness of 1 mm were annealed at 823 K for 2 h and chemically treated to increase the surface area and to create a film of CuO and ZnO. This was done by treatment of the alloys with an aqueous solution containing 15 wt% NH$_4$Cl in contact with air. During this treatment, etching of the copper surface occurred, and the solution turned blue. Finally, the chips were washed with distilled water and dried in an oven at 383 K.

3.2.2 Catalyst characterization

The BET specific surface area of the catalysts was determined using nitrogen adsorption measurements at 77 K. The data were obtained using an automatic volumetric device (ASAP 2400). XRD measurements were carried out with a Siemens D-500 diffractometer (CuK$_\alpha$ radiation; graphite monochromator). The scanning range was $15 - 85°$ (2θ) with a scanning step size of 0.05° (2θ).

3.2.3 Setup

Glycerol (purity > 99%) was supplied by Chemproha, The Netherlands. The RSCW of glycerol was investigated in the bench scale setup with a capacity of approximately 1 L aqueous feed/h. The system was constructed from Incoloy 825 and further details are provided in Chapter 2. The reactor configuration used in this chapter is depicted schematically in Fig. 3.2.

A premixed feed was introduced into the system through a high pressure pump. The reactor consisted of three insulated electrically heated reactor tubes in series. In all experiments, the first reactor tube was used as a feed pre-heater and did not contain catalyst. The other two reactors were partially filled with catalyst (see Table 3.2 for exact amounts).

Table 3.2 Catalyst intakes.

Catalyst	Quantity in R2[a]	Quantity in R3[b]
	(g)	(g)
Pt/CeZrO$_2$	15.7	15.9
Ni/ZrO$_2$	5.0	5.0
Ni/CaO-6Al$_2$O$_3$	8.2	8.2
NiCu/CeZrO$_2$	8.9	9.1
CuZn	7.7	7.7

[a]R2 = reactor 2, [b]R3 = reactor 3

The reactor effluent was cooled in a double-walled cooler using tap water. The product gas was separated from the liquid phase in a high pressure separator (HPS) before depressurization,

quantification (Gallus 2000 G1.6 gas meter), and analysis. The water phase in the HPS was subsequently depressurized and sent to a low pressure separator (LPS). Gases released from the water phase in the LPS were quantified with a similar gas meter and analyzed. The total gas yield was taken as the sum of gas flows from the HPS and the LPS. Setup control and data logging were conducted by a computer equipped with the Adamview software package. For the experiments, the reactor temperature was varied from 648 K – 973 K, resulting in (approximated) residence times of 8 – 87 s, with the shortest residence time at the highest temperature. The weight hourly space velocity (WHSV) was between 3.0 and 9.7 g glycerol/g cat./h (from here on the unit h^{-1} is used). The feed concentration was kept constant at 10 wt%. The pressure was maintained between 25.5 and 27.0 MPa.
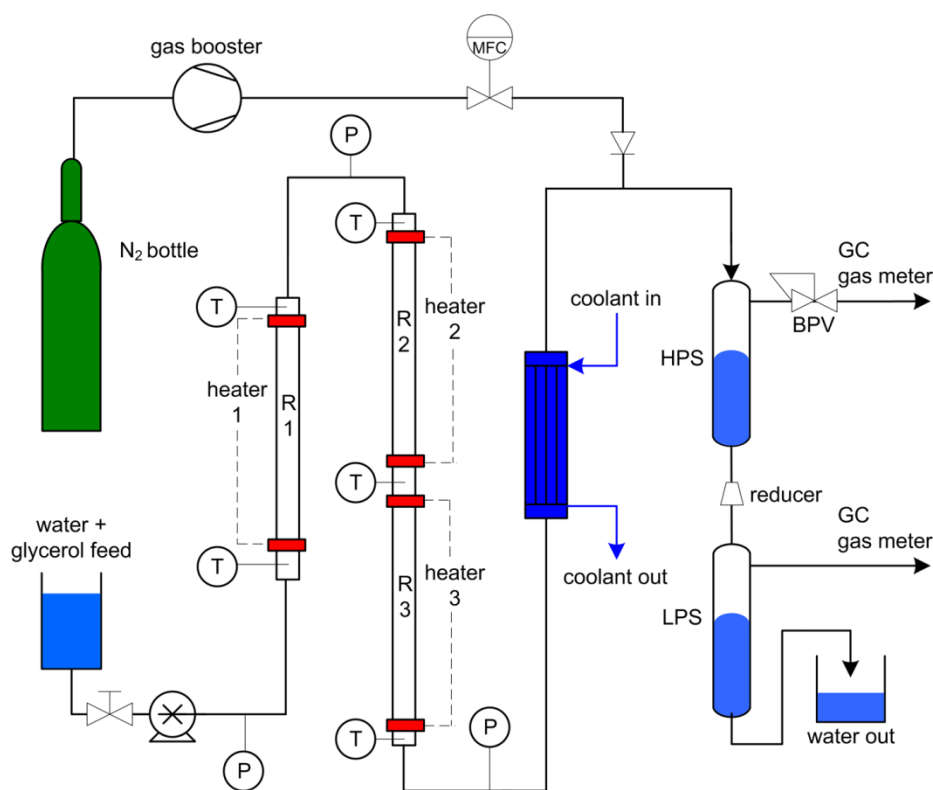
Fig. 3.2 Schematic representation of the continuous setup.

3.2.4 Analyses

The gas compositions were analyzed using an online dual-column gas chromatograph (GC 955, Syntech Spectras) equipped with thermal conductivity detectors. CO was analyzed over a molecular sieves 5 Å column ($L = 1.6$ m), CO_2, CH_4, and C_{2+} using a Chromosorb 102 column ($L = 1.6$ m), both using helium as carrier gas. H_2 was analyzed on the molecular sieves column using argon as carrier gas. The total organic carbon (TOC) content of the effluent water was analyzed using a TOC analyzer (TOC-V$_{CSN}$, Shimadzu).

3.2.5 Definitions and equilibrium calculations

The temperatures of the three reactors were measured at the outer surface of the reactor tubes at two locations. It is not possible to measure the temperature of the flow leaving the catalyst bed, so the temperature of an experiment was taken as the average temperature of the last reactor. The carbon-to-gas efficiency (C_{GE}) is defined as the ratio between the molar carbon flow in the product gas (ϕ_C) and the molar carbon flow in the feed ($\phi_{C,feed}$):

$$C_{GE} = \frac{\sum_i \phi_{C,i}}{\phi_{C,feed}} \cdot 100\% \qquad \text{(Eq. 2.7)}$$

The molar carbon flow in the feed was calculated from the glycerol concentration and feed flow. The molar carbon flow in the gas was calculated from the gas flow and composition. The (carbon) conversion (ζ) is the conversion calculated by means of the molar carbon flow of the feed and the molar carbon flow of the effluent water:

$$\zeta = \frac{\phi_{C,feed} - \phi_{C,effluent}}{\phi_{C,feed}} \cdot 100\% \qquad \text{(Eq. 2.10)}$$

In the absence of coke formation the C_{GE} and ζ are equal. The C_{GE} and ζ for a typical experiment were the average values during the operating time of 2 – 4 h. The residence time (τ) is calculated with Eq. 2.11:

$$\tau = \frac{V_r \cdot \rho_{T,P}}{\phi_{m,STP}} \qquad \text{(Eq. 2.11)}$$

with V_r as the geometric reactor volume, $\rho_{T,P}$ as the water density at (average) process temperature and pressure and $\phi_{m,STP}$ as the mass flow at standard conditions. For all residence time calculations the feed was assumed to consist of pure water.

Equilibrium gas yields for glycerol reforming were calculated from literature data for the equilibrium constants for the WGS reaction and methanation as a function of the temperature, using an in-house-developed Matlab routine [30]. Thermodynamic calculations at the prevailing reaction conditions and feed concentrations indicate that the Boudouard equilibrium involving CO, CO_2 and C is shifted completely to the CO side and as such this reaction was not considered. The Soave-Redlich-Kwong equation of state was used to correct for nonideality [31]. Thermodynamic properties such as critical properties and acentric factors were obtained from Reid [32].

3.3 Results and discussion

3.3.1 Glycerol reforming in supercritical water

A total of 5 to 8 experiments were conducted at different temperatures for each catalyst. Relevant details of the experiments are given in Table 3.3, together with data from previous noncatalyzed experiments taken from Chapter 2. The carbon balance closures for Ni/CaO-6Al$_2$O$_3$, NiCu/CeZrO$_2$, and CuZn are very good and reproducible. In case of Pt/CeZrO$_2$ and Ni/ZrO$_2$ the closure of the carbon balance is less, indicating carbon losses, most probably by coke formation on the catalyst. As mentioned before, the difference between C_{GE} and ζ is a good indicator for coke formation but also the experimental error has to be taken into account. The average absolute difference in carbon balance closure for the noncatalytic experiments is 3.1% which can be considered as the average experimental error. Values that are significantly higher indicate coke formation. The average difference between C_{GE} and ζ is a factor of 2-3 higher for Pt/CeZrO$_2$ and Ni/ZrO$_2$ compared to the other catalysts (Table 3.3).

Table 3.3 Relevant data on the experiments conducted.

Catalyst	No. of exp.	T (K)	C-balance (%)	Average $\|C_{GE} - \zeta\|$ (%)	Pressure build-up
Pt/CeZrO$_2$	8	623-933	82.8-97.9	7.7	Yes
Ni/ZrO$_2$	5	721-912	85.5-98.4	6.0	Yes
Ni/CaO-6Al$_2$O$_3$	7	658-931	95.4-99.8	2.1	No
NiCu/CeZrO$_2$	7	648-966	95.6-102.4	2.1	Yes
CuZn	5	833-954	96.0-99.3	3.5	No
No catalyst[a]	6	879-898	94.5-99.8	3.1	No

[a]Results were obtained in the reactor configuration shown in Fig. 2.2B from Chapter 2.

The C_{GE} and ζ for the five catalysts are shown as a function of the temperature in Fig. 3.3. In this figure one data point for a noncatalytic glycerol reforming experiment (at 947 K) is included as reference. Apparently, both C_{GE} and ζ are much higher if a catalyst is present, typically yielding values of 80 to 100% for the catalytic experiment versus 40% for the noncatalytic experiment. All catalysts are active in the decomposition of glycerol into gaseous components.

For Pt/CeZrO$_2$, Ni/ZrO$_2$, and NiCu/CeZrO$_2$ a pressure build-up in the reactor was observed. In case of the former two catalysts, coke formation was likely responsible as it was observed visually at the catalysts surface and the inner surface of the reactor. For NiCu/CeZrO$_2$, coke formation could not be observed visually and the increase in pressure drop was caused by disintegration of the solid structure of the catalyst into a paste.
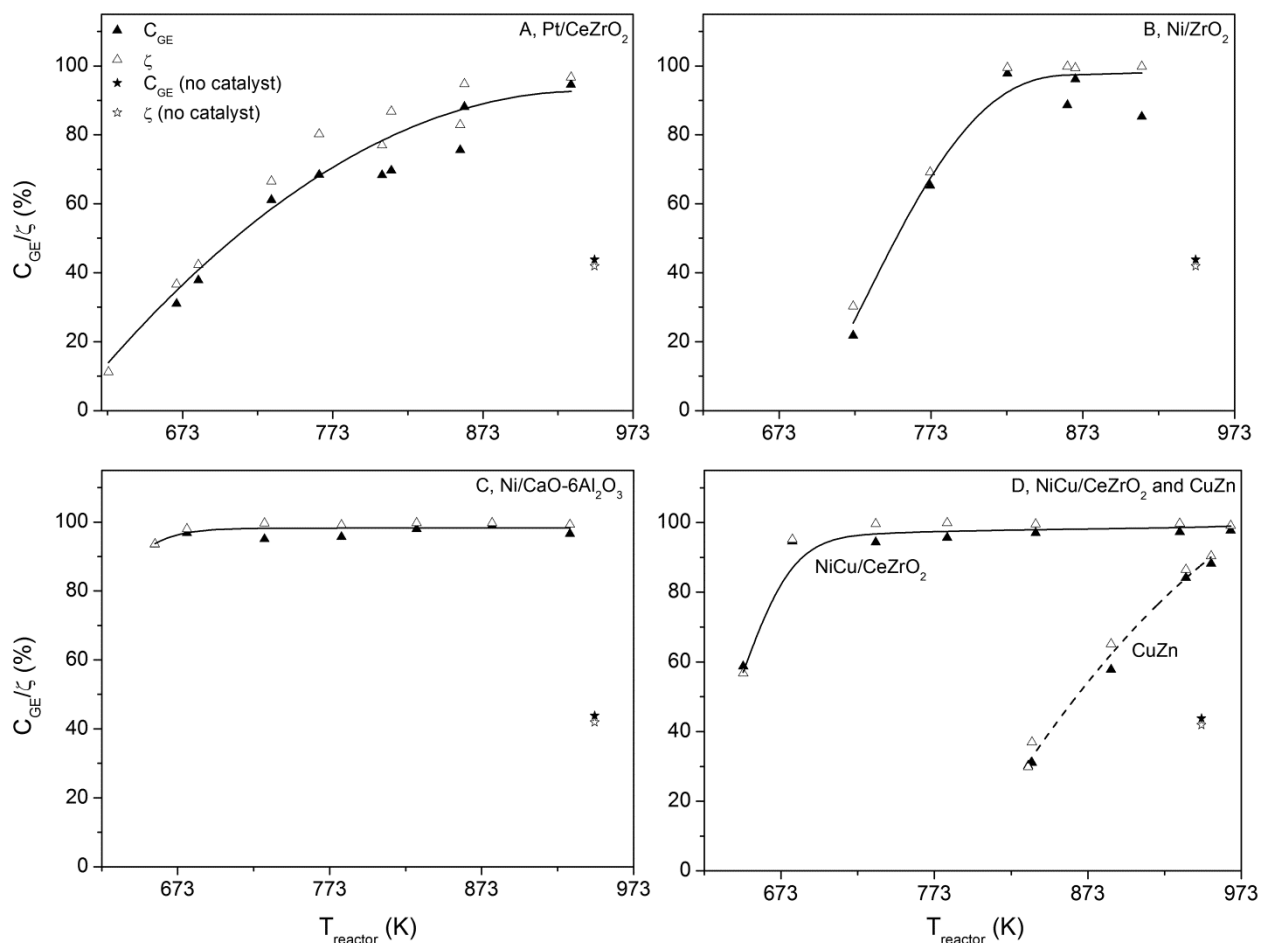
Fig. 3.3 C_{GE} and ζ as a function of the temperature for five different catalysts: Pt/CeZrO$_2$ (A, *GHSV* = 3 h^{-1}), Ni/ZrO$_2$ (B, *GHSV* = 9.7 h^{-1}), Ni/CaO-6Al$_2$O$_3$ (C, *GHSV* = 5.9 h^{-1}), and NiCu/CeZrO$_2$ (D, *GHSV* = 4.6 h^{-1}) and CuZn (D, *GHSV* = 6.4 h^{-1}). Experimental conditions: τ = 8 − 87 s, *P* = 25.5 − 27.0 MPa, [feed] = 10 wt%. The solid lines are for illustrative purposes only.

The exit gas flows versus runtime were measured and the results for some typical experiments with the different catalysts are given in Fig. 3.4. For experiments with Pt/CeZrO$_2$ and Ni/ZrO$_2$, the gas flow dropped approximately 10% during 2 − 3 h of operation (see Fig. 3.4), an indication for deactivation of the catalyst. The reduction in gas flow hardly influenced the gas composition. For the other catalyst the gas flow remained more or less constant, which can be seen in Fig. 3.4. Deactivation can be caused by changes in catalyst structure (for Pt/CeZrO$_2$ increase in crystallite size of Pt and for Ni/ZrO$_2$ changes in support morphology, see Section 3.3.2) or coke formation, as visually observed for most experiments, or combinations thereof. Unfortunately, we were not able to determine the exact amount of coke deposition on the catalyst to assess the impact of coke formation on catalyst performance.
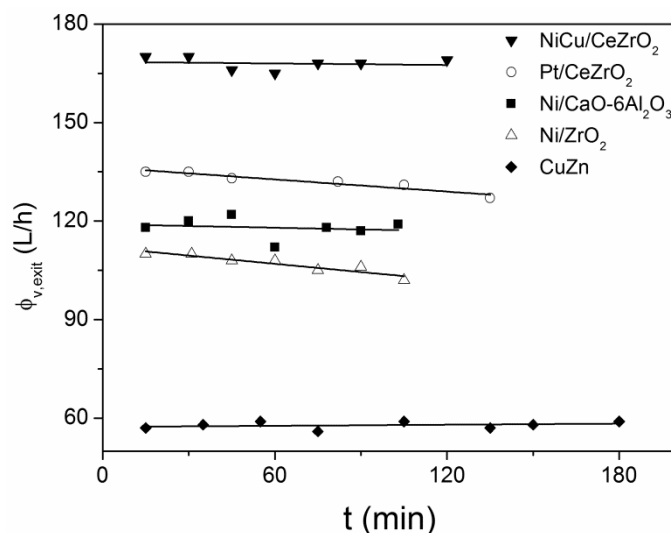
Fig. 3.4 Exit gas flows for typical reforming experiments. Gas flows were measured at ambient conditions. Catalyst and operating temperature of R3: Pt/CeZrO$_2$ (932 K), Ni/ZrO$_2$ (863 K), Ni/CaO-6Al$_2$O$_3$ (730 K), NiCu/CeZrO$_2$ (781 K), and CuZn (836 K), P = 25.5 − 27.0 MPa. The solid lines are trend lines and for illustrative purposes only.

The observed activation energies for glycerol reforming for Pt/CeZrO$_2$ and CuZn in our reactor system were calculated assuming a first order decomposition reaction in glycerol and plug flow behavior in the reactor tubes. From the conversion data, the reactor volume, and the volumetric flow (using the density of SCW for the complete flow) the reaction rate constant was calculated. The observed activation energy was then calculated using the Arrhenius equation. The observed activation energy for Pt/CeZrO$_2$ and CuZn are 93 ± 16 kJ/mol and 148 ± 29 kJ/mol (95% confidence limits) respectively, as compared to 196 kJ/mol for reforming without catalysts and 183 kJ/mol for reforming crude glycerin (glycerol derived from biodiesel production containing NaCl) [7]. The catalysts reduce the observed activation energy of glycerol decomposition, which allows for less severe operating conditions, but these observed activation energies should be treated with some care. The values, in particular in the case of Pt/CeZrO$_2$, may not be constant as some catalyst deactivation was observed (Fig. 3.4), which is expected to lead to higher activation energies. For the other catalysts, no or too few data points are available with conversions significantly lower than 100% to calculate the activation energy.

The gas composition for catalytic and noncatalytic reforming is illustrated in Table 3.4 and compared with equilibrium data. The main components in the noncatalytic experiments at 898 K are H$_2$ and CO. The concentrations of CO$_2$ and CH$_4$ are around 12 vol% and higher hydrocarbons are present as well. The WGS reaction hardly proceeds in the absence of catalysts. The gas composition is significantly influenced by the presence of catalysts. The equilibrium composition for the WGS reaction is reached in the presence of four of the five catalysts. The only exception is CuZn, which has less activity for the WGS reaction than the other catalysts, but more activity than in case of the noncatalytic experiment. CH$_4$ was present for all catalyst ranging from 8.8 − 22.6 vol%. The CH$_4$ concentration of 22.6 vol% for Ni/ZrO$_2$ is

significantly higher than the equilibrium value. An hypothesis for this high CH_4 concentration is that due to coke deposition at the reactor wall the temperature of the medium could not have reached the temperature recorded for reactor 3 and equilibrium was reached at a lower temperature than recorded. The equilibrium concentration of 22.6 vol% CH_4 corresponds to a temperature of 872 K assuming complete glycerol conversion.

Table 3.4 Comparison of the gas composition for catalytic and noncatalytic reforming.

Catalyst	T	ζ	H_2	CO	CO_2	CH_4	C_2H_6	C_{2+}[a]
	(K)	(%)				(vol%)		
Pt/CeZrO$_2$	932	97	51.0	0.4	34.6	8.8	4.4	0.9
Ni/ZrO$_2$	912	99	41.9	0.7	34.8	22.6	0.0	0.0
Ni/CaO-6Al$_2$O$_3$	931	99	51.1	0.8	32.4	15.7	0.0	0.0
NiCu/CeZrO$_2$	933	99	53.4	0.8	32.2	13.5	0.0	0.0
CuZn	937	87	44.8	13.6	24.8	11.9	4.1	0.8
No catalyst[b]	898	85	35.6	33.2	12.9	11.6	5.4	1.3
Equilibrium 1[c]	898	100	47.4	1.1	33.0	18.5	0.0	0.0
Equilibrium 2[c]	933	100	52.6	1.5	31.8	14.1	0.0	0.0
Equilibrium (no methanation)[c]	933	100	69.2	2.7	28.1	0.0	0.0	0.0

[a]Sum of the concentrations of C_2H_4, C_3H_6, and C_3H_8.
[b]Results taken from an experiment conducted in the research study described in Chapter 2.
[c]Equilibria are calculated for 25.0 MPa.

In case of Pt/CeZrO$_2$ and CuZn, significant amounts of higher hydrocarbons are present in the gas phase. Thus, methanation or the reforming of higher hydrocarbons is not or hardly promoted, as the concentrations of CH_4 and the higher hydrocarbons for these catalysts are similar to the concentrations obtained in noncatalytic reforming. For noncatalytic reforming methanation was shown to be negligible and CH_4 was formed directly as a primary gas phase product during decomposition [5, 7].

The gas compositions (vol%) for the different catalysts versus the temperature are shown in Fig. 3.5. The lines represent equilibrium values in case of complete glycerol conversion. For Pt/CeZrO$_2$, the following assumptions were used to calculate the equilibrium composition. All hydrocarbons were considered as primary products and only the WGS reaction was taken into account in the equilibrium calculation. The average hydrocarbon concentration over the whole temperature range (CH_4 = 6.0 vol%, C_2H_6 = 3.9 vol%, C_3H_8 = 0.7 vol%) was taken as a constant value. Methanation was assumed to be absent and this reaction was neglected (see Fig. 3.5A).
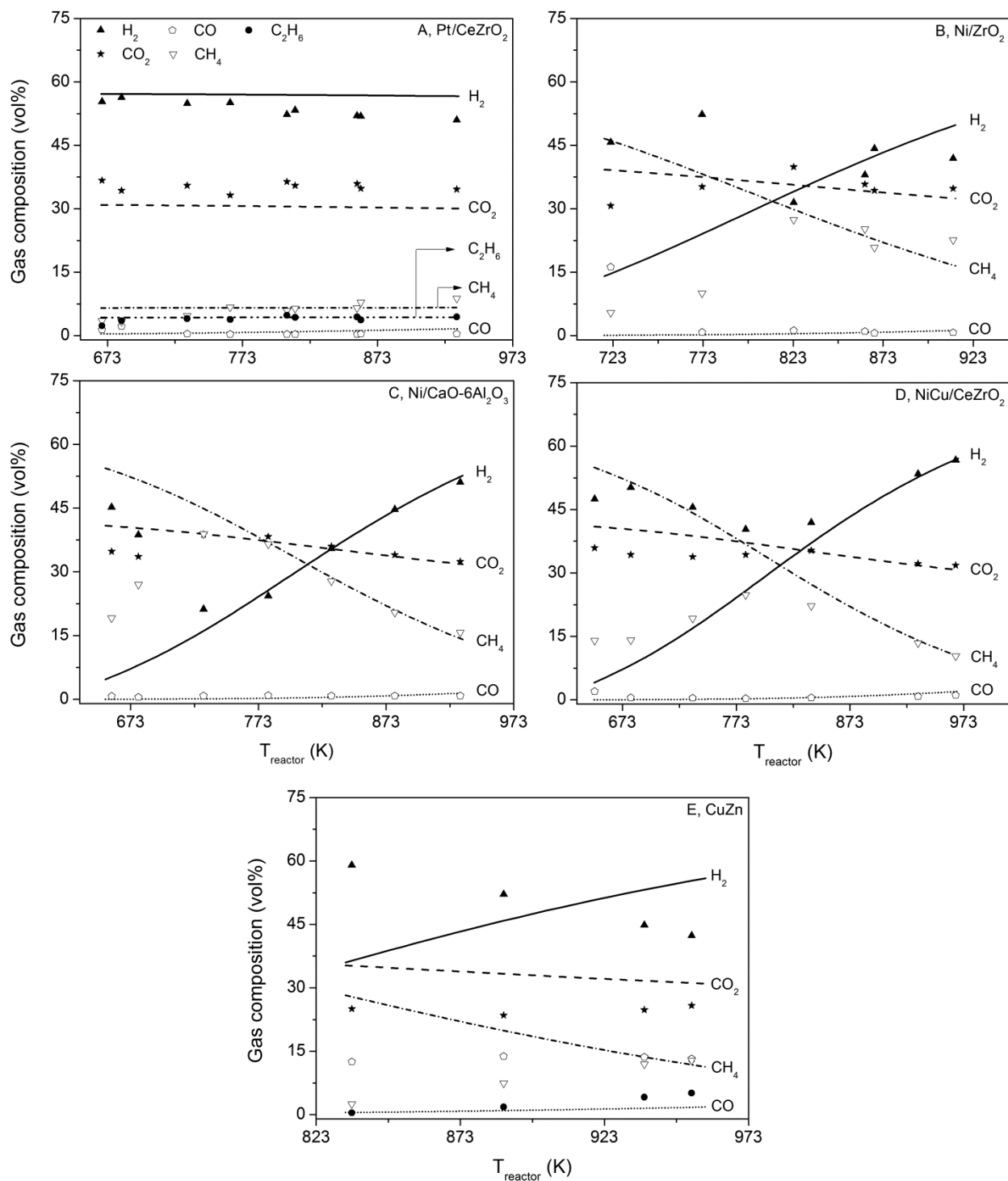
Fig. 3.5 The gas composition as a function of the temperature for five different catalyst: Pt/CeZrO$_2$ (A, *GHSV* = 3 h^{-1}), Ni/ZrO$_2$ (B, *GHSV* = 9.7 h^{-1}), Ni/CaO-6Al$_2$O$_3$ (C, *GHSV* = 5.9 h^{-1}), NiCu/CeZrO$_2$ (D, *GHSV* = 4.6 h^{-1}), and CuZn (E, *GHSV* = 6.4 h^{-1}). Experimental conditions: τ = 8 − 87 s, *P* = 25.5 − 27.0 MPa, [feed] = 10 wt%. The lines represent the equilibria. For the equilibrium calculation of Pt/CeZrO$_2$ (A) only the WGS reaction was taken into account.

For $Pt/CeZrO_2$, the product gas contains mainly H_2 and CO_2 and traces of CO. The concentration of CH_4 and C_2H_6 varies between 3.3 – 8.8 vol% and 2.3 – 4.8 vol% respectively. The concentration of H_2 and CO_2 shows a slightly decreasing trend, while the concentration of hydrocarbons increases somewhat over the temperature range. The concentrations of H_2, CO_2, and CO follow a trend predicted by the equilibrium calculation although the values deviate slightly (see Fig. 3.5A). This is likely caused by the assumption of constant hydrocarbon concentrations and the formation of coke in these experiments. The similar trends of the experimental data and the equilibrium predictions without methanation justify the assumption of neglecting methanation. Thus, for $Pt/CeZrO_2$ it is likely that the CH_4 present is mainly a primary gas phase reforming product, as in case of noncatalytic experiments [7]. With no or hardly any methanation activity the equilibrium gas composition appears to be almost independent of the temperature. The WGS reaction is at or close to equilibrium as almost no CO is present in the gas.

For the other catalysts the gas compositions show a stronger temperature dependence. For Ni/ZrO_2 (Fig. 3.5B) some CO is still present at low temperatures, but is absent at higher temperatures. The CH_4 concentration in particular increases, even exceeding the equilibrium concentrations (an explanation is given before). The trends observed for the gas phase concentrations for $Ni/CaO-6Al_2O_3$, and $NiCu/CeZrO_2$ (Fig. 3.5C-D) versus temperature are rather similar, but the concentrations of the components differ. Although $Ni/CaO-6Al_2O_3$ has a lower Ni loading this catalyst seems more active in promoting methanation than $NiCu/CeZrO_2$ as equilibrium values are reached at lower temperatures. At higher temperatures, the experimental concentrations are in agreement with the calculated equilibrium values for both catalysts. The presence of Cu in $NiCu/CeZrO_2$ possibly reduces the methanation activity of Ni. The effect, however, seems less pronounced than observed in the literature [16]. Comparing the catalysts containing Ni or NiCu with the Pt catalyst, a substantial amount of higher hydrocarbons is present when the Pt catalyst is used (as in noncatalytic reforming, see Table 3.4 and Chapter 2). When Ni or NiCu are present, the higher hydrocarbons may be reformed into smaller components that react further through the WGS reaction and methanation.

CuZn (see Fig. 3.5E) is the least active catalyst and the gas composition deviated substantially from the gas compositions obtained with the other catalysts. At higher temperatures, a substantial amount of CO (> 13 vol%) is still present, while the CH_4 and C_2H_6 concentrations are similar to experiments with $Pt/CeZrO_2$ and noncatalytic experiments. For CuZn, both methanation and the WGS reaction do not reach equilibrium.

Catalysts can act upon glycerol decomposition in three ways, viz. (i) initial decomposition of glycerol into water-soluble intermediate products, (ii) the conversion of these intermediate products to gas, and (iii) gas phase reactions. No conclusions can be drawn on the former two as in the majority of the experiments complete glycerol conversion was obtained and no effluent samples were analyzed for intermediate organic products. Obviously, the catalysts influence the gas phase reactions as the gas phase composition is a strong function of the temperature (Fig. 3.5), approaching equilibria at the higher temperatures (which was not the case for experiments

with pure glycerol without catalysts). The variations in the gas phase compositions for the different catalyst and the different temperatures can be rationalized by assuming that glycerol decomposes into H_2, CO, CH_4, and C_2 and C_3 hydrocarbons. CO_2 is formed in the WGS reaction. The catalysts promoting methanation (Ni and NiCu) reform the C_2/C_3 hydrocarbons and only H_2, CO, CO_2, and CH_4 remain present in the gas phase, which would also be expected from thermodynamics. The methanation activity determines the final composition. For the other catalysts ($Pt/CeZrO_2$ and CuZn) all gas products originally formed remain present and the WGS activity of the catalyst determines the final composition.

Although the presence of any of the catalysts influences the gas phase composition significantly, the actual compositions are not particularly attractive for a subsequent reaction to methanol. The values of some performance indicators (C_{GE}, S_N, and C_xH_y; sum of the concentrations of all $C_1 - C_3$ hydrocarbons) for the different catalysts are shown in Fig. 3.6. The performance indicators are a qualitative measure for the quality of the syngas in combination with the performance of the catalyst. For methanol synthesis, an S_N as close as possible to 1.33 (see Eq. 7.2 in Chapter 7), a high C_{GE}, and low C_xH_y content are preferred.

The extremities of the performance indicators are: $22 \leq C_{GE} \leq 99\%$, $-0.45 \leq S_N \leq 0.96$, and $3.5 \leq C_xH_y \leq 39.3$ vol%. The S_N follows more or less the inverse trend of the C_xH_y content and goes through a minimum for the Ni containing catalysts. The other catalysts have a gradually decreasing S_N and increasing C_xH_y content. The highest S_N value is 0.96 for CuZn at 836 K and a C_{GE} of 31%. The highest S_N value at C_{GE}'s exceeding 95% is 0.76 for $NiCu/CeZrO_2$ at around 973 K. Both S_N values are far from the preferred value of 1.33, due to the formation of C_xH_y. Because the gas composition obtained with the Ni based catalyst is close to equilibrium at the higher temperatures (see Figs. 3.5B-D), the S_N can be improved by further increasing the temperature or reducing the feed concentration. For the production of 'green' natural gas $Ni/CaO-6Al_2O_3$ and to a lesser extent $NiCu/CeZrO_2$ appear to be attractive catalysts based on their methanation activity.
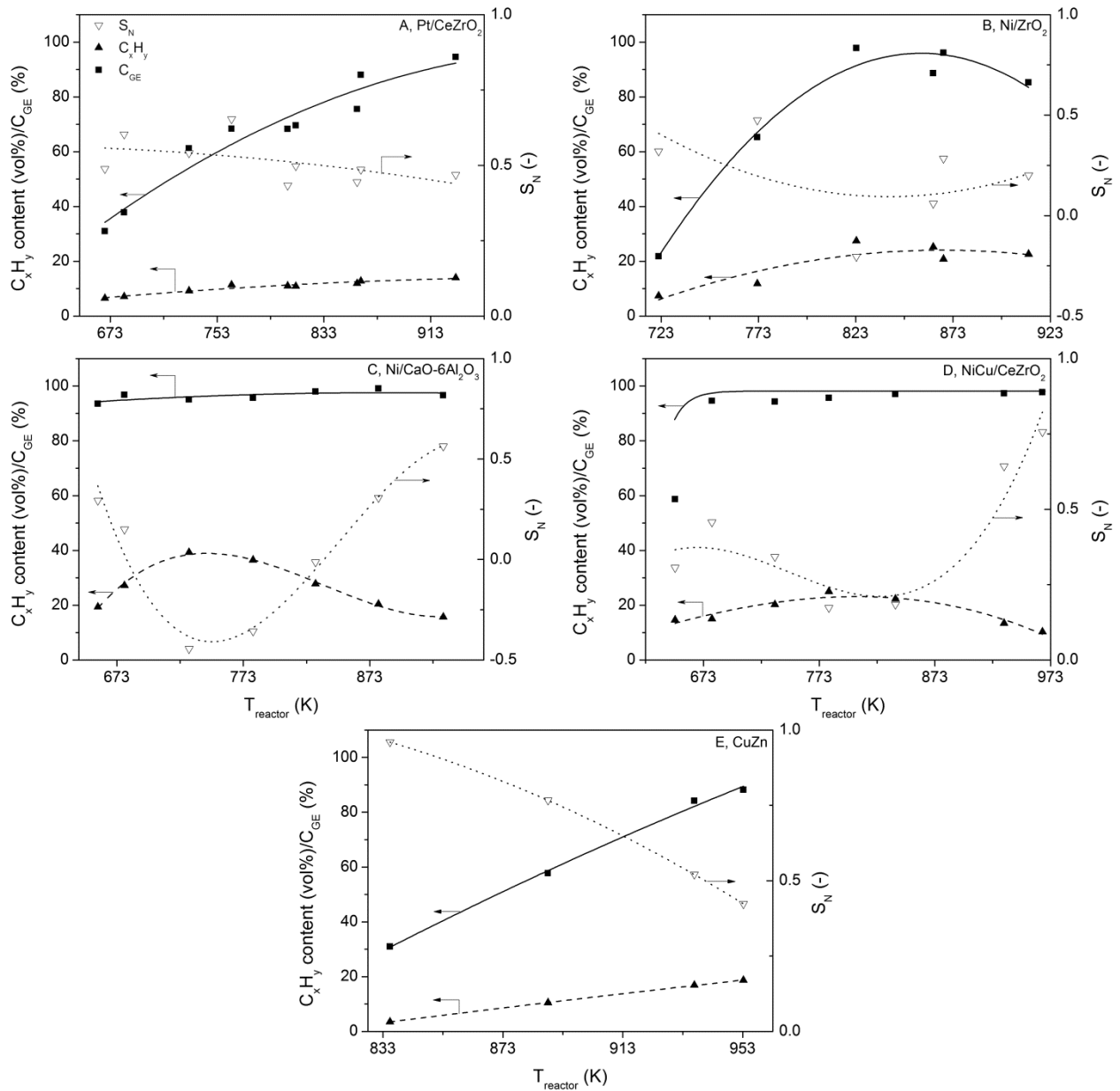
Fig. 3.6 Values of the performance indicators qualitatively defining the performance of the catalyst and the quality of the syngas. Pt/CeZrO$_2$ (A, *GHSV* = 3 h^{-1}), Ni/ZrO$_2$ (B, *GHSV* = 9.7 h^{-1}), Ni/CaO-6Al$_2$O$_3$ (C, *GHSV* = 5.9 h^{-1}), NiCu/CeZrO$_2$ (D, *GHSV* = 4.6 h^{-1}), and CuZn (E, *GHSV* = 6.4 h^{-1}). Experimental conditions: τ = 8 − 87 s, *P* = 25.5 − 27.0 MPa, [feed] = 10 wt%. The lines are trend lines and for illustrative purposes only.

In Fig. 3.7 the gas yields (in mol/mol feed) are plotted as a function of the operating temperature for Ni/CaO-6Al$_2$O$_3$ and NiCu/CeZrO$_2$ for experiments with C_{GE} and ζ exceeding 96%. Initially, the CH$_4$ yields increases with temperature at the expense of H$_2$ and CO$_2$. Above a certain temperature (748 K for Ni/CaO-6Al$_2$O$_3$ and 798 K for NiCu/CeZrO$_2$), the CH$_4$ yield decreases again, and the H$_2$ and CO$_2$ yield increases. In both cases, the yield of CO is negligible.

Apparently, at low temperatures methanation is kinetically limited, while at higher temperatures thermodynamic limitations play a major role. Although both catalysts show similar trends in gas yields, CH_4 production at lower temperatures is substantially higher for $Ni/CaO-6Al_2O_3$.
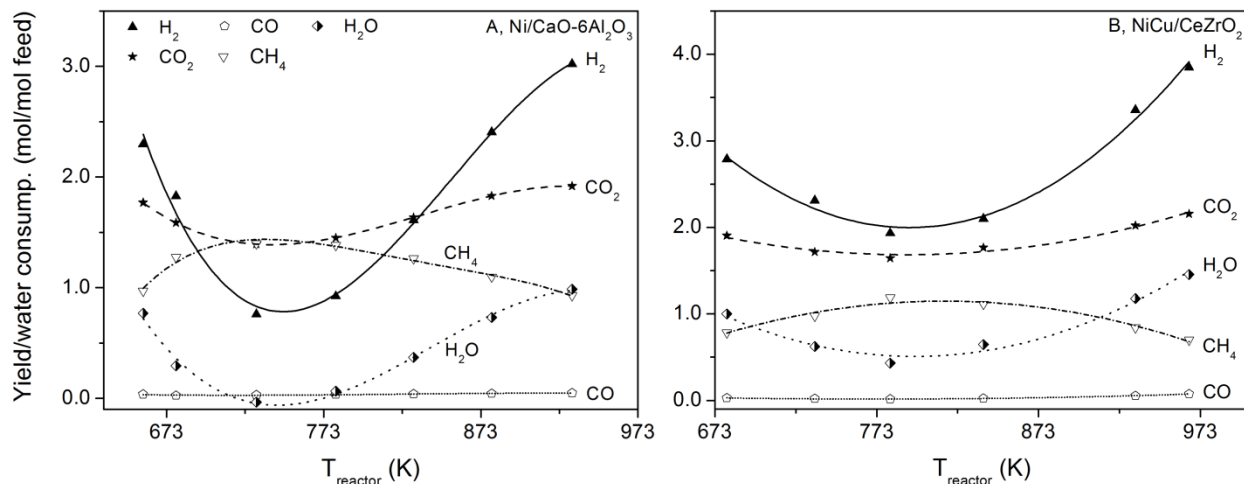
Fig. 3.7 The gas yields and the water consumption as a function of the temperature for $Ni/CaO-6Al_2O_3$ (A, $GHSV = 5.9 \ h^{-1}$), and $NiCu/CeZrO_2$ (B, $GHSV = 4.6 \ h^{-1}$). Experimental conditions: $\tau = 8 - 21$ s, $P = 25.5 - 27.0$ MPa, [feed] = 10 wt%. The lines are trend lines and for illustrative purposes only.

From the glycerol feed concentration, gas yields, and carbon concentration in the effluent water, and assuming that the only organic component in the effluent water is nonconverted glycerol, the overall element balances for carbon, hydrogen, and oxygen can be derived based on glycerol. The carbon balance closure is close to 100% (see Table 3.3), however, the closure of the balances for H and O are in between 90 and 150%. For all experiments, this difference can be attributed to reactions involving water which lead to a net water production or consumption. From the element balances, the overall water production/consumption can thus be derived and the lines are shown in Fig. 3.7 as well. Water production or consumption is due to the WGS reaction and methanation.

In the literature Ru based catalysts for the RSCW of glycerol were investigated (see Table 3.1). These catalysts can be used for methanation, which is also the case for the Ni based catalysts investigated here. In this study, the opportunities in the catalytic RSCW of glycerol are extended with experiments with a Pt based catalyst and a CuZn alloy. Both catalysts showed completely different behavior, with low or no methanation activity and some WGS activity. Besides quantification of the performance of the catalysts in glycerol reforming, the catalysts are characterized, to gain more understanding in the influence of RSCW on the catalyst structure.

3.3.2 Catalysts characterization before and after the experiments

In Table 3.5 relevant properties of the catalysts are shown. The spent catalysts samples were taken out of the reactor after having been in contact with water at supercritical conditions for more than 20 h. Notably, the specific surface area was reduced for all the porous catalysts, but increased for the CuZn alloy. For the latter, the increase is probably due to leaching in SCW. It proved not possible to quantify the extent of leaching e.g. by analyses of the Cu content in the effluent water. The main reason is that the reactor wall contains Cu (Incoloy 825), which may also be prone to leaching. The decrease of the surface area for $NiCu/CeZrO_2$ is the most dramatic with a factor of approximately 15, and the solid structure of the catalyst had collapsed into a paste. The other catalysts maintained their original solid structure. The reduction in specific surface area might be due to the collapse of the porous structure, sintering, and coke deposition on the catalyst leading to pore blockage.

Table 3.5 Relevant catalyst properties before and after reaction.

Catalyst	Fresh[a] (m^2/g)	Spent[a] (m^2/g)	Visual coke formation[b]	Appearance spent cat.
$Pt/CeZrO_2$	35	16	+	Solid
Ni/ZrO_2	20	13	+	Solid
$Ni/CaO-6Al_2O_3$	20	12	+/-	Solid
$NiCu/CeZrO_2$	151	9	+/-	Paste
CuZn (alloy)	0.3	1.2	-	Solid

[a]BET surface area.
[b]+ = coke clearly visible, +/- coke slightly visible, - = no coke formation visible

X-Ray diffraction patterns were measured for fresh and spent catalysts. These patterns are shown in Figs. 3.8 – 3.12. In each of these figures the lower pattern represents the diffraction pattern of the fresh catalyst and the upper pattern is the diffraction pattern of the spent catalyst.

In Fig. 3.8 the XRD spectra for $Pt/Ce_{0.08}Zr_{0.92}O_2$ are shown. In the fresh sample a tetragonal phase of ZrO_2 or $Ce_{0.08}Zr_{0.92}O_2$ is present. Pt was not detected in the fresh sample, probably due to the small crystallite size and low loading. The spent catalyst contains tetragonal ZrO_2 (or $Ce_{0.08}Zr_{0.92}O_2$). A small amount of monoclinic ZrO_2 was detected. The lattice parameters of the tetragonal phase are slightly larger than those for pure tetragonal ZrO_2 which indicates a modification of the tetragonal ZrO_2 structure by Ce. In the spent sample Pt with a crystallite size of 20 nm was detected. The crystallite size of Pt increased probably due to the agglomeration of Pt crystallites at these harsh conditions.
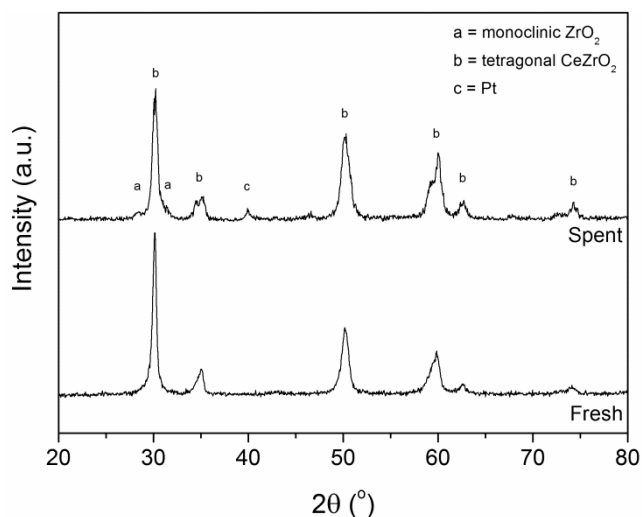
Fig. 3.8 Diffraction pattern of Pt/CeZrO$_2$, fresh and spent catalyst. Monoclinic ZrO$_2$ (a), tetragonal CeZrO$_2$ (b), Pt (c).

The diffraction patterns of Ni/ZrO$_2$ are given in Fig. 3.9. The fresh sample contains cubic NiO, monoclinic ZrO$_2$, and probably small quantities of tetragonal ZrO$_2$. The XRD spectrum of the fresh sample has a very small peak at 30.5^o which is the strongest reflection angle of the tetragonal phase. The spent sample contains a larger amount of tetragonal ZrO$_2$ and apparently a part of the monoclinic ZrO$_2$ phase is converted into tetragonal ZrO$_2$. NiO, present in the fresh sample is completely converted into metallic Ni. In the spent sample no NiO phase was detected. The size of Ni crystallites in the spent sample is approximately 50 nm.
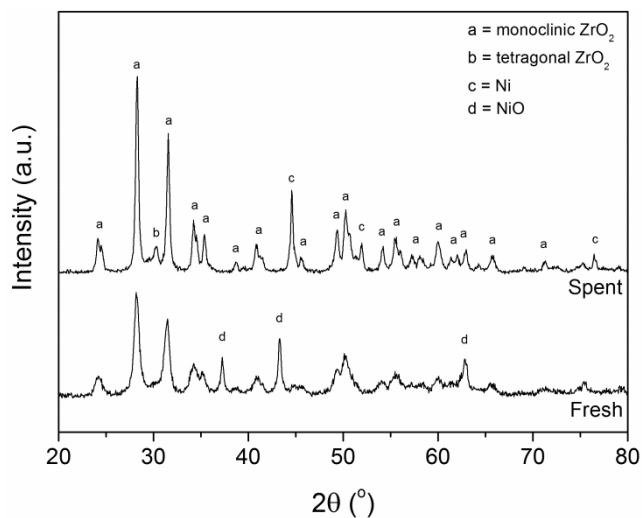
Fig. 3.9 Diffraction pattern of Ni/ZrO$_2$, fresh and spent catalyst. Monoclinic ZrO$_2$ (a), tetragonal ZrO$_2$ (b), Ni (c), NiO (d).

Diffraction patterns for Ni/CaO-6Al$_2$O$_3$ are shown in Fig. 3.10. Both samples contain a hexagonal CaO-6Al$_2$O$_3$ phase and an α-Al$_2$O$_3$ phase, and are very crystalline as can be seen from the narrow peaks. The peaks that are not labeled have reflections for both phases at similar positions. The fresh sample contains cubic NiO, while this phase is not present in the spent sample. The spent sample contains only Ni (crystallite size 40 nm) in the metallic form. As with Ni/ZrO$_2$ after subjection to SCW, Ni(0) is present, which remained in the reduced form after exposure to air upon opening the reactor and collecting the catalyst. A small amount of CaO$_3$ is present, indicated by a diffraction peak at 29.4°, labeled with a 'c' in the diffraction pattern.
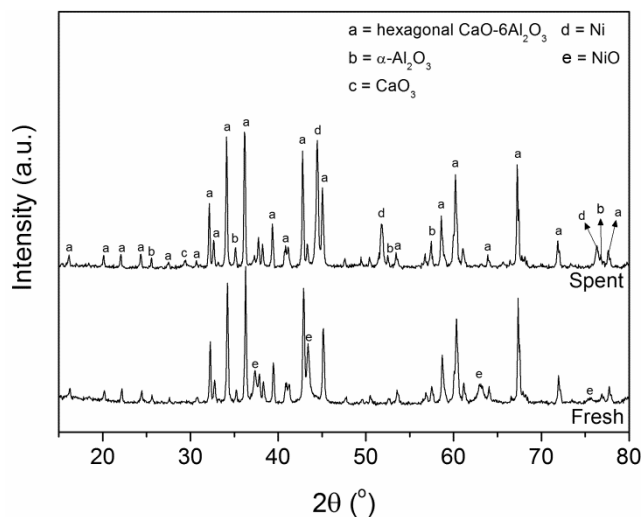
Fig. 3.10 Diffraction pattern of Ni/CaO-6Al$_2$O$_3$, fresh and spent catalyst. CaO-6Al$_2$O$_3$ (a), α-Al$_2$O$_3$ (b), CaO$_3$ (c), Ni (d), NiO (e).

Diffraction patterns of NiCu/Ce$_{0.46}$Zr$_{0.54}$O$_2$ are shown in Fig. 3.11. The fresh sample is practically amorphous, however, broad peaks are visible of a cubic NiO phase. Most probably, these reflections can be attributed to a solid solution of Ni$_{1-x}$Cu$_x$O (a = 4.185 Å) on the basis of NiO. Some diffuse peaks from CeZrO$_2$ were observed as well. The pattern of the spent sample differs significantly from the fresh sample and crystallized phases are present. The first two peaks (at 18.1° and at 25.0°) and several small reflections in the spent sample correspond with a hydroxy copper carbonate phase.

The peaks marked 'c' in Fig. 3.11 deviate slightly from the diffraction peak position for pure metallic Ni which can be due to the presence of Cu in a Ni$_{1-x}$Cu$_x$ alloy. The peaks marked 'b' in Fig. 3.11 represent a cubic solid solution of CeZrO$_2$ probably with a slight distortion. Furthermore, it is possible that a small quantity of other Ce(Zr) oxides is present. The amorphous phase of the fresh sample was converted in SCW into a crystalline solid solution of CeZrO$_2$. The poorly crystallized Ni$_{1-x}$Cu$_x$ oxides were converted to metallic Ni$_{1-x}$Cu$_x$ (crystallite size 42 nm). The structural stability of NiCu/CeZrO$_2$ and the specific surface area (see Table 3.5), however, deteriorated substantially. Remarkably, this structural disintegration did not reduce the activity of the catalyst, indicating that enough specific surface area remained present to

retain activity. For a MnO_2/CeO_2 catalyst in SCW oxidation, similar phenomena of catalyst disintegration and structural changes were observed that did not affect the catalyst activity adversely [33]. On the contrary, the structural change even had a positive effect on the activity of the catalyst. The instability of $NiCu/CeZrO_2$ in SCW can be caused by the high specific surface area of the catalyst, the presence of an amorphous phase and a high CeO_2 content. Stability issues have been reported for Al_2O_3 modified with higher loadings of Ce [34], while pure ZrO_2 supports remain stable [35].
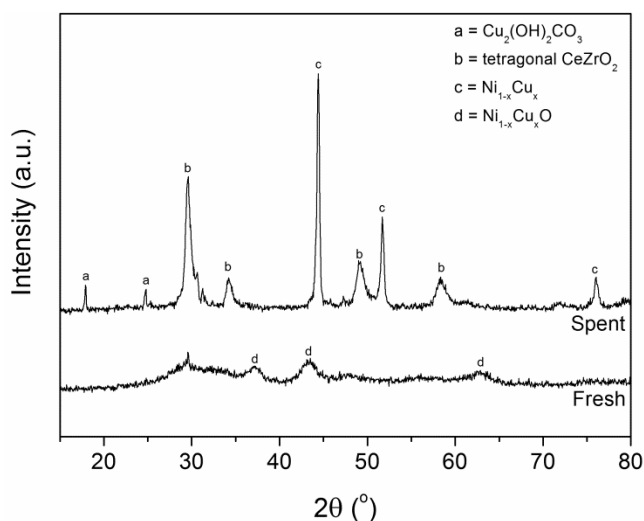
Fig. 3.11 Diffraction pattern of $NiCu/CeZrO_2$, fresh and spent catalyst. Monoclinic $Cu_2(OH)_2CO_3$ (a), tetragonal $CeZrO_2$ (b), $Ni_{1-x}Cu_x$ (c), $Ni_{1-x}Cu_xO$ (d).

The diffraction patterns of the CuZn alloy are shown in Fig. 3.12. The surface of the fresh sample contains hexagonal ZnO and monoclinic CuO. The average crystallite sizes for both phases are similar and are approximately 50 nm. Some weak reflections are visible in the pattern which are uncharacteristic for the specified phases. These reflection can be assigned to the presence of some impurities (NiO and MgO) in the sample. The spent sample contains the same ZnO phase as the fresh sample and metallic Cu.
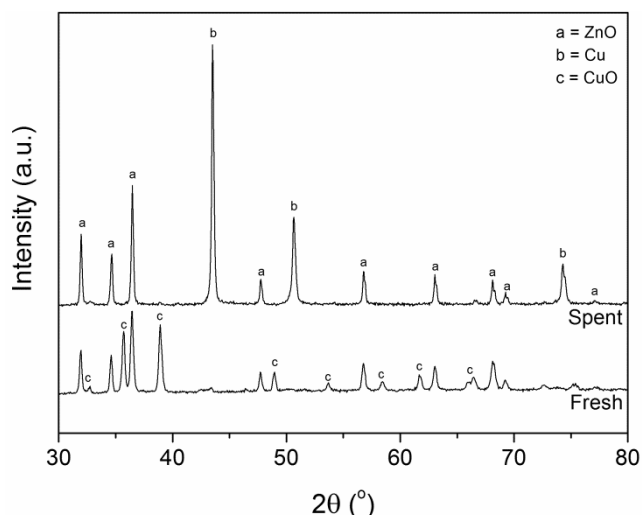
Fig. 3.12 Diffraction pattern of CuZn, fresh and spent catalyst. ZnO (a), Cu (b), CuO (c).

3.4 Conclusion

The influence of five different catalysts (Pt/CeZrO$_2$, Ni/ZrO$_2$, Ni/CaO-6Al$_2$O$_3$, NiCu/CeZrO$_2$, and CuZn, a nonporous alloy) on the reforming of glycerol in supercritical water was studied. The presence of a catalyst significantly promoted the decomposition of glycerol, but also the water-gas shift reaction. The catalysts containing Ni also promoted methanation, but the rate of methanation appeared lower than the water-gas shift reaction. For all catalysts except CuZn the water-gas shift reaction reached equilibrium while the methanation equilibrium was reached only at the higher temperatures (> 773 K). When using Pt/CeZrO$_2$ and Ni/ZrO$_2$ coke formation and pressure build-up were observed. In the experiments with Ni/CaO-6Al$_2$O$_3$, NiCu/CeZrO$_2$, and CuZn the coke formation was limited, however, the NiCu/CeZrO$_2$ catalyst disintegrated and its solid structure was lost, but reforming activity remained.

The gas composition was a strong function of the reactor temperature as expected from thermodynamics and a wide range of gas compositions was obtained. Except for NiCu/CeZrO$_2$ the catalyst structures remained largely intact in supercritical water and only minor changes in the support structure were observed. The surface area of all porous catalysts decreased. The S_N value of the gas compositions for the different catalyst was below 1 and therefore not very attractive for methanol synthesis. However, Ni/CaO-6Al$_2$O$_3$ strongly promotes methanation and has potential for the production of 'green' natural gas by reforming in supercritical water.

3.5 References

1   P. Basu, V. Mettanant, Biomass gasification in supercritical water - A review, Int. J. Chem. Reactor Eng., 7 (2009) 1-61.
2   G. Brunner, Near critical and supercritical water. Part I. Hydrolytic and hydrothermal processes, J. Supercrit. Fluids, 47 (2009) 373-381.
3   A. Kruse, Hydrothermal biomass gasification, J. Supercrit. Fluids, 47 (2009) 391-399.
4   J.A. Libra, K.S. Ro, C. Kammann, A. Funke, N.D. Berge, Y. Neubauer, M.M. Titiric, C. Fühner, O. Bens, J. Kern, K.H. Emmerich, Hydrothermal carbonization of biomass residuals: A comparative review of the chemistry, processes and applications of wet and dry hydrolysis, Biofuels, 2 (2011) 89-124.
5   A.A. Peterson, F. Vogel, R.P. Lachance, M. Fröling, M.J. Antal Jr., J.W. Tester, Thermochemical biofuel production in hydrothermal media: A review of sub- and supercritical water technologies, Energy Environ. Sci., 1 (2008) 32-65.
6   H. Schmieder, J. Abeln, N. Boukis, E. Dinjus, A. Kruse, M. Kluth, G. Petrich, E. Sadri, M. Schacht, Hydrothermal gasification of biomass and organic wastes, J. Supercrit. Fluids, 17 (2000) 145-153.
7   J.G. van Bennekom, R.H. Venderbosch, D. Assink, H.J. Heeres, Reforming of methanol and glycerol in supercritical water, J. Supercrit. Fluids, 58 (2011) 99-113.
8   A.J. Byrd, K.K. Pant, R.B. Gupta, Hydrogen production from glycerol by reforming in supercritical water over Ru/Al2O3 catalyst, Fuel, 87 (2008) 2956-2960.
9   M. Schubert, Catalytic hydrothermal gasification of biomass - Salt recovery and continuous gasification of glycerol solutions, ETH, Zürich, (2010).
10   M.H. Waldner, F. Vogel, Renewable production of methane from woody biomass by catalytic hydrothermal gasification, Ind. Eng. Chem. Res., 44 (2005) 4543-4551.
11   A. Nakamura, E. Kiyonaga, Y. Yamamura, Y. Shimizu, T. Minowa, Y. Noda, Y. Matsumura, Detailed analysis of heat and mass balance for supercritical water gasifications, J. Chem. Eng. Jpn., 41 (2008) 1-12.
12   Y. Yoshida, K. Dowaki, Y. Matsumura, R. Matsuhashi, D. Li, H. Ishitani, H. Komiyama, Comprehensive comparison of efficiency and CO_2 emissions between biomass energy conversion technologies - position of supercriticalwater gasifcation in biomass technologies, Biomass Bioenergy, 25 (2003) 257-272.
13   J.G. van Bennekom, J. Vos, R.H. Venderbosch, M.A.P. Torres, V.A. Kirilov, H.J. Heeres, Z. Knez, M. Bork, J.M.L. Penninger, Supermethanol: Reforming of crude glycerine in supercritical water to produce methanol for re-use in biodiesel plants, in: 17th European Biomass Conference and Exhibition, Hamburg, (2009) 899-902.
14   A.G. Chakinala, D.W.F. Brilman, W.P.M. van Swaaij, S.R.A. Kersten, Catalytic and non-catalytic supercritical water gasification of microalgae and glycerol, Ind. Eng. Chem. Res., 49 (2010) 1113-1122.
15   M.J. Antal Jr., S.G. Allen, D. Schulman, X. Xu, R.J. Divilio, Biomass gasification in supercritical water, Ind. Eng. Chem. Res., 39 (2000) 4040-4053.
16   J.B. Gadhe, R.B. Gupta, Hydrogen production by methanol reforming in supercritical water: Suppression of methane formation, Ind. Eng. Chem. Res., 44 (2005) 4577-4584.
17   S.R.A. Kersten, B. Potic, W. Prins, W.P.M. van Swaaij, Gasification of model compounds and wood in hot compressed water, Ind. Eng. Chem. Res., 45 (2006) 4169-4177.
18   F.L.P. Resende, Supercritical water gasification of biomass, University of Michigan, (2009).
19   G. van Rossum, B. Potic, S.R.A. Kersten, W.P.M. van Swaaij, Catalytic gasification of dry and wet biomass, Catal. Today, 145 (2009) 10-18.
20   D. Xu, S. Wang, X. Hu, C. Chen, Q. Zhang, Catalytic gasification of glycine and glycerol in supercritical water, Int. J. Hydrogen Energy, 34 (2009) 5357-5364.
21   X. Xu, Y. Matsumura, J. Stenberg, M.J. Antal Jr., Carbon-catalyzed gasification of organic feedstocks in supercritical water, Ind. Eng. Chem. Res., 35 (1996) 2522-2530.
22   A. Kruse, E. Dinjus, Influence of salts during hydrothermal biomass gasification: The role of the catalysed water–gas shift reaction, Z. Phys. Chem., 219 (2005) 341-366.
23   J.M.L. Penninger, M. Rep, Reforming of aqueous wood pyrolysis condensate in supercritical water, Int. J. Hydrogen Energy, 31 (2006) 1597-1606.
24   D.C. Elliot, Catalytic hydrothermal gasification of biomass, Biofuels, Bioprod. Biorefin., 2 (2008) 254-265.
25   E. Supp, How to produce methanol from coal, Springer-Verlag, Berlin, (1990).

26   Y. Guo, S.Z. Whang, D.H. Xu, Y.M. Gong, H.H. Ma, X.Y. Tang, Review of catalytic supercritical water gasification for hydrogen production from biomass, Renewable Sustainable Energy Rev., 14 (2010) 334-343.

27   R.R. Davda, A review of catalytic issues and process conditions for renewable hydrogen and alkanes by aqueous-phase reforming of oxygenated hydrocarbons over supported metal catalysts, Appl. Catal., B, 56 (2005) 171-186.

28   D.F. Smith, B.F. Branting, The equilibrium between methanol, carbon monoxide and hydrogen, J. Am. Chem. Soc., 51 (1929) 129-139.

29   V.A. Yakovlev, S.A. Khromova, O.V. Sherstyuk, V.O. Dundich, D.Y. Ermakov, V.M. Novopashina, M.Y. Lebedev, O. Bulavchenko, V.N. Parmon, Development of new catalytic systems for upgraded bio-fuels production from bio-crude-oil and biodiesel, Catal. Today, 144 (2009) 362-366.

30   M.V. Twigg, Catalyst Handbook, second edition ed., Wolfe Publishing Ltd., 1989.

31   G. Soave, Equilibrium constants from a modified Redlich-Kwong equation of state, Chem. Eng. Sci., 27 (1972) 1197-1203.

32   R.C. Reid, J.M. Prausnitz, B.E. Poling, The properties of gases and liquids, Fourth Edition ed., McGraw-Hill, Inc., New york, (1987).

33   Z.Y. Ding, L. Li, D. Wade, E.F. Gloyna, Supercritical water oxidation of NH_3 over a MnO_2/CeO_2 Catalyst, Ind. Eng. Chem. Res., 37 (1998) 1707-1716.

34   A.J. Byrd, R.B. Gupta, Stability of cerium-modified γ-alumina catalyst support in supercritical water, Appl. Catal. A, 381 (2010) 177-182.

35   B. Yan, Supercritical water gasification with Ni/ZrO_2 catalyst for hydrogen production from model wastewater of polyethylene glycol J. Supercrit. Fluids, 50 (2009) 155-161.

4 Methanol synthesis beyond chemical equilibrium

Abstract

In commercial methanol production from syngas, the conversion is thermodynamically limited to 30 – 70% leading to large recycles of nonconverted syngas. This problem can be overcome to a significant extent by *in situ* condensation of methanol during its synthesis which is possible nowadays due to the availability of highly active catalysts allowing for lower reactor temperatures. For the first time, *in situ* methanol condensation at 20 MPa and 473 K was demonstrated visually in a view cell. The condensation of reaction products (mainly methanol and water) drives the equilibrium reactions nearly to completion, as is demonstrated experimentally in a packed bed reactor and supported by thermodynamic calculations. Contrary to conventional methanol synthesis, once-through operation becomes possible avoiding recycling of unconverted syngas, which can be economically beneficial for industrial stakeholders.

4.1 Introduction

Methanol is the simplest of all alcohols and has a wide application range. The global annual production was approximately 38 million metric tons in 2007 and is expected to grow [1]. Methanol is mainly used for the production of bulk chemicals like formaldehyde, acetic acid, and a wide variety of application products including polymers and paints. In addition, methanol has high potential as a clean and renewable energy carrier [2]. Methanol is produced from syngas, a mixture of H_2, CO, and minor quantities of CO_2 and CH_4. Methanol synthesis proceeds in gas-solid catalytic reactors where three reactions at the catalyst surface are important: (i) hydrogenation of CO, (ii) the (reverse) water-gas shift reaction, and (iii) hydrogenation of CO_2:

$CO + 2\ H_2$	$\rightleftharpoons$	CH_3OH	$\Delta_r H^0_{298}$ = -90.64 kJ/mol	(Eq. 1.1)
$CO_2 + H_2$	$\rightleftharpoons$	$CO + H_2O$	$\Delta_r H^0_{298}$ = +41.17 kJ/mol	(Eq. 1.2)
$CO_2 + 3\ H_2$	$\rightleftharpoons$	$CH_3OH + H_2O$	$\Delta_r H^0_{298}$ = -49.47 kJ/mol	(Eq. 1.3)

There is discussion about the actual reactions proceeding in methanol synthesis [3], however, for this research study the contribution of each individual reaction is not important. For the sake of completeness all three reactions are shown. Methanol synthesis is exothermic and reversible. The conversion of $CO+CO_2$ at chemical equilibrium is a function of the pressure and temperature (see Fig. 4.1).
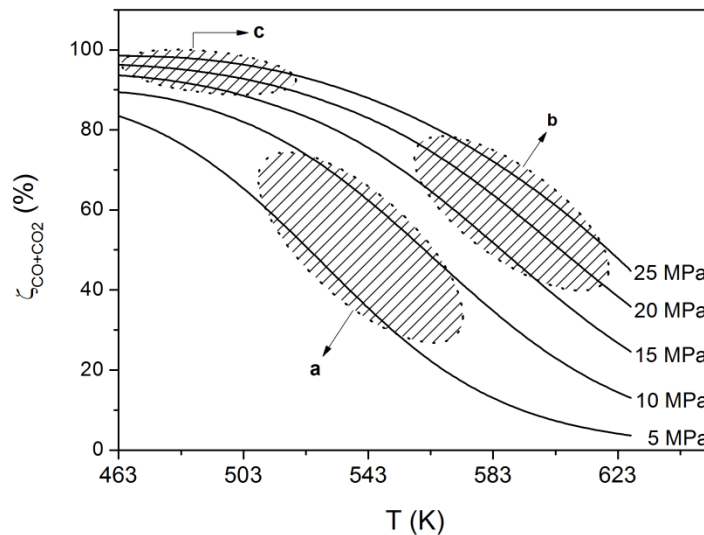
Fig. 4.1 Equilibria in methanol synthesis. Approximate conditions for: Conventional processes (a), BASF's high pressure process (b), this work (c). Syngas: $H_2/CO/CO_2/CH_4$ = 67.0/24.4/3.5/5.1 vol%.

The first large-scale methanol synthesis plant was constructed by BASF in the 1920s and had to be operated at high temperatures (573 – 633 K) to compensate for the low catalyst activity [4, 5]. In order to obtain reasonable conversions high pressures (15 – 25 MPa) were needed. With

the availability of more active Cu based catalysts and advanced syngas purification techniques operation at lower pressures and temperatures became possible. As a result, the so-called *low-pressure* methanol synthesis process (5 – 10 MPa, 490 – 570 K) was developed by ICI in the 1960s. The majority of the high pressure units has been converted to the low pressure system since then [5, 6]. Both methanol synthesis processes require large recycle flows of syngas due to the limited conversion per reactor pass [6].

The development of more active catalysts allows for even lower reactor temperatures (473 > *T* > 520 K) while high reaction rates are maintained [7]. The combination of high pressures (15 – 25 MPa) and low temperatures, which are the envisaged conditions for this research study, favors high equilibrium conversions towards methanol.

Several studies have been conducted to circumvent the limitations imposed by thermodynamic equilibria and mainly involve *in situ* methanol removal. Examples are methanol adsorption on fine alumina powder or the use of a solvent such as tetraethylene glycol, n-butanol, or n-hexane [8-10]. An alternative method is based on the *in situ* separation of reaction products by condensing them on the surface of a condenser inside the reactor, close to the catalyst bed [11]. All methods led to higher syngas conversions, but have main drawbacks such as the introduction of other chemicals, complicated operation, or low space time yields. An attractive concept to move beyond chemical equilibrium is to apply *in situ* condensation of methanol without using adsorbents or additional coolers. Condensation is expected to occur at high pressure and low temperatures. To the authors knowledge, condensation has only been shown indirectly by experimental observations of conversions higher than the equilibrium conversions or calculations based on thermodynamic models, [12-15] though has never been demonstrated visually before.

Here, we provide the proof of principle for methanol condensation at high pressure (20 MPa) and relatively low temperature (473 K) in a so-called view cell with a transparent window to allow visual observation of the methanol synthesis reactions. View cells have been used to investigate phase behavior and precipitation [16-21]. Its potential for chemical reactions and *in situ* spectroscopy has been recognized [22-26], though to the authors knowledge, a view cell has not been used so far to perform reactions with heterogeneous catalysts in a stirred cell configuration. In this study the cell contains a typical commercial heterogeneous methanol catalyst (Cs doped $Cu/ZnO/Al_2O_3$) with high activity.

4.2 Materials and methods

Experiments were performed in a view cell and a packed bed reactor. A schematic representation of the view cell is given in Fig. 4.2. The experiments to visualize condensation were performed in a view cell reactor. The view cell is a high pressure reactor (32 – 64 mL), which can be operated at temperatures up to about 473 K (electrical heating) and pressures up to 60 MPa. A transparent sapphire window allows the observation of the phenomena taking place inside the view cell. The view cell is equipped with either a small basket or a propeller-

shaped stirrer. In all view cell experiments cylindrical catalyst pellets were used with a diameter and height of approximately 5 mm. The catalyst used was a commercial Cs doped $Cu/ZnO/Al_2O_3$ catalyst, but any methanol synthesis catalyst could have been used. The view cell was operated in semi-batch mode at constant pressure (20 MPa) and temperature (473 K). The setup for the view cell contained a gas mixing section which can be used to make any mixture of the connected pure gases. The gas mixture was pressurized and stored in the gas storage bomb. The view cell was fed from the storage bomb. The pressure was maintained in the view cell with a pressure controller (PC). The view cell was operated in semi-batch mode at constant pressure (20 MPa) and temperature (473 K). All reactor exits were closed. The experiments in the view cell were conducted with two home-made gas compositions; $H_2/CO/CO_2/CH_4$ = 65.0/25.0/5.0/5.0 vol% and $H_2/CO/CO_2$ = 70.0/28.1/1.9 vol%.
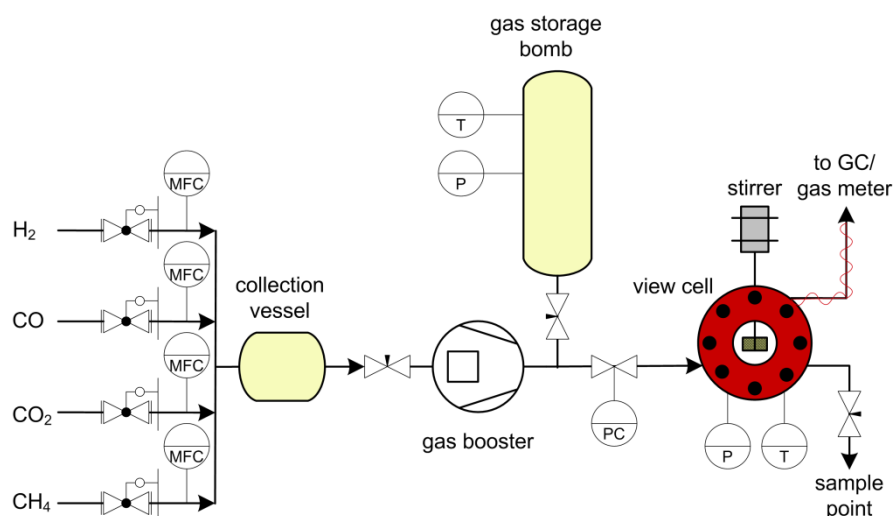
Fig. 4.2 Schematic flow diagram of the view cell setup including the gas mixing section. GC = gas chromatograph.

Detailed descriptions of the packed bed reactor are given in Chapter 5 and 6. The two packed bed reactors were operated in continuous mode and contained an excess of catalyst (approximately 50 g per reactor). The reactor setup consisted of two packed bed reactors. The first packed bed reactor had a sharp temperature rise and a high conversion is already obtained. The second reactor is operated almost isothermally and allows the reaction to proceed till equilibrium. The exit flow was quantified and analyzed. The process conditions and syngas compositions used in the experiments are given in Table 4.1. Syngas 1 resembles a gas which is typically used in methanol synthesis. Syngas 2 has a similar H_2 content but now CO_2 is the main carbon oxide. Such a syngas is interesting as the topic of methanol synthesis from H_2 from water and CO_2 from air is gaining more attention [27].

Table 4.1 Process conditions of the experiments conducted in the packed bed setup.

Syngas	T	P	H_2	CO	CO_2	CH_4
	(K)	(MPa)	(vol%)	(vol%)	(vol%)	(vol%)
1	468 – 543	15 – 20	67.0 – 68.0	24.0 – 24.4	3.0 – 3.5	5.0 – 5.1
2	484 – 543	20	69.9	5.0	20.0	5.1

4.3   Results and discussion

The catalyst pellets were positioned around a propeller-shaped stirrer or placed in a small basket. Prior to the experiment the catalyst was activated by reduction (2 h at 443 K, 2 h at 473 K, 2 h at 493 K, 10 vol% H_2 in N_2, 3 Nm^3/kg cat./h, 0.2 MPa). The initially black (Cu(II) oxide) catalyst (Fig. 4.3A) turned reddish (Fig. 4.3B). There is debate about the active Cu species in methanol synthesis. It can be Cu(0) or Cu(I) oxide, possibly in interaction with the other catalyst constituents [28]. Both species are red and we could not establish which species was observed. The catalyst retains its reddish color during methanol synthesis.
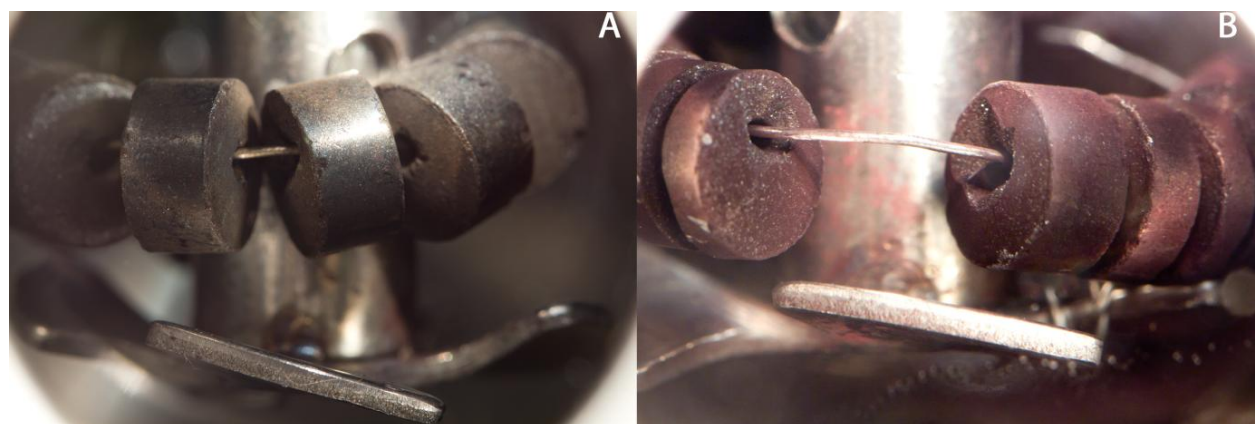
Fig. 4.3 Visual observation of catalyst reduction. Fresh unreduced catalyst (A). The catalyst after reduction (B). Pellet diameter = 5 mm.

The view cell was operated in a semi-batch mode and methanol synthesis was initiated by feeding syngas (H_2/CO/CO_2 = 70.0/28.1/1.9 vol%). The most striking and most relevant observation here is the *in situ* liquid phase formation at 20.0 MPa and 473 K (Fig. 4.4). Conditions for condensation are a function of the syngas composition and liquid formation was also observed at 17.5 MPa and 473 K for a syngas with composition: H_2/CO/CO_2/CH_4 = 65.0/25.0/5.0/5.0 vol%.
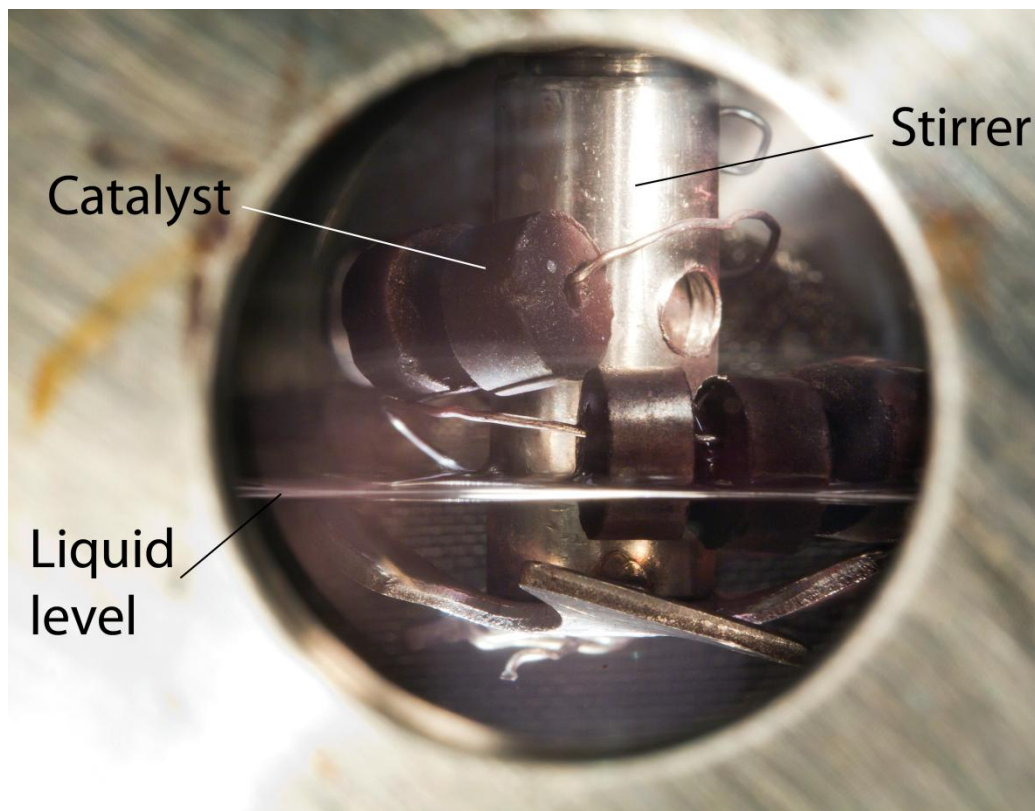
Fig. 4.4 Liquid formation in a view cell. P = 20.0 MPa, T = 473 K, Syngas: $H_2/CO/CO_2$ = 70.0/28.1/1.9 vol%.

Upon prolonged reaction times, the liquid accumulated and part of the catalyst became immersed in the liquid phase which can be seen in the Movies 1 – 3 (see supplementary materials of the original publication in Chem. Eng. Sci. at Science Direct). Screenshots of the movies are given in Fig. 4.5 with explanatory labels. In Movie 1 and 2 the view cell contains a basket with catalyst. The basket has a Teflon body with open cavities to contain catalyst particles. A woven wire mesh of stainless steel was wound around the Teflon body to keep the catalyst in place. In Movie 1 (Fig. 4.5A) the interior of the view cell is visible. The view is slightly tilted due to some technical issues (light reflection) during recording. In reality, the location where the methanol accumulates is the lowest point and bottom of the reactor. The basket contains the catalyst and the formation of the first droplets is shown. It is not clear if the droplets originate from the basket or condense in the back of the view cell and come forward. The first droplets evaporated till the saturated vapor pressure was reached in the entire view cell. As from this moment, a liquid phase remains at the bottom of the view cell.

The liquid level continues to rise after a lasting liquid level was formed. In Movie 2 (Fig. 4.5B) a considerable amount of liquid was formed. The basket was brought to a stop in the movie and the liquid present at the outer wall of the basket reflected the light.

Movie 3, was recorded in the same configuration as shown in Figs. 4.3 and 4.4. The basket was replaced by a stirrer and a catalytic chain. Droplet formation was not observed on the

catalyst particles themselves, but started somewhere in the reactor at probably a slightly colder spot.

Even after complete immersion of the catalyst particles in the liquid, the methanol synthesis reaction was still ongoing as fresh syngas feed was bubbling through the liquid. The liquid phase consists of mainly methanol and water, the exact composition being a function of conversion, process conditions, and syngas composition.
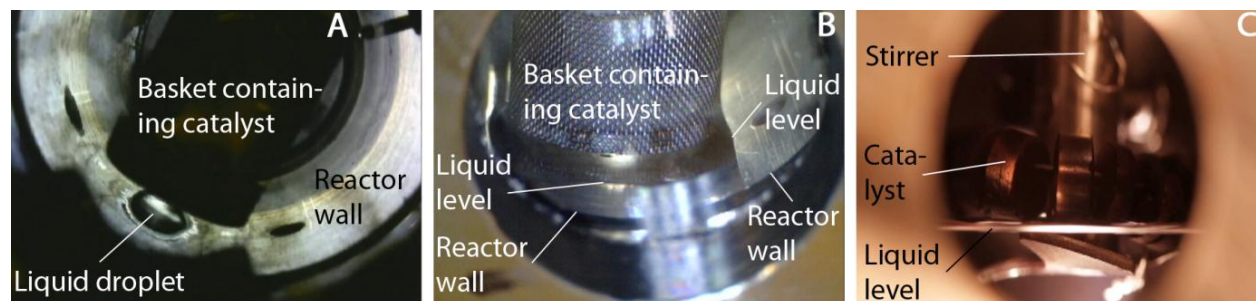
Fig. 4.5 Screenshots of the movies to visualize methanol condensation during synthesis. Formation of the first droplets, view is slightly tilted (A). A significant amount of liquid has been formed (B). Liquid formation with catalyst directly attached to the propeller shaped stirrer (C).

Further experimental studies to support the visual observations in the view cell and to use *in situ* condensation for achieving higher methanol conversions than at conventional conditions were conducted in a packed bed reactor (see Table 4.1). These experiments will be dealt with in detail in Chapter 5 and 6, but for clarity some results are also presented in this chapter. Experiments with different flow rates were conducted for syngas 1 to ensure that equilibrium was reached and that the reactions were not conducted in the kinetic regime. Methanation and the formation of higher hydrocarbons were negligible. The $CO+CO_2$ conversion at 468 K was 99.5% for syngas 1, which is 7.7% higher than the equilibrium conversion at 7.5 MPa (a typical pressure for conventional methanol synthesis). For syngas 2, the difference between methanol synthesis at 20 and 7.5 MPa is more pronounced. The $CO+CO_2$ conversion at 484 K was 92.5% which is 46.9% higher than the equilibrium conversion at 7.5 MPa. The model used to calculate the equilibria is described in Chapter 5.

The experimental and predicted equilibrium conversions are shown in Fig. 4.6A and Table 4.2). At temperatures above 495 K for syngas 1 and 507 K for syngas 2 only a gas phase is present, while at lower temperatures condensation occurs. Methanol production continues in the two phase system until phase and chemical equilibrium are reached.
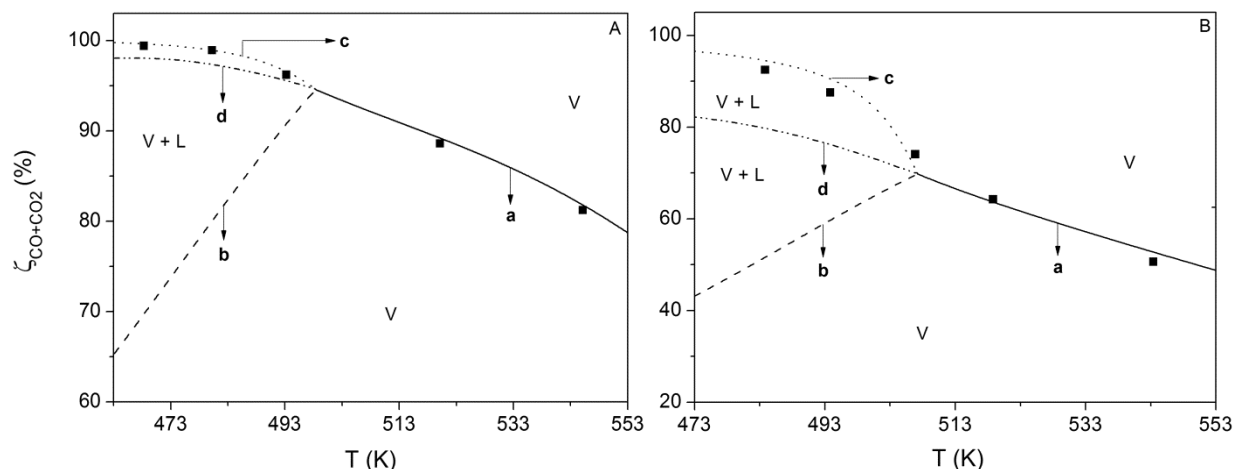
Fig. 4.6 Equilibrium diagrams for methanol synthesis. Syngas 1 (A): $H_2/CO/CO_2/CH_4$ = 67.0/24.4/3.5/5.1 vol%, P = 19.7 MPa (equilibrium calculation). Syngas 2 (B): $H_2/CO/CO_2/CH_4$ = 69.9/5.0/20.0/5.1 vol%, P = 20.3 MPa (equilibrium calculation). Gas phase equilibrium curve (a), dew point curve (b), equilibrium curve including liquid formation (c), extrapolation of the gas phase equilibrium curve (d). Symbols: experimental data; lines: model results.

Table 4.2 Experimental results of methanol synthesis in the packed bed reactor.

	Conditions			Composition exit streams						Purity[a]	Conv. and C-bal.		
	T	P	$GHSV$	H_2	CO	CO_2	C_xH_y	Org.[e]	H_2O	MeOH	ζ_{CO+CO2}	ζ_{H2}	C-bal.
	(K)	(MPa)	(h^{-1})			(vol%)		(g/h)	(g/h)	(mol%)	(%)	(%)	(%)
1^b	469	15.3	$1.1 \cdot 10^3$	69.0	0.0	1.9	29.1	22.2	1.7	99.7	98.8	82.3	96
2^b	470	15.3	$2.2 \cdot 10^3$	68.7	0.0	2.5	28.8	42.9	3.0	99.5	98.4	82.7	94
3^c	468	20.7	$1.7 \cdot 10^3$	59.5	0.1	0.9	39.5	35.0	3.3	99.5	99.5	88.5	93
4^c	469	19.2	$1.7 \cdot 10^3$	59.3	0.3	1.3	39.1	36.3	3.3	99.6	99.3	88.5	96
5^c	480	20.8	$1.6 \cdot 10^3$	61.5	0.1	2.1	36.3	33.6	3.0	99.3	98.9	87.2	94
6^c	493	19.7	$1.7 \cdot 10^3$	63.4	0.3	6.1	30.3	33.9	2.7	99.2	96.2	84.1	93
7^c	520	19.6	$1.7 \cdot 10^3$	65.8	1.5	11.6	21.1	31.9	1.9	98.6	88.6	76.2	95
8^c	545	19.5	$1.7 \cdot 10^3$	66.2	4.0	15.1	16.7	30.0	1.4	97.8	81.2	69.8	97
9^d	484	20.5	$5.3 \cdot 10^2$	47.6	0.1	19.7	37.1	10.4	4.1	99.9	92.5	91.6	103
10^d	494	20.5	$5.3 \cdot 10^2$	49.7	0.2	22.7	30.4	9.4	4.3	99.9	87.5	88.8	99
11^d	507	20.4	$7.5 \cdot 10^2$	58.5	0.3	22.8	18.5	10.7	4.6	99.9	74.1	76.4	98
12^d	519	20.0	$2.0 \cdot 10^3$	64.3	0.4	21.9	12.7	25.3	11.9	99.9	64.2	63.1	99
13^d	543	20.0	$2.0 \cdot 10^3$	66.2	1.1	22.5	10.0	18.9	8.9	99.9	50.6	50.4	97

[a]Methanol purity of the organic fraction.
[b]Experiments were conducted with $H_2/CO/CO_2/CH_4$ = 68.0/24.0/3.0/5.0 vol%.
[c]Experiments were conducted with $H_2/CO/CO_2/CH_4$ = 67.0/24.4/3.5/5.1 vol%.
[d]Experiments were conducted with $H_2/CO/CO_2/CH_4$ = 69.9/5.0/20.0/5.1 vol%.
[e]Total mass flow of organic components leaving the system.

The conversion of $CO+CO_2$ is nearly complete for syngas 1 at the lowest temperatures in the range. The experimental conversions coincide nicely with the conversion predicted by the model. The conversion of all components decreased with increasing temperature as dictated by

thermodynamics. The effect of condensation was the most pronounced for syngas 2 (Fig. 4.6B). Here, the experimental conversion is even 12.7% higher than the extrapolated gas phase equilibrium curve (ζ = 79.8% vs. 92.5% at 484 K).

As shown above, methanol synthesis with *in situ* condensation requires elevated pressures and is a function of the gas composition. For syngas 1 a dew point is obtained at 473 K for pressures over 12 MPa (based on thermodynamic calculations). Compression of syngas to such elevated pressures is an energy intensive process that will negatively affect process economics. A promising technique to avoid the compression step is the reforming of suitable feedstocks in supercritical water [29, 30]. This technology produces high pressure syngas without gas compression and can be operated energetically efficient [31]. The syngas composition is a function of the process conditions and the use of a catalyst. In Table 4.3 some typical gas compositions for glycerol reforming are given. More information on gas compositions obtained in glycerol reforming can be found in Chapters 2, 3, and 7. The gas can subsequently be used to produce methanol.

Table 4.3 Gas compositions obtained in glycerol reforming.

	Catalyst	T	P	[Glycerol]	H_2	CO	CO_2	C_xH_y
		(K)	(MPa)	(wt%)	(vol%)	(vol%)	(vol%)	(vol%)
1	-	743 – 923	25 ± 2	15 – 20	26 – 51	20 – 37	6 – 22	9 – 30
2	Pt/CeZrO$_2$	623 – 931	25 ± 2	10	51 – 56	0 – 2	34 – 37	6 – 13
3	CuZn	833 – 954	25 ± 2	10	42 – 60	12 – 14	24 – 26	3 – 19
4	Ni/CaO-6Al$_2$O$_3$	658 – 998	26 ± 2	4 – 10	21 – 67	1	30 – 39	2 – 39

4.4 Conclusion

High pressure methanol synthesis with *in situ* formation of a liquid phase is visualized for the first time in a view cell reactor supported by experiments in a packed bed reactor. The experimental data obtained in the packed bed reactor were successfully supported by thermodynamic modeling. These findings can have some positive consequences for methanol synthesis. Higher conversions than predicted by gas phase thermodynamics are obtained and, at appropriate conditions, almost complete conversion of the limiting component is achieved. As a consequence, recycle streams and associated bleed/purge streams are not required, a broader range of syngas composition may be applied and throughputs for a given reactor volume may be increased, leading to higher methanol production levels. A possible additional advantage compared to conventional low pressure operation is enhanced reaction rates due to higher partial pressures of the reactants, though this needs further experimental confirmation.

4.5 References

1   M. Berggren, Methanol industry in focus, milestones, www.methanol.org (accessed 19 January 2012)
2   G.A. Olah, A. Goeppert, G.K.S. Prakash, Beyond oil and gas: The methanol economy, Wiley-VCH, Weinheim, (2006).
3   G.C. Chinchen, P.J. Denny, J.R. Jennings, M.S. Spencer, K.C. Waugh, Synthesis of methanol. Part 1. Catalysts and kinetics, Appl. Catal., 36 (1988) 1-65.
4   A. Mittasch, K. Winkler, M. Pier, Verfahren zur Gewinnung organischer Verbindungen durch katalytische Gasreaktionen, German patent 441433, (1923).
5   J. Skrzypek, J. Stoczynski, S. Ledakowicz, Methanol synthesis, Polish Scientific Publishers PWN, Warsaw, (1994).
6   E. Supp, How to produce methanol from coal, Springer-Verlag, Berlin, (1990).
7   Y. Zhang, Q. Sun, J. Deng, D. Wu, S. Chen, A high activity Cu/ZnO/Al2O3 catalyst for methanol synthesis: Preparation and catalytic properties, Appl. Catal., A, 158 (1997).
8   P. Reubroycharoen, T. Vitidsant, K. Asamic, Y. Yoneyama, N. Tsubaki, Accelerated methanol synthesis in catalytically active supercritical fluid, Catal. Commun., 4 (2003) 461-464.
9   K.R. Westerterp, M. Kuczynski, C.H.M. Kamphuis, Synthesis of methanol in a reactor system with interstage product removal, Ind. Eng. Chem. Res., 28 (1989) 763-770.
10   M. Kuczynski, M.H. Oyevaar, R.T. Pieters, K.R. Westerterp, Methanol synthesis in a countercurrent gas-solid-solid trickle flow reactor, an experimental study, Chem. Eng. Sci., 42 (1987) 1887-1898.
11   B. Haut, V. Halloin, H.B. Amor, Development and analysis of a multifunctional reactor for equilibrium reactions: Benzene hydrogenation and methanol synthesis Chem. Eng. Process., 43 (2004) 979-986.
12   M. Castier, P. Rasmussen, A. Fredenslund, Calculation of simultaneous chemical and phase equilibria in nonideal systems, Chem. Eng. Sci., 44 (1989) 237-248.
13   J.B. Hansen, F. Joensen, High conversion of synthesis gas into oxygenates, in: A. Holmen (Ed.) Proceeding of the NGCS, Elsevier Science Publishers B.V., Oslo, (1991) 457-467.
14   E.L. Sorensen, J. Perregaard, Condensing methanol synthesis and ATR - The technology choice for large-scale methanol production, Stud. Surf. Sci. Catal., 147 (2004) 7-12.
15   H.F.A. Topsoe, J.B. Hansen, Method of preparing methanol, United States patent 5262443, (1993).
16   M.L. Japas, E.U. Franck, High pressure phase equilibria and PVT-data of the water-nitrogen system to 673 K and 250 MPa, Ber. Bunsen Ges. Phys. Chem., 89 (1985) 793-800.
17   F.J. Armellini, J.W. Tester, Experimental methods for studying salt nucleation and growth from supercritical water, J. Supercrit. Fluids, 4 (1991) 254-264.
18   J.N. Jaubert, P. Borg, L. Coniglio, D. Barth, Phase equilibria measurements and modeling of EPA and DHA ethyl esters in supercritical carbon dioxide, J. Supercrit. Fluids, 20 (2001) 145-155.
19   T. Adrian, S. Oprescu, G. Maurer, Experimental investigation of the multiphase high-pressure equilibria of carbon dioxide-water-(1-propanol), Fluid Phase Equilibr., 132 (1997) 187-203.
20   J.A. Briones, J.C. Mullins, M.C. Thies, B.U. Kim, Ternary phase equilibria for acetic acid-water mixtures with supercritical carbon dioxide, Fluid Phase Equilib., 36 (1987) 235-246.
21   P.L. Cheong, D. Zhang, K. Ohgaki, B.C.Y. Lu, High pressure phase equilibria for binary systems involving a solid phase, Fluid Phase Equilib., 29 (1986) 555-562.
22   S. Lefèvre, O. Boutin, J.H. Ferrasse, L. Malleret, R. Faucherand, A. Viand, Thermodynamic and kinetic study of phenol degradation by a non-catalytic wet air oxidation process, Chemosphere, 84 (2011) 1208-1215.
23   M. Caravati, J.D. Grunwaldt, A. Baiker, Benzyl alcohol oxidation in supercritical carbon dioxide: Spectroscopic insight into phase behaviour and reaction mechanism, Phys. Chem. Chem. Phys., 7 (2005) 278-285.
24   R.N. Occhiogrosso, M.A. McHugh, Critical-mixture oxidation of cumene, Chem. Eng. Sci., 42 (1987) 2478-2481.
25   T. Moreno, M.A.M. Lopez, I.H. Illera, C.M. Piqueras, A.S. Arranz, J.G. Serna, M.J. Cocero, Quantitative Raman determination of hydrogen peroxide using the solvent as internal standard: Online application in the direct synthesis of hydrogen peroxide, Chem. Eng. J., 166 (2011) 1061-1065.

26   M.S. Schneider, J.D. Grunwaldt, T. Bürgi, A. Baiker, High pressure view-cell for simultaneous in situ infrared spectroscopy and phase behavior monitoring of multiphase chemical reactions, Rev. Sci. Instrum., 74 (2003) 4121-4128.

27   C. Graves, S.D. Ebbesen, M. Mogensen, K.S. Lackner, Sustainable hydrocarbon fuels by recycling CO_2 and H_2O with renewable or nuclear energy, Renewable Sustainable Energy Rev., 15 (2011) 1-23.

28   J.B. Hansen, P.E.H. Nielsen, Methanol Synthesis, in: G. Ertl, H. Knözinger, F. Schüth, J. Weitkamp (Eds.) Handbook of heterogeneous catalysis, Wiley-VCH Verlag, Weinheim, (2008) 2920-2949.

29   A. Kruse, Supercritical water gasification, Biofuels, Bioprod. Biorefin., 2 (2008) 415-437.

30   M. Modell, Gasification and liquefaction of forest products in supercritical water, in: R.P. Overend (Ed.) Fundamentals of thermochemical biomass conversion Elsevier, London, (1985).

31   A. Nakamura, E. Kiyonaga, Y. Yamamura, Y. Shimizu, T. Minowa, Y. Noda, Y. Matsumura, Detailed analysis of heat and mass balance for supercritical water gasifications, J. Chem. Eng. Jpn., 41 (2008) 1-12.

5 Modeling and experimental studies on phase and chemical equilibria in high pressure methanol synthesis

Abstract

A solution method was developed to calculate the simultaneous phase and chemical equilibria in high pressure methanol synthesis (P = 20 MPa, 468 < T < 548 K). Algorithms were developed that explicitly consider the existence of a condensed phase and include dew point calculations. A modification of the Soave-Redlich-Kwong equation of state was used to correct for nonideal effects. Binary interaction coefficients were derived from literature data on high pressure binary vapor-liquid equilibria. Predicted equilibrium conversions, with and without the formation of a liquid phase, were successfully verified with new experimental results on high pressure methanol synthesis obtained in a packed bed methanol synthesis reactor. Experimental data coincide very well with model predictions for the equilibrium conversion and gas composition. Remarkably, in some situations the model calculations appeared to predict condensation followed by a disappearing liquid phase (retrograde-like behavior) with increasing extent of the methanol synthesis reactions. Finally, at equilibrium only a vapor phase remained present.

5.1 Introduction

Methanol is an important bulk chemical with an estimated global annual production of 38 million metric tons in 2007 [1]. Methanol is mostly produced from syngas, a gas consisting of predominantly H_2 and CO usually obtained from natural gas. Three reactions are important in the synthesis of methanol: the hydrogenation of CO (Eq. 1.1), the reverse water-gas shift (WGS) reaction (Eq. 1.2), and the hydrogenation of CO_2 (Eq. 1.3):

$$CO + 2\,H_2 \;\rightleftharpoons\; CH_3OH \qquad\qquad \Delta_r H^0_{298} = \text{-90.64 kJ/mol} \qquad\qquad \text{(Eq. 1.1)}$$

$$CO_2 + H_2 \;\rightleftharpoons\; CO + H_2O \qquad\qquad \Delta_r H^0_{298} = \text{+41.17 kJ/mol} \qquad\qquad \text{(Eq. 1.2)}$$

$$CO_2 + 3\,H_2 \;\rightleftharpoons\; CH_3OH + H_2O \qquad \Delta_r H^0_{298} = \text{-49.47 kJ/mol} \qquad\qquad \text{(Eq. 1.3)}$$

Both methanol synthesis reactions (Eqs. 1.1 and 1.3) are exothermic and proceed with volume contraction. All three reactions are reversible and their progress is thermodynamically limited.

In commercial methanol synthesis, roughly two processes (differing in process conditions) can be distinguished. From the 1920s to the 1960s, methanol was synthesized at high pressures and high temperatures ($P > 15$ MPa and $T > 573$ K). From the 1960s onward, more active catalyst became available, allowing for lower operating pressures and temperatures ($P < 10$ MPa and $T < 573$ K), and thus reduced gas compression duty, less formation of byproducts, and cheaper equipment [2, 3]. Thermodynamically, the most favorable conditions for methanol synthesis are high pressures and relatively low temperatures ($P > 15$ MPa and $T < 523$ K). Methanol synthesis at these conditions is the focus of the Supermethanol project [4] and has not been explored experimentally yet. At these conditions methanol can condense to form a liquid phase in the reactor [5-7]. Condensation of methanol is described in detail in Chapter 4. Formation of such a liquid phase has severe consequences not only for design of methanol reactors but also for modeling of the equilibria in methanol synthesis, as restrictions due to chemical equilibrium are, to a large extent, eliminated in the presence of a dew point [6]. Catalysts may deactivate faster with condensation, although no problems concerning mechanical integrity and activity of the catalyst were observed during 5 months of operation [6].

Equilibrium modeling in methanol synthesis has been conducted by several researchers. Graaf *et al.* measured and modeled equilibria at conditions ranging from 1 to 8 MPa and from 473 to 543 K [8]. Equilibrium data could be described most accurately using the Soave-Redlich-Kwong (SRK) equation of state (EOS). Danes and Geana modeled the equilibria in high pressure methanol synthesis for stoichiometric syngases at 10 – 41 MPa and 523 – 673 K [9]. The most accurate description of the experimental data was obtained using a modified Himpan EOS. Skrzypek *et al.* conducted equilibrium calculations for a large range of pressures (5 – 30 MPa) and temperatures (425 – 675 K), but in spite of the high pressure in combination with low temperatures (425 – 500 K) condensation was not considered [10]. Chang *et al.* found that their equilibrium model based on the SRK EOS or Peng-Robinson EOS did not converge at 473 K and

30.0 MPa, most probably due to condensation [5]. This result attracted attention, and methanol synthesis at these conditions with a syngas composition of $H_2/CO/CO_2/CH_4$ = 74/15/8/3 vol% became one of the reference cases in several publications on modeling simultaneous phase and chemical equilibria purely on a theoretical basis. No experimental data were used or available.

Castier *et al.* developed an equilibrium model with a stoichiometric formulation based on minimization of the Gibbs free energy followed by checking the phase stability with the tangent plane criterion [11]. A similar approach for checking the phase stability was used by Stateva and Wakeham with a newly developed algorithm for solution of chemical equilibria in any number of prescribed phases [12]. Gupta *et al.* derived a set of coupled nonlinear equations that describe the stability and multiphase behavior of both nonreacting and reacting systems [13]. Jalali and Seader adopted a nonlinear optimization method using homotopy continuation to locate all minima in the Gibbs free energy function to ascertain a global stable solution [14]. In the method by Avami and Saboohi, the extended τ-method was used for phase identification and phase and chemical equilibrium calculations [15]. Except for Gupta *et al.* [13], all authors employ the SRK EOS for the methanol synthesis case. None of these models is validated with experimental data at relevant process conditions. Although the models do take into account formation of a liquid phase, calculation of the dew point as a function of the extent of the reactions is not considered. For reactor and catalyst design it is important to know when and where condensation starts. When methanol synthesis is conducted with *in situ* condensation, operating conditions may be selected based on the difference between the conversion at phase and chemical equilibrium and the conversion at which condensation starts. The larger the difference the higher the overall driving force in methanol synthesis. The actual reaction rates result from a tradeoff between two opposing effects: (i) the rate constants increase with increasing temperature, while (ii) the driving forces at the dew point decrease with increasing temperature.

In this chapter a solution model is reported based on a modified SRK EOS, suited for polar mixtures, which enables calculation of the simultaneous phase and chemical equilibria that occur during high pressure methanol synthesis. The model includes, in contrast to the models known from the literature, the calculation of the dew point as a function of temperature and conversion occurring in methanol synthesis. The binary interaction coefficients of the EOS were fitted to literature data on binary systems at relevant temperatures for methanol synthesis. Notably, validation of the model was obtained from new experimental results on high pressure methanol synthesis (P = 20 MPa, 468 < T < 548 K) from two syngas mixtures, one with H_2 as the limiting component and the other with $CO+CO_2$ as the limiting components.

5.2 Thermodynamic framework

5.2.1 Equation of state

A modification of the SRK EOS was used in this work. The SRK EOS was originally developed for hydrocarbon systems [16]. Mathias showed that vapor-liquid equilibria (VLE) in a polar system

containing water and methanol, an important binary mixture in methanol synthesis, can be accurately described using his modification [17]. For pure substances the original SRK EOS reads

$$P = \frac{RT}{V-b} - \frac{a(T)}{V(V+b)}$$
(Eq. 5.1)

Or written in a different way

$$Z^3 - Z^2 + (A - B - B^2)Z - AB = 0$$
(Eq. 5.2)

where A and B are auxiliary variables. All variables are defined in Section 5.8. Values for a and b (see Eq. 5.1) are calculated using critical temperatures, critical pressures, and acentric factors (see Table A.1 in Appendix A). When mixtures are involved, a and b become composition dependent; furthermore a is temperature dependent. For each component of the mixture a_i and b_i read

$$a_i(T) = a_{c,i}\alpha_i(T)$$
(Eq. 5.3)

$$b_i = 0.08664 \frac{RT_{c,i}}{P_{c,i}}$$
(Eq. 5.4)

a_i (Eq. 5.3) is composed of a critical parameter, $a_{c,i}$,

$$a_{c,i} = 0.42747 \frac{R^2 T_{c,i}^2}{P_{c,i}}$$
(Eq. 5.5)

and a temperature dependent parameter, α_i.

$$\alpha_i^{0.5} = 1 + m_i\left(1 - \sqrt{T_{R,i}}\right) - p_i(1 - T_{R,i})(0.7 - T_{R,i})$$
(Eq. 5.6)

In comparison with the SRK EOS, an additional parameter, p_i, is added to α_i to correct for the presence of polar components. The polarity correction parameter, p_i, is empirical and improves prediction of the vapor pressure of polar substances of the original SRK EOS [17]. The parameter m_i was obtained by fitting the α_i equation to a detailed set of pure hydrocarbon vapor pressure data [18].

$$m_i = 0.48508 + 1.55191\omega_i - 0.15613\omega_i^2$$
(Eq. 5.7)

Mathias adapted Eq. 5.3 for components at supercritical temperatures [17]. However, this α_i is not considered here because it proved to be less accurate in the description of binary VLE.

The SRK EOS of pure fluids is extended to mixtures according to the concept of a *one-fluid* mixture. Then, Eq. 5.1 retains its original form and the mixture parameters are calculated using simple mixing rules with a quadratic dependence on the mole fractions.

$$a = \sum_{i=1}^{n}\sum_{j=1}^{n} y_i y_j a_{ij}$$

(Eq. 5.8)

Binary interaction parameters (k_{ij}, see Eq. 5.9) are empirical parameters and take into account the difference in the interaction of unlike molecules. They are used to obtain the most accurate fit of the EOS to experimental VLE.

$$a_{ij} = \sqrt{a_i a_j}\,(1-k_{ij})$$

(Eq. 5.9)

For b the original mixing rules from Soave are used without binary interaction parameters [16].

$$b = \sum_{i=1}^{n} y_i b_i$$

(Eq. 5.10)

Then the fugacity coefficient can be obtained from [19]

$$\ln \phi_i = \frac{1}{RT}\int_{V}^{\infty}\left[\left(\frac{\partial P}{\partial n_i}\right)_{T,V,n_{j\neq i}} - \frac{RT}{V}\right]dV - \ln Z$$

(Eq. 5.11)

resulting in the following equation for the fugacity of the vapor phase [20]:

$$\ln \phi_i^V = \frac{b_i}{b}(Z-1) - \ln(Z-B) - \frac{A}{B}\left[\frac{2\sum_{j=1}^{n} y_j a_{ij}}{a} - \frac{b_i}{b}\right]\ln\left(1+\frac{B}{Z}\right)$$

(Eq. 5.12)

5.2.2 Vapor-liquid equilibria (dew point calculations)

For a vapor-liquid multicomponent mixture at equilibrium the fugacities for components in the liquid and vapor phase are equal. The fugacity of component i in the vapor phase is related to the pressure via the fugacity coefficient

$$\phi_i^V = \frac{f_i^V}{y_i P} \tag{Eq. 5.13}$$

and is calculated using the modified SRK EOS. At the high pressure applied here, an activity coefficient approach to calculate the fugacity of the components in the liquid phase is inappropriate [21]; therefore, an EOS approach is used to calculate the fugacity of the liquid phase as well:

$$\phi_i^L = \frac{f_i^L}{x_i P} \tag{Eq. 5.14}$$

A dew point is reached in a system when, for each component, the following conditions are fulfilled:

$$y_i \phi_i^V = x_i \phi_i^L \tag{Eq. 5.15}$$

5.2.3 Combined phase and chemical equilibria calculations

Starting with a given syngas composition, calculation of the equilibrium composition, including condensation, requires the simultaneous solution of a set of equations that describe the chemical and phase equilibria. The equilibrium constants for reactions 1, 2, and 3 (Eqs. 1.1-1.3) are based on fugacities and given by Graaf *et al.* [8]:

$$K_{f,1} = \left[\frac{f_{CH_3OH}}{f_{CO}f_{H_2}^2}\right]_{eq} = \left[\frac{\phi_{CH_3OH}}{\phi_{CO}\phi_{H_2}^2}\right]_{eq} \cdot \left[\frac{P_{CH_3OH}}{P_{CO}P_{H_2}^2}\right]_{eq} = K_{\phi,1} \cdot K_{P,1} \tag{Eq. 5.16}$$

$$K_{f,2} = \left[\frac{f_{CO}f_{H_2O}}{f_{CO_2}f_{H_2}}\right]_{eq} = \left[\frac{\phi_{CO}\phi_{H_2O}}{\phi_{CO_2}\phi_{H_2}}\right]_{eq} \cdot \left[\frac{P_{CO}P_{H_2O}}{P_{CO_2}P_{H_2}}\right]_{eq} = K_{\phi,2} \cdot K_{P,2} \tag{Eq. 5.17}$$

$$K_{f,3} = K_{f,1} \cdot K_{f,2} = K_{\phi,1} \cdot K_{P,1} \cdot K_{\phi,2} \cdot K_{P,2} \tag{Eq. 5.18}$$

Thermodynamically, two reactions are sufficient to calculate the equilibrium composition. If the reactions given in Eq. 1.1 and Eq. 1.2 are at equilibrium, then the reaction given in Eq. 1.3 is automatically at equilibrium (see Eq. 5.18). $K_{f,h}$ is equal to $K_{P^0,h}$. By definition, $K_{P^0,h}$ is a function of the temperature only, and its value is determined from thermodynamic data. Graaf *et al.* determined smoothed relations for the equilibrium constants for the temperature range of $473 - 573$ K [8]:

$$K_{P^0,1} = 10^{\left(\frac{5139}{T} - 12.621\right)} \tag{Eq. 5.19}$$

$$K_{P^o,2} = 10^{\left(\frac{-2073}{T} + 2.029\right)}$$ (Eq. 5.20)

Methanol synthesis including liquid formation thus comprises 3 reactions (Eqs. 1.1-1.3) and 6 phase equilibrium equations, involving CO, CO_2, H_2, CH_4, methanol, and water. CH_4 is considered as inert. In one of the gases used for experimental validation (see Section 5.5), C_2H_6 is present which is also considered as inert. In the equilibrium calculation for this gas mixture the CH_4 concentration includes both CH_4 and C_2H_6. The distribution of the components over the vapor and liquid phase is calculated with the element and inert balances. The element balances for carbon, hydrogen, and oxygen are, respectively:

$$\sum_{i=1}^{5} F_{C,i}^{V,in} = \sum_{i=1}^{5} F_{C,i}^{V} + \sum_{i=1}^{5} F_{C,i}^{L}$$ (Eq. 5.21)

$$\sum_{i=1}^{5} F_{H,i}^{V,in} = \sum_{i=1}^{5} F_{H,i}^{V} + \sum_{i=1}^{5} F_{H,i}^{L}$$ (Eq. 5.22)

$$\sum_{i=1}^{5} F_{O,i}^{V,in} = \sum_{i=1}^{5} F_{O,i}^{V} + \sum_{i=1}^{5} F_{O,i}^{L}$$ (Eq. 5.23)

The inert balance for CH_4 is:

$$F_{CH_4}^{V,in} = F_{CH_4}^{V} + F_{CH_4}^{L}$$ (Eq. 5.24)

To calculate the equilibria, a set of equations including the two chemical equilibrium equations (Eqs. 5.16 and 5.17), 6 phase equilibrium concentrations (Eq. 5.15), 3 element balances (Eqs. 5.21-5.23), and an inert balance (Eq. 5.24) is solved simultaneously.

5.3 Determination of k_{ij} and validation of the modified SRK EOS

Binary interaction parameters (k_{ij}, see Eq. 5.9) are empirical parameters and take into account the difference in the interaction of unlike molecules. Their importance lies in their ability to make a particular EOS predict the correct phase behaviour [19]. Binary interaction parameters are temperature dependent and cannot be found in the literature for the binary pairs involved in methanol synthesis at temperatures around 473 K. Therefore the binary interaction parameters were fitted to literature data measured at relevant temperatures for methanol synthesis.

The liquid phase in methanol synthesis is primarily a binary mixture of water and methanol (*vide infra*). Furthermore, the vapor phase at equilibrium contains a significant amount of methanol at 20 MPa. To have an accurate description of the methanol synthesis system a good description of the water-methanol VLE is required. The binary interaction coefficient was fitted to literature data obtained at 473 and 523 K [22]. The fit is shown in Fig. 5.1 using k_{ij} = -0.075. Although only 'simple' mixing rules are applied an accurate fit is obtained.
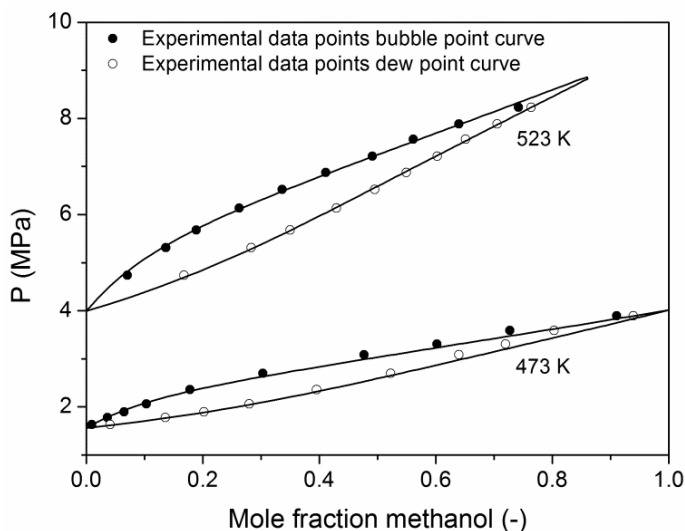
Fig. 5.1 VLE of water and methanol. Symbols: experimental data [22]; lines: model predictions using k_{ij} = -0.075.

Binary interaction coefficient for VLE of methanol and H_2, CO, CO_2, and CH_4 respectively were fitted to VLE data from Brunner *et al.* [23]. The experimental data points for each binary mixture were selected at temperatures the closest to methanol synthesis conditions, see Fig. 5.2 and Table A.2 in Appendix A for the binary interaction coefficients found. Also here, the behavior of the VLE is described qualitatively correct, but the discrepancies between the experimental data and the model predictions are somewhat larger than for the water-methanol system. The H_2, CO, and CH_4 dew point curves are accurately predicted, while the predictions of the bubble point curves are less accurate. For CO_2 the number of data points is limited. The qualitative

description of the system is good, but both the prediction of the dew point curve and the bubble point curve differ from the experimental values.
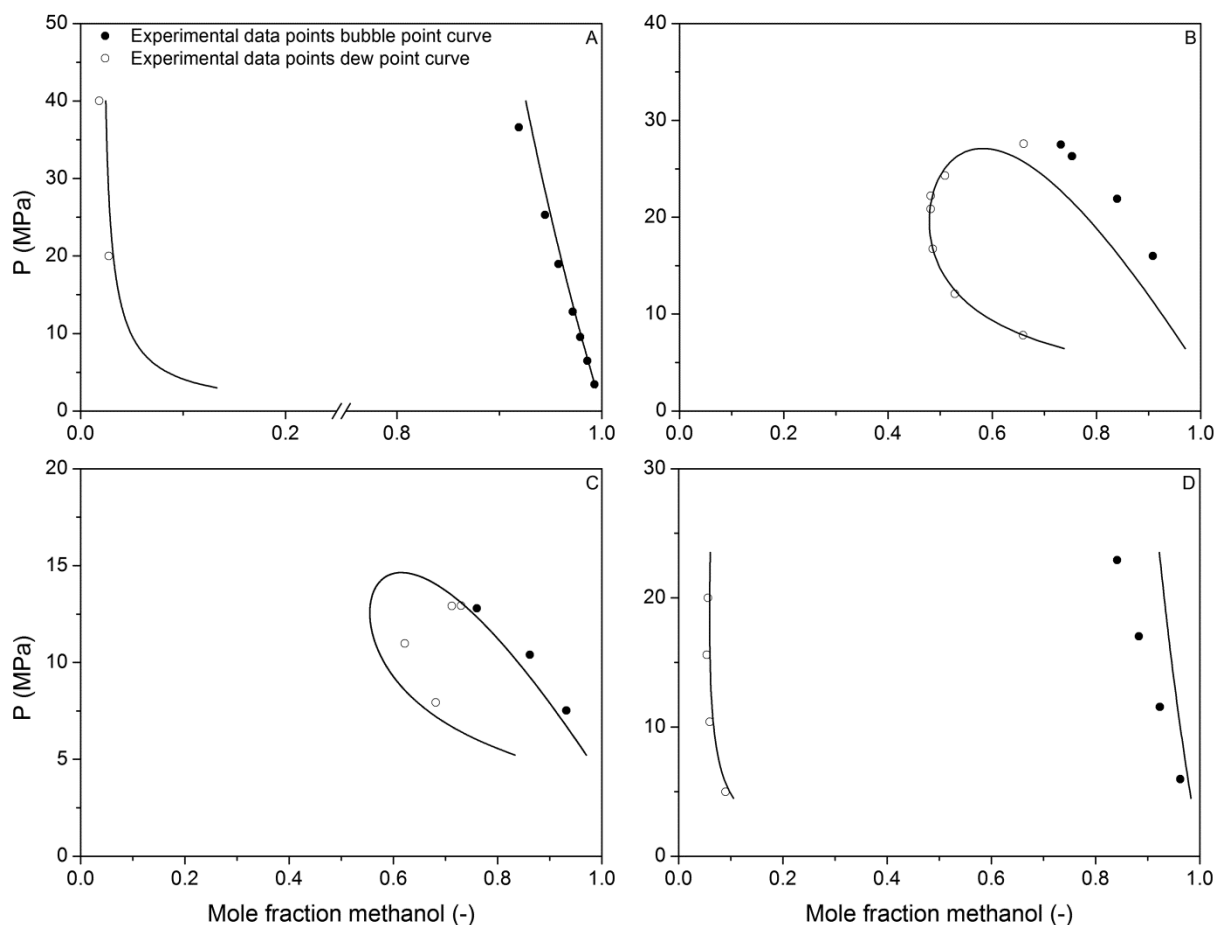
Fig. 5.2 VLE diagrams of methanol-H_2 at 373 K (A, k_{ij} = -0.125), methanol-CO at 473 K (B, k_{ij} = -0.37), methanol-CO_2 at 473 K (C, k_{ij} = 0.10), methanol-CH_4 at 373 K (D, k_{ij} = 0.046). Symbols: experimental data [23]; lines: model predictions.

In Fig. 5.3 the solubility of H_2, CO, and CH_4 in water and the VLE of the CO_2-water binary mixture are given. The predictions of the solubility data and the VLE of the water-CO_2 binary mixture are very accurate. The solubility predictions for CO differ slightly from the experimental values, but the number of data points is limited. As for methanol binary systems (Fig. 5.1 and 5.2) the binary interaction parameters were derived from these data (Fig. 5.3). The binary interaction parameters for the other binary pairs are taken from the Aspen Hysys database for the SRK EOS and can be found in Table A.2 in Appendix A.
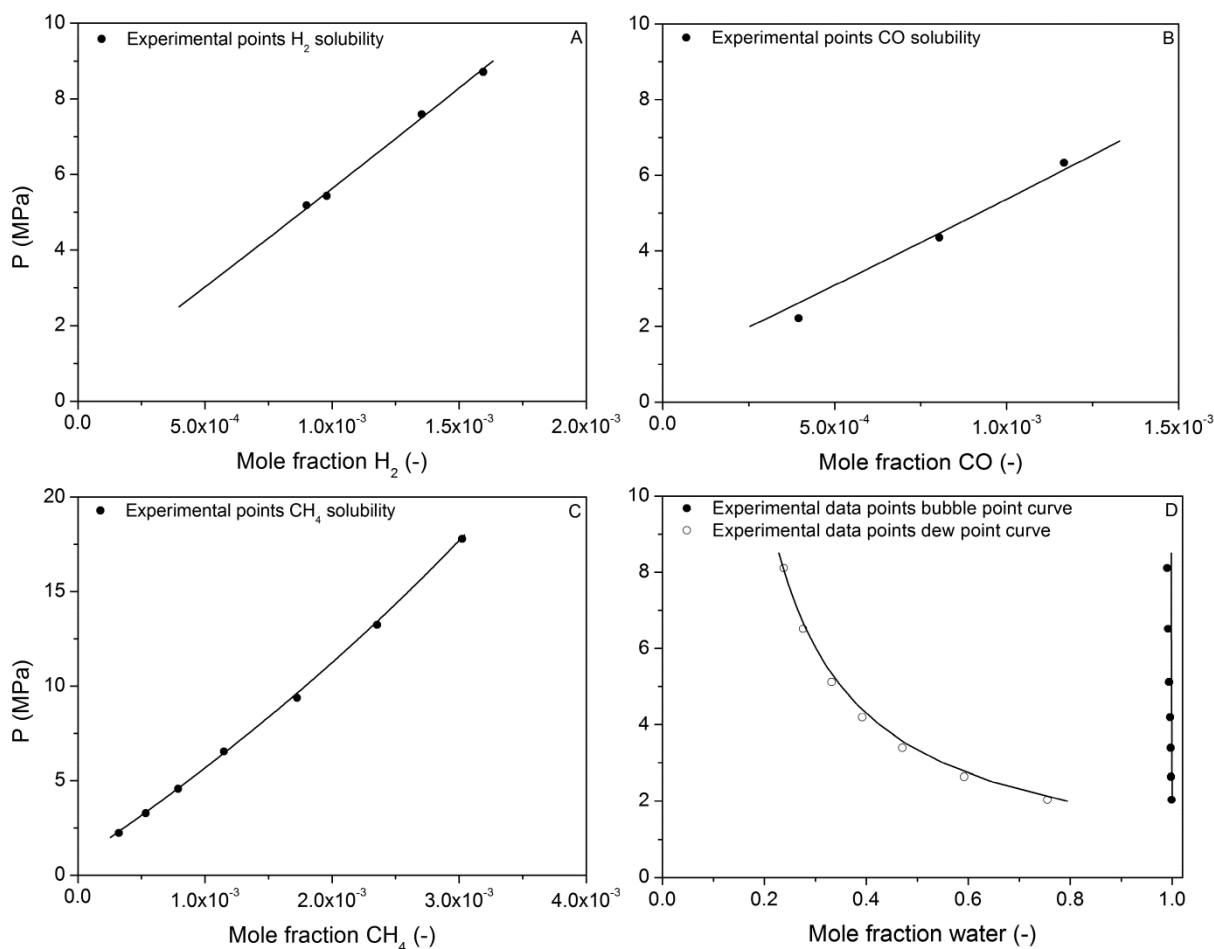
Fig. 5.3 Solubility of H_2 in water at 423 K (A, k_{ij} = -0.745) [24], solubility of CO in water at 448 K (B, k_{ij} = -0.474) [25], solubility of CH_4 in water at 444 K (C, k_{ij} = 0.014) [26], VLE diagram of water-CO_2 at 473 K (D, k_{ij} = 0.30) [27]. Symbols: experimental data; lines: model predictions.

5.4 Model structure and calculation procedure

Several models in the literature use integration of a set of differential equations, including kinetic equations if reactions are considered, to calculate steady-state solutions or equilibria [28-30]. Such methods have good stability and convergence characteristics, as a realistic approach toward the chemical equilibrium is followed. In the case of equilibrium calculations with a reactor in a packed bed configuration, the amount of catalyst is taken as infinite to ensure that equilibrium is reached.

Here, model calculations were performed for an isothermal packed bed reactor at constant pressure. The model requires the following input: syngas composition, pressure, temperature, critical temperatures, critical pressures, and acentric factors. The values for the latter three properties were taken from the literature [21] and are shown in Table A.1 in Appendix A. As we are interested in the vapor composition and conversion at the dew point, dynamic vapor

compositions were used that occur during methanol synthesis. Kinetic equations used to obtain the dynamic vapor compositions were taken from the literature for the MK-101 methanol synthesis catalyst [31]. Calculation of the dew point as a function of vapor compositions occurring in methanol synthesis cannot be done with conventional models [11-15], as the dynamic compositions can only be obtained using kinetic equations, which are not present in the literature models. When exclusively the phase and chemical equilibrium are of interest, only the set of equations described in Section 5.2.3 can be solved. The complexity of the model can be further reduced using simplified kinetic equations for methanol synthesis reactions.

Two different algorithms, A and B, were developed. Algorithm A is the simplest model and can be used in most situations. In some cases, algorithm A does not result in a physically realistic solution (negative liquid phase). This phenomenon occurs when a dew point is present and a liquid is formed, but this liquid disappears at further increase of the conversion. In this situation, no solution exists for the phase equilibrium equations (Eq. 5.15) and algorithm B is required.

5.4.1 Algorithm A: Single integration followed by solving a set of equations

The macroscopic behavior of the isothermal packed bed at fixed pressure can be described with a simple continuity differential equation (Eq. 5.25) until the dew point is reached, which is visualized in Fig. 5.4.

$$\frac{dF_i^V}{dWt_{cat}} = r_i^{'} (i = CO, CO_2, CH_3OH, H_2, H_2O, CH_4)$$

(Eq. 5.25)
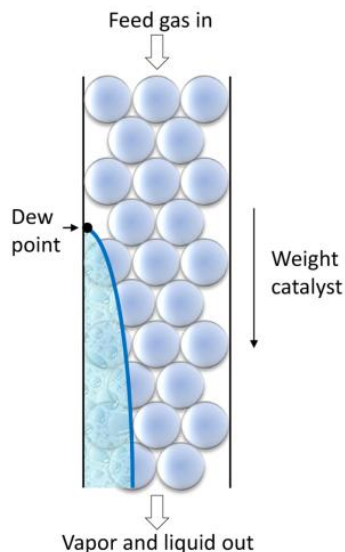
Fig. 5.4 Simplified representation of liquid formation in a packed bed reactor.

The structure of the algorithm is shown in the block diagram in Fig. 5.5. After initialization of the input parameters, the local vapor composition of the system is calculated as a function of the accumulative weight of the catalyst. After each subsequent integration step (Euler method), the difference between the actual methanol fugacity ($f^V_{methanol,n}$) and the methanol fugacity after the previous integration step ($f^V_{methanol,n-1}$) divided by the standard pressure is calculated. If this value is smaller than 10^{-10}, the vapor mixture is considered to be at chemical equilibrium. Then the actual concentration and conversion are given as output. If the difference is larger than 10^{-10} the dew point temperature and composition of the liquid phase are calculated.
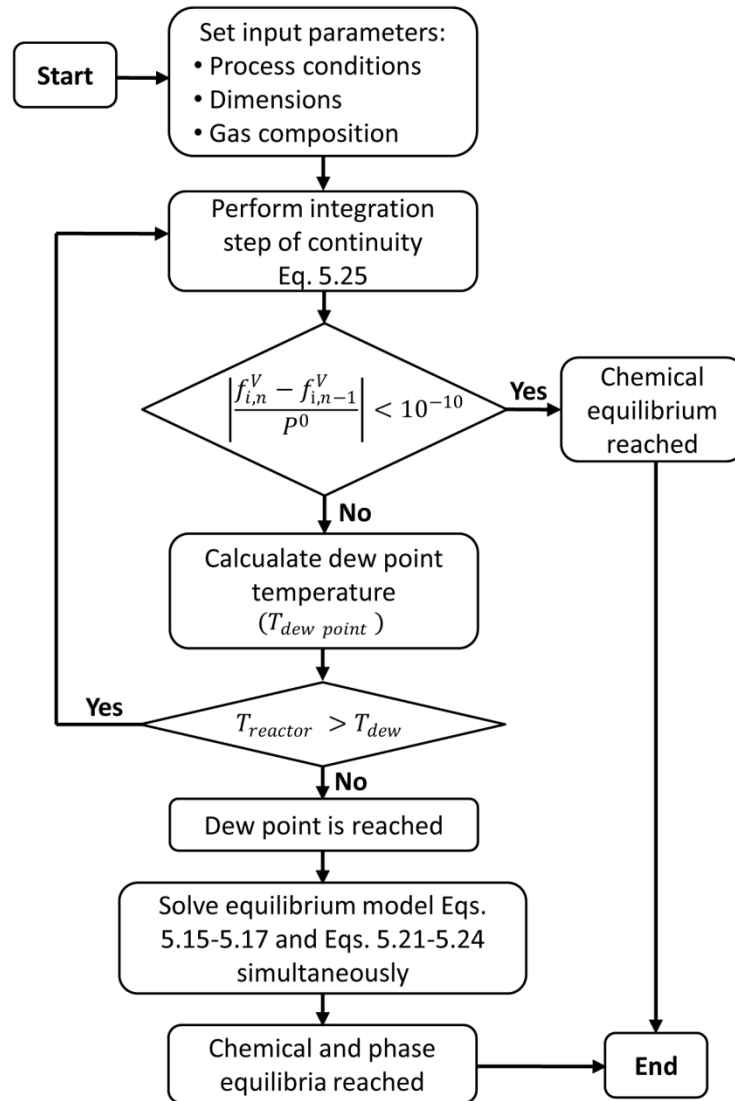
Fig. 5.5 Block diagram for algorithm A of the equilibrium model for an isothermal packed bed reactor (routine: single integration followed by solving a set of equations).

At low conversions, the dew point temperature is much lower than the reactor temperature. When the methanol concentration increases the dew point temperature of the mixture increases. As long as the reactor temperature is higher than the dew point temperature the integration procedure is repeated, until either the chemical equilibrium is reached or the dew point temperature becomes equal to the reactor temperature (see Fig. 5.6). Then the conversion and composition at the dew point are provided as output. The pressure and composition of the vapor phase are used as input for the dew point calculations, resulting in the composition of the liquid phase at the dew point.
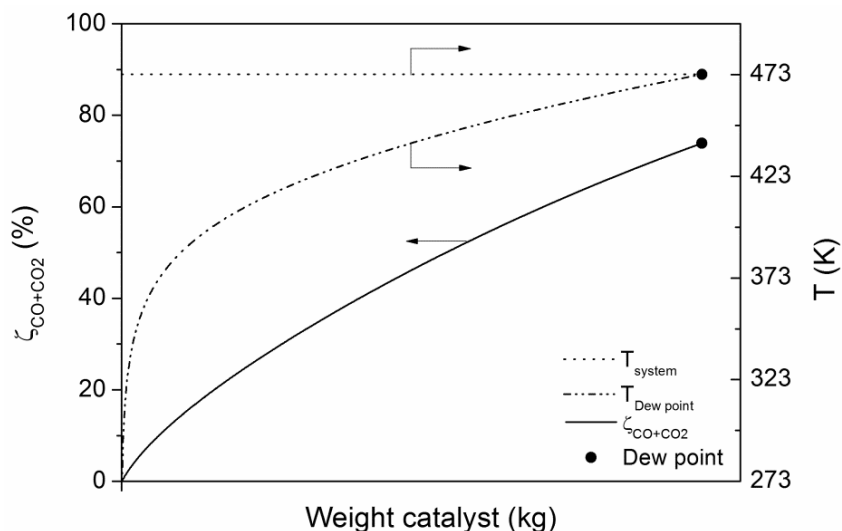
Fig. 5.6 ζ_{CO+CO2} accompanied by the dew point temperature of the system as a function of the weight of catalyst. $P = 20.0$ MPa, $T = 473$ K, syngas: $H_2/CO/CO_2/CH_4 = 67.0/24.4/3.5/5.1$ vol%.

In general, when a dew point occurs chemical equilibrium has not been reached yet. Then, the vapor phase reaction continues and more liquid condenses. Finally, in a reactor with an infinite amount of catalyst, phase and chemical equilibria are reached. The simultaneous phase and chemical equilibria are calculated by solving the set of 12 equations as described in Section 5.2.3. The concentration and conversion of the reactants are output of the model.

5.4.2 Algorithm B: Double integration

The first part of algorithm B is equal to algorithm A. The system is integrated until the dew point is reached. From here on, algorithm B is different (see the block diagram in Fig. 5.7). Integration of the system (also with the Euler method) is continued but now taking into account the continuity equations for the vapor phase (Eq. 5.26) and the continuity equation for the liquid phase (Eq. 5.27).

$$\frac{dF_i^V}{dWt_{cat}} = r_i{}' - G_{i,cond}$$

(Eq. 5.26)

$$\frac{dF_i^L}{dWt_{cat}} = G_{i,cond}$$

(Eq. 5.27)
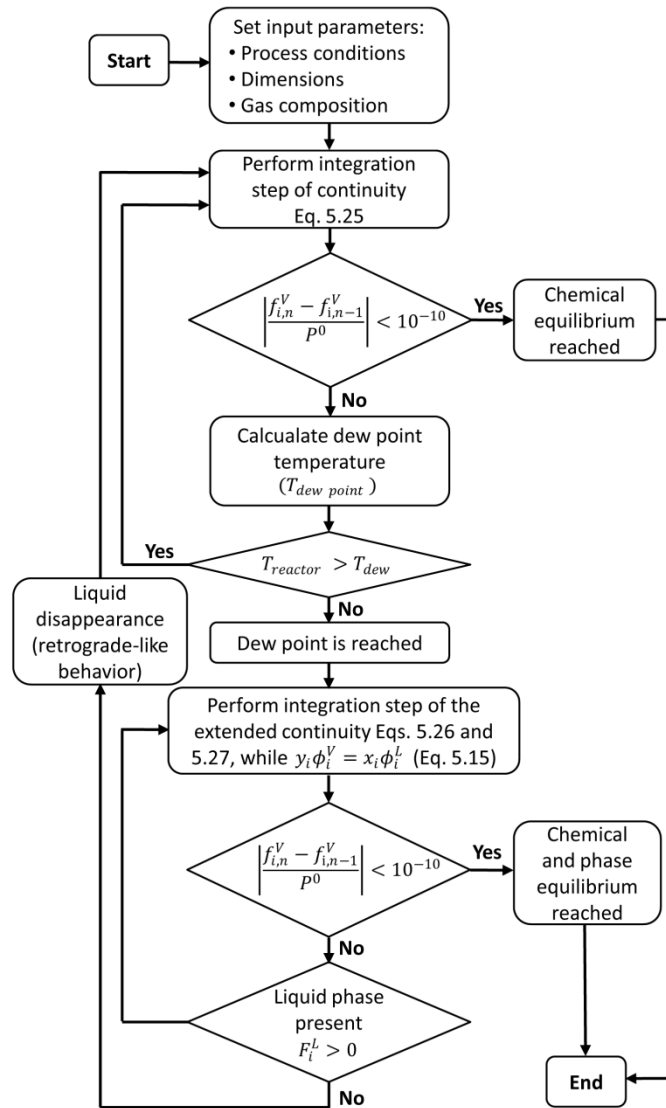
Fig. 5.7 Block diagram for algorithm B of the equilibrium model for an isothermal packed bed reactor (routine: double integration).

Eq. 5.26 and Eq. 5.27 are integrated in such a way that there is phase equilibrium of the system after every integration step. This is done by first calculating the reaction rate in an integration

step and then calculating the condensation rate resulting in a composition of the vapor and liquid phase that satisfies the conditions given in Eq. 5.15 for each component.

After each integration step in the second integration routine the change in methanol fugacity of the vapor phase is calculated. As long as the change in fugacity divided by the standard pressure is larger than 10^{-10} and a liquid phase exists ($F_i^L > 0$) the integration is repeated. After several integration steps either the simultaneous phase and chemical equilibria are reached or the liquid phase disappears ($F_i^L = 0$). When the chemical and phase equilibria are reached the equilibrium data is given as output. When the liquid phase disappears the vapor composition and conversion at the point of liquid disappearance are given as output and the first integration procedure is repeated until chemical equilibrium of the vapor phase only is reached.

Algorithm B can be used for all cases in which algorithm A is used. Calculation time in algorithm B, however, is longer, because a second integration routine is required. Algorithm A is the algorithm generally preferred except for the cases in which a physically unrealistic liquid phase composition is calculated. The algorithms considered in this work were solved using Matlab. Data relevant for this work can be found in Appendix A.

5.5 Experimental validation

5.5.1 Materials

Premixed syngases were supplied by Westfalen-AG, Germany. The composition of the syngases is given in Table 5.1. The methanol synthesis catalyst was a commercial methanol synthesis catalyst (Cs doped $Cu/ZnO/Al_2O_3$).

Table 5.1 Composition of the syngas used for the experimental validation of the model.

	H_2 (vol%)	CO (vol%)	CO_2 (vol%)	CH_4 (vol%)	C_2H_6 (vol%)
Syngas 1	67.0	24.4	3.5	5.1	-
Syngas 2	54.2	28.9	10.9	4.0	2.0

5.5.2 Setup description

In Fig. 5.8 a schematic flow sheet of the setup is given. The gas bottle containing syngas was connected to a booster (Maximator) to pressurize the syngas to the desired pressure. Syngas was fed from the booster to the setup via a Brooks mass flow controller (MFC). The gas was preheated in a preheater (P1) consisting of a tube with a heating jacket. Heating oil was flown through the annular zone and syngas passed through the tube. The same principle was applied for the two methanol synthesis packed bed reactors (R1 and R2) in series, which were located directly after the preheater.
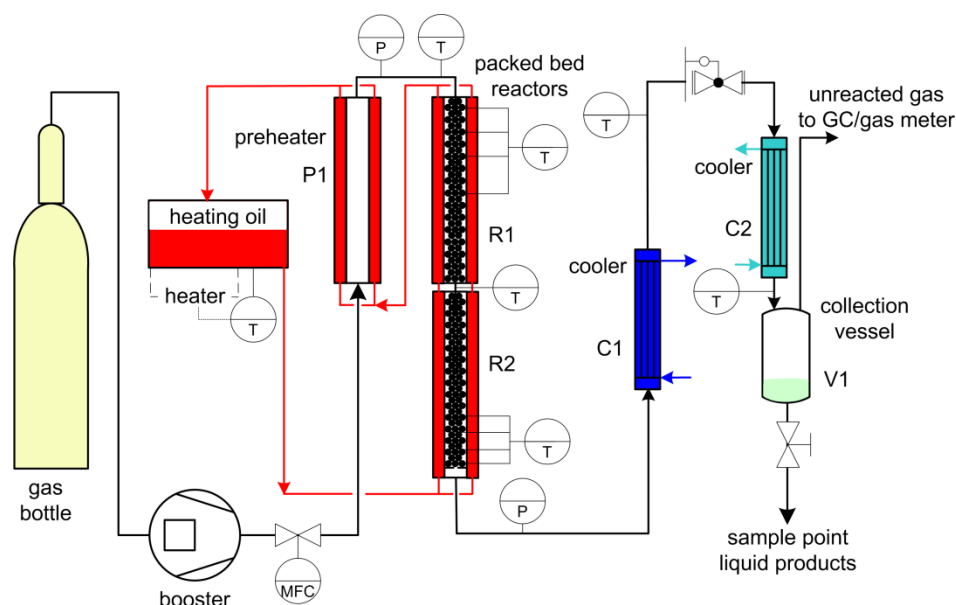
Fig. 5.8 Schematic flow sheet of the methanol synthesis setup.

The inner diameter of the reactor tube was 10 mm, and the length of each reactor was 500 mm. In these reactors the heating oil acted in the beginning of the first reactor bed as heating medium and further down as coolant. The first reactor bed contained a thermowell which recorded the temperature at 5, 10, 20, and 30 cm from the top of the catalyst bed. Methanol synthesis took place when the gas entered the packed bed. Due to the exothermicity of the reaction the temperature in the packed bed increased in the first part of the first reactor; then the temperature went down, approaching the temperature of the oil. Subsequently, the vapor entered the second reactor, which ensured that the equilibrium was reached. The temperature of the second reactor was measured with a thermowell at four locations (11, 7, 4, and 0.1 cm from the end of the reactor, R2) in the center of the catalyst bed. The temperature of the last four thermocouples was constant within 1 K and slightly below the temperature of the heating oil, due to small heat losses to the surroundings. The temperature of the last thermocouple was used as the temperature at which equilibrium was calculated. The two packed bed reactors were filled with 50 and 51 g of catalyst, respectively. The catalyst pellets were crushed, and particle sizes between 1 and 2 mm were used. At 468 K and 15 MPa, experiments with two different space velocities ($1.1 \cdot 10^3$ and $2.2 \cdot 10^3$ m^3 syngas/m^3 cat./h) were used to ascertain that equilibrium was reached.

After the reactor, the mixture of organics, water, and vapor was cooled in a cooler (C1) by tap water before the mixture was depressurized to 1 MPa through a back-pressure valve. In a second cooler (C2), which was operated at 253 K, the remaining condensables were condensed. After depressurization to atmospheric pressure via a pressure reducer the liquid was collected in a measuring cylinder (V1), which could be tapped. The dry gas was quantified by a gas meter (Gallus G1.6) and analyzed by a gas chromatograph (GC). Experiments were conducted at pressures around 20 MPa and temperatures of the heating jacket of 473, 498, 523, and 548 K.

All parts of the system that were heated or cooled were well insulated with glass wool. The process pressure was determined by taking the average pressure of the two pressure meters.

5.5.3 Analyses

Dry gas composition was analyzed using an online dual-column GC (GC 955, Syntech Spectras) equipped with thermal conductivity detectors. CO was analyzed over a molecular sieves 5 Å column (L = 1.6 m) with helium as the carrier gas. CO_2, CH_4 and C_{2+} were analyzed on a Chromosorb 102 column (L = 1.6 m) with helium as the carrier gas. H_2 was analyzed on the molecular sieves column using argon as the carrier gas.

5.6 Results and discussion

The case of methanol synthesis from $H_2/CO/CO_2/CH_4$ = 74/15/8/3 vol% at 473 K and 30.0 MPa has been used as a modeling example in several publications, though experimental validation is lacking [11-15]. The results from the literature and the results from the present study are shown in Table 5.2.

Table 5.2 Composition of the vapor and liquid equilibria in methanol synthesis predicted by several authors. P = 30 MPa, T = 473 K, syngas: $H_2/CO/CO_2/CH_4$ = 74/15/8/3 vol%.

	Feed	[11]	[13]	[12]	[14]	[15]	This work
Vapor phase							
CO^a	15	$6 \cdot 10^{-3}$	0.01	$1.3 \cdot 10^{-3}$	$6.2 \cdot 10^{-3}$	Traces	$8.6 \cdot 10^{-3}$
CO_2^a	8	0.05	0.04	Traces	0.05	Traces	0.06
$Methanol^a$	0	20.53	20.40	21.20	20.42	16.55	20.23
H_2^a	74	65.89	66.93	64.93	66.02	70.91	65.51
$Water^a$	0	4.73	3.74	4.64	4.71	3.53	5.06
CH_4^a	3	8.75	9.15	9.23	8.79	9.02	9.13
Phase fraction	-	0.5112	0.5258	0.4968	0.4863	0.4825	0.4848
Liquid phase							
CO^a	-	Traces	Traces	Traces	Traces	Traces	$1.8 \cdot 10^{-3}$
CO_2^a	-	0.02	0.01	Traces	0.02	Traces	0.02
$Methanol^a$	-	63.54	67.09	63.71	63.43	66.87	63.43
H_2^a	-	9.62	4.20	9.48	9.76	5.47	10.49
$Water^a$	-	24.36	27.32	24.88	24.29	25.33	23.87
CH_4^a	-	2.46	1.56	1.93	2.48	2.33	2.19
Phase fraction	-	0.4888	0.4742	0.5032	0.5137	0.5175	0.5152

[a]All concentrations are expressed in vol%.

Although all models have a (slightly) different approach to calculate the equilibrium composition, the differences are rather small and probably caused by the use of different thermodynamic data, binary interaction coefficients, and in one case the use of a different EOS. The equilibrium compositions predicted with the model developed in this study are well within

the variations of the compositions predicted by the models from literature, validating our approach (i.e., the algorithms in combination with the selected EOS).

5.6.1 Modeling of high pressure methanol synthesis

In the following section the model predictions and experimental results for two representative syngases will be discussed (see Table 5.1 for their composition). Syngas 1 is similar to a gas used in commercial methanol synthesis, while syngas 2 is similar to gas that can be obtained in a biomass-reforming process [32].

Syngas 1

Experimental and calculated results for syngas 1 are shown in Fig. 5.9. The equilibrium conversion of $CO+CO_2$ (Fig. 5.9A) and the equilibrium conversion of H_2 (Fig. 5.9B) are shown as a function of the temperature at 19.7 MPa. The diagram consists essentially of three parts.

1. Vapor (or gas) phase equilibrium curve: At high temperatures, in Fig. 5.9 from 498 K onward, only a vapor phase exists. Conversion of $CO+CO_2$ or H_2 is a function of temperature and can be predicted on the basis of the chemical equilibrium of the vapor phase.
2. Dew point curve: At temperatures below 498 K, a dew point is present. The dew point curve represents the combination of temperature and conversion at which condensation starts. Methanol synthesis and condensation continue beyond the dew point.
3. Curve for the equilibrium including liquid formation: When a dew point is present, chemical and phase equilibrium coexist. Equilibrium conversion including liquid formation (dotted line) is higher than the extrapolation of the vapor phase equilibrium curve (not shown in the figure).
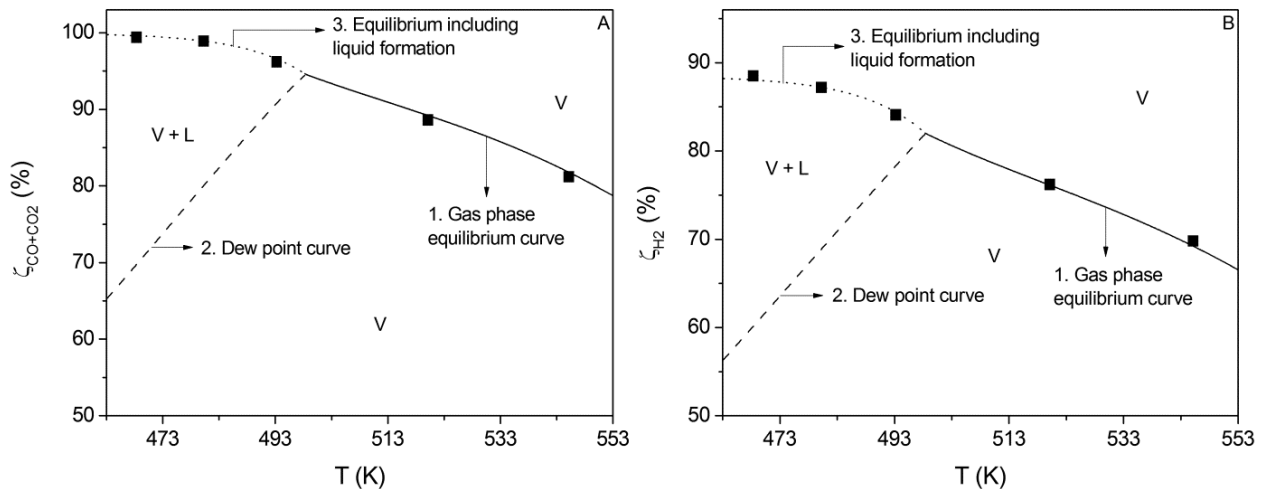
Fig. 5.9 Equilibrium diagram for methanol synthesis including a dew point curve for ζ_{CO+CO2} (A) and ζ_{H2} (B). *P* = 19.7 MPa, syngas: $H_2/CO/CO_2/CH_4$ = 67.0/24.4/3.5/5.1 vol%. Symbols: experimental data; lines: model results.

The model predictions are in very good agreement with experimental data (relative error in the data is estimated to be 1%) for the whole temperature range. Both model and experimental data follow the same trend. In this system a single combination of temperature and conversion exists where the vapor composition at the dew point is equal to the chemical equilibrium composition. In this point the three lines in the diagram come together. This point is from here on referred to as the 'max dew point'.

The max dew point temperature is a function of the pressure and is calculated for the pressure range of 11 – 30 MPa. The results are shown in Fig. 5.10. At the lower pressures the max dew point temperature increases with increasing pressure, reaching a maximum at 23.5 MPa. In this pressure range, the temperature at which the composition of the vapor phase at the dew point becomes equal to the chemical equilibrium composition shifts to higher temperatures, implying that the temperature range in which a liquid phase can be obtained in methanol synthesis becomes larger. Interestingly, at pressures above 23.5 MPa the max dew point temperature becomes lower again. A possible explanation is that the critical temperature of the mixture decreases with increasing pressure. For this syngas composition, no liquid phase exists at any pressure at temperatures above 501 K.
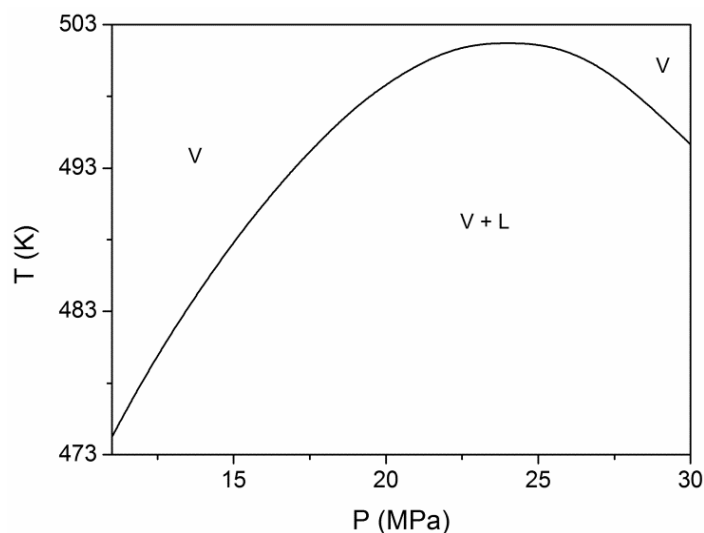
Fig. 5.10 Pressure of the max dew point vs. temperature. Syngas: $H_2/CO/CO_2/CH_4$ = 67.0/24.4/3.5/5.1 vol%.

The equilibrium gas composition (excluding water and methanol) as a function of temperature is shown in Fig. 5.11. In this calculation it is assumed that all dissolved permanent gases are released during depressurization. Thus, at the end of the process the liquid phase consists of methanol and water only.

The concentration of inert gas (viz. CH_4 in the present model) is the highest at the lowest temperature and decreases with increasing temperature. The equilibrium concentrations of H_2, CO, and CO_2 increase with temperature. A discontinuity can be seen at the max dew point

temperature (498 K). Experimental data nicely coincide with the model calculations and follow similar trends. Predictions seem to be rather accurate, although experiments were conducted at harsh conditions with relatively large deviations from ideal behavior. At the two higher temperatures the concentrations of CO and CO_2 differ slightly from the predicted values.
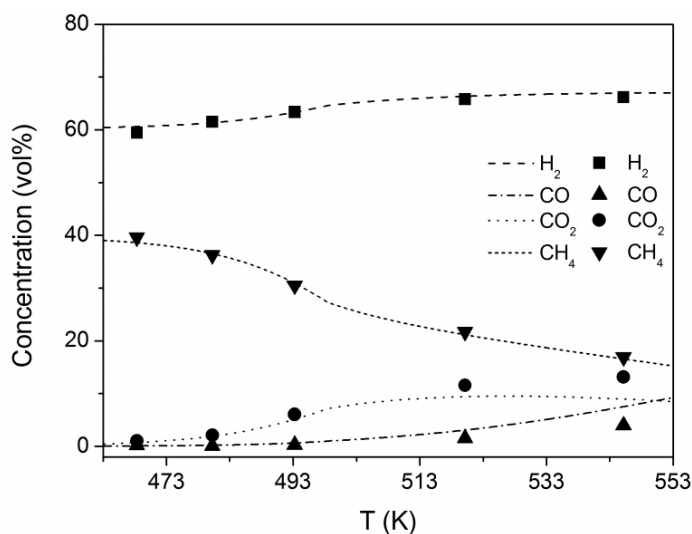
Fig. 5.11 Equilibrium concentration of the permanent gases after methanol synthesis. P = 19.7 MPa, syngas: $H_2/CO/CO_2/CH_4$ = 67.0/24.4/3.5/5.1 vol%. Symbols: experimental data; lines: model results.

The modeling results for the vapor fraction of the system at equilibrium together with the vapor phase composition are shown in Fig. 5.12. At 468 K approximately 33% of the total amount of moles present is in the vapor phase, while the remainder is in the liquid phase. At temperatures exceeding the max dew point temperature only a vapor phase exists.

The composition of the vapor phase shows different trends at temperatures below and above the temperature of the max dew point. At temperatures above the max dew point the vapor concentrations show a regular trend, but below the max dew point methanol, water, and H_2 show inverse behavior. The concentrations of methanol and water increase with increasing temperature until the max dew point. The concentration of CO_2 increases over the complete temperature interval. It should be realized that it is difficult to explain the trends for the individual components in detail, as the exact composition of the system depends on the temperature, equilibrium conversion, and interaction between the different components.
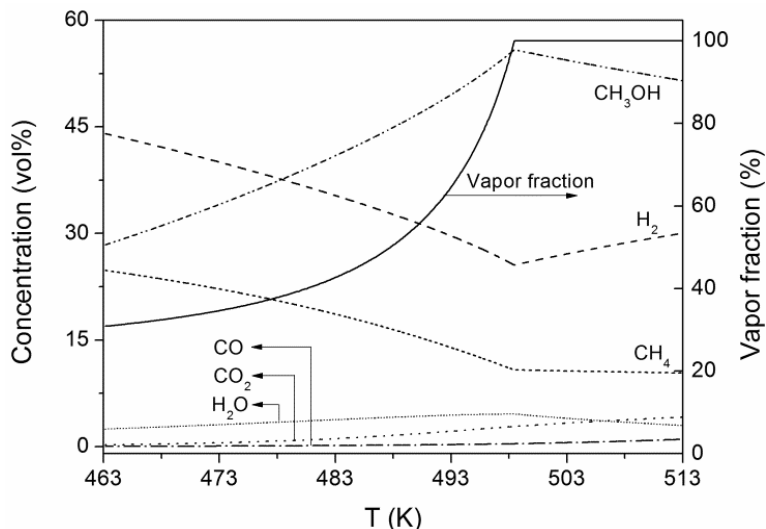
Fig. 5.12 Vapor phase concentrations and the vapor fraction at equilibrium as a function of temperature. P = 19.7 MPa, syngas: $H_2/CO/CO_2/CH_4$ = 67.0/24.4/3.5/5.1 vol%. Solid line: vapor phase fraction; dotted lines: concentration of the vapor component.

If a liquid phase is present part of the gases will dissolve. The composition of the liquid phase as a function of temperature is presented in Fig. 5.13. At 468 K approximately 67% of the total amount of moles is in the liquid phase. The number of moles in the liquid phase decreases at higher temperatures, and above 498 K no liquid phase is predicted anymore. The concentration of methanol is relatively constant over the temperature interval and slightly below 80%. The remaining 20% is water and dissolved components. Experimental data to justify these modeling results and the data presented in Fig. 5.13 are not available.
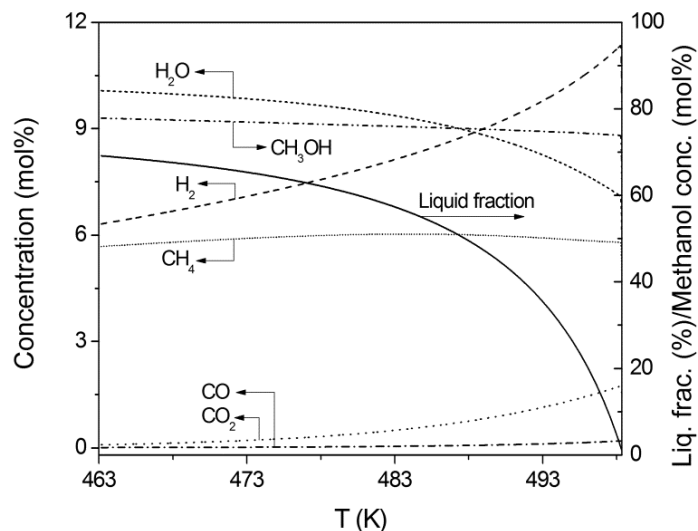
Fig. 5.13 Liquid phase concentrations and liquid fraction as a function of temperature. P = 19.7 MPa, syngas: $H_2/CO/CO_2/CH_4$ = 67.0/24.4/3.5/5.1 vol%. Solid line: liquid phase fraction; dotted lines: concentration of the liquid component.

107

Syngas 2

Similar calculations and experiments as for syngas 1 were conducted using syngas 2. The results are shown in Fig. 5.14. The equilibrium predictions of the model coincide very well with the experimental data for the two lower temperatures, but the experimental data points differ from the predictions at the two higher temperatures. This is probably due to formation of higher alcohols, which is common for a system at higher temperatures with high CO partial pressures [33, 34] but not included in our model.

Remarkable phenomena are calculated for certain combinations of vapor composition and process conditions. For this system, three different types of behavior can be distinguished. Fig. 5.14 shows that at higher temperatures (T > 475.4 K) only a vapor phase exists and at the lower temperature (T < 469.5 K) a vapor phase and a liquid phase coexist at equilibrium. However, at temperatures between 469.5 and 475.4 K a dew point is calculated, initially followed by condensation but then devolving to evaporation until at a certain conversion the liquid phase has disappeared. Apparently, the liquid phase present vanishes, due to a changing vapor and liquid composition.

This phenomenon resembles retrograde condensation, although it occurs as a function of increasing reaction extent and not at equilibrium. In natural gas systems, condensation is regularly observed upon pressure reduction at constant temperature [35]. As retrograde condensation is reversible, increasing the pressure of such a system will result in the disappearance of the liquid phase. For syngas 2, liquid disappearance is not observed with increasing pressure but with increasing methanol content of the mixture (increasing reaction extent). This behavior cannot be predicted using algorithm A as after the dew point a simultaneous chemical and phase equilibrium is calculated which does not exist in this situation.
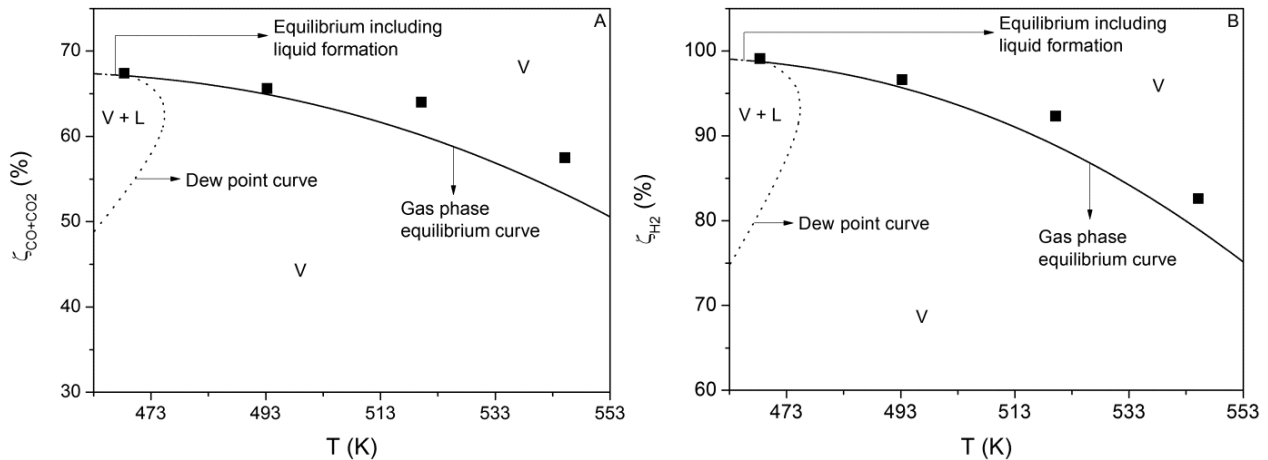
Fig. 5.14 Equilibrium diagram for methanol synthesis including the dew point curve for ζ_{CO+CO2} (A) and ζ_{H2} (B). Symbols: experimental data; lines: model results. P = 19.4 MPa. Syngas: $H_2/CO/CO_2/CH_4/C_2H_6$ = 54.2/28.9/10.9/4.0/2.0 vol%.

The approach toward the chemical/phase equilibrium or the combination of both for three different types of behavior in this system is illustrated in Figs. 5.15 and 5.16. These figures show the molar flows in the vapor and liquid phase as a function of the weight of the catalyst in the isothermal packed bed reactor. The total molar flow in the vapor phase decreases, because methanol synthesis is accompanied by molar contraction. When the situation in Fig. 5.15A (463 K) is considered, a dew point is reached at a certain conversion. A liquid phase starts to appear, and initially the molar flow in the vapor phase decreases faster before leveling off when equilibrium is approached. Finally, a stable chemical and phase equilibrium is reached. At 483 K (Fig. 5.15B) only a vapor phase is present and no liquid phase is formed.
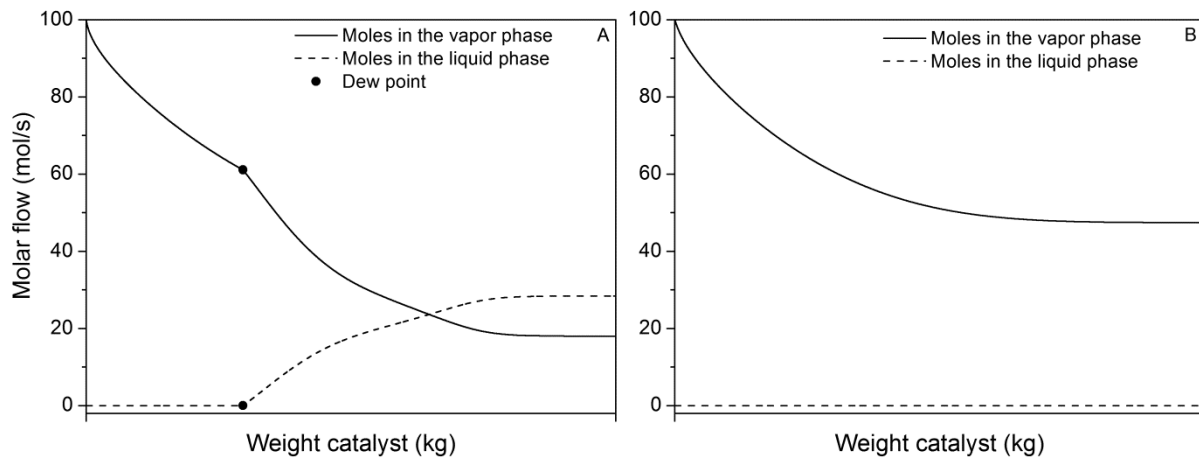
Fig. 5.15 Molar flow vs. weight of catalyst, illustrating the approach toward chemical/phase equilibrium, as obtained from algorithm B. P = 19.4 MPa, T = 463 K (A), 483 K (B), F_{in} = 100 mol/s with composition $H_2/CO/CO_2/CH_4/C_2H_6$ = 54.2/28.9/10.9/4.0/2.0 vol%.

The situation is different at 473 K (Fig. 5.16). The dew point is reached when the temperature of the packed bed reactor becomes equal to the dew point temperature and a liquid phase starts to appear. As the reaction proceeds the liquid phase starts to vanish until a point of complete liquid disappearance is reached. It can be seen that from this point on the dew point temperature of the mixture is below the temperature of the system, indicating that no liquid phase is predicted at these conditions. Finally, at equilibrium only a vapor phase exists, which is the reason why algorithm A does not have a realistic solution.
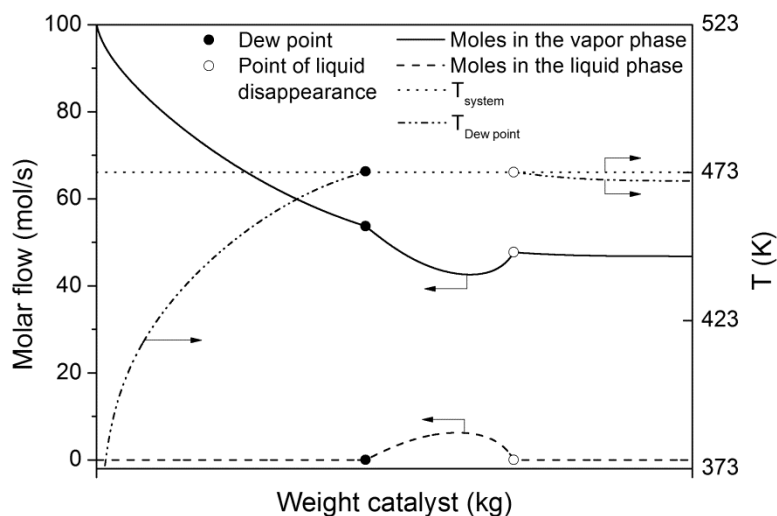
Fig. 5.16 Molar flow vs. weight of catalyst, illustrating the approach towards chemical/phase equilibrium, as obtained from algorithm B. $P = 19.4$ MPa, $T = 473$ K, $F_{in} = 100$ mol with composition $H_2/CO/CO_2/CH_4/C_2H_6 = 54.2/28.9/10.9/4.0/2.0$ vol%.

5.7 Conclusion

Phase equilibria and chemical equilibria for high pressure methanol synthesis are calculated simultaneously using a modified Soave-Redlich-Kwong equation of state. The model developed is solved in two stages. In the first stage a dew point, if present, is calculated by integration of kinetic equations for an isothermal system, which is a unique feature of the model in comparison to the models known in the literature. The second stage of the model can be solved in two different ways. Either a set of equations is solved to calculate the simultaneous phase and chemical equilibria (algorithm A) or the integration procedure of the packed bed reactor is continued for a combination of a vapor phase and a liquid phase (algorithm B). The binary vapor-liquid equilibrium of methanol and water can be predicted accurately with the equation of state used by fitting binary interaction coefficients to literature data. Both the phase and the chemical equilibria in methanol synthesis are presented is a single diagram in which clearly a vapor-liquid area can be distinguished. The shape of the diagram appears to be a strong function of the composition of the syngas. In contrast to models from the literature dealing with high pressure methanol synthesis the model predictions in this study are experimentally verified. The thermodynamic equilibria, including both phase and chemical equilibria, coincide nicely with the experimental data obtained here on high pressure methanol synthesis.

Condensation of methanol has beneficial consequences for methanol synthesis as conversions higher than the chemical equilibrium are obtained. The conversion of the limiting component is almost complete at low temperatures, which omits the necessity of a recycle stream. High pressure methanol synthesis thus has potential, in particular in combination with reforming in supercritical water (Supermethanol project) in which a syngas at high pressure is produced by pressurizing a liquid.

5.8 Nomenclature

a	Attractive parameter of EOS	T_R	Reduced temperature (T/T_c)
$A = \dfrac{aP}{R^2T^2}$	Reduced attractive parameter of the EOS	x	Mole fraction in the liquid phase
		y	Mole fraction in the vapor phase
b	Repulsive parameter of the EOS	V	Volume (m^3)
$B = \dfrac{bP}{RT}$	Reduced repulsive parameter of the EOS	Wt	Catalyst weight (kg)
		Z	Compressibility
$\Delta_r H_{298}$	Reaction enthalpy at 298 K (J·mol^{-1})		
f_i^e	Fugacity (Pa)		*Greek symbols*
F_i^e	Local molar flow (mol·s^{-1})	α	Adimensional factor for a
G_i^e	Local condensation rate (mol·kg cat^{-1}·s^{-1})	ϕ_i^e	Fugacity coefficient of component i in phase e
k_{ij}	Binary interaction parameter	ω	Acentric factor
$K_{f,h}$	Chemical equilibrium constant based on fugacities		
			Subscripts
$K_{\phi,h}$	Deviation of $K_{P,h}$ from the ideal gas law	$cond$	Condensation
		dew	Dew point
$K_{P,h}$	Chemical equilibrium constant based on partial pressures	h	Reaction identification (h = 1,2, or 3)
$K_{P^0,h}$	Theoretical chemical equilibrium constant	i,j	Component identification ($i, j = CO, CO_2, CH_3OH, H_2, H_2O, CH_4$)
m	Characteristic constant	cat	Catalyst
n	Number of moles	c	Critical property
p	Polar parameter	C	Carbon
P	Pressure (Pa)	H	Hydrogen
P_c	Critical pressure (Pa)	O	Oxygen
R	Universal gas constant (8.314 J·mol^{-1}·K^{-1})		
			Superscripts
r_i'	Reaction rate per weight of catalyst (mol·kg cat.$^{-1}$·s^{-1})	e	Phase identification (e = V or L)
		in	Inlet
T	Absolute temperature (K)	L	Liquid phase
T_c	Critical temperature (K)	V	Vapor phase
		0	Indicates standard pressure

5.9 References

1   M. Berggren, Methanol industry in focus, milestones, www.methanol.org (accessed 19 January 2012)

2   J. Skrzypek, J. Stoczynski, S. Ledakowicz, Methanol synthesis, Polish Scientific Publishers PWN, Warsaw, (1994).

3   E. Supp, How to produce methanol from coal, Springer-Verlag, Berlin, (1990).

4   J.G. van Bennekom, J. Vos, R.H. Venderbosch, M.A.P. Torres, V.A. Kirilov, H.J. Heeres, Z. Knez, M. Bork, J.M.L. Penninger, Supermethanol: Reforming of crude glycerine in supercritical water to produce methanol for re-use in biodiesel plants, in: 17th European Biomass Conference and Exhibition, Hamburg, (2009) 899-902.

5   T. Chang, R.W. Rousseau, P.K. Kilpatrick, Methanol synthesis reactions: Calculations of equilibrium conversions using equations of state, Ind. Eng. Chem. Process Des. Dev., 25 (1986) 477-481.

6   J.B. Hansen, F. Joensen, High conversion of synthesis gas into oxygenates, in: A. Holmen (Ed.) Proceeding of the NGCS, Elsevier Science Publishers B.V., Oslo, (1991) 457-467.

7   E.L. Sorensen, J. Perregaard, Condensing methanol synthesis and ATR - The technology choice for large-scale methanol production, Stud. Surf. Sci. Catal., 147 (2004) 7-12.

8   G.H. Graaf, P.J.J.M. Sijtsema, E.J. Stamhuis, G.E.H. Joosten, Chemical equilibria in methanol synthesis, Chem. Eng. Sci., 41 (1986) 2883-2890.

9   F.E. Danes, D. Geana, Calcul de l'équilibre chimique à la synthèse du méthanol par les équations d'état des gaz hautement comprimés, Rev. Roum. Chim., 26 (1981) 947-954.

10   J. Skrzypek, M. Lachowska, D. Serafin, Methanol synthesis from CO_2 and H_2: Dependence of equilibrium conversions and exit equilibrium concentrations of components on the main process variables, Chem. Eng. Sci., 45 (1990) 89-96.

11   M. Castier, P. Rasmussen, A. Fredenslund, Calculation of simultaneous chemical and phase equilibria in nonideal systems, Chem. Eng. Sci., 44 (1989) 237-248.

12   R.P. Stateva, W.A. Wakeham, Phase equilibrium calculations for chemically reacting systems, Ind. Eng. Chem. Res., 36 (1997) 5474-5482.

13   A.K. Gupta, P.R. Bishnoi, N. Kalogerakis, A method for the simultaneous phase equilibria and stability calculations for multiphase reacting and non-reacting systems, Fluid Phase Equilib., 63 (1991) 65-89.

14   F. Jalali, J.D. Seader, Homotopy continuation method in multi-phase multi-reaction equilibrium systems, Comput. Chem. Eng., 23 (1999) 1319-1331.

15   A. Avami, Y. Saboohi, A simultaneous method for phase identification and equilibrium calculations in reactive mixtures, Chem. Eng. Res. Des., 89 (2011) 1901-1908.

16   G. Soave, Equilibrium constants from a modified Redlich-Kwong equation of state, Chem. Eng. Sci., 27 (1972) 1197-1203.

17   P.M. Mathias, A versatile equilibrium equation of state, Ind. Eng. Chem. Process Des. Dev., 22 (1983) 385-391.

18   M.S. Graboski, T.E. Daubert, A modified Soave equation of state for phase equilibrium calculations. 1. Hydrocarbon systems, Ind. Eng. Chem. Process Des. Dev., 17 (1978) 443-448.

19   R.C. Reid, J.M. Prausnitz, B.E. Poling, The properties of gases and liquids, Fourth Edition ed., McGraw-Hill, Inc., New york, (1987).

20   M.S. Graboski, T.E. Daubert, A modified Soave Equation of state for phase equilibrium calculations. 3. Systems containing hydrogen, Ind. Eng. Chem. Process Des. Dev., 18 (1979) 300--306.

21   B.E. Poling, J.M. Prausnitz, J.P. O'Connel, The properties of gases and liquids, 5 ed., McGraw-Hill, Singapore, (2007).

22   J. Gmehling, D.D. Liu, J.M. Prausnitz, High-pressure vapor-liquid equilibria for mixtures containing one or more polar components, Chem. Eng. Sci, 34 (1979) 951-958.

23   E. Brunner, W. Hültenschmidt, G. Schlichthärle, Fluid mixtures at high pressures IV. Isothermal phase equilibria in binary mixtures consisting of (methanol + hydrogen or nitrogen or methane or carbon monoxide or carbon dioxide), J. Chem. Thermodyn., 19 (1987) 273-291.

24   G. Kling, G. Maurer, The solubility of hydrogen in water and in 2-aminoethanol at temperatures between 323 K and 423 K and pressures up to 16 MPa J. Chem. Thermodyn., 23 (1991) 531-541.

25   S.B. Dake, R.V. Chaudhari, Solubility of CO in aqueous mixtures of methanol, acetic acid, ethanol, and propionic acid J. Chem. Eng. Data, 30 (1985) 400-403.

26   O.L. Culberson, J.J. McKetta, Phase equilibria in hydrocarbon-water system. The solubility of methane in water at pressures to 10,000 psia, Pet. Trans. AIME, 3 (1951) 223-226.

27   G. Müller, E. Bender, G. Maurer, Das Dampf-Flüssigkeitsgleichgewicht des ternären Systems Ammoniak-Kohlendioxid-Wasser bei hohen Wassergehalten im bereich zwischen 373 und 473 Kelvin., Ber. Bunsen Ges. Phys. Chem., 92 (1988) 148-160.

28   A.V. Mironova, V.S. Beskov, A.V. Krasavin, Kinetic method of calculation of chemical equilibrium, Theor. Found. Chem. Eng., 45 (2011) 319-322.

29   M.A. Al-Arfaj, W.L. Luyben, Effect of number of fractionating trays on reactive distillation performance AIChE J., 46 (2000) 2417-2425.

30   J.G.M. Winkelman, H. Sijbring, A.A.C.M. Beenackers, Modeling and simulation of industrial formaldehyde absorbers, Chem. Eng. Sci., 47 (1992) 3785-3792.

31   G.H. Graaf, E.J. Stamhuis, A.A.C.M. Beenackers, Kinetics of low-pressure methanol synthesis, Chem. Eng. Sci., 43 (1988) 3185-3195.

32   J.G. van Bennekom, R.H. Venderbosch, D. Assink, H.J. Heeres, Reforming of methanol and glycerol in supercritical water, J. Supercrit. Fluids, 58 (2011) 99-113.

33   B. Denise, R.P.A. Sneeden, Hydrocondensation of carbon dioxide: IV, J. Mol. Catal., 17 (1982) 359-366.

34   K.J. Smith, R.B. Anderson, A chain growth scheme for the higher alcohols synthesis, J. Catal., 85 (1984) 428-436.

35   C.J. Peters, T.W. de Loos, J. de Swaan Arons, On the retrograde condensation of one or two liquids, Fluid Phase Equilib., 70 (1991) 185-197.

6 High pressure methanol synthesis from syngas using a Cu/ZnO/Al$_2$O$_3$ catalyst

Abstract

Methanol synthesis from syngas was investigated for various gas compositions at new exceptional conditions of high pressures (up to 20 MPa) combined with relatively low temperatures (465 to 545 K). A total of 60 experiments were conducted in a packed bed reactor using a conventional Cs doped Cu/ZnO/Al$_2$O$_3$ catalyst. Methanol condensation was observed in the high pressure low temperature regime, allowing for nearly complete conversions of the limiting components. The experimental syngas conversions and off gas concentrations nicely coincide with equilibrium calculations incorporating the formation of liquid methanol. Pressure, temperature, and gas composition affected the methanol quality in terms of the presence of water and higher alcohols (mainly ethanol, propanol, 2-methyl-1-propanol, and 1-butanol). The higher alcohol content was negligible when the gas contained large amounts of CO$_2$, while higher CO concentrations and temperatures led to substantial higher alcohol concentrations in the liquid product (up to 14 wt%).

6.1 Introduction

Methanol has high potential as a clean and renewable energy carrier/fuel [1]. It is an important bulk chemical and used for the production of formaldehyde, acetic acid and MTBE. Methanol is mostly produced from syngas, a mixture consisting of predominantly H_2, CO, CO_2, and CH_4. Syngas can be derived from natural gas, coal or biomass. Three coupled equilibrium reactions of which two are independent are involved in methanol synthesis, viz. (i) the hydrogenation of CO (Eq. 1.1), (ii) the (reverse) water-gas shift (WGS) reaction (Eq. 1.2), and (iii) the hydrogenation of CO_2 (Eq. 1.3):

$$CO + 2\,H_2 \;\rightleftharpoons\; CH_3OH \qquad \Delta_r H^0_{298} = -90.64 \text{ kJ/mol} \qquad \text{(Eq. 1.1)}$$

$$CO_2 + H_2 \;\rightleftharpoons\; CO + H_2O \qquad \Delta_r H^0_{298} = +41.17 \text{ kJ/mol} \qquad \text{(Eq. 1.2)}$$

$$CO_2 + 3\,H_2 \;\rightleftharpoons\; CH_3OH + H_2O \qquad \Delta_r H^0_{298} = -49.47 \text{ kJ/mol} \qquad \text{(Eq. 1.3)}$$

An important specification of the quality of the syngas is the stoichiometric number (S_N) defined as [2]:

$$S_N = \frac{(H_2 - CO_2)}{(CO + CO_2)} \qquad\qquad \text{(Eq. 1.4)}$$

If S_N is equal to 2, there is exactly enough H_2 present to convert all CO and CO_2 to methanol. For S_N > 2, CO+CO_2 are the limiting components, while for S_N < 2, H_2 is limiting. Methanol synthesis has been under investigation since the beginning of the 20th century. In the early days, methanol synthesis was conducted industrially at 25 MPa and temperatures up to 623 K [3]. In the 1960s, improved syngas purification techniques allowed the use of more active Cu based catalysts and this led to the development of the low pressure process (5 − 10 MPa) at temperatures typically from 493 − 573 K. Nowadays, nearly all methanol is produced via the low pressure process. The conversion of syngas to methanol per reactor pass is between 30 − 70% due to the unfavorable thermodynamic equilibrium conversion at low pressures. Thus, to obtain complete conversion of the valuable syngas, recycle streams are required. Recycles ratios (recycle stream/feed) are roughly in the range of 3 − 4 to 1 [2].

High pressure methanol synthesis is interesting from an equilibrium point of view as higher syngas conversions are attainable [4, 5]. In the high pressure low temperature range, condensation of methanol (and water) can increase the equilibrium conversion further (see Chapter 4 and 5). Experimental data on high pressure methanol synthesis are scarce, in contrast to experimental data on low pressure methanol synthesis [6-10]. The accuracy of the high pressure equilibrium experiments conducted in the 1920s and 1930s is doubtful and in these experiments usually only CO and H_2 were considered [11-14]. Discrepancies between different publications are relatively large as not all investigators measured exit gas compositions and did not consider the formation of byproducts like higher alcohols (HA) which are likely to be formed

at such conditions [15]. In the 1980s, an equilibrium model was developed based on Russian high pressure data for a syngas composed of mainly H$_2$ and CO (10.1 < P < 40.5 MPa, 573 < T < 623 K) [16]. The equilibrium data could most accurately be described using a modified Himpan equation of state. Kinetic data are scarce as well, and only a few publications deal with reaction rates in high pressure methanol synthesis [17-19].

Although not always taken into account, the formation of HA in methanol synthesis can be substantial, in particular at the higher temperatures, and was already reported in the 1930s [20, 21]. In these experiments, a mixture of methanol and linear and branched primary and secondary alcohols was obtained from CO and H$_2$ at high pressure. The stoichiometry of the overall reaction is given in Eq. 6.1 (with n as number).

$$n\ CO + 2n\ H_2 \longrightarrow C_nH_{2n+1}OH + (n-1)\ H_2O \qquad\qquad (Eq.\ 6.1)$$

Hydrocondensation of lower alcohols to form HA was proposed as the main reaction mechanism. Later studies by Nunan *et al.* and Elliot and Pennella with labeled carbon atoms revealed that chain growth occurs mainly via the addition of intermediate C$_1$-oxygenates to adsorbed species [22-24].

Smith and Anderson described their experimental data quantitatively with a chain growth scheme considering additions of C$_1$ and C$_2$ species on α- and β-carbon atoms (see scheme 6.1 for an example, as a simplification adsorbed methanol is taken as reactant) [25]. The scheme was based on synthesis experiments over a K doped Cu/ZnO catalyst at 10.4 MPa and 458 K.
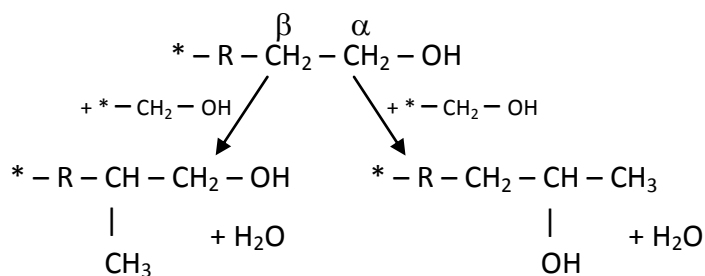
Scheme 6.1 Simplified reaction of an adsorbed intermediate with adsorbed methanol to HA.
$* - R$ implies an adsorbed surface species.

Chain growth occurs by addition to an $\alpha-$ or $\beta-$carbon as shown in Scheme 6.1. For example, 2-butanol (if R = CH$_3$ in Scheme 6.1), is formed when addition occurs to the α-carbon and 2-methyl-1-propanol is formed by addition to the β-carbon. In a kinetic study, this model was extended with linear chain growth of primary alcohols accounting for e.g. the formation of 1-pentanol [26]. The branched alcohols are termination products and considered as inert [22]. β-addition is faster compared to α-addition with K$_2$CO$_3$ promoted Cu/ZnO catalysts and this explains the relatively high yields of 2-methyl-1-propanol (up to 18% of the total HA content in

some cases). In HA synthesis also hydrocarbons can be formed [22, 27]. Thermodynamics dictate that HA and hydrocarbons become more favorable in the following order for the same n-value [28]:

$C_nH_{2n} > C_nH_{2n+1}OH > C_nH_{2n+2}$
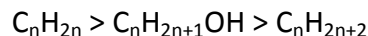
The formation of hydrocarbons can be prevented (to a large extent) by using an appropriate catalyst. In the kinetic regime, HA production is a function of the temperature and the residence time, while the influence of the pressure seems marginal [15]. At longer residence times the HA concentration decreases in favor of hydrocarbons [27]. The H_2/CO ratio is important for HA formation, as higher amounts of HA are observed at lower ratios (around 1) than the stoichiometric ratio of 2, rationalized by observations that the rate of chain growth is approximately proportional to the CO partial pressure, while the rate of chain termination depends on the H_2 partial pressure [25]. HA synthesis is also accompanied by CO_2 production, as part of the water formed in HA synthesis reacts with CO in the water-gas shift reaction (Eq. 1.2) [21]. Water competitively adsorbs with intermediate species and in turn suppresses the formation of HA [15, 21, 29].

In this chapter, the experimental results of high pressure methanol synthesis are described with various syngas compositions and process conditions using a typical Cs doped Cu/ZnO/Al$_2$O$_3$ catalyst. As far as we know, the conditions employed here, i.e. high pressure of up to 20 MPa and low temperature of 465 to 545 K, have not been studied before. The focus is mainly on high conversion runs (close to, or at equilibrium) and these were realized by using low gas hourly space velocities (*GHSV*), high catalyst intake, and low feed flow rates. The gas composition was varied to simulate gas compositions typically used in conventional methanol synthesis, a gas rich in CO_2, and gas that can be obtained from the reforming of a typical biomass feed (glycerol) in supercritical water [30, 31]. The experimental data are compared with theoretical thermodynamic equilibria. In addition, the composition of the liquid product (methanol, water, and HA) was determined to assess the influence of process conditions and gas composition on the product quality.

6.2 Description of the equilibrium model

An equilibrium model was developed for methanol synthesis which is described in Chapter 5. This theoretical model not only focuses on chemical gas phase equilibria but also includes the possible formation of a liquid phase. Here, only a short description of the model is given. The Soave-Redlich-Kwong equation of state, with a modification for polar components, is used to correct for nonideal behavior of the system [32]. A set of equations is solved accounting for the chemical and phase equilibria, and conservation of mass with a nonnegativity constraint. An example of such an equilibrium diagram is given in Fig. 6.1 for syngas 1 (H$_2$/CO/CO$_2$/CH$_4$:

70/5/20/5 vol%). The vapor and liquid phase are indicated with 'V' and 'L' respectively. The figure comprises 4 curves:

- ➢ Curve 1 (solid) represents the gas phase equilibrium.
- ➢ Curve 2 (dashed) is the conversion at which a dew point is reached.
- ➢ Curve 3 (dotted) represents the equilibrium if both conditions, chemical and phase equilibrium, are met.
- ➢ Curve 4 (dashed-dotted) is an extrapolation of the gas phase equilibrium curve (curve 1) to lower temperatures.

The four curves merge in point A, which represents the highest temperature (507 K in this example) at which a liquid phase is formed. At this temperature, the dew point temperature of the mixture is equal to the reactor temperature and the gas composition is equal to the equilibrium composition. Curve 4 is an extrapolation of the gas phase equilibrium curve without taking into account condensation. The difference between chemical equilibria (curve 4) and the combination of chemical and phase equilibria (curve 3) is indicated by the arrow marked 'B' in Fig. 6.1 and is the additional conversion that can be obtained due to condensation. It is clear that condensation is favorable for obtaining high equilibrium conversions.
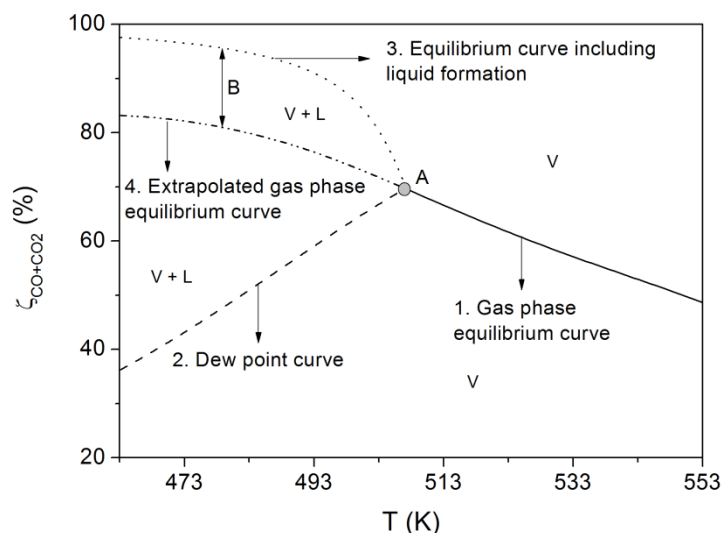
Fig. 6.1 Example of an equilibrium conversion diagram including chemical and phase equilibria. *P* = 20.3 MPa, syngas: H$_2$/CO/CO$_2$/CH$_4$ = 70/5/20/5 vol%.

6.3 Materials and methods

6.3.1 Materials

Model syngases were supplied by Westfalen-AG, Germany and their composition is given in Table 6.1. The relative deviation in the gas composition is 2% for each component. A commercial methanol synthesis catalyst (Cs doped Cu/ZnO/Al$_2$O$_3$) was used. All alcohols used

for calibration purposes were supplied by Sigma-Aldrich, The Netherlands and have a purity of at least 99%.

Table 6.1 Gas composition of the different syngases.

Syngas	H_2 (vol%)	CO (vol%)	CO_2 (vol%)	CH_4 (vol%)	N_2 (vol%)	C_2H_6 (vol%)	S_N (-)	Remarks
1	69.9	5.0	20.0	5.1		-	2.0	CO_2 rich
2	67.0 – 68.0	24.0 – 24.4	3.0 – 3.5	5.0 – 5.1	-	-	2.3	Typical Industrial syngas
3	54.5	19.7	20.3	4.0	1.0	-	0.9	Simulated RSCW gas (CO_2 rich)
4	54.2	28.9	10.9	4.0	-	2.0	1.1	Simulated RSCW gas (CO_2 lean)

6.3.2 Description of the setup

In Fig. 6.2 a schematic flow sheet of the setup is shown. The syngas was pressurized to the desired pressure using a gas booster (Maximator). The flow rate was regulated using a Brooks mass flow controller (MFC). The gas was preheated in a preheater (P1) consisting of an empty tube (*ID* = 10 mm, *L* = 500 mm) surrounded by an annular heating jacket. Methanol synthesis was conducted in two packed bed reactors (R1 and R2) in series each with the same dimension as the preheater. Both packed beds were filled with catalyst (50 and 51 g). The catalyst particles were crushed to obtain particles sizes between 1 and 2 mm.
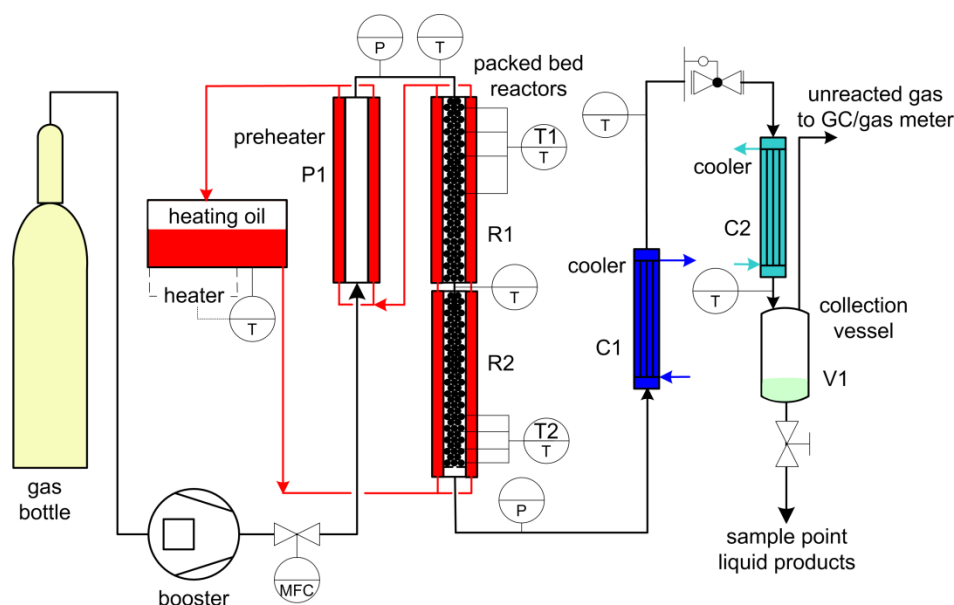
Fig. 6.2 Schematic flow sheet of the methanol synthesis setup.

Both packed bed reactors (R1 and R2) contained thermowells (T1 and T2 respectively) to record the temperature inside the catalyst bed. In the first packed bed reactor (R1) the temperature

was recorded at 5, 10, 20, and 30 cm from the top of the catalyst bed. The temperature of the second packed bed reactor (R2) was recorded at 4 locations in the last 10 cm of the catalyst bed. The temperature measured at the reactor exit (the last thermocouple of T2) in the centre of the catalyst bed was taken as the temperature for equilibrium calculations. When the exit gas was at or close to equilibrium the temperatures of the 4 thermocouples (T2) were within 1 K.

In a typical experiment, methanol synthesis occurred mainly in the first packed bed reactor (R1). Due to the exothermicity of the reaction the temperature increased in the first part of the packed bed and decreased in the second part and approached the oil temperature. The temperature in the second packed bed reactor was constant in most experiments and the exit temperature was at most 4 K below the temperature of the heating oil. After the second packed bed (R2), the reactor effluent was cooled in a cooler (C1) by tap water before depressurization to 1 MPa through a back-pressure valve. In a second cooler (C2), which was operated at 253 K the remaining condensables were liquefied. However, complete condensation proved cumbersome and entrainment of small amounts of methanol was observed in the tubing between the collection vessel (V1) and the gas meter and in the gas meter itself. After depressurization via a reducer the liquid was collected in a collection vessel (V1). The gas was quantified by a gas meter (Gallus G1.6) and analyzed by gas chromatography (GC). Experiments were conducted at pressures of 7.5 ± 1, 15 ± 1, and 20 ± 1 MPa and temperatures of the heating oil between 473 and 548 K. All parts of the system that were heated or cooled were well insulated with glass wool. The process pressure was determined by taking the average pressure of the two pressure meters. The gas hourly space velocities (*GHSV*) expressed as m^3 feed/m^3 cat./h (from here on the dimension h^{-1} is used) were varied between $0.5 \cdot 10^2 - 2.2 \cdot 10^2$ h^{-1}.

The experiments were conducted with a large amount of catalyst to aim for equilibrium conversions. The experimental data are shown in Appendix B. For some experiments duplicate experiments were performed. The relative deviation in the CO+CO$_2$ and H$_2$ conversion was below 2.5%. The conversions for syngas 2b at 15 MPa and 467-468 K were measured at two different space velocities (*GHSV* = $1.1 \cdot 10^2$ and $2.2 \cdot 10^2$ h^{-1}, exp. 26 and 27 respectively). The same was done for syngas 3 in exp. 40 and 41. The difference between the conversions measured was small indicating that equilibrium was reached.

The accuracy of each experiment was determined by the closure of the carbon balance. In the calculation of the carbon balances the organic fraction is assumed to consist of pure methanol. In the majority of the experiments the carbon balance closure is below 100% as small amounts of methanol do not condense in the second cooler (C2) and/or evaporate from the collection vessel (V1). The exit temperature of the second cooler (C2) for experiments with syngas 1 and the majority of syngas 2 was around 263 K and these experiments appeared to be the most accurate, as the closure of the carbon balances were in between 90 and 103%. For the remainder of the experiments with syngas 2, and all experiments with syngases 3 and 4, exit temperatures between 283 and 288 K were measured, due to which less methanol condensed and left the cooler in the vapor phase. The exit gas flows for these experiments were corrected

for the methanol present in the vapor phase. The carbon balances of these experiments were between 87 and 103%.

6.3.3 Analyses

The dry gas composition was analyzed using an online dual-column GC (GC 955, Syntech Spectras) equipped with thermal conductivity detectors. CO was analyzed over a molecular sieves 5 Å column (L = 1.6 m) with helium as carrier gas. CO_2, CH_4, and C_{2+} were analyzed on a Chromosorb 102 column (L = 1.6 m) with helium as carrier gas. H_2 was analyzed on the molecular sieves column using argon as carrier gas. The water content of the methanol was determined by Karl Fischer-titration. The composition of the organics in the liquid phase was determined with a GC (HP 5890 series II) equipped with a flame ionization detector (FID) using a Restek RTX-1701 column (L = 60 m, ID = 0.25 mm) coupled with a mass spectrometer (MS, HP 5972 series). The FID was used for quantification and the MS for identification. The FID was calibrated for the main constituents of the organic phase: methanol, ethanol, 1-propanol, 2-propanol, 1-butanol, 2-butanol, 1-pentanol, 2-methyl-1-propanol, and 2-methyl-1-butanol.

The composition of the organic phase and the water content were determined with different techniques. The total is not normalized to 100%. Any deviation from 100% reflects mainly the accuracy of the measurement methods used.

6.3.4 Statistical analyses of HA formation as a function of process conditions for syngas 4

The experimental results for each response (the concentrations of the most abundant higher alcohols) were analyzed statistically by means of the Design Expert 8 software package (Stat-Ease Inc.). The responses were modeled with a quadratic model using the following standard expression:

$$y_k = b_0 + \sum_i b_i x_i + \sum_i b_{ii} x_i^2 + \sum_i \sum_j b_{ij} x_i x_j \qquad \text{(Eq. 6.2)}$$

Here, i and j (i ≠ j) represent the independent variables T and P, while b_i, b_{ii}, b_{ij} are the regression coefficients which were obtained by statistical analyses of the data. The significant factors were selected based on their p-value in the ANOVA analyses. Factors with a p-value below 0.05 were regarded as significant and included in the response model. Step-wise elimination was applied to eliminate all statistically insignificant terms. After each elimination step a new ANOVA table was generated until all insignificant factors were removed.

6.4 Results and discussion

6.4.1 Overview of experiments

Sixty methanol synthesis experiments were conducted in a packed bed reactor using low *GHSV* values (< 2.2·10^3 h^{-1}) to aim for equilibrium conversions at the exit of the reactor. Four different syngases were used, see Table 6.1 for details. The results of all experiments are summarized in Table B.1 and B.2 in Appendix B. Table B.1 contains the reactions conditions, outlet gas and liquid composition, and both the experimental and theoretical equilibrium conversion. Table B.2 contains the composition of the liquid products.

Syngas 1 is a gas rich in H$_2$ with CO$_2$ as the main carbon oxide and a S_N of 2. Syngas 2 is typically used in conventional methanol synthesis with H$_2$ and CO as the main constituents and a S_N of 2.3. Syngases 3 and 4 are representative for syngases that can be obtained in the reforming of biomass in supercritical water. The S_N is below 2 (respectively 0.9 and 1.1) for both gases and H$_2$ is the limiting component. In the next sections, the major findings for each of the four syngas compositions will be further elucidated.

6.4.2 Results for syngas 1 (H$_2$/CO/CO$_2$/CH$_4$ = 70/5/20/5 vol%).

The experimental conversions for syngas 1 are shown in Fig. 6.3 as a function of the temperature at a fixed pressure of 20 ± 1 MPa. The highest conversions were obtained at 484 K, viz. 92% for both CO+CO$_2$ and H$_2$. A clear sharp increase in the conversion for this syngas was observed when the temperature was lowered to below approximately 507 K. Though puzzling at first instance, it appears that this is the condition at which condensation and thus the formation of a liquid phase occurs (see also Chapter 4). This observation was supported by model equilibrium calculations, see Fig. 6.1 for details (see also Chapter 5).

In general, the experimental data coincide nicely with the theoretical predictions including the occurrence of condensation at temperatures below 507 K. However, the experimental conversions at the lowest temperature in the range are considerably lower than the calculated equilibrium conversions. Likely, equilibrium is not reached due to the reduced reaction rates at this temperature. Deviations between experiments and model are noticeable for the conversions of the individual components CO and CO$_2$. This is particularly evident for CO, as the feed concentration of this component is low. The concentration of CO in the feed is only 5 vol% and the exit concentration is an order of magnitude lower. If for example part of the CO is converted to CO$_2$ via the water-gas shift reaction (Eq. 1.2), indicating an error in the model predictions at the higher temperatures, the influence of the deviation on the conversion of CO is larger than on CO$_2$.
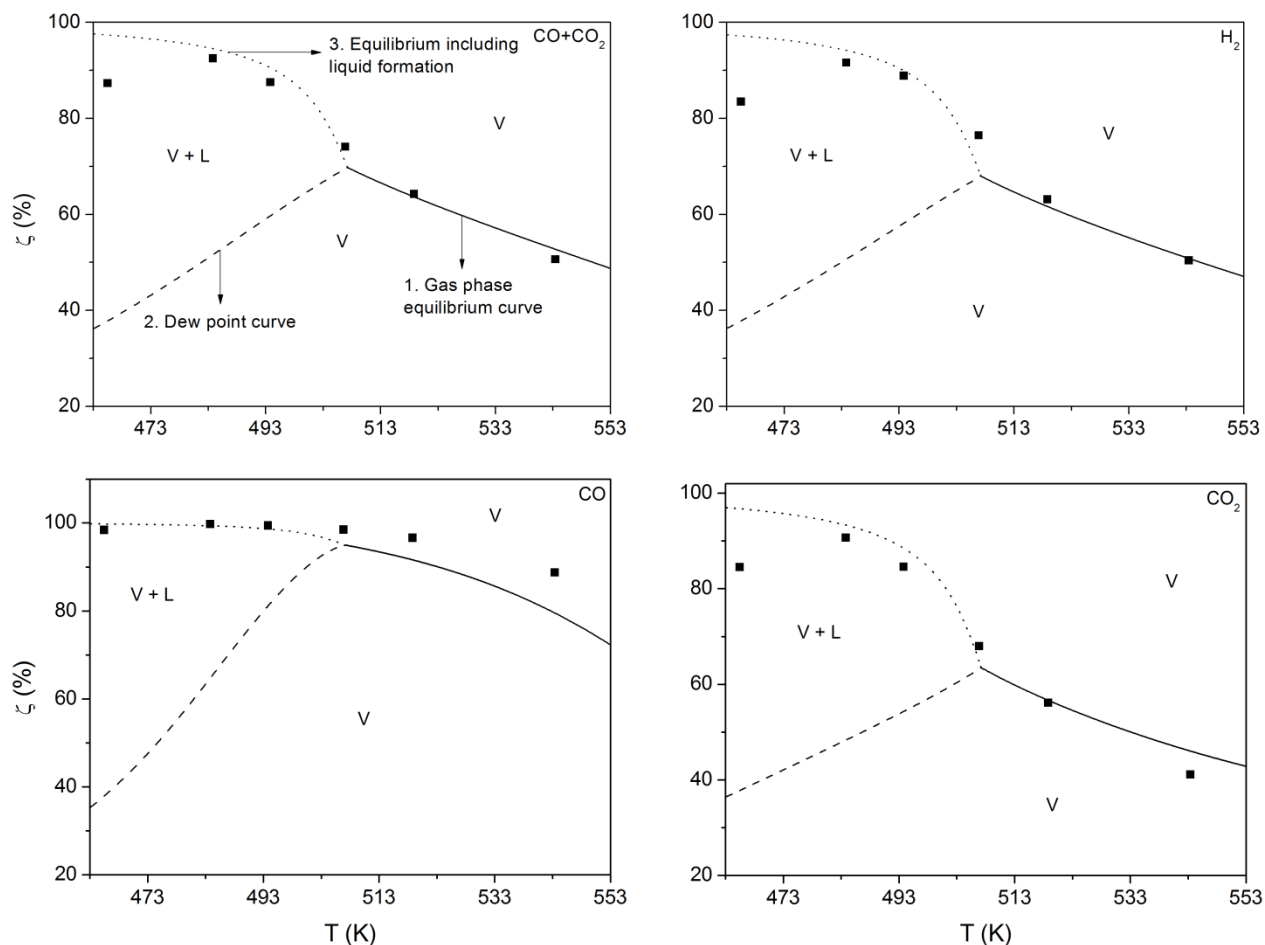
Fig. 6.3 Experimental conversion for syngas 1 including model predictions + dew point curves. *P* = 20.3 MPa (equilibrium calculation), syngas: $H_2/CO/CO_2/CH_4$ = 70/5/20/5 vol%. Symbols: experimental data; curves: model predictions.

The gas composition at the outlet of the reactor is shown in Fig. 6.4 for an experiment with syngas 1 at 20 ± 1 MPa. The higher temperature data (*T* > 510 K) correspond nicely with the equilibrium composition. At temperatures below the discontinuity, the area in which liquid formation is predicted, the experimental data follow the theoretical predictions (473 > *T* > 510 K) but deviations become noticeable as equilibrium is not reached, confirming the results shown in Fig. 6.3. Similar results are obtained for the lower pressures of 8 and 15 MPa.
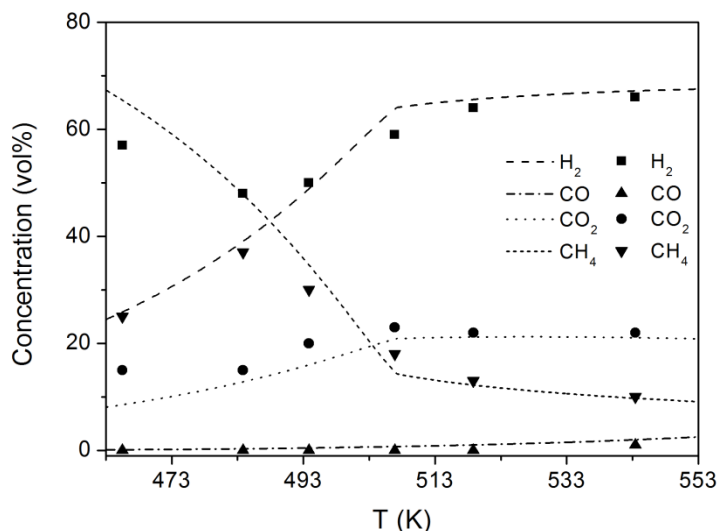
Fig. 6.4 Outlet gas composition for syngas 1. *P* = 20.3 MPa (equilibrium calculation), syngas: H$_2$/CO/CO$_2$/CH$_4$ = 70/5/20/5 vol%. Symbols: experimental data; curves: model predictions.

The experimental conversions at lower pressures (8 and 15.4 MPa) are shown in Fig. 6.5. At a pressure of 15.4 MPa the interval, in which both a vapor and a liquid phase exist, is much smaller than for 20.3 MPa. The highest temperature at which a dew point can be reached is 491 K, which is 16 K lower than at 20.3 MPa. At the lowest pressure (8.0 MPa) no dew point is predicted by the equilibrium model and experimental data points at temperatures exceeding 490 K coincide nicely with the equilibrium predictions. At lower temperatures, the experimental conversions are again lower than predicted by the equilibrium model, likely due to kinetic constraints.

The composition of the liquid products obtained with syngas 1 is given in Table B.2 in Appendix B. The liquid consists mainly of methanol (65 − 72 wt%) and water (27 − 34 wt%). In some liquid products, HA were found, though the amounts were very small (< 0.1 wt%). A clear relation between the water content and process conditions (pressure and temperature) is not observed. The equilibrium model predicts a slight increase in methanol concentration and a slight decrease in water concentration as a function of the temperature in the range of 463 to 543 K. The changes in the equilibrium composition depend on the system of three reactions (Eqs. 1.1 − 1.3), but can be rationalized accordingly. The increase in methanol is caused by a sharper decrease in CO$_2$ conversion, leading to methanol and water, compared to the decrease of CO conversion, leading to methanol only, with only small contributions of the WGS reaction. At temperatures exceeding 543 K the water concentration increases due to a larger share of the reverse WGS reaction (Eq. 1.2).
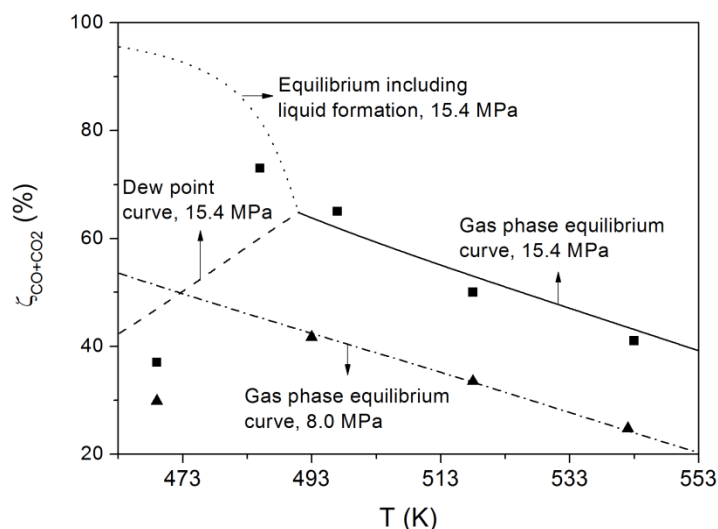
Fig. 6.5 Experimental conversion for syngas 1 including model predictions + dew point curves. P = 8.0 and 15.4 MPa (equilibrium calculations), syngas: $H_2/CO/CO_2/CH_4$ = 70/5/20/5 vol%. Symbols: experimental data; curves: model predictions.

6.4.3 Results for syngas 2a/2b: $H_2/CO/CO_2/CH_4$ = 67 − 68/24/3 − 4/5 vol%.

Syngas 2 represents a conventional methanol synthesis syngas, with a S_N of 2.3. A graphical representation of the results for syngas 2 is given in Fig. 6.6. At the lower temperatures, the conversion of CO and CO_2 are predicted accurately, however, above 495 K the conversion of both components starts to differ from the model predictions. The CO conversion is higher than predicted whereas the CO_2 conversion is lower. The deviations from the predicted values seem to be large for CO_2, but it should be kept in mind that the feed concentration of CO_2 is much lower than the feed concentration of CO. At the highest temperatures, the CO_2 conversion even becomes negative, indicating a net CO_2 production. The difference from the model prediction is larger for this syngas than for syngas 1 and points most probably at the formation of HA, in particular at the highest temperature, which is known from literature at these conditions [15, 33]. For example, for a $Cu/Zn/Al_2O_3$ + 0.85 wt% Cs catalyst (P = 10 MPa, T = 573 K, *GHSV* = 4000 h^{-1}, H_2/CO = 1) a HA content of 13.7 wt% was reported in the literature [15].

Analyses of the organic fraction in the liquid phase (GC-MS/FID) indeed revealed an increase in HA up to 3.7 wt% at the highest temperature. Due to the formation of water in HA synthesis part of the CO is converted to CO_2 resulting in higher CO conversions and lower CO_2 conversion than predicted.
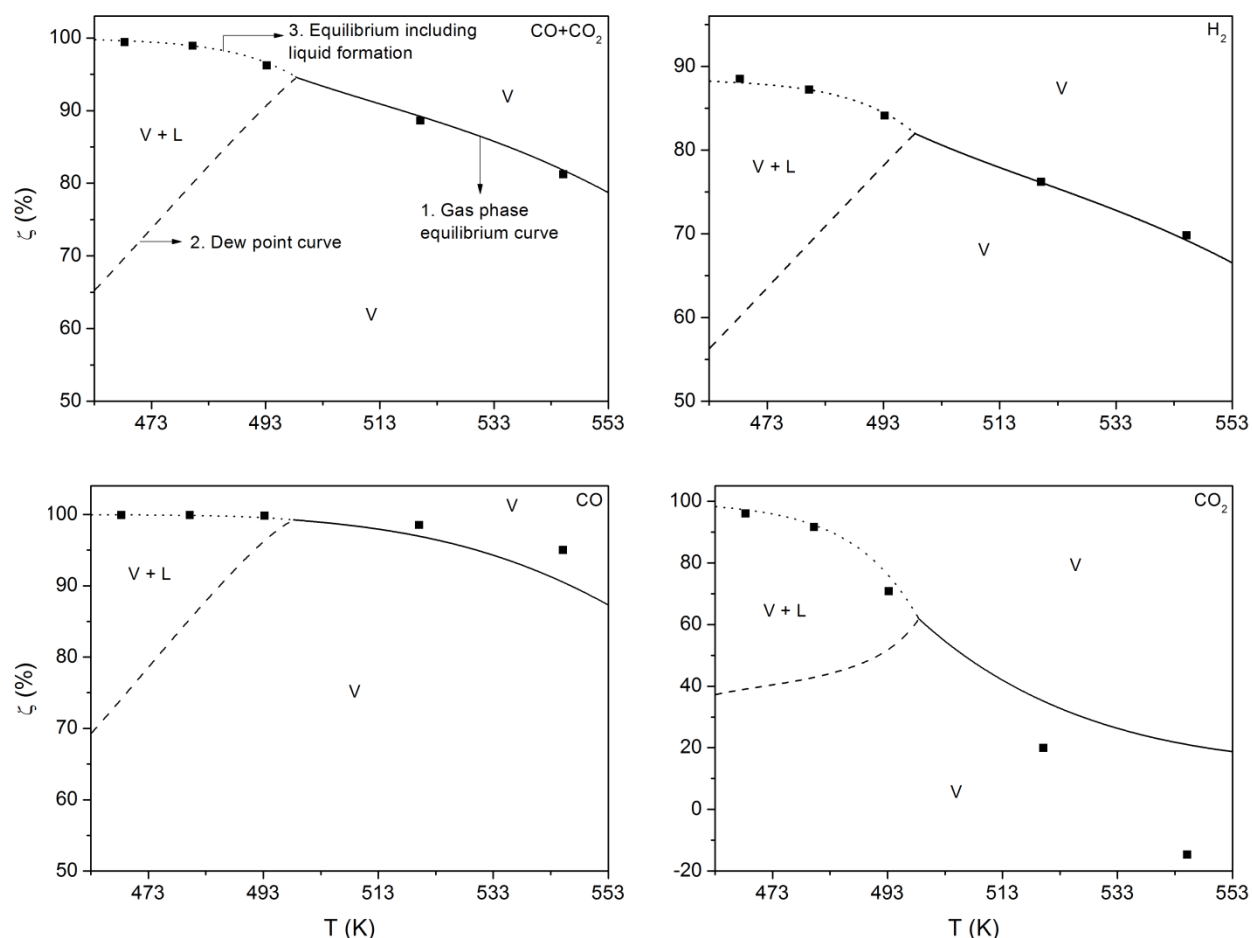
Fig. 6.6 Experimental conversion for syngas 2 including model predictions + dew point curves. *P* = 19.7 MPa, syngas: H$_2$/CO/CO$_2$/CH$_4$ = 67/24/4/5 vol%. Symbols: experimental data; curves: model predictions.

The data obtained at 7.8 MPa and 15.1 MPa can also be accurately described with the model, although a small amount HA (< 3.0 wt%) was produced at the higher temperatures. The conversion increases with increasing pressure and decreases with increasing temperature as thermodynamics dictate. The difference in conversion between the two pressures becomes larger at the higher temperatures.

At the lower temperatures the concentration of HA is very low (see Table B.2 in Appendix B), but at the higher temperatures the concentration increases. The main HA present were ethanol and 1-propanol. The methanol concentration for syngas 2 was between 89.7 and 97.1 wt% with a corresponding water concentration of 2.6 – 9.0 wt%. Compared to syngas 1 (CO$_2$-rich), the methanol concentration is higher and water concentration obviously lower as less CO$_2$ was converted in the case of syngas 2.

6.4.4 Results for syngas 3: H$_2$/CO/CO$_2$/CH$_4$/N$_2$ = 55/20/20/4/1 vol%.

For the RSCW-like syngases 3 and 4, H$_2$ is the limiting component. For syngas 3, the conversion results are shown in Fig. 6.7. At the lowest temperatures, the equilibrium conversion was not

reached, but again, at the other temperatures the equilibrium predictions coincide nicely with the experimental data. At a pressure of 19.4 MPa a dew point was calculated for temperatures below 480 K. The presence of this dew point, however, does not have a significant influence on the equilibrium conversion.

The liquid phase, for experiments with syngas 3, contains mainly water and methanol, while the HA concentration is low (at most 2.5 wt%). The HA content increased with temperature at 14.9 and 19.4 MPa. The water content (24.6 and 20.5 wt% for exp. 42 and 43) seems rather high and can neither be explained by the CO_2 conversion nor by the HA quantity. Probably, due to high surroundings temperatures (± 305 K) a disproportionate amount of CH_3OH compared to H_2O has been evaporated from the liquid collection vessel leading to higher water concentrations than expected.
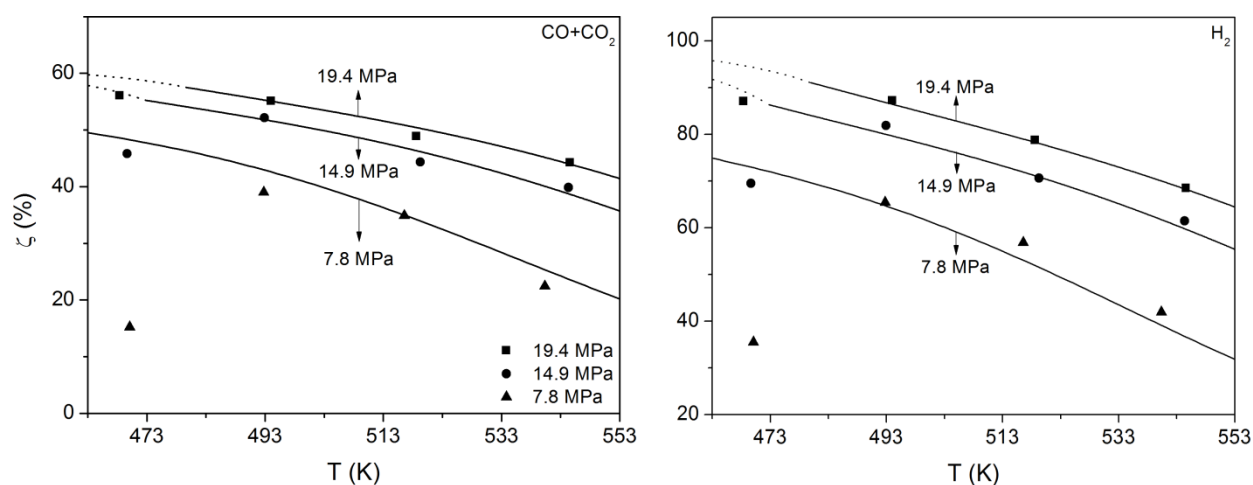
Fig. 6.7 Experimental conversion for syngas 3 at three different pressures including model predictions. P = 7.8, 14.9, and 19.4 MPa (equilibrium calculations); syngas: $H_2/CO/CO_2/CH_4/N_2$ = 55/20/20/4/1 vol%. Symbols: experimental data; curves: model results.

6.4.5   Results for syngas 4: $H_2/CO/CO_2/CH_4/C_2H_6$ = 54/29/11/4/2 vol%.

The composition of syngas 4 is comparable to syngas 3, except for the CO/CO_2 ratio, which is approximately three times higher than for syngas 3. The experimental conversion at different pressures as a function of the temperatures is shown in Fig. 6.8. The maximum theoretical conversion, 67.5% for $CO+CO_2$ and 100% for H_2, is not an equilibrium conversion, but the conversion when the limiting component H_2 is converted completely. The conversion of $CO+CO_2$ and H_2 increased with increasing pressure and decreasing temperature and approached the highest theoretical conversion at the highest pressure and lowest temperature. The reaction products were methanol, water, and a substantial amount of HA. The conversions at 19.8 MPa can be found in Fig. 5.14 in Chapter 5. When the experimental conversions are compared to the model predictions, good agreement is found for the lowest temperature, while at higher temperatures large differences are obtained. The differences can be attributed to the formation

of HA, which is by far the most significant for syngas 4, and most probably due to the high CO partial pressures.
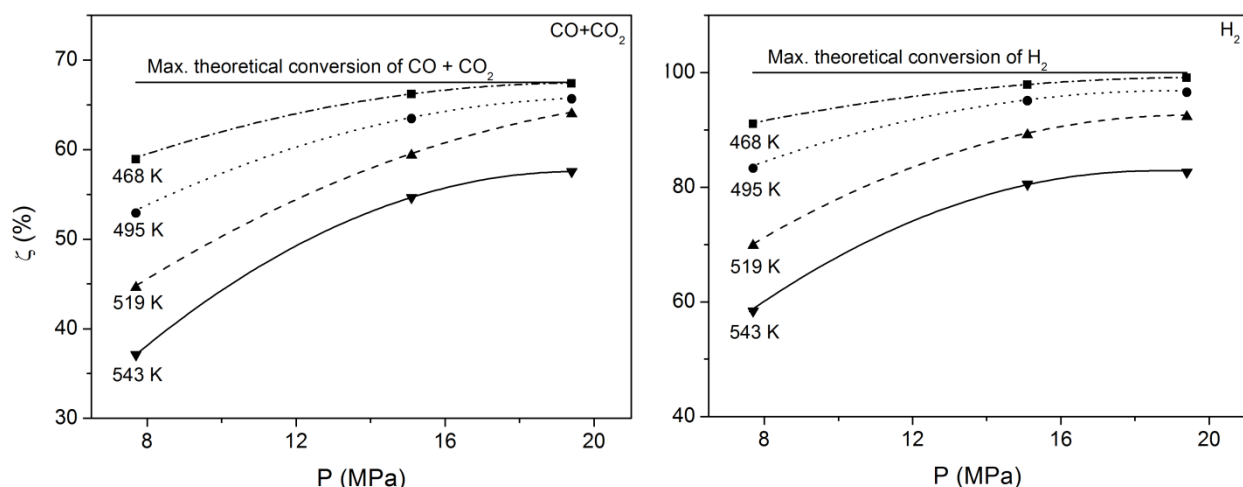
Fig. 6.8 Experimental conversion for syngas 4 as a function of the pressure for 4 temperatures. Syngas: H$_2$/CO/CO$_2$/CH$_4$/N$_2$ = 54/29/11/4/2 vol%. The lines are trend lines and they are for indicative purposes only.

6.4.6 HA formation for syngas 4

HA concentration for syngas 4 can be as high as 13.9 wt% (see Table B. 2 in Appendix B, exp. 48-60). This value is comparable to a concentration of 13.7 wt% reported in the literature for a Cu/Zn/Al$_2$O$_3$ + 0.85% Cs catalyst (P = 10 MPa, T = 573 K, $GHSV$ = 4000 h^{-1}, H$_2$/CO = 1). In dedicated HA synthesis the yields can be much higher as HA yields of 58 wt% have been reported for a ZnO/Cr$_2$O$_3$ + 3% K$_2$O catalyst (P = 8.5 MPa, T = 678 K, $GHSV$ = 8000 h^{-1}, H$_2$/CO = 1) [15]. Based on thermodynamics, the formation of HA is expected [33, 34], but is not included in the equilibrium model used in this study, as the focus is on methanol synthesis. The main HA formed in the experiments were ethanol and 1-propanol followed by 1-butanol, 2-methyl-1-propanol, and 2-methyl-1-butanol (Eq. 6.1 and Scheme 6.1). The product distribution seems to follow the Smith-Anderson growth pathway (similar product ratios were observed), although also some 1-pentanol and larger primary alcohols were detected [25, 26]. Besides the HA indicated above, small amounts of more than 100 organic products were identified by GC-MS, including esters, aldehydes, and HA even up to 1-undecanol. These components were not quantified, because their concentrations were estimated to be below 0.05 wt% in general. The concentration of the most abundant alcohols (methanol, ethanol, 1-propanol, 1-butanol, 2-butanol, and 2-methyl-1-propanol) is given in Fig. 6.9 as a function of the process conditions. The methanol concentration clearly decreases over the temperature range in favor of the HA, with ethanol being the predominant one.
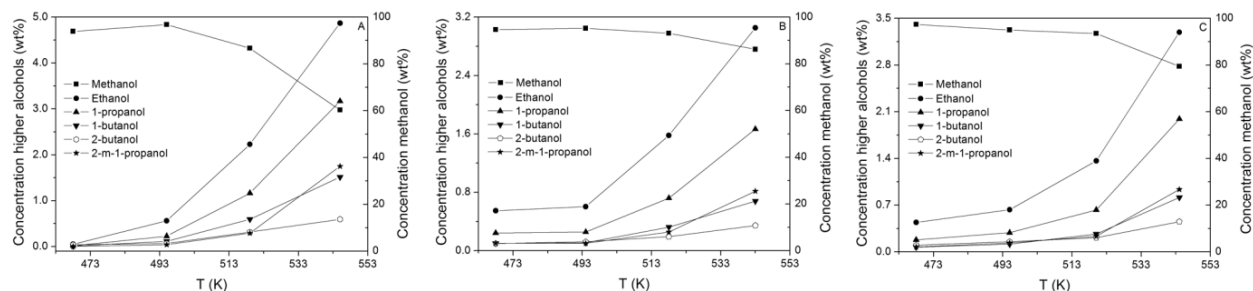
Fig. 6.9 Alcohol concentration for syngas 4 as a function of the temperature for 7.6 MPa (A), 15.1 MPa (B), 19.9 MPa (C). Syngas: $H_2/CO/CO_2/CH_4/C_2H_6$ = 54/29/11/4/2 vol%.

The concentration of individual HA components increases exponentially with the temperature, which is in agreement with literature data [15, 22]. It is known that Cs (the dopant of the catalyst used in this study) promotes the formation of ethanol, but enhances the C_3 alcohol formation to an even greater extent (see Table 6.2) [22].

Table 6.2 Alcohol yields over Cu/ZnO catalysts from the literature [22]. P = 7.6 MPa, T = 583 K, $GHSV$ = 3260 L/kg cat./h, H_2/CO = 0.45. Other organic products and hydrocarbons are omitted.

	Methanol	Ethanol	1 -propanol	2-methyl-1-propanol	1-butanol	2-methyl-1-butanol
Catalyst				(g/kg cat./h)		
Cu/ZnO	204	22.6	10.1	20.7	3.4	8.6
0.34 mol% Cs on Cu/ZnO	157	17.0	38.1	48.6	8.2	15.5

The HA yield for ethanol and 1-propanol, the most abundant species, were modeled using nonlinear multivariable regression based on two independent parameters (T and P). The 13 experiments for syngas 4 were best modeled using quadratic models for the individual components data. The R^2, $R^2_{adjusted}$, and R^2_{PRESS} are given in Table 6.3, and indicate that the models are suitable to navigate the design space.

Table 6.3 Regression coefficients for ethanol and 1-propanol.

Variable (x_i)		Ethanol Coefficient	1-propanol Coefficient
	Intercept (b_0)	149.51	115.08
T (x_1)	b_1	-0.662	-0.501
P (x_2)	b_2	1.152	0.774
$x_1 x_2$	b_{12}	-0.00236	-0.00159
x_1^2	b_{11}	0.00073	0.00054
x_2^2	b_{22}	ns.[a]	ns.[a]
	R^2	0.98	0.95
	$R^2_{adjusted}$	0.97	0.93
	R^2_{PRESS}	0.91	0.80

[a]n.s.: nonsignificant terms

The parity plots of the models are given in Fig. 6.10 and they confirm the good predictive capability of the model.
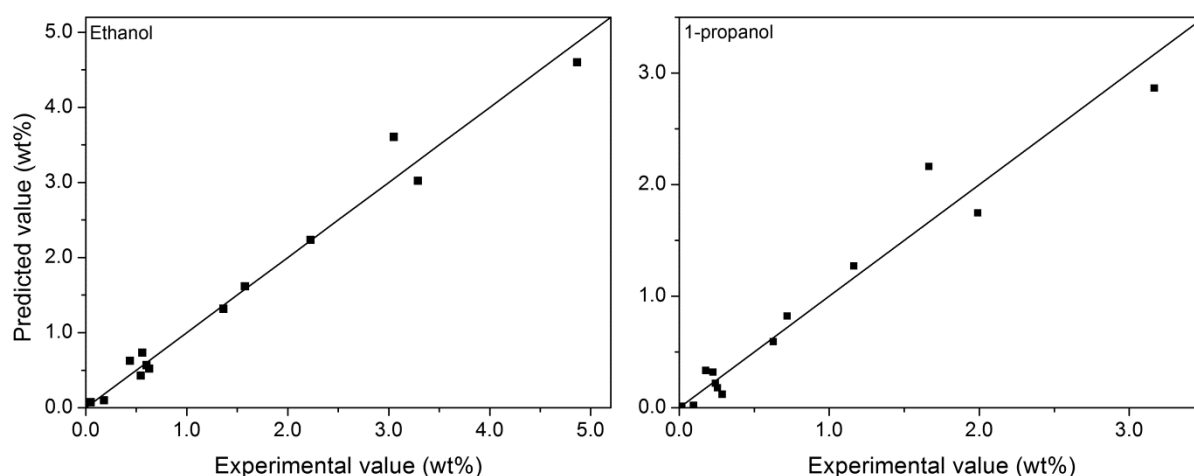
Fig. 6.10 Parity plot for the experimental and predicted values of the concentration of ethanol and 1-propanol.

The combined effect of pressure and temperature on the HA synthesis is visualized in 3D graphs in Fig. 6.11. The concentration of ethanol and 1-propanol shows similar trends. The concentration increases with temperature. The pressure effect is more complex and higher pressure seems to have a slight promoting effect on the HA synthesis at lower temperatures and a suppressing effect at the higher temperatures. The highest quantity of HA is obtained at the combination of the lowest pressure and the highest temperature. An hypothesis for this phenomenon is that the competitive adsorption of water with intermediate species that form the HA starts to play a more predominant role at higher pressures [29]. Due to a larger quantity of HA at the higher temperatures more H$_2$O is produced.
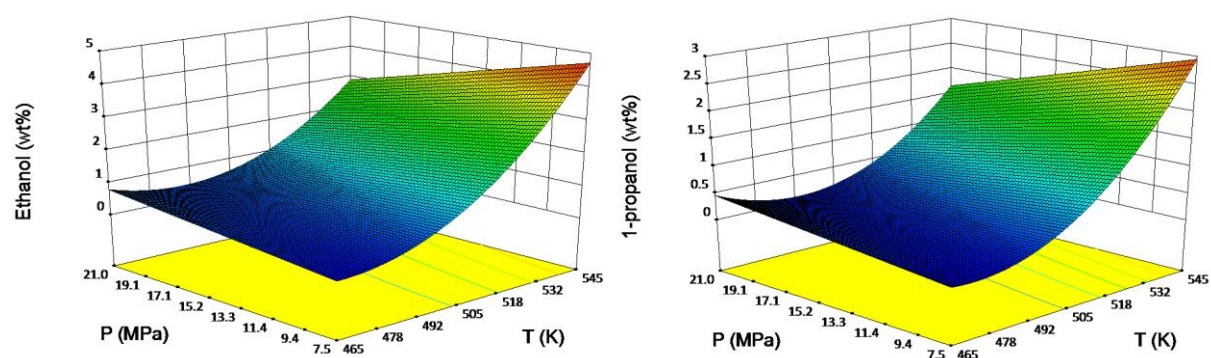
Fig. 6.11 Statistical dependence of the HA concentration as a function of the pressure and temperature, ethanol (A), 1-propanol (B). Syngas: $H_2/CO/CO_2/CH_4/N_2$ = 54/29/11/4/2 vol%, *GHSV* = 1.8/1.9·10^3 h^{-1}.

Besides the absolute pressure and temperature, the gas composition plays an important role in the formation of HA, which could not be modeled successfully using the statistical models described in this section. The HA concentration increases generally with a decreasing H_2/CO ratio, which is known from literature [15]. The maximum HA content as a function of the H_2/CO ratio is depicted in Table 6.4. The HA content cannot be solely related to the H_2/CO ratio as the CO_2 concentration plays an important role. If the H_2/CO ratio decreases and the CO/CO_2 ratio as well (syngas 2 vs. 3), the HA yield can go down. This is most probably caused by the conversion of CO_2 to methanol yielding water which is known to suppress the formation of HA [15, 20]. When CO_2 is the most abundant carbon oxide (syngas 1) hardly any HA were observed.

Table 6.4 HA content for the different syngases.

Syngas	H_2/CO (-)	CO/CO_2 (-)	S_N (-)	HA at 8 ± 1 MPa (wt%)	HA at 20 ± 1 MPa (wt%)
1	14.0	0.3	2.0	0.1	0.1
2	2.8	6.0	2.3	6.0	3.7
3	2.8	1.0	0.9	0.1	1.7
4	1.9	2.6	1.1	13.9	8.6

6.5 Conclusion

A detailed study of once-through high pressure methanol synthesis was performed in a packed bed reactor over a Cs doped $Cu/ZnO/Al_2O_3$ catalyst. The main focus was on equilibrium data, which were obtained by conducting experiments at relatively low *GHSV* values (0.5·10^3 – 2.2·10^3 h^{-1}) and measuring the exit gas compositions. In the high pressure, low temperature regime the conversion of the limiting components was almost complete, due to the *in situ* formation of a liquid phase. The exit gas compositions and the high conversions (up to 99.5%) measured at these conditions can be accurately predicted with a theoretical equilibrium model. The syngas

conversion increased with increasing pressure and decreasing temperature as thermodynamics dictate. The formation of higher alcohols in methanol synthesis was a function of mainly the temperature and the syngas composition. For a syngas composed of mainly H$_2$ and CO, higher alcohol concentrations up to 14 wt% were observed.

The results imply that methanol synthesis in a once-through mode at high pressure is possible as high (equilibrium) conversions of the limiting component in the syngas were obtained. Thus, recycle streams used in conventional methanol synthesis can be omitted leading to process simplifications. However, such a process is attractive only if syngas at 20 MPa or more is available (without an energy intensive gas compression step). A pressurized syngas can be obtained e.g. in biomass reforming in supercritical water where syngas at pressures > 22.1 MPa is obtained by pumping a carbon containing liquid (or slurry) to high pressure, prior to its gasification. Advantageously, pressurizing a liquid consumes much less energy than gas compression and, when biomass resources are used, 'renewable', green methanol is produced. Reactions rates in high pressure methanol synthesis are expected to be higher than for the conventional low pressure processes, leading to either smaller reactors or possibilities for higher throughputs in existing ones. These studies are in progress and some preliminary results are reported in Appendix C and D.

6.6 References

1   G.A. Olah, A. Goeppert, G.K.S. Prakash, Beyond oil and gas: The methanol economy, Wiley-VCH, Weinheim, (2006).
2   E. Supp, How to produce methanol from coal, Springer-Verlag, Berlin, (1990).
3   J. Skrzypek, J. Stoczynski, S. Ledakowicz, Methanol synthesis, Polish Scientific Publishers PWN, Warsaw, (1994).
4   J.G. van Bennekom, J.G.M. Winkelman, R.H. Venderbosch, S.D.G.B. Nieland, H.J. Heeres, Modeling and experimental studies on phase and chemical equilibria in high-pressure methanol synthesis, Ind. Eng. Chem. Res., 51 (2012) 12233-12243.
5   J.B. Hansen, F. Joensen, High conversion of synthesis gas into oxygenates, in: A. Holmen (Ed.) Proceeding of the NGCS, Elsevier Science Publishers B.V., Oslo, (1991) 457-467.
6   T. Chang, R.W. Rousseau, P.K. Kilpatrick, Methanol synthesis reactions: Calculations of equilibrium conversions using equations of state, Ind. Eng. Chem. Process Des. Dev., 25 (1986) 477-481.
7   G.H. Graaf, P.J.J.M. Sijtsema, E.J. Stamhuis, G.E.H. Joosten, Chemical equilibria in methanol synthesis, Chem. Eng. Sci., 41 (1986) 2883-2890.
8   H. Liu, Z. Luo, B. Zhu, Study of chemical equilibria in methanol synthesis, Fuel Sci. Technol. Int., 12 (1994) 815-827.
9   J. Skrzypek, M. Lachowska, D. Serafin, Methanol synthesis from CO$_2$ and H$_2$: Dependence of equilibrium conversions and exit equilibrium concentrations of components on the main process variables, Chem. Eng. Sci., 45 (1990) 89-96.
10   L. Hui, L. Zanchun, Z. Bingchen, Study of chemical equilibria in methanol synthesis, Fuel Sci. Technol. Int., 12 (1994) 815-827.
11   B.S. Lacy, R.G. Dunning, H.H. Storch, Equilibrium in the synthesis and decomposition of methanol, J. Am. Chem. Soc., 52 (1930) 926-938.
12   D.M. Newitt, B.J. Byrne, H.W. Strong, Equilibrium in the system methyl alcohol-hydrogen-carbonic oxide, Proc. R. Soc. London, Ser. A, A123 (1928) 236-252.

13   D.F. Smith, B.F. Branting, The equilibrium between methanol, carbon monoxide and hydrogen, J. Am. Chem. Soc., 51 (1929) 129-139.

14   E.F. von Wettberg, B.F. Dodge, The methanol equilibrium, Ind. Eng. Chem., 22 (1930) 1040-1046

15   P. Forzatti, E. Tronconi, I. Pasquin, Higher alcohol synthesis, Catal. Rev. Sci. Eng., 33 (1991) 109-168.

16   F.E. Danes, D. Geana, Calcul de l'équilibre chimique à la synthèse du méthanol par les équations d'état des gaz hautement comprimés, Rev. Roum. Chim., 26 (1981) 947-954.

17   C.E. Brown, C.O. Bennet, Methanol synthesis catalysis in an internally recycled reactor, AIChE J., 16 (1970) 817-823.

18   W. Kotowski, The yield of methanol synthesis from various $CO+CO_2+H_2$ mixtures, Przem. Chem., 44 (1965) 66-71.

19   G. Natta, Synthesis of methanol, in: P.H. Emmett (Ed.) Catalysis: Hydrogenation and dehydrogenation, Rheinhold, New York, (1955) 349-411.

20   C.D. Graves, Higher alcohols formed from carbon monoxide and hydrogen, Ind. Eng. Chem., 23 (1931) 1381-1385.

21   P.K. Frolich, D.S. Cryder, Catalysts for the formation of alcohols from carbon monoxide and hydrogen, Ind. Eng. Chem., 22 (1930).

22   J.G. Nunan, C.E. Bogdan, K. Klier, K.J. Smith, C.W. Young, R.G. Herman, Higher alcohol and oxygenate synthesis over cesium-doped Cu/ZnO catalysts, J. Catal., 116 (1989) 195-221.

23   J.G. Nunan, R.G. Herman, K. Klier, Higher alcohol synthesis and oxygenate synthesis over Cs/Cu/ZnO/M_2O_3 (M = Al, Cr) catalysts, J. Catal., 116 (1989) 222-229.

24   D.J. Elliot, F. Pennella, Mechanism of ethanol formation from synthesis gas over Cu/O/ZnO/Al_2O_3, J. Catal., 114 (1988) 90-99.

25   K.J. Smith, R.B. Anderson, A chain growth scheme for the higher alcohols synthesis, J. Catal., 85 (1984) 428-436.

26   K.J. Smith, R.G. Herman, K. Klier, Kinetic modeling of higher alcohol synthesis over alkali-promoted Cu/ZnO and MoS2 catalysts, Chem. Eng. Sci., 45 (1990) 2639-2646.

27   B. Denise, R.P.A. Sneeden, Hydrocondensation of carbon dioxide: IV, J. Mol. Catal., 17 (1982) 359-366.

28   X. Xiaoding, E.B.M. Doesburg, J.J.F. Scholten, Synthesis of higher alcohols from syngas - recently patented catalysts and tentative ideas on the mechanism, Catal. Today, 2 (1987) 125-170.

29   E. Tronconi, N. Ferlazzo, P. Forzatti, I. Pasquon, Synthesis of alcohols from carbon oxides and hydrogen. 4. Lumped kinetics for the higher alcohol synthesis over a Zn-Cr-K oxide catalyst, Ind. Eng. Chem. Res., 26 (1987) 2122-2129.

30   J.G. van Bennekom, R.H. Venderbosch, D. Assink, H.J. Heeres, Reforming of methanol and glycerol in supercritical water, J. Supercrit. Fluids, 58 (2011) 99-113.

31   J.G. van Bennekom, R.H. Venderbosch, D. Assink, K.P.J. Lemmens, H.J. Heeres, Bench scale demonstration of the Supermethanol concept: The synthesis of methanol from glycerol derived syngas, Chem. Eng. J., 207-208 (2012) 245-253.

32   P.M. Mathias, A versatile equilibrium equation of state, Ind. Eng. Chem. Process Des. Dev., 22 (1983) 385-391.

33   G.C. Chinchen, P.J. Denny, J.R. Jennings, M.S. Spencer, K.C. Waugh, Synthesis of methanol. Part 1. Catalysts and kinetics, Appl. Catal., 36 (1988) 1-65.

34   V. Subramani, S.K. Gangwal, A review of recent literature to search for an efficient catalytic process for the conversion of syngas to ethanol, Energy Fuels, 22 (2008) 814-839.

7 Bench scale demonstration of the Supermethanol concept
The synthesis of methanol from glycerol derived syngas

Abstract

An integrated process for the synthesis of methanol from aqueous glycerol involving reforming of the feed to syngas followed by methanol synthesis is successfully demonstrated in a continuous bench scale unit. Glycerol reforming was carried out at pressures of 24 – 27 MPa and temperatures of 948 – 998 K with a throughput of approximately 1 kg aqueous feed/h (3 – 10 wt% glycerol) leading to high glycerol conversions (95.0 – 99.9%) and syngas with a composition range of $H_2/CO/CO_2/C_xH_y$ = 44 – 67/1 – 21/16 – 34/2 – 18 vol%. The effluent water of the process was recycled at high pressure, reducing the water consumption of the process significantly. Subsequent syngas conversion to methanol was carried out in a packed bed reactor at temperatures between 468 and 518 K and pressures between 24 and 27 MPa using a commercial methanol catalyst (Cs doped $Cu/ZnO/Al_2O_3$). The maximum yield of methanol based on glycerol intake was 0.62 kg methanol/kg glycerol for an experiment with a time on stream of 16 h, which corresponds to a carbon conversion (carbon in methanol over carbon in glycerol) of 60%. This value is close to the maximum theoretical yield of 78% based on stoichiometric considerations.

7.1 Introduction

Methanol, the simplest of all alcohols, has a wide application range. It is mainly used for the production of bulk chemicals like formaldehyde, acetic acid, and a wide variety of application products including polymers, paints, and adhesives. In addition, methanol can be used as a clean and renewable energy carrier [1]. The global annual production of methanol is on the rise and amounted approximately 38 million metric tons in 2007 [2]. Typically, methanol is produced from syngas, a mixture of predominantly H_2, CO and minor quantities of CO_2 and CH_4. Methanol is commercially produced mainly in gas-solid catalytic reactors and involves three equilibrium reactions, viz.: (i) hydrogenation of CO (Eq. 1.1), (ii) the (reverse) water-gas shift (WGS) reaction (Eq. 1.2), and (iii) hydrogenation of CO_2 (Eq. 1.3) [3]:

$CO + 2\ H_2$	$\rightleftharpoons$	CH_3OH	$\Delta_r H^0_{298}$ = -90.64 kJ/mol	(Eq. 1.1)
$CO_2 + H_2$	$\rightleftharpoons$	$CO + H_2O$	$\Delta_r H^0_{298}$ = +41.17 kJ/mol	(Eq. 1.2)
$CO_2 + 3\ H_2$	$\rightleftharpoons$	$CH_3OH + H_2O$	$\Delta_r H^0_{298}$ = -49.47 kJ/mol	(Eq. 1.3)

The stoichiometric ratio (S_N) of the syngas is defined as [4]:

$$S_N = \frac{(H_2 - CO_2)}{(CO + CO_2)} \qquad \text{(Eq. 1.4)}$$

With S_N equal to 2, all reactants can be converted to methanol. For $S_N > 2$, CO+CO_2 are the limiting components, while for $S_N < 2$, H_2 is limiting.

In view of environmental issues and diminishing fossil fuel reserves, the production of chemicals and fuels from renewable carbon sources has attracted considerable interest [1]. Methanol is commonly produced from fossil resources like natural gas or coal, however, biomass can also be used as resource. This allows the synthesis of green methanol which not only has an environmental bonus but may also lead to considerable variable costs reductions when the biomass is a waste product with a zero or negative value.

Methanol synthesis from biomass was already proposed during the first oil crisis in the 1970s [1]. In the 1980s a comprehensive review was published on the production of methanol from syngas derived from wood. Different gasification technologies were proposed and demonstration projects of these technologies were discussed [5, 6]. In the mid 1990s several projects on methanol synthesis from biomass were initiated such as the Hynol project in the USA and the BLGMF (black liquor gasification with motor fuels production) project in Sweden [7-9]. Unfortunately no experimental data of these processes is available in the open literature.

Methanol production from biomass was experimentally demonstrated by reforming pyrolysis oil into H_2 and CO_2 followed by catalytic syngas conditioning (to H_2/CO/CO_2/N_2 = 59/31/9/1 vol%) and subsequent methanol synthesis in a packed bed (533 K and 5.0 MPa) [10]. An overall carbon conversion of 23% was obtained at a production rate of 1.32 kg methanol/kg cat./h. At

industrial scale, Chemrec in Sweden produces methanol and dimethyl ether (DME) from syngas obtained by entrained flow gasification of black liquor [11, 12]. The plant capacity is 4 tons of DME per day and the first DME and methanol were produced in 2011. The production of methanol from glycerol was demonstrated on an industrial scale by BioMCN in The Netherlands [13]. Glycerol, produced as byproduct in biodiesel synthesis, became an interesting biomass resource as the biodiesel production increased in the 2000s. BioMCN has adapted their natural gas reforming unit to a unit suitable for steam reforming of glycerol to syngas. Subsequently the syngas is converted to methanol in conventional packed bed methanol synthesis reactors. The capacity of their plant is 250 ML of methanol/y [13].

Most publications on methanol production from biomass are desk-top studies and data comparison is difficult [8, 9, 14-18]. These studies often combine biomass gasification and conventional methanol synthesis with, in some cases, electricity production [8, 9, 16, 18]. Another concept of using biomass to produce methanol is the co-processing of biomass and fossil resources, e.g. co-gasification of biomass with coal or natural gas [14, 15, 17]. The advantage of this approach is that the S_N can be adjusted without gas conditioning or removal of CO_2 as the S_N of syngas from biomass is < 2 and of natural gas > 2 [14].

The concepts involved in the current processes for the synthesis of methanol from biomass generally involve an initial gasification step at elevated temperatures and pressures. Our interest involves syngas production by a hydrothermal process, viz. conversion of a wet biomass stream to syngas by reforming in supercritical water (RSCW), followed by methanol synthesis.

RSCW has been under investigation since the late 1970s and several comprehensive reviews have been published [19-23]. One of the advantages of RSCW is that the syngas is produced at elevated pressures (> 22.1 MPa). This is particularly advantageous for the subsequent methanol synthesis. At higher pressures the chemical equilibria, as given in Eqs. 1.1-1.3, favor the reaction products, methanol and water, and high conversions (up to 98%, depending on gas composition, temperature, and pressure) can be obtained in a single reactor pass. In Fig. 7.1 the equilibrium conversions for conventional methanol synthesis, BASF's high pressure methanol synthesis (1920 – 1960), and the current work at relevant process conditions are given [4].

Even more advantageously, conversions can be higher than expected purely based on gas phase equilibria, as at high pressure and 'low' temperature (e.g. 20 – 25 MPa and 473 K) a liquid methanol phase is formed (see Chapters 4 and 5). At certain process conditions and syngas compositions, equilibrium conversions of $CO+CO_2$ can exceed 99.5%. Thus, a combination of the RSCW of a suitable biomass resource for high pressure syngas production followed by methanol synthesis may have advantages compared to gasification and low pressure methanol synthesis concepts.

In this chapter an experimental demonstration of the integration of the RSCW of glycerol (a model biomass resource) and methanol synthesis in a dedicated continuous bench scale unit is presented aiming at maximizing the methanol yield per kg of glycerol. The performance of the process in terms of glycerol conversion, methanol yield, and carbon balances will be evaluated and discussed and strong and weak points of the concept are addressed. The use of recycling

the effluent water in the reformer section at high pressure is demonstrated which has, to the authors' knowledge, not been shown before and is an absolute novelty of this paper.
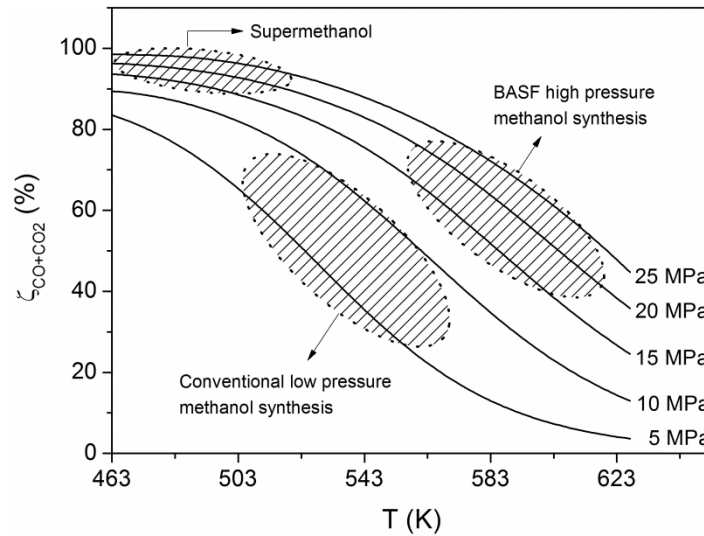
Fig. 7.1 Equilibria in methanol synthesis for different pressures ($H_2/CO/CO_2/CH_4 = 67/24/4/5$ vol%). The condition ranges for conventional methanol synthesis, BASF's high pressure methanol synthesis process and the range envisaged in this study are roughly indicated.

7.2 Theoretical considerations

The ideal syngas for methanol synthesis has an S_N of 2 (see Eq. 1.4). However, even if glycerol decomposes solely in H_2, CO, and CO_2 the maximum S_N is 1.33, and this value is not affected by the progress of the WGS reaction. This is illustrated in Eqs. 7.1 and 7.2. In Eq. 7.1, glycerol decomposition into syngas including the reversible WGS reaction is given. The syngas composition at equilibrium, expressed in terms of x, is a function of the temperature and the water concentration.

$$C_3H_8O_3 \xrightarrow{+ \text{x } H_2O} (3 - x) \text{ CO} + (4 + x) \text{ H}_2 + x \text{ CO}_2 \tag{Eq. 7.1}$$
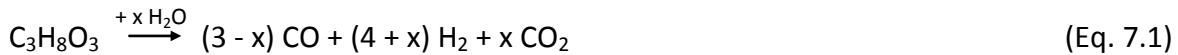
Application of the definition for S_N and introduction of gas phase compositions in terms of x, see Eq. 7.2, confirms that the S_N value is 1.33 at most and independent of the progress of the WGS reaction:

$$S_N = \frac{(H_2 - CO_2)}{(CO + CO_2)} = \frac{(4 + x - x)}{(3 - x + x)} = \frac{4}{3} \tag{Eq. 7.2}$$

The S_N value, though, can be increased by the addition of H_2 to or removal of CO_2 from the syngas. To obtain the highest methanol yield per kg glycerol, glycerol reforming followed by

syngas conversion should proceed according to the stoichiometry as shown in Eq. 7.3. Glycerol is selectively converted to H_2, CO and CO_2. Subsequently, all H_2 and CO react to methanol while the CO_2 remains.

$$3\ C_3H_8O_3 + 2\ H_2O \longrightarrow 7\ CO + 14\ H_2 + 2\ CO_2 \longrightarrow 7\ CH_3OH + 2\ CO_2 \tag{Eq. 7.3}$$
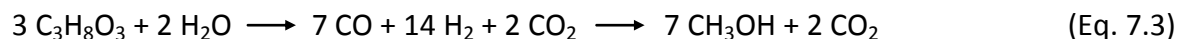
In this case, 2.33 mol carbon/mol glycerol end up in methanol (77.8% on carbon basis or 0.81 kg methanol/kg glycerol on weight basis), which is the absolute theoretical maximum. Actual yields will be lower due to the fact that both glycerol reforming and methanol synthesis involve equilibrium reactions and the occurrence of other reactions like the formation of higher hydrocarbons, higher alcohols (HA), and methanation (see Eq. 2.2).

$$CO + 3\ H_2 \rightleftharpoons CH_4 + H_2O \tag{Eq. 2.2}$$

To gain insight into the effect of the equilibria on process performance theoretical yields including equilibria were determined. The chemical equilibria involved in glycerol reforming (Eq. 1.2 and Eq. 2.2) as a function of process conditions were calculated by solving a set of equations using the model described in Chapter 2. The equilibria in methanol synthesis including liquid formation were calculated with a more sophisticated model (see Chapter 5). In the model a set of equations was solved accounting for the chemical equilibria (theoretical equilibrium constants), phase equilibria (fugacity of the vapor phase is equal to the fugacity of the liquid phase), and conservation of mass with a nonnegativity constraint.

The model for glycerol reforming predicts that a syngas with an S_N of 0.85 (H_2/CO/CO_2/CH_4 = 58.0/2.1/30.4/9.5 vol%) is obtained when a 10 wt% glycerol feed is reformed at 973 K and 24 MPa. In the subsequent methanol synthesis at 24 MPa and 473 K, the equilibrium model predicts the presence of a dew point and thus the formation of a liquid phase. The carbon conversion (carbon in methanol over carbon in glycerol) is 44% which is equal to 0.46 kg methanol/kg glycerol. This yield is substantially lower than the theoretical maximum based on Eq. 7.3 (0.81 kg methanol/kg glycerol) and this lower yield is caused mainly by the formation of CH_4 in the reforming step, at the expense of H_2 and CO. CH_4 is inert in methanol synthesis and its formation increases the H_2 deficiency of the gas mixture.

7.3 Materials and methods

7.3.1 Materials

Glycerol (purity > 99%) was supplied by Chemproha, The Netherlands. Deionized water was used with a conductivity below 3 μS/cm. In some reforming experiments (exp.) a Ni/CaO-6Al$_2$O$_3$ catalyst was used. This catalyst is known to promote the decomposition of glycerol, reforming of higher hydrocarbons, and methanation, and its properties and preparation procedure can be

found in Chapter 3. A commercial Cs doped $Cu/ZnO/Al_2O_3$ catalyst was used for methanol synthesis.

7.3.2 Setup description

The setup consisted of a reformer section, a high pressure gas-liquid separator and a subsequent methanol synthesis reactor system. An extensive description of the reformer section of the setup is given in Chapter 2. A schematic flow sheet of the setup is given in Fig. 7.2. The reformer section was operated in continuous mode with a throughput of 1 L aqueous feed/h. Glycerol and water were introduced to the system from feed containers F1 or F2 through a pump and subsequently reformed in five reforming reactors (R1 – R5) in series. The temperature in each reactor can be adjusted individually. The setup contained *in situ* separation of the water and gas phase after the reformer section in a high pressure separator (HPS). The liquid phase in the HPS, can either be depressurized and transferred to a low pressure separator (LPS) or recycled via a recycle pump. In the former operating mode (using the LPS), the gases dissolved in the aqueous liquid phase were released, quantified (Gallus G1.6 gas meter) and analyzed (gas chromatography, GC). In the latter operation mode (recycle mode) the gases remained dissolved and glycerol feed was injected in the recycle stream before the first reforming reactor (R1). If required all reforming reactors can easily be filled with catalyst. The glycerol feed concentration was typically between 3 – 10 wt%, the pressure around 24 – 27 MPa, the temperature of the reformer section between 948 – 998 K, and the residence time ranged from 30 – 35 s.

The gas phase from the HPS was directly fed to the methanol synthesis section without upgrading or selective removal of components. In one of the experiments external H_2 was added via the gas booster. The methanol section contained three tubular packed bed reactors (P1 – P3, each L = 500 mm, *ID* = 10 mm) surrounded by heating jackets. A heating/cooling medium was flown through the heating jacket to control the temperature in the reactors. Temperatures were recorded at 4 positions inside the packed bed P2 (at locations 2 to 30 cm from the entrance) and at the exit of packed bed reactor P2 and P3. Two or three of the tubular reactors were filled with catalyst particles (1 < d_p < 3 mm). The mixture of methanol, water, and unconverted gases from the last packed bed (P3) was cooled (cooler C2) using tap water, depressurized and cooled (cooler C3) to temperatures below 263 K to trap all condensables. Liquid samples were collected in a vessel and unconverted gas was quantified (Gallus G1.6 gas meter) and analyzed by GC. The methanol synthesis reactors were operated at temperatures from 468 – 518 K and at similar pressure as the reformer section.
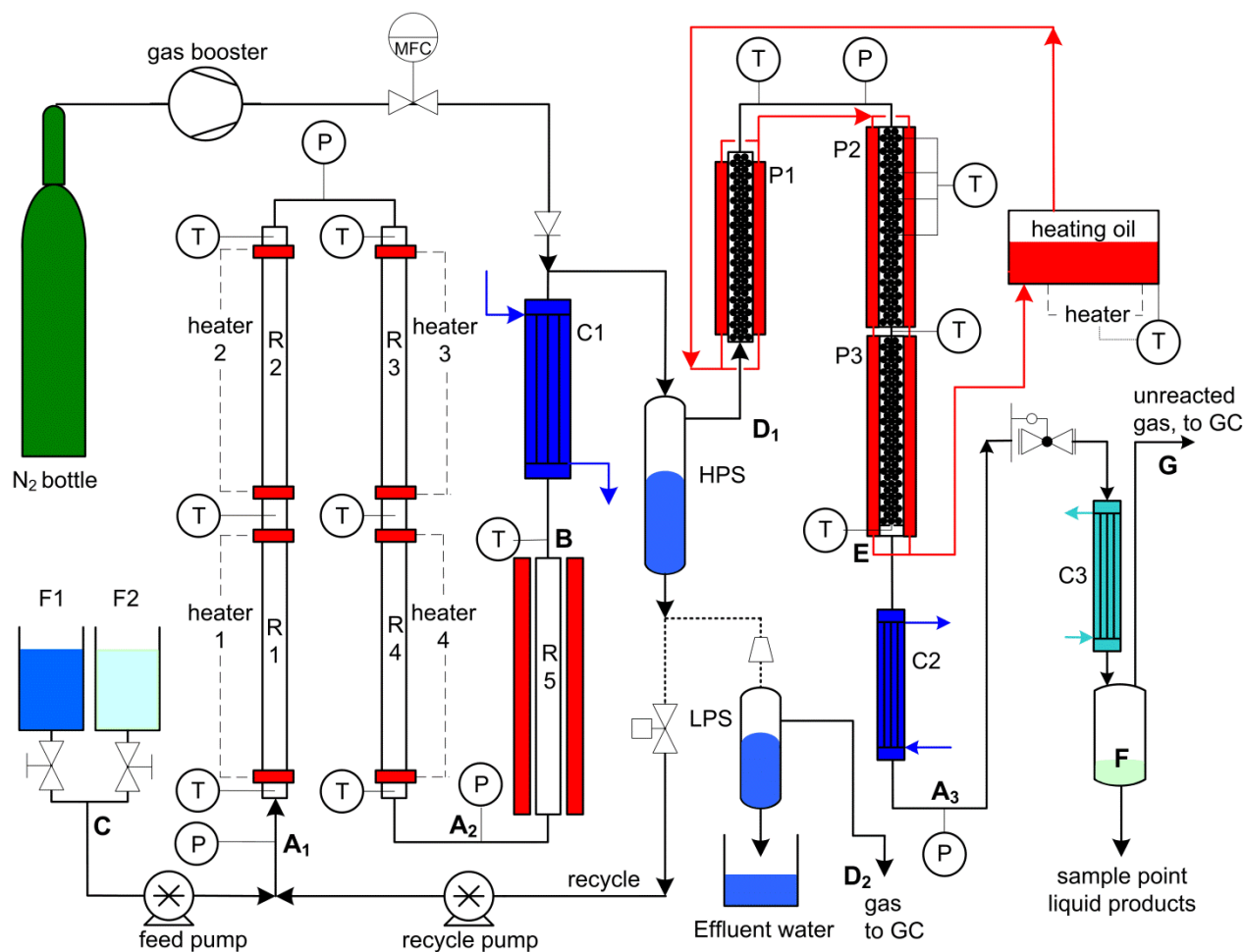
Fig. 7.2 Flow sheet of the integrated Glycerol-to-Methanol setup. The left part of the figure is the reformer section of the process and the right part is the methanol synthesis section. HPS and LPS refer to high pressure separator and low pressure separator respectively. F = feed container, C = cooler, P = packed bed reactor. The bold capital letters correspond to the locations where relevant process parameters were measured.

Several process parameters were logged during operations. The locations are indicated with letters in bold in Fig. 7.2. The process pressure was the average of **A₁₋₃**, the temperature of reactor R5 (T_{R5}) was measured at **B** at the end of reactor R5, the glycerol feed flow at **C**, the gas flow of the HPS and LPS at **D₁** and **D₂** respectively, the temperature at the end of the methanol synthesis bed at **E**, the amount of liquid product at **F**, and the unconverted gas flow at **G**.

7.3.3 Product analyses

The gas composition of the off gas from the reforming process and methanol synthesis was analyzed using an online dual-column gas chromatograph (GC 955, Syntech Spectras) equipped with thermal conductivity detectors. CO was analyzed and quantified using a molecular sieves 5Å column (L = 1.6 m) with He as carrier gas. CH_4, CO_2, and C_{2+} were analyzed on a Chromosorb 102 column (L = 1.6 m) with He as carrier gas. H_2 was analyzed on the molecular sieves column

using Ar as carrier gas. The total organic carbon (TOC) content of the effluent water from the RSCW process was analyzed using a TOC analyzer (TOC-V$_{CSN}$, Shimadzu). Before the TOC measurement, the effluent sample was diluted appropriately to obtain values within the measuring range of the apparatus. The water content of the methanol was determined by Karl Fischer-titration. The composition of the organics in the liquid phase after the methanol synthesis reactor was determined with a GC (HP 5890 series II) equipped with a flame ionization detector (FID) over a Restek RTX-1701 column (L = 60 m, ID = 0.25 mm) coupled with a mass spectrometer (MS, HP 5972 series). The FID was used for the quantification of the components and the MS for the identification of the components. The FID was calibrated for the main constituents of the organic fraction: methanol, ethanol, 1-propanol, 2-propanol, 1-butanol, 2-butanol, 1-pentanol, 2-methyl-1-propanol, and 2-methyl-1-butanol.

7.3.4 Experimental program for experiments in the integrated setup

A total of 9 experiments were performed aiming at increasing the methanol yield. An overview of the experiments is presented in Table 7.1 and a short resume is given below. The first 2 experiments were conducted using the LPS without recycling the effluent water. Part of the gas produced is lost as it dissolves in the water that leaves the process. In the second experiment external H_2 is added between the reformer section and the methanol synthesis reactors. As H_2 is the limiting component the S_N of the gas can be improved and thus the carbon conversion to methanol.

In exp. 3 – 6 the effluent water from the reformer is recycled after the HPS. Operating with a recycle stream at high pressure in RSCW is a unique feature. As a consequence of the recycle stream no gas is lost in the reformer section through the LPS and additionally, the water consumption of the process can be reduced significantly. In these experiments the glycerol reforming is carried out catalytically by using a CH_4 reforming catalyst (Ni/CaO-6Al$_2$O$_3$) in combination with higher temperatures. All C_{2+} hydrocarbons can be reformed and the CH_4 equilibrium concentration decreases (with higher temperatures) yielding a more favorable gas composition [24].

Finally, in exp. 6 an extra methanol synthesis packed bed (P1) is added to achieve equilibrium gas phase conditions at the outlet and the methanol section now consists of 3 packed bed reactors (P1 – P3) in series. The 3 packed beds were operated at different temperatures, viz. ± 518 K (P1), ± 503 K (P2), and 481 – 482 K (P3). The reaction rate in methanol synthesis depends strongly on temperature. Higher temperatures lead to higher reaction rates. In the first packed bed (P1) the reaction rate will be relatively high while the second (P2) and third (P3) are used to achieve equilibrium.

Table 7.1 Overview of experiments in the integrated unit.

Exp.	Catalyst (g)			Recycle	Catalyst (g)			Remarks
	R3	R4	R5		P1	P2	P3	
1	-	-	-	-	-	50	51	-
2a/2b	-	-	-	-	-	50	51	H_2 added after reformer section
3a/3b	10	10	3	✓	-	50	51	Ni/CaO-6Al$_2$O$_3$ used in reformer section
4	10	10	3	✓	-	50	51	Ni/CaO-6Al$_2$O$_3$ used in reformer section
5	10	10	3	✓	-	50	51	Ni/CaO-6Al$_2$O$_3$ used in reformer section
6-1	10	10	3	✓	51	50	51	Ni/CaO-6Al$_2$O$_3$ used in reformer, P1-P3 at different T
6-2[a]	10	10	3	✓	51	50	51	Ni/CaO-6Al$_2$O$_3$ used in reformer, P1-P3 at different T

[a]The catalyst in the reformer was replaced by fresh catalyst.

7.3.5 Definitions

The conversion of glycerol to gas (ζ_{gly}) in the reformer is defined as the difference between the molar carbon flow of glycerol in the feed and the molar carbon flow of the effluent ($\phi_{C,gly}$ - $\phi_{C,effluent}$) over the molar carbon flow of glycerol in the feed ($\phi_{C,gly}$):

$$\zeta_{gly} = \frac{\phi_{C,gly} - \phi_{C,effluent}}{\phi_{C,gly}} \cdot 100\% \qquad \text{(Eq. 7.4)}$$

The overall carbon conversion to methanol (ζ_C) in the integrated unit is the molar carbon flow in methanol ($\phi_{C,MeOH}$) over the molar carbon flow of glycerol in the feed.

$$\zeta_C = \frac{\phi_{C,MeOH}}{\phi_{C,gly}} \cdot 100\% \qquad \text{(Eq. 7.5)}$$

The methanol yield (η) is the mass flow of methanol (ϕ_{MeOH}) produced over the mass flow of glycerol (ϕ_{gly}) fed.

$$\eta = \frac{\phi_{MeOH}}{\phi_{gly}} \qquad \text{(Eq. 7.6)}$$

The conversion of gas component i (ζ_i) in methanol synthesis is defined as the molar conversion rate ($\phi_{i,in}$ - $\phi_{i,off}$) over the molar flow of component i ($\phi_{i,in}$) originally present after glycerol reforming.

$$\zeta_i = \frac{\phi_{i,in} - \phi_{i,off}}{\phi_{i,in}} \cdot 100\% \qquad \text{(Eq. 7.7)}$$

The energetic efficiency (higher heating value, HHV) is defined as:

$$\eta_{HHV} = \frac{HHV_{MeOH}}{HHV_{gly}} \cdot \eta \cdot 100\%$$
(Eq. 7.8)

7.4 Results

For the experiments, process conditions were varied, the use of a catalyst in the reformer section was evaluated, recycle of the liquid effluent of the HPS was assessed, and the addition of external H_2 was investigated with the primary objective to achieve high methanol yields. This requires proper operating conditions for each reactor section (reformer, methanol synthesis) to limit byproduct formation (e.g. CH_4, higher hydrocarbons, and HA) and to allow operation at high equilibrium conversions in methanol synthesis. An overview of the experiments is presented in Table 7.1. In this section, both the results for the overall integrated process will be discussed as well as the results for the reformer section in these experiments. Typical run times for the experiments were 6 – 10 h and steady state was reached in approximately 2 h.

7.4.1 Reformer performance

Typical conditions for the reformer section (see Fig. 7.2) were 24 – 27 MPa and 948 – 998 K. At these conditions the residence times of the reformer section (R1 – R5) were in the range of 30 – 35 s. The composition and quantity of the off gas were analyzed to determine the carbon balance. The hydrocarbon concentration in the off gas is the summation of the concentrations of CH_4 and C_2H_6. The glycerol conversion was determined based on the quantity of carbon in the effluent water (see Eq. 7.4). The main results of the glycerol reformer section are summarized in Table 7.2. The locations given in the last row of the table correspond to the position in the experimental setup where the parameters were measured, marked with bold capital letters in Fig. 7.2.

Carbon balance closure for the reformer is very satisfactorily and was between 95 and 104%. The glycerol conversion was almost complete for all experiments, which is in line with Chapter 2 and 3. Syngas composed of: $H_2/CO/CO_2/C_xH_y$ = 44 – 67/1 – 21/16 – 34/2 – 18 vol% was obtained. The results for each experiment will be discussed separately in the following section. Exp. 1 is selected as base case and the results of the other experiments will be compared to this experiment.

Base case
Exp. 1 was conducted with a glycerol feed concentration of 10 wt%. The setup was operated without a catalyst in the reformer section and in a once-through mode. Part of the gas (ca. 13%) dissolves in the effluent stream from the LPS (see Fig. 7.2) and is not used for the subsequent methanol synthesis. The product gas has a relatively low S_N value of 0.74, which is mainly caused by the formation of hydrocarbons (18.1 vol% with approximately ⅔ CH_4 and ⅓ C_2H_6).

Exp. 2 – 6

Exp. 2 was conducted at the same conditions as the base case. The only difference is that approximately 100 NL/h of external H_2 was added to the syngas after the reformer section. The gas composition, given in Table 7.2, is the gas composition of the reformer gas including the additional H_2. The S_N of the gas increased to 2.66. The ratio between CO, CO_2, and CH_4 changed slightly in comparison with the base case, which can be due to the H_2 addition or some scattering in the experimental data. The hydrocarbon concentration is still high and the gas flow has almost doubled.

Table 7.2 Reforming results (before methanol synthesis).

Exp.		P	T_{R5}	ϕ_{gly}	Feed	ϕ_v	H_2	CO	CO_2	C_xH_y	S_N	ζ_{gly}	C_{bal}
		(MPa)	(K)	(g/h)	(wt%)	(NL/h)	(vol%)	(vol%)	(vol%)	(vol%)	(-)	(%)	(%)
1	HPS	27	948	106	10.4	97	44.3	21.2	16.5	18.1	0.74	96.2[a]	95.8
1	LPS					14	21.9	8.4	62.0	7.7	-		
2[c]	HPS	27	948	112	10.4	191	67.3	10.2	11.0	11.6	2.66	95.0[a]	102.7
2[c]	LPS					11	15.1	4.4	74.9	5.5	-		
3	HPS	24	998	97	± 10	151	54.9	1.6	32.5	11.0	0.66	99.9[b]	97.1
4	HPS	24	998	35	± 4	65	59.4	1.1	33.5	6.0	0.75	99.9[b]	103.7
5	HPS	24	998	38	± 4	70	61.4	1.1	32.1	5.3	0.88	99.9[b]	99.0
6-1	HPS	26	998	34	± 3	60	59.7	1.0	32.2	7.1	0.83	99.9[b]	101.1
6-2	HPS	26	998	35	± 4	71	66.4	1.3	30.0	2.4	1.17	99.9[b]	94.8
Loc.[e]		A_{1-3}	B	C		D_1/D_2[d]							

[a]Based on carbon content in the effluent water.
[b]Experiment conducted in recycle mode. Glycerol conversion is estimated based on previous work [24].
[c]External H_2 is co-fed after the reforming process, the composition provided is after H_2 addition.
[d]D_1 for the HPS gas and D_2 for the LPS gas.
[e]Locations where the parameters were measured (see Fig. 7.2).

In exp. 3, a different approach was followed to increase the S_N compared to the base case. To avoid the addition of external (fossil derived) H_2, the hydrocarbon content had to be reduced. A Ni/CaO-6Al$_2$O$_3$ catalyst was used to reform the higher hydrocarbons and to promote glycerol decomposition, but besides these two reactions the WGS reaction was promoted as well [24]. The temperature was slightly increased compared to the base case to have a more advantageous equilibrium composition (less CH_4) and the effluent water was recycled at high pressure. Recycling the effluent water drastically reduces the water consumption of the process and the recycle flow was adjusted in such a way that the reactor inlet flow was comparable to the inlet flow in the base case. Compared to the base case no gas was lost through the effluent stream from the LPS. The gas composition obtained over this catalyst differed substantially from the base case. The CO concentration was reduced from 21 vol% to 1 – 2 vol% and the concentration of the hydrocarbons was significantly lower and approached equilibrium ($C_2H_6 = 0$ vol% and $CH_4 \approx 11$ vol%). The S_N value was slightly lower than the base case.

In exp. 4 – 6-1 the glycerol feed concentration was reduced to 4 wt%. The H_2 and CO_2 concentration increased compared to the base case, whereas the CO and hydrocarbon concentration were lower, resulting in slightly more attractive S_N values of 0.75 – 0.88. The higher hydrocarbon content increased from exp. 5 to exp. 6-1 which indicated a decrease in the higher hydrocarbon reforming performance of the catalyst. Therefore, in exp 6.2, a fresh reforming catalyst was used leading to the lowest hydrocarbon concentration and the highest H_2 concentration of all experiments. For instance, C_2H_6, which accounted for ⅓ of the hydrocarbon content in the base case, could not be detected in the product gas. The S_N increased to 1.17 which is close to the theoretical maximum of 1.33 (Eq. 7.2).

7.4.2 Performance of the integrated process

The results for the integrated process, including methanol synthesis, are presented in Table 7.3. For some experiments methanol synthesis was operated at two different temperatures. These experiments are marked as e.g. 2a and 2b. The equilibria in methanol synthesis were calculated with the data from Table 7.2 as input and, if applicable, condensation of methanol was accounted for in the equilibrium calculations (see Chapter 5). The equilibrium data should be considered with some care, because the results are based on the assumption of constant gas composition and gas flow from the reformer section. As for the reforming experiments, all methanol synthesis experiments have good closures of the carbon balance (93 – 100%), particularly when regarding the complexity of the integrated process. A detailed summary of the experimental results of the integrated process is given below. As in section 7.4.1, exp. 1 is considered as base case and the results of the other experiments are compared to this experiment.

Table 7.3 Results of methanol synthesis from glycerol-derived syngas.

Exp.	T	ϕ_{gly}	$\phi_{v,off}$	H_2	CO	CO_2	C_xH_y	L. yield[a]	η	MeOH[b]	H_2O	ζ_{CO+CO2}	ζ_{H2}	ζ_C	C_{bal}
	(K)	(g/h)	(NL/h)			(vol%)		(g/h)	(kg MeOH/ kg glycerol)	(wt%)				(%)	
1	468	106.1	37.1	3.3	2.2	43.6	50.9	28.9	0.27	98.9	1.1	57.5	97.4	25.8	94.6
equi	468	-	35.6	4.8	2.1	43.7	49.6	29.7	0.28	98.5	1.5	59.3	96.4	28.0	-
2a[c]	468	112.2	136.6	67.3	2.9	13.3	16.4	31.9	0.25	87.2	12.8	49.7	34.4	23.8	98.4
equi	468	-	49.5	55.0	0.0	0.4	44.6	74.7	0.52	77.5	22.5	99.5	80.5	49.1	-
2b[c]	518	111.7	88.9	65.8	0.3	6.9	26.9	56.1	0.40	80.3	19.7	81.0	58.3	38.6	98.1
equi	518	-	71.5	61.0	0.6	7.6	30.9	62.5	0.45	79.8	20.2	86.9	68.9	43.1	-
3a	498	96.7	82.5	41.6	0.4	40.0	18.1	41.3	0.29	67.0	33.0	35.4	58.8	27.4	96.2
equi	498	-	60.7	25.5	0.7	46.1	27.6	50.5	0.35	66.1	33.9	44.9	81.4	33.1	-
3b	518	96.5	67.3	34.4	0.4	42.6	22.5	56.8	0.39	65.8	34.2	43.8	72.2	37.1	100.0
equi	518	-	72.8	33.7	1.2	42.1	23.0	43.7	0.30	65.9	34.1	38.8	70.5	28.6	-
4	483	35.3	33.9	48.9	0.6	39.9	10.7	14.4	0.27	65.4	34.6	39.0	57.0	25.5	93.2
equi	483	-	16.8	15.1	0.6	61.1	23.2	27.0	0.50	65.2	34.8	53.9	93.4	47.7	-
5	493	37.7	22.5	37.9	0.4	44.9	16.8	27.1	0.47	65.3	34.7	56.0	80.0	44.9	96.8
equi	493	-	16.9	20.4	0.8	57.7	21.2	29.3	0.51	65.2	34.8	57.2	91.9	48.5	-
6-1	482	33.9	12.5	15.7	0.3	53.4	30.6	28.3	0.55	66.1	33.9	66.4	94.5	52.8	95.5
equi	482	-	15.0	13.2	0.5	57.1	29.1	25.9	0.50	65.1	34.9	56.5	94.5	47.6	-
6-2	481	35.0	10.9	20.0	0.3	59.5	20.2	33.4	0.62	65.1	34.9	70.5	95.4	59.6	93.8
equi	481	-	9.5	10.8	0.6	69.6	19.0	34.7	0.65	65.3	34.7	70.0	97.8	62.1	-
Loc.[d]	E	C	G	-	-	-	-	F	-	-	-	-	-	-	-

[a] Yield of liquid products.
[b] The liquid phase is assumed to consist of water and methanol. The concentration here is calculated by 100 wt% – (water concentration).
The exact composition of the organic phase is given in Table 7.4.
[c] External H_2 is added to the reforming gas.
[d] Locations where the parameters were measured (see Fig. 7.2).

Base case
In exp. 1, the methanol synthesis reactors were operated at 468 K. Hydrocarbons are inert in methanol synthesis and their concentration increased strongly in the off gas of the methanol synthesis reactor to over 50 vol%. The H_2 and CO concentration were 3 and 2 vol%, respectively. The CO_2 concentration increased compared to the gas composition from the reformer as mainly CO was converted to methanol. The gas composition and liquid yield at the exit of the methanol reactor were close to equilibrium, with the liquid yield slightly lower and experimental conversion slightly higher than equilibrium. The overall carbon conversion was 26% which is equal to a methanol yield of 0.27 kg methanol/kg glycerol. The conversion of 26% is the highest conversion possible with such a syngas composition.

Exp. 2 – 6
In exp. 2 the S_N was increased by the addition of external H_2 and the syngas flow for the methanol synthesis section doubled. The methanol synthesis was operated at 468 K (exp. 2a) and 518 K (exp 2b). In exp. 2a the residence time of the packed bed reactor was too short at these low temperatures to achieve gas phase equilibrium and the carbon conversion and methanol yield were similar as in the base case. In contrast to the base case, the gas composition remained far from equilibrium, which is mainly visible in the low conversion of CO_2 and the low water content of the liquid product. For this situation the addition of H_2 is not recommendable.

In exp. 2b, the reactor temperature was increased to achieve equilibrium and to obtain higher yields. The carbon conversion became closer to the equilibrium values (ζ_C = 39% vs. 43% at equilibrium) and the off gas composition was closer to equilibrium, though equilibrium was not yet attained. Approximately 81% (equilibrium = 87%) of the carbon oxides present in the gas phase was converted to methanol and a methanol yield of 0.40 kg methanol/kg glycerol was obtained, which is significantly higher than the base case, but at the cost of the addition of external H_2.

In exp. 3, the gas composition after reforming is significantly different as for the base case. Almost all CO is converted to CO_2. From the literature, it is known that methanol can be successfully synthesized solely from CO_2 [25-28]. Methanol synthesis was operated at 498 K (exp. 3a) and 518 (exp. 3b). The carbon conversion and methanol yield in exp. 3a were below equilibrium and similar to the base case, although the composition of the syngas was completely different. Nonetheless, based on equilibria higher conversions are possible in exp. 3a. Increasing the temperature (exp. 3b) led to higher carbon conversion and methanol yields (ζ_C = 37 ,η = 0.39 kg methanol/kg glycerol) than the base case. The conversions and yields are slightly higher than the predicted equilibrium values due to technical issues leading to some extra methanol release from the system.

To obtain significant higher conversions than the base case, the temperature of the methanol synthesis reactors was reduced in combination with a reduction of the flow rate and the hydrocarbon content of the syngas. The latter two targets were realized jointly by reducing the

feed concentration with a factor of almost 3. In exp. 4, methanol synthesis was operated at 483 K. The carbon conversion and methanol yield were comparable to the base case, but remained far from equilibrium. A slight increase in the packed bed temperature of 10 K (exp. 5) resulted in a significant increase in the carbon conversion to 45% (η = 0.47 kg methanol/kg glycerol), which is significantly higher than the base case but still below equilibrium. Even though the gas flow to the packed bed was reduced, the residence time remained too short to achieve equilibrium.

An increase in reactor length (exp. 6-1) and variable operating temperatures of the three packed bed reactors (P1 – P3 in Fig. 7.2) caused a significant increase in the carbon conversion to 53% which is equal to a yield of 0.55 kg methanol/kg glycerol. This carbon conversion and yield are more than double the values of the base case.

7.4.3 Long duration experiment in the integrated unit

In a long duration run (exp. 6-2, 20 h) at the same conditions as exp. 6-1, but using a fresh reforming catalyst, a considerably lower hydrocarbon concentration in the gas phase after the reformer was observed. As a consequence the corresponding carbon conversion in the methanol synthesis unit increased to 60% (η = 0.62 kg methanol/kg glycerol). Nevertheless, even higher methanol yields are possible as equilibria were not yet achieved. In the first 4 h of the long duration experiment, only the reformer section was operated. Methanol synthesis was carried out over a 16 h period and the hourly liquid methanol yields and volumetric flows at the exit of the methanol synthesis unit (point **G** in Fig. 7.2) are shown in Fig. 7.3A.
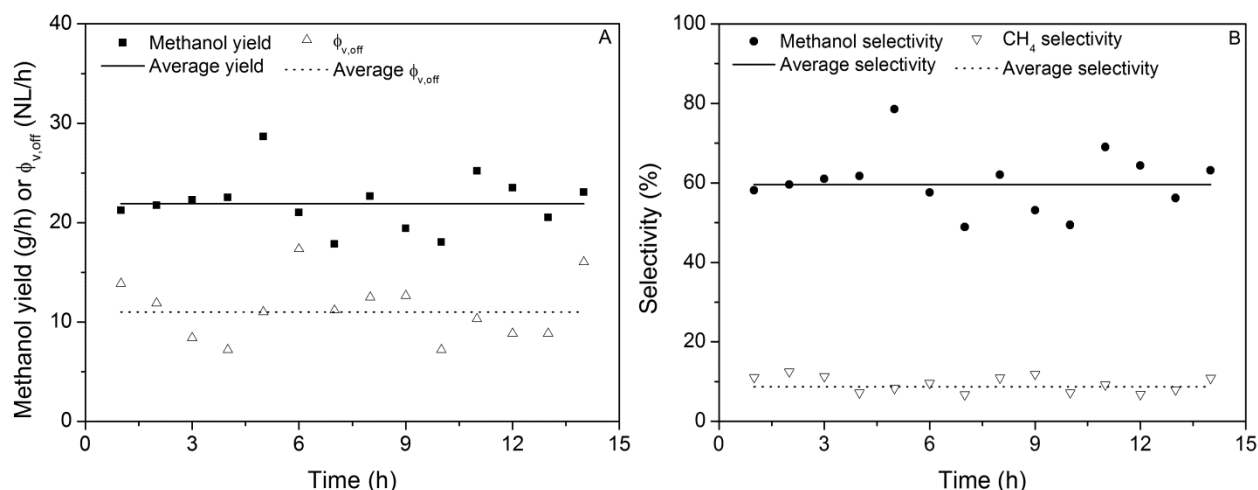
Fig. 7.3 Methanol yields from glycerol and volumetric flow at the exit of the methanol reactor of the long duration experiment (A). Carbon selectivity towards methanol and CH_4 (B).

Though some scattering in the methanol yield can be noted (due to some pressure fluctuation and uncontrolled release by the back-pressure valve during the experiment), the integrated system was running steadily and the methanol yield was more or less constant. The selectivity (mol carbon in product/mol carbon in glycerol · 100%) is depicted in Fig. 7.3B. An average value

of 8.7% of the carbon present in glycerol ends up as CH_4 and the methanol selectivity is equal to the carbon conversion and amounts 60% on average. The scattering in the methanol selectivity is similar to the scattering in the methanol yield in Fig. 7.3A. The selectivity towards CH_4 is also more or less constant. It seems that no deactivation or reduced activity for both the reformer section and the methanol synthesis section were observed during the course of the experiment.

7.4.4 Liquid composition after methanol synthesis reactor

The composition of the liquid product after the methanol synthesis reactor for all experiments is given in Table 7.4. The liquid phase was analyzed on methanol, water, and the eight most common HA. In general, the concentration of HA was very low (< 0.23 wt% of the total and < 0.24 wt% of the organic fraction), probably due to the low temperatures of the methanol synthesis and the high CO_2 content of the syngas [29]. Ethanol was the most predominant HA, with a maximum concentration of 1.2 wt‰. Noticeably, when methanol was predominantly synthesized from CO_2 (exp. 3 – 6) the concentrations of HA were negligible. This is in agreement with literature data which show that the concentrations of HA are low when mainly CO_2 is converted to methanol and decrease at higher H_2/CO ratios in the syngas feed [29, 30].

7.5 Discussion

The experiments conducted in this research study were aimed at obtaining high carbon conversions and methanol yields when reforming aqueous glycerol solutions to syngas followed by methanol synthesis. The gas composition after reforming appeared to be the most critical factor and has a major effect on the final methanol yield. Particularly the formation of hydrocarbons should be avoided in the reformer section as hydrocarbons are inert in the subsequent methanol synthesis. Therefore, hydrocarbon reduction was the main objective in the experimental program and was pursued by the application of catalysts, higher reforming temperature, and reduction of the feed concentration. Application of a suitable catalyst ($Ni/CaO-6Al_2O_3$) indeed led to a considerable reduction in the amount of hydrocarbons in the reformer off gas, though as a consequence almost all CO was converted to CO_2. Further research will be required to identify reformer catalysts that promote glycerol decomposition rates and hydrocarbon reforming, but do not enhance the WGS reaction. In this respect, Ir based catalysts are promising because of good performance in aqueous phase reforming [31].

The conversion of CO to CO_2 in the reformer section, as observed when using the $Ni/CaO-6Al_2O_3$ catalyst, is not detrimental for the subsequent methanol synthesis. With the commercial methanol synthesis catalyst used in this study, CO_2 hydrogenation is possible, as was also proven here, though the overall reaction rates in methanol synthesis are lower than in case of CO hydrogenation [28]. An advantage, however, of CO_2 hydrogenation is the high purity of the organic fraction, as the formation of HA is suppressed by most probably the presence of water [32].

Table 7.4 Composition of the liquid phase.

Exp.	T	Liquid product					Higher alcohols							
		MeOH	H_2O	HA	Total[a]	Purity[b]	EtOH	1-pro-panol	2-pro-panol	2-methyl-1-propanol	1-bu-tanol	2-bu-tanol	2-methyl-1-butanol	1-pen-tanol
(-)	(K)	(wt%)					(wt‰)							
1	468	97.8	1.1	0.23	99.1	99.8	1.15	0.02	0.69	0.15	0.17	0.00	0.09	0.08
2a	468	87.4	12.8	0.09	100.2	99.9	0.07	0.03	0.33	0.00	0.01	0.11	0.00	0.00
2b	518	80.8	19.7	0.17	100.7	99.8	0.69	0.23	0.31	0.08	0.08	0.22	0.05	0.03
3a	498	66.5	33.0	0.00	99.5	99.9	0.00	0.02	0.01	0.00	0.00	0.01	0.00	0.00
3b	518	65.8	34.2	0.01	100.0	99.9	0.03	0.01	0.01	0.00	0.00	0.01	0.00	0.00
4	483	65.9	34.6	0.00	100.5	99.9	0.00	0.00	0.00	0.00	0.00	0.00	0.00	0.00
5	493	64.6	34.7	0.00	99.3	99.9	0.00	0.00	0.00	0.00	0.00	0.00	0.00	0.00
6-1	482	67.1	33.9	0.01	100.9	99.9	0.05	0.01	0.00	0.00	0.00	0.01	0.00	0.00
6-2	481	65.1	34.9	0.01	100.0	99.9	0.05	0.01	0.00	0.00	0.00	0.01	0.00	0.00

[a]Summation of the methanol, water, and higher alcohols concentrations.
[b]Methanol content of the organic fraction.

The highest methanol yield (exp. 6.2) was 76% of the theoretical maximum (η = 0.62 vs. 0.81 kg methanol/kg glycerol). This experimental value is remarkably high, particularly when considering that in the calculation of the theoretical maximum, equilibria are not considered and the formation of reforming products other than H_2, CO, and CO_2 (e.g. hydrocarbons) is ignored.

Table 7.5 gives an overview of the various types of processes reported in the literature and an indication of the efficiencies. Direct comparison of the efficiencies is difficult as in most cases different assumptions and process units are considered. The efficiencies of study 3 and study 5 (this work) can be compared directly as they consider only the HHV of the product and the feed without energy consumption or production. The η_{HHV} in this work is clearly higher. For study 1 and study 2, also (part of) the energy consumption of the process is taken into account resulting in lower efficiencies and yields [33]. As such, direct comparison with our process is cumbersome. Major assumptions were made to calculate the yield and efficiency for study 4 and this value should be considered purely as indicative [34]. The η_{HHV} in study 5 (this work) is about a factor 2 higher.

The main challenges for subsequent process research and development studies on the integrated concept proposed in this chapter are to be found in the reformer section. Process improvements involve heat integration, reduction of operating temperatures in the reformer section and the usage of higher glycerol feed, without lowering the quality of the syngas.

7.6 Conclusion

A successful experimental demonstration of glycerol conversion to methanol was shown by the integration of two processes. Glycerol was reformed in supercritical water to syngas and the syngas was subsequently converted to methanol. The continuous setup was modified during the experimental program to increase the methanol yields. The effluent water of the reformer section was recycled at high pressure, to reduce the water consumption of the process. The highest methanol yield of 0.62 kg methanol/kg glycerol was obtained using a methanation catalyst in the reformer section and recycling of the effluent water. Glycerol was converted to mainly H_2 and CO_2 and smaller amounts of CH_4 and CO. In the most successful experiment, 60% of the carbon present in the glycerol ends up in methanol. These yields are close to the equilibrium yields and higher than experimental and case studies reported in the literature. The integrated setup was operated smoothly for more than 16 h without catalyst deactivation.

Table 7.5 Summary of the results of literature studies to the production of methanol from biomass.

Study	Feedstock	Gasification	Secondary process	Methanol synthesis	η[a]	η_x (%)	Type of study	Ref.
1	Biomass (not otherwise classified)	Indirectly fired atmospheric gasification with steam	Gas cleaning, compression to 1.4 Mpa, steam reforming at 1223 K	Conventional methanol synthesis reactor at 5.1 Mpa and 533 K	0.47[b]	51[b]	Desk-top	[14]
2	Biomass (not otherwise classified)	Indirectly fired atmospheric gasification with steam	Gas cleaning, steam reforming at 1.6 MPa and 1163 K, partial WGS at 603 K	Conventional methanol synthesis reactor at 10.6 MPa and 533 K	0.52[c]	54[c]	Desk-top	[16]
3	Wood (not otherwise classified)	Gasification at 2.0 MPa, with steam and O_2 addition.	High temperature gas filtering and WGS	Conventional methanol synthesis reactor at 6.7 MPa, T unknown	0.56[d]	63[d]	Desk-top	[18]
4	Pyrolysis oil from rice husk	Not specified in detail (steam reforming)	Catalytic and electrochemical gas conditioning using char	Packed bed reactor at 5.0 MPa and 533 K	0.34[e]	31[e]	lab scale	[10]
5	Glycerol	RSCW (26 Mpa, 998 K)	-	High pressure methanol synthesis at 26 MPa, 518-482 K	0.62[f]	78[f]	bench scale	This work

[a]Units: kg methanol/kg biomass.

[b]$\eta_x = \eta_{thermal}$. Moisture content of the biomass is 10 wt%, the efficiency reported is thermal efficiency and it is unknown whether this is η_{HHV} or η_{LHV} (LHV = lower heating value). In this calculation all the energy for biomass drying, crude methanol distillation, and electrical power required in the process are obtained from the feed [14].

[c]$\eta_x = \eta_{HHV}$. The efficiency is an overall efficiency accounting for the energy requirements and production in the process [16]. A HHV value of 20 MJ/kg dry wood is assumed [37].

[d]$\eta_x = \eta_{HHV}$. η (kg methanol/kg dry biomass) is corrected for the moisture content originally present in the biomass. The η_{HHV} is calculated based on HHV of the feed and the products, neither electricity consumption nor valuable output are considered [18].

[e]$\eta_x = \eta_{HHV}$. η is in kg methanol/kg pyrolysis oil. It is assumed that all carbon present in the pyrolysis oil is converted to gas. The η and η_{HHV} are not corrected for the uptake of carbon occuring during gas conditioning. Elemental compostion of the pyrolysis oil is assumed to be $CH_{1.55}O_{0.5}$ with a HHV of 24.8 MJ/kg [38].

[f]$\eta_x = \eta_{HHV}$ (calculated with eq. 13). Only the energy content of the feed and methanol product are considered. η is in kg methanol/kg glycerol.

7.7 References

1   G.A. Olah, A. Goeppert, G.K.S. Prakash, Beyond oil and gas: The methanol economy, Wiley-VCH, Weinheim, (2006).

2   M. Berggren, Methanol industry in focus, milestones, www.methanol.org (accessed 19 January 2012)

3   S. Lee, Methanol synthesis technology, CRC Press Inc., Boca Raton, Florida, (1990).

4   E. Supp, How to produce methanol from coal, Springer-Verlag, Berlin, (1990).

5   A.A.C.M. Beenackers, W.P.M. van Swaaij, Methanol from wood II. Current research and development programs, Int. J. Sol. Energy, 2 (1984) 487-519.

6   A.A.C.M. Beenackers, W.P.M. van Swaaij, Methanol from wood I. Process principles and technologies for producing methanol from biomass, Int. J. Sol. Energy, 2 (1984) 349-367.

7   Y. Xiuli, Synthesizing methanol from biomass-derived syngas, in: Department of mechanical engineering, The university of Hong Kong, Hong Kong, (2005).

8   J.M. Norbeck, K. Johnson, Evaluation of a process to convert biomass to methanol fuel, in: U.S.E.P. Agency (Ed.), Cincinnati, (2000).

9   T. Ekbom, M. Lindblom, N. Berglin, P. Ahlvik, Cost-competitive, efficient biomethanol production from biomass via black liquor gasification, Nykomb Synergetics AB, (2003).

10   Y. Xu, T.Q. Ye, S.B. Qiu, S. Ning, F.Y. Gong, Y. Liu, Q.X. Li, High efficient conversion of CO_2-rich bio-syngas to CO-rich bio-syngas using biomass char: A useful approach for production of bio-methanol from bio-oil, Bioresour. Technol., 102 (2011) 6239-3245.

11   Chemrec, The Bio-DME project – From wood to wheel, www.chemrec.se (accessed 07 February 2012)

12   P. Salomonsson, BioDME, www.biodme.eu (accessed 22 March 2012)

13   BioMCN, BioMCN opens largest 2nd generation biofuel plant, www.biomcn.eu (accessed 07 February 2012)

14   R.H. Borgwardt, Methanol production from biomass and natural gas as transporation fuel, Ind. Eng. Chem. Res., 37 (1998) 3760-3767.

15   T. Chmielniak, M. Sciazko, Co-gasification of biomass and coal for methanol synthesis, Appl. Energy, 74 (2002) 393-403.

16   C.N. Hamelinck, A.P.C. Faaij, Future prospects for production of methanol and hydrogen from biomass, J. Power Sources, 111 (2002) 1-22.

17   H. Li, H. Hong, H. Jin, R. Cai, Analysis of a feasible polygeneration system for power and methanol production taking natural gas and biomass as materials, Appl. Energy, 87 (2010) 2846-2853.

18   G.L.M.A. van Rens, G.H. Huisman, H. de Lathouder, R.L. Cornelissen, Performance and exergy analysis of biomass-to-fuel plants producing methanol, dimethylether or hydrogen, Biomass Bioenergy, 35 (2011) S145-S154.

19   P. Basu, V. Mettanant, Biomass gasification in supercritical water - A review, Int. J. Chem. Reactor Eng., 7 (2009) 1-61.

20   G. Brunner, Near critical and supercritical water. Part I. Hydrolytic and hydrothermal processes, J. Supercrit. Fluids, 47 (2009) 373-381.

21   D.C. Elliot, Catalytic hydrothermal gasification of biomass, Biofuels, Bioprod. Biorefin., 2 (2008) 254-265.

22   A. Kruse, Hydrothermal biomass gasification, J. Supercrit. Fluids, 47 (2009) 391-399.

23   A.A. Peterson, F. Vogel, R.P. Lachance, M. Fröling, M.J. Antal Jr., J.W. Tester, Thermochemical biofuel production in hydrothermal media: A review of sub- and supercritical water technologies, Energy Environ. Sci., 1 (2008) 32-65.

24   J.G. van Bennekom, V.A. Kirillov, Y.I. Amosov, T. Krieger, R.H. Venderbosch, D. Assink, K.P.J. Lemmens, H.J. Heeres, Explorative catalyst screening studies on reforming of glycerol in supercritical water, J. Supercrit. Fluids, 70 (2012) 171-181.

25   K.G. Chanchlani, R.R. Hudgins, P.L. Silveston, Methanol synthesis form H_2, CO, and CO_2 over Cu ZnO catalysts, J. Catal., 136 (1992) 59-75.

26   H.H. Kung, G. Liu, D. Wilcox, The effect of CO_2 and H_2O in the methanol synthesis reaction on Cu-Zn-O, in: ACS fuels fall meeting, Philadelphia, (1984) 194-195.

27   J. Skrzypek, M. Lachowska, D. Serafin, Methanol synthesis from CO_2 and H_2: Dependence of equilibrium conversions and exit equilibrium concentrations of components on the main process variables, Chem. Eng. Sci., 45 (1990) 89-96.

28   K. Klier, V. Chatikavanij, R.G. Herman, G.W. Simmons, Catalytic synthesis of methanol from CO/H_2. IV. The effects of carbon dioxide J. Catal., 74 (1982) 343-360.

29   B. Denise, R.P.A. Sneeden, Hydrocondensation of carbon dioxide: IV, J. Mol. Catal., 17 (1982) 359-366.

30   K.J. Smith, R.B. Anderson, A chain growth scheme for the higher alcohols synthesis, J. Catal., 85 (1984) 428-436.

31   R.R. Davda, A review of catalytic issues and process conditions for renewable hydrogen and alkanes by aqueous-phase reforming of oxygenated hydrocarbons over supported metal catalysts, Appl. Catal., B, 56 (2005) 171-186.

32   P. Forzatti, E. Tronconi, I. Pasquin, Higher alcohol synthesis, Catal. Rev. Sci. Eng., 33 (1991) 109-168.

33   K. Raveendran, A. Ganesh, Heating value of biomass and biomass pyrolysis products, Fuel, 75 (1996) 1715-1720.

34   H.S. Heo, H.J. Park, J.I. Dong, S.H. Park, S. Kim, D.J. Suh, Y.W. Suh, S.S. Kim, Y.K. Park, Fast pyrolysis of rice husk under different reaction conditions, J. Ind. Eng. Chem., 16 (2010) 27-31.

8 Perspective, outlook, and conclusions

8.1 Introduction

Biomass is the only renewable feedstock to produce chemicals and fuels. That makes the topic of biomass conversion into fuels or chemicals a very important and growing research area. Methanol was discovered by the Scottish scientist Robert Boyle in 1661 [1, 2]. He succeeded in producing methanol from biomass by distillation of wood. Since then the feedstocks for methanol production changed to fossil resources, but, after the first oil crisis in the 1970s, methanol production from biomass regained considerable attention. The processes targeted for biomass conversion into methanol have changed to processes analogous to methanol production from fossil resources. However, mankind is back to how it all started, methanol from biomass.

The work described in this dissertation is centered on a European project referred to as Supermethanol. The intention of this project was to design a blueprint for a process to convert glycerol into methanol. In this dissertation, the complete process from feed (glycerol) to products (methanol) was investigated separately, and in an integrated mode. In the following section the results obtained for the different processes will be discussed and put into perspective.

8.2 Considerations

In the process of converting glycerol into methanol with syngas as the intermediate product, the quality of the syngas is an important parameter. The quality is usually determined by the value of the stoichiometric number (S_N, see Eq. 1.4). An optimal syngas for methanol synthesis has a S_N close to 2. Without addition or removal of components to or from the gas phase the maximum S_N that can be obtained in glycerol reforming is 1.33 (see Chapter 3 and 7). The conversion of carbon in glycerol or biomass into methanol is limited due to the H_2 deficiency of these resources. Effectively, not all carbon in the biomass can be converted to methanol. However, the syngas can be used as such, or after some conditioning steps.

8.3 Glycerol reforming in supercritical water

The work described in Chapters 2 and 3 on the reforming in supercritical water (RSCW) of glycerol was aimed at deriving relations between process conditions, conversions, and gas compositions/yields. Glycerol decomposes into water-soluble intermediates and these compounds are subsequently converted into gas phase components. The carbon-to-gas efficiency (C_{GE}) for glycerol appeared to be a function of the process severity (combination of residence time and temperature). Surprisingly, the gas composition is also related to the glycerol conversion. For our system (without dedicated catalysts), the only relevant gas phase reaction turned out to be the water-gas shift (WGS) reaction (Eq. 1.2). In methanol reforming at similar conditions gas was produced with more or less similar H_2/CO/CO_2 concentrations as in glycerol reforming, but almost no CH_4 was found indicating that CH_4 is hardly formed through gas phase methanation (Eq. 2.2, 2.3). As a consequence, CH_4 and higher hydrocarbons are produced as primary gas phase products. This complicates the picture of producing a syngas with an attractive S_N.

Generally, the carbon from glycerol ends up in CO_x and C_yH_z with a ratio of 2 : 1. All carbon and hydrogen present as hydrocarbons cannot be converted into methanol without an additional reforming step or using catalytic reforming.

In catalytic reforming it was observed that the temperature could be reduced significantly while maintaining high glycerol conversions. For some Ni based catalyst (see Chapter 3), complete glycerol conversion to gas was obtained at operating temperatures as low as 700 K. For some catalysts coke formation was observed, but the amount was hard to quantify and long duration runs were not performed to determine the influence of coke formation on the catalyst activity and pressure build-up.

Ni catalysts strongly promote methanation (see Eq. 2.2). This property is both advantageous and disadvantageous. As higher hydrocarbons are thermodynamically unstable at the conditions employed in this work they are all reformed. The CH_4 concentrations will be at their equilibrium concentration at temperatures exceeding 750 K for our system. All catalysts tested (Pt, Ni(Cu), Cu, as active metals) promote the WGS reaction and as a result most CO is converted into CO_2. With these catalysts, either a gas rich in CH_4 and CO_2 (673 K ≤ T ≤ 773 K) or a gas rich in H_2 and CO_2 (T ≥ 873 K) can be obtained, which is attractive when H_2 or CH_4 are the desired products, but not particularly when syngas (H_2 and CO) is the desired product.

It is possible to produce a gas with a S_N ≥ 1, but then high temperatures (T ≥ 873 K) and low feed concentrations ([feed] ≤ 5 wt%) are required (see Chapter 7). The main constituents of such a gas are H_2 and CO_2. For a more energy efficient process, temperatures need to be lowered, feed concentrations should be higher and, if the targeted product is syngas, methanation and the WGS reaction should be suppressed. In this respect, Ir based catalysts hold promise as in aqueous phase reforming it was found that these catalysts promote C-C scission and thus glycerol decomposition, but they do not promote methanation and the WGS reaction.

According to various studies, RSCW is the most efficient conversion technology for wet, preferably liquid, biomass (see Chapter 1). The process would even be more attractive when the water consumption can be reduced. In the experiments regarding the integrated setup (Chapter 7) we demonstrated the recycling of water at high pressure. For the experiments with effluent water recycle the setup was filled with water at start-up and during operation only the water required for the water-gas shift reaction was added. Recycling effluent water reduces the water consumption considerably, but is only possible when components, such as salts, than can build-up in the recycle stream, are absent.

The salts present in glycerol remain an issue in RSCW. Crude glycerin can be reformed to gas, but without prior salt removal, reactor plugging will take place sooner or later. The setup (Konti II) operated by the group of Vogel and the Verena pilot plant by the group of Kruse employ salt separation and successful reforming of biomass containing salts was reported [3, 4]. Salt separation, however, is never complete and some salts will enter the reactor [5, 6]. When operating with water recycling at high pressure the salts may accumulate in our system.

In conclusion, the gas compositions obtained in glycerol reforming are not particularly attractive for methanol synthesis, due to H_2 deficiency. However, when such a syngas is mixed with a syngas obtained in CH_4 steam reforming, a much more attractive gas mixture is produced. The reforming studies provided valuable insight in glycerol decomposition into gas phase products and steer opportunities of the gas composition towards products rich in H_2, rich in CH_4, or a more syngas-like gas and reducing the water consumption of the system.

8.4 Methanol synthesis

Methanol synthesis was investigated for a wide range of syngas compositions, either model gases or gases derived from glycerol RSCW. Basically, all extremes were investigated. The most striking result in the methanol synthesis was the *in situ* formation of a liquid phase at 473 K and 20.0 MPa in a unique view cell reactor (see Chapter 4). Although condensation was predicted based on indirect experimental evidence, it has never been shown before.

Condensation of methanol has serious consequences for methanol synthesis as the reaction products are withdrawn from the gas phase and consequently the equilibrium is shifted towards the reaction products. In such a situation almost complete conversion of the limiting components is obtained as was demonstrated experimentally (see Chapter 5 and 6). When complete conversion of the limiting component is obtained recycle streams, which are common for conventional methanol synthesis, can be omitted leading to reduced reactor volumes. However, due to the higher pressure the wall thickness of the reactors should be increased, leading to higher investment costs. Furthermore, it would be very interesting to have a calculation in which the operating costs of low pressure methanol synthesis including gas recycle are compared to high pressure methanol synthesis without recycle, both processes starting with syngas at atmospheric pressure. For the time being such a calculation for the high pressure process requires too many assumptions to arrive at an accurate estimation.

One of the reasons to abandon the high pressure methanol synthesis process in the 1960s (see Chapter 1 and 4) is the energy cost of syngas compression. In the GtM-concept the costs of syngas compression are negligible as the high pressure syngas is produced by pressurizing a liquid through pumping.

Considering the importance of *in situ* condensation a separate chapter (Chapter 5) was dedicated to the development of a theoretical model to be able to predict the equilibrium conversion when condensation occurs. The predictions of the model are good, in particular at lower temperatures, while at higher temperature the predictions are less accurate as different phenomena start playing a role. A considerable amount of higher alcohols can be formed even with highly selective methanol catalysts, the exact amount depending on the syngas composition.

For reactor design and equipment size estimation, kinetics of the chemical reactions involved in methanol synthesis have to be known. For low pressure methanol synthesis more than 10 different kinetic equations can be found in the literature (see Appendix C). However, kinetic equations in the high pressure regime are not available. In Appendix C kinetics are derived for high pressure methanol synthesis. The accuracy of the data set is not fully satisfactorily, due to the experimental conditions (high pressure in combination with low temperature). Therefore a rough kinetic model was derived. When this model was compared to low pressure kinetics the methanol synthesis reaction rates turn out to be significantly higher at high pressure. In designing reactors, higher reaction rates will, in general, reduce the reactor volume. In practice, when reaction rates are higher the cooling duty needs to be sufficient to prevent overheating and to keep the system at conditions at which condensation would occur. The reaction rates, determined in Appendix C, do not include the formation of a liquid. Measuring these reaction rates and designing a reactor for such a process is very complex and can be a topic of a complete Ph.D. research study. These design calculations should confirm if high pressure methanol synthesis remains attractive when gas compression is included. If that would be the case, high pressure methanol synthesis might become interesting again from an industrial point of view without the coupling with a RSCW process.

8.5 Applicability of the Supermethanol concept

In Chapter 7 a proof of principle is presented for the production of methanol from glycerol. The functionality of the system is demonstrated during a run of more than 16 h and the methanol yield is 0.62 kg methanol/kg glycerol. The highest methanol yields are obtained when the glycerol is catalytically reformed at high temperature to mainly H_2 and CO_2, which are subsequently converted into methanol. In addition, the recycling of effluent water at high pressure is demonstrated.

Uhde High Pressure Technology designed the Glycerol-to-Methanol (GtM) unit and an incomplete simplified schematic flow sheet is given in Fig. 8.1. In the configuration depicted in

Fig. 8.1, the effluent water of the reforming reactor (R1) is recycled. Heat integration is only taken into account in one heat exchanger (HE2) and one reactor (R2).

Glycerol and water are fed independently through pumps (P1 and P2 respectively). The glycerol is preheated to decrease the viscosity and increase pumpability. In a heat exchanger (HE1) the glycerol is heated before it enters separator S1. Here, the glycerol is evaporated and a brine composed of concentrated salts leaves the separator. The desalination unit is not proven technology at the moment and its functionality cannot be ascertained, but it is a critical unit operation in the process. The desalinated glycerol (still containing small amounts of salts) is injected in a preheated water stream, before the glycerol/water mixture enters the reformer (R1). Glycerol is reformed in the reactor and a gas is produced. The reactor effluent is cooled using a counter current heat exchanger (HE2) to heat up the mixture of fresh and recycle water. The mixture of gas and water is cooled further in a heat exchanger (HE3) and separated in a high pressure separator (S2). The gas is fed to the methanol synthesis unit. Part of the water stream leaving the high pressure separator is purged to prevent build-up of salts. The rest is recycled through pump (P3), mixed with fresh water, and heated in the heat exchanger (HE2). Subsequently fresh glycerol is injected in the stream.
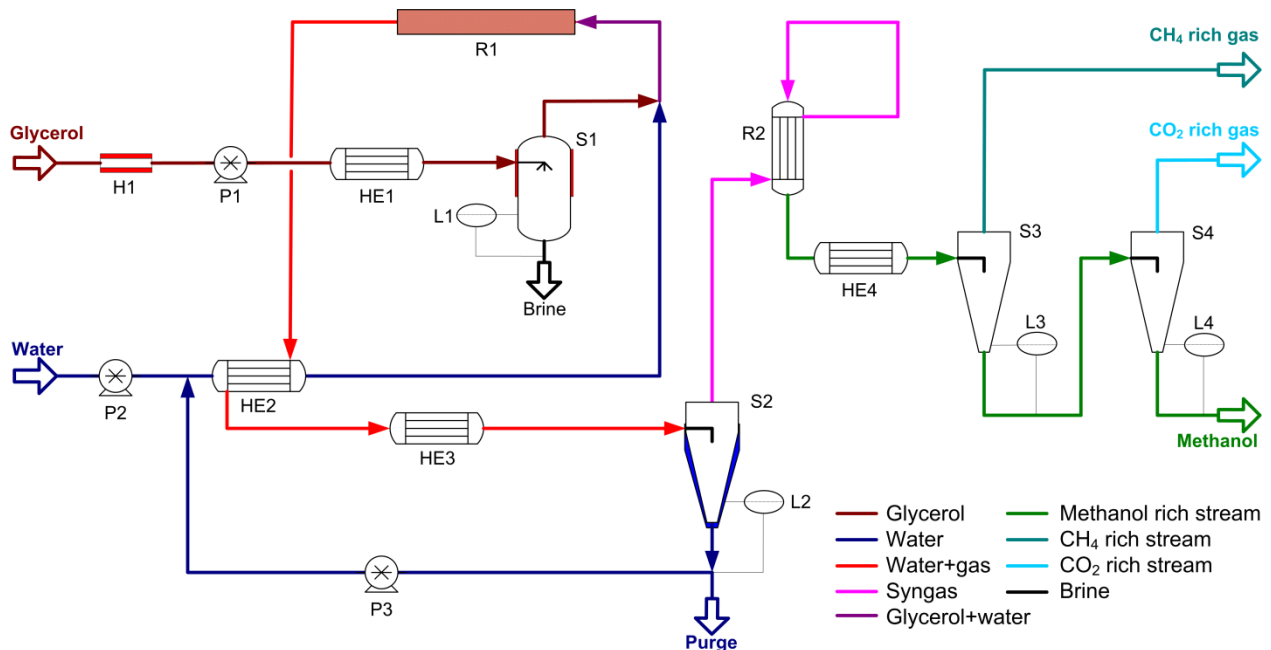
Fig. 8.1 Schematic flow sheet of the GtM-concept designed by Uhde without heat integration except for heat exchanger HE2 and reactor R2. L = level controller, H = heater, HE = heat exchanger, P = pump, R = reactor, S = separator.

The syngas leaving the separator (S2) is heated and fed to a packed bed methanol synthesis reactor (R2). Methanol synthesis takes place and heat is withdrawn from the system. The gas mixture including methanol is cooled in a heat exchanger (HE4). In a separator (S3) a gas stream rich in CH_4 is separated from the methanol stream. Then, the methanol stream is depressurized

and separated (S4) in a CO_2-rich stream and a stream containing all condensables (mainly methanol). Methanol purification is not considered.

The capital expenditures (CAPEX) costs were calculated by Uhde for 3 configurations:

➢ Case A: Unit (feed: 1.0 t/h glycerol, product: 0.23 t/h methanol) with 30% conversion per pass including ash removal. Crude glycerin as raw material. RSCW part of the unit constructed from Inconel 617. CAPEX = 24 M€.
➢ Case B: Case A + external H_2 to increase the conversion (feed: 1.0 t/h glycerol, product: 0.31 t/h methanol). CAPEX = 30 M€.
➢ Case C: Unit (feed: 3.0 t/h glycerol, product: 2.0 t/h methanol) with 100% conversion without ash removal. RSCW part of the unit constructed from Inconel 617. CAPEX = 26 M€.

The CAPEX costs are rather high, which is mainly caused by the reforming section covering more than 80% of the investment costs. Due to the severe conditions expensive alloys and large tube thicknesses are required. In Case C, the most attractive situation, the production costs per ton methanol are in an optimistic estimation around 550 to 750 €/t, while Acciona (the biodiesel producers involved in the project) paid an average of 350 €/t for their methanol from 2006 – 2011. In this calculation, pure glycerol is used as feedstock and estimated to be available on-site for 100 to 300 €/t, the depreciation time is 20 y, and no costs are calculated for waste water treatment and methanol purification.

When glycerol-derived methanol is used as fuel additive higher prices can be charged for the methanol, as it qualifies as second generation (2G) biofuel. Under current legislation so-called 'double counting' is applicable when glycerol is used as feedstock for 2G biofuel production. Just recently (October 2012), the European Commission proposed that 2G fuels made from certain feedstocks, including glycerol, shall be considered to be counted four times their energy content. This means that if, for example, 5% (energy content) blending with biofuels is required only 2.5% (and in future maybe 1.25%) of glycerol-derived methanol needs to be added on an energy basis. The remainder of the blending material can then be ordinary (cheaper) petrol. The 'multiple-counting' mechanism allows higher prices to be charged for green methanol. Furthermore carbon credits can influence the process economics positively. These support mechanisms put the opportunities of the process proposed in this dissertation in a more positive perspective.

8.6 Applications beyond Supermethanol

RSCW of glycerol or biomass is shown to be a versatile technique to produce renewable gas. Gas rich in CH_4 (+ CO_2), rich in H_2 (+ CO_2), or a syngas can be produced. The gases require cleaning, which can be done by absorption in water or aqueous ethanolamine, pressure swing adsorption, or in case of H_2 membrane filtration (Pd-membranes). The CH_4 can finally be used as green gas, while the H_2 can be stored at high pressure without or with limited additional compression. Then the H_2 can be used for fuel cells or other processes that require H_2. An example of such a

process is ammonia synthesis which requires H_2 at high pressure and for which compression can be avoided when RSCW is used.

All chemicals that are produced nowadays from syngas from fossil resources can be produced from renewable syngas, although the syngas may require (more) conditioning. For products as methanol, higher alcohols, and Fischer-Tropsch (FT) diesel S_N values of around 2 are needed from a stoichiometric point of view. The S_N value of syngas from glycerol reforming is relatively low for these kinds of applications, but can still be used. For dimethyl ether (DME) usually H_2 to CO ratios of 1 are used. In FT, Fe based catalyst can also cope with S_N's < 2 [7]. If a certain type of Fe based catalysts is used the composition of the FT liquids can be tuned to low olefins which can be used as feedstock for biobased plastics [8]. Sasol announced that the company starts research to produce synthetic fuel from biomass [9]. That means that even large industrial players have become aware of the potential of biomass. To the author's knowledge, FT at high pressure (> 20.0 MPa) has never been investigated and it is unclear if operating at high pressure is advantageous and profitable.

In higher alcohols synthesis (HAS), S_N values around 1 are preferred (see also Chapter 6) [10]. When methanol was synthesized from a gas with a S_N of 1.1 up to 14 wt% of the liquid product consisted of higher alcohols, despite the fact that a dedicated methanol synthesis catalyst was used which is supposed to suppress the formation of higher alcohols. It might be expected that over dedicated catalysts for HAS higher yields can be obtained. HAS from biomass has thus potential and further research is justified.

Pyrolysis is expected to be one of the key technologies to produce biobased fuels and chemicals [11]. Pyrolysis oil (PO) can be directly fired or upgraded for the production of chemicals or fuels. During the upgrading process the PO is treated with H_2 at high pressure (20 MPa) and separates into a dark organic phase (sugar derivatives) and an aqueous phase containing smaller organic molecules. RSCW of the aqueous phase can supply (part of) the H_2 for the upgrading of the PO. It is unclear whether pure H_2 is required for the upgrading or that also mixtures containing H_2, CO, CO_2, and C_xH_y can be used. The remaining combustible components can be used to produce heat for the RSCW process. The combination of PO upgrading combined with in situ H_2 production is in its infancy and investigated for the first time in the GAP project (BTG, University of Groningen, Albemarle), which runs from 2010 – 2013.

Finally, methanol synthesis as 'sequestration' opportunity for CO_2 is an interesting topic. An extensive review of the state of the art of this topic using CO_2 and water as a resource for syngas was published in 2011 [12]. According to this article the most promising route for syngas production was the electrolysis of H_2O and CO_2 in a solid oxide cell to produce a mixture of CO and H_2. The first commercial plant for methanol synthesis from CO_2 and H_2 has been erected by Carbon Recycling International (CRI) in Iceland [13]. The results obtained in this dissertation on methanol synthesis from H_2 and CO_2 can contribute to the development of improved versions of this process.

8.7 References

1   G.A. Olah, A. Goeppert, G.K.S. Prakash, Beyond oil and gas: The methanol economy, Wiley-VCH, Weinheim, (2006).

2   E. Supp, How to produce methanol from coal, Springer-Verlag, Berlin, (1990).

3   N. Boukis, U. Galla, H. Müller, E. Dinjus, Biomass gasification in supercritical water. Experimental progress achieved with the Verena pilot plant, in: 15th European biomass conference & exhibition, Berlin, Germany, (2007).

4   J. Müller, M. Schubert, F. Vogel, Hydrothermal gasification of wet biomass for SNG production: Optimization of salt separation and preheating, in: 8th European congres of chemical engineering, Berlin, Germany, (2011).

5   M. Schubert, J.W. Regler, F. Vogel, Continuous salt precipitation and separation from supercritical water. Part 2: Type 2 salts and mixtures of two salts, J. Supercrit. Fluids, 52 (2010) 113-124.

6   M. Schubert, J.W. Regler, F. Vogel, Continuous salt precipitation and separation from supercritical water. Part 1: Type 1 salts, J. Supercrit. Fluids, 52 (2010) 99-112.

7   A.P. Steynberg, M.E. Dry, Fischer-Tropsch technology, in: G. Centi (Ed.) Studies in Surface Science and Catalysis, Elsevier, Amsterdam, (2004).

8   H.M.T. Galvis, J.H. Bitter, C.B. Khare, M. Ruitenbeek, A.I. Dugulan, K.P. de Jong, Supported iron nanoparticles as catalysts for sustainable production of lower olefins, Sci., 335 (2012) 835-838.

9   Sasol, Sasol achieves approval for 100% synthetic jet fuel, www.sasol.com (accessed 15 May 2012)

10   P. Forzatti, E. Tronconi, I. Pasquin, Higher alcohol synthesis, Catal. Rev. Sci. Eng., 33 (1991) 109-168.

11   D. Shantz, M. Karanjikar, Developing new paradigms for biofuels separations to enable an alternative fuels future, National Science Foundation, Washington D.C., (2011).

12   C. Graves, S.D. Ebbesen, M. Mogensen, K.S. Lackner, Sustainable hydrocarbon fuels by recycling CO_2 and H_2O with renewable or nuclear energy, Renewable Sustainable Energy Rev., 15 (2011) 1-23.

13   CRI, www.carbonrecycling.is (accessed 13 July 2012)

Appendix A
Physical properties and k_{ij} for the equilibrium model

Table A.1 Critical properties, acentric factors, and polarity correction factors for the components involved in methanol synthesis.

Property	CO	CO_2	Methanol	H_2	Water	CH_4
P_c (MPa)	3.494	7.374	8.097	1.293	22.064	4.599
T_c (K)	132.85	304.12	512.64	32.98	647.14	190.56
ω (-)	0.045	0.225	0.565	-0.217	0.344	0.011
p (-)	0	0	0.2359	0	0.1277	0

The thermodynamic properties are taken from [1] and the polarity corrections from [2].

Table A.2 Binary interaction parameters (k_{ij}) for the modified SRK equation of state.

Component	CO	CO_2	Methanol	H_2	Water	CH_4
CO	-	0.1164	-0.37	-0.0007	-0.474	0.0204
CO_2	0.1164	-	0.10	0.1164	0.30	0.0956
Methanol	-0.37	0.10	-	-0.125	-0.075	0.046
H_2	-0.0007	0.1164	-0.125	-	-0.745	0.001
Water	-0.474	0.30	-0.075	-0.745	-	0.014
CH_4	0.0204	0.0956	0.046	0.001	0.014	-

The binary interaction parameters for methanol + water, methanol + $CO/CO_2/H_2/CH_4$, and water + $CO/CO_2/H_2/CH_4$ are determined from experimental data. The other binary interaction parameters are taken from the Aspen Hysys database.

A.1 References

1   B.E. Poling, J.M. Prausnitz, J.P. O'Connel, The properties of gases and liquids, 5 ed., McGraw-Hill, Singapore, (2007).
2   P.M. Mathias, A versatile equilibrium equation of state, Ind. Eng. Chem. Process Des. Dev., 22 (1983) 385-391.

Appendix B
Experimental results of high pressure methanol synthesis in a packed bed

Chapter 6 is based on a total of 60 experiments, aiming at high conversion (equilibrium). The results of all these experiments are given in this appendix. The experimental conditions, conversions (experimental and theoretical equilibria), and balances are given in Table B.1. The composition of the liquid product is given in Table B.2.

Table B.1 Experimental results.

No.	Feed	Conditions			Composition exit streams						Conversion (experimental vs. equilibrium)								Balances		
		T	P	GHSV	H₂	CO	CO₂	CₓHᵧ	Org.*	H₂O	ζ_{CO+CO2}		ζ_{H2}		ζ_{CO}		ζ_{CO2}		C	H	O
(-)	(-)	(K)	(MPa)	(h⁻¹)	(vol%)				(g/h)	(g/h)	Exp.	Eq.	Exp.	Eq.	Exp.	Eq.	Exp.	Eq.		(%)	
1	1	469	7.9	$1.0 \cdot 10^3$	68.2	0.8	23.6	7.1	4.6	2.3	29.8	53.0	29.7	50.0	88.7	94.9	15.1	42.5	94.0	94.3	100.1
2	1	493	8.0	$1.0 \cdot 10^3$	67.5	0.5	22.8	8.2	7.3	3.0	41.7	44.0	39.7	41.0	93.4	86.4	28.7	33.4	94.9	95.6	98.1
3	1	518	8.0	$1.0 \cdot 10^3$	68.0	1.4	22.9	7.5	5.6	2.6	33.5	34.9	33.3	32.5	81.0	67.7	21.6	26.7	94.7	94.8	99.1
4	1	542	8.1	$1.0 \cdot 10^3$	68.0	2.9	22.1	7.0	3.8	2.0	24.8	25.9	26.9	25.1	56.7	36.9	16.8	23.1	95.5	93.9	98.7
5	1	469	15.0	$1.5 \cdot 10^3$	68.1	0.6	23.2	7.8	9.0	3.6	37.1	93.9	35.7	93.5	91.6	99.4	23.5	92.6	93.8	93.9	96.9
6	1	485	15.8	$0.5 \cdot 10^3$	61.5	0.2	22.2	16.1	7.3	3.2	73.3	81.0	73.7	79.8	98.9	97.5	66.8	76.8	96.8	95.9	98.8
7	1	497	15.5	$0.5 \cdot 10^3$	64.3	0.3	22.3	13.1	6.5	2.7	64.9	61.8	64.3	59.5	97.9	94.0	56.6	53.7	99.8	99.1	101.1
8	1	518	15.0	$1.5 \cdot 10^3$	65.7	0.6	23.4	10.1	14.9	5.7	50.2	52.8	51.2	50.4	93.6	86.3	39.3	44.5	98.9	96.1	100.0
9	1	543	15.5	$1.5 \cdot 10^3$	66.6	1.5	23.0	8.8	11.3	5.4	41.3	43.2	43.1	41.4	81.6	69.5	31.2	36.7	96.7	95.4	100.9
10	1	465	20.2	$0.5 \cdot 10^3$	57.3	0.4	15.3	25.1	8.7	3.2	87.3	97.4	83.4	97.2	98.4	99.8	84.5	96.7	95.0	94.6	88.8
11	1	484	20.5	$0.5 \cdot 10^3$	47.6	0.1	15.1	37.1	10.4	4.1	92.5	94.5	91.6	94.2	99.7	99.4	90.7	93.3	102.9	101.6	101.3
12	1	494	20.5	$0.6 \cdot 10^3$	49.7	0.2	19.7	30.4	9.4	4.3	87.5	90.5	88.8	89.9	99.4	98.7	84.5	88.5	98.9	98.5	102.0
13	1	507	20.4	$0.8 \cdot 10^3$	58.5	0.3	22.7	18.5	10.7	4.6	74.1	70.9	76.4	69.1	98.5	95.2	67.9	64.8	97.6	94.9	98.4
14	1	519	20.0	$2.0 \cdot 10^3$	64.3	0.4	21.9	12.7	25.3	11.9	64.2	63.6	63.1	61.6	96.6	91.6	56.1	56.6	98.5	100.2	103.1
15	1	543	20.0	$2.0 \cdot 10^3$	66.2	1.1	22.5	10.0	18.9	8.9	50.6	52.7	50.4	50.8	88.7	79.5	41.1	46.0	96.8	97.3	100.7
16	2#	468	20.7	$1.7 \cdot 10^3$	59.5	0.1	0.9	39.4	35.0	3.3	99.5	99.6	88.5	88.1	99.9	99.9	96.8	97.3	92.7	94.5	95.4
17	2#	469	19.2	$1.7 \cdot 10^3$	59.3	0.3	1.3	39.1	36.3	3.3	99.3	99.6	88.5	88.0	99.9	99.9	95.2	97.1	95.9	97.0	98.8
18	2	480	20.8	$1.6 \cdot 10^3$	61.5	0.1	2.1	36.3	33.6	3.0	98.9	99.1	87.2	87.4	99.9	99.9	91.6	93.6	93.6	95.7	96.3
19	2#	493	19.7	$1.7 \cdot 10^3$	63.4	0.3	6.1	30.3	33.9	2.7	96.2	96.6	84.1	84.4	99.8	99.6	70.8	76.0	93.2	95.3	96.1
20	2#	520	19.6	$1.7 \cdot 10^3$	65.8	1.5	11.6	21.1	31.9	1.9	88.6	89.7	76.2	76.6	98.5	97.3	19.9	36.9	95.2	97.0	100.7
21	2#	545	19.5	$1.7 \cdot 10^3$	66.2	4.0	13.1	16.7	30.0	1.4	81.2	82.5	69.8	69.9	95.0	91.2	-14.7	21.8	97.3	98.2	104.7
22	2	471	7.8	$1.3 \cdot 10^3$	69.3	4.1	9.9	16.7	24.6	1.3	85.0	88.8	70.6	71.3	95.0	97.7	5.0	17.5	100.9	100.9	108.4
23	2	496	7.9	$1.3 \cdot 10^3$	69.6	4.5	10.1	15.7	22.6	0.7	82.7	82.2	67.2	65.7	94.0	91.2	-8.3	9.5	97.7	98.2	102.0
24	2	520	8.0	$1.3 \cdot 10^3$	68.7	9.3	9.5	12.5	19.0	0.6	71.4	71.0	58.5	56.7	84.1	78.9	-30.3	7.3	96.7	97.0	102.2
25	2	544	7.6	$1.3 \cdot 10^3$	68.0	13.2	9.2	9.7	12.7	0.6	54.9	54.8	45.6	43.8	70.1	60.7	-66.5	7.2	92.1	93.1	100.5
26	2	469	15.3	$1.1 \cdot 10^3$	69.0	0.0	1.9	29.1	22.2	1.7	98.8	99.0	82.3	82.6	99.9	99.9	89.0	91.6	96.1	97.8	98.1
27	2	470	15.3	$2.2 \cdot 10^3$	68.7	0.0	2.5	28.8	42.9	3.0	98.4	98.9	82.7	82.5	99.9	99.9	86.0	90.8	94.2	95.2	95.7
28	2	470	15.3	$2.2 \cdot 10^3$	68.7	0.0	3.1	28.2	46.2	3.5	97.9	98.9	81.2	82.5	99.9	99.9	80.9	90.8	100.7	102.1	103.7
29	2	495	14.9	$2.2 \cdot 10^3$	69.6	0.9	9.1	20.4	38.5	1.8	91.2	91.8	75.7	74.6	99.1	98.3	27.8	39.1	91.2	92.3	94.6
30	2	520	15.0	$2.2 \cdot 10^3$	70.1	2.5	10.6	16.8	35.7	1.0	85.5	86.0	69.3	69.3	96.9	94.1	-5.6	21.8	91.6	93.1	94.8
31	2	544	15.0	$2.2 \cdot 10^3$	69.1	5.6	11.3	14.0	29.8	1.1	76.1	77.5	61.3	62.2	91.1	85.3	-43.5	15.0	90.0	92.4	96.3

*Org. = Organics.

#Corrected $\phi_{v,off}$ due to the presence of methanol vapor in the exit.

•All conversions are in %.

Continuation of Table B.1.

No.	Feed	Conditions			Composition exit streams						Conversion (experimental vs. equilibrium)								Balances		
		T	P	GHSV	H_2	CO	CO_2	C_xH_y	Org.*	H_2O	ζ_{CO+CO2}		ζ_{H2}		ζ_{CO}		ζ_{CO2}		C	H	O
		(K)	(MPa)	(h^{-1})			(vol%)		(g/h)	(g/h)	Exp.	Eq.	Exp.	Eq.	Exp.	Eq.	Exp.	Eq.		(%)	
(-)	(-)																				
32	2	493	20.6	$1.7 \cdot 10^3$	68.3	0.1	4.2	27.4	33.1	2.1	97.1	97.6	81.6	81.1	99.9	99.6	74.5	81.3	93.2	94.0	94.5
33	2	506	20.5	$1.7 \cdot 10^3$	69.0	0.3	7.8	22.9	31.1	1.6	93.6	94.6	78.4	77.7	99.7	99.0	44.5	59.6	91.2	92.0	93.7
34	2	519	20.9	$1.7 \cdot 10^3$	68.6	0.9	9.5	20.9	29.4	1.6	90.5	91.8	75.4	74.9	99.1	97.7	22.3	44.4	90.7	92.0	94.5
35	3#	470	7.8	$1.7 \cdot 10^3$	47.1	16.9	28.6	7.4	6.2	0.6	15.2	48.6	35.5	73.4	35.9	93.1	-5.0	5.5	96.5	85.1	100.8
36	3#	493	7.9	$1.7 \cdot 10^3$	38.7	7.0	43.1	11.3	17.9	1.8	39.0	42.3	65.4	63.7	82.8	81.2	-3.4	4.5	95.0	89.9	101.8
37	3#	517	8.0	$1.7 \cdot 10^3$	42.7	10.9	36.4	10.0	17.4	1.4	34.9	34.0	56.8	51.6	69.5	64.3	1.4	4.6	97.3	94.4	101.3
38	3#	540	7.9	$1.7 \cdot 10^3$	46.4	14.9	30.6	8.1	10.5	0.8	22.4	24.2	41.9	37.5	48.4	43.6	-2.8	5.3	97.0	89.8	101.0
39	3#	470	14.7	$1.7 \cdot 10^3$	37.9	5.1	44.4	12.6	21.2	1.0	45.8	57.0	69.5	89.9	88.8	98.2	4.1	16.9	92.7	89.8	96.0
40	3#	493	14.9	$0.8 \cdot 10^3$	27.7	2.7	53.5	16.2	9.4	0.7	52.3	52.6	82.7	81.5	95.4	95.3	10.5	11.2	87.1	79.9	91.0
41	3#	492	14.8	$1.6 \cdot 10^3$	28.2	2.5	53.1	16.2	24.5	1.7	52.8	52.6	82.5	81.5	95.7	95.3	11.2	11.2	94.0	91.2	96.8
42	3#	519	14.9	$1.6 \cdot 10^3$	36.6	5.5	45.4	12.6	18.1	5.1	44.4	46.2	70.6	70.9	87.9	85.3	2.1	8.3	91.1	94.0	104.9
43	3#	544	14.9	$1.6 \cdot 10^3$	41.5	9.4	38.2	10.9	16.4	3.2	39.8	39.1	61.5	60.4	75.9	71.4	4.8	7.8	91.8	93.0	100.4
44	3#	468	19.4	$1.6 \cdot 10^3$	23.3	1.5	56.9	18.3	25.2	5.9	56.1	59.4	87.1	95.0	97.8	98.8	15.6	21.1	94.2	100.9	105.1
45	3#	494	19.5	$1.6 \cdot 10^3$	22.8	1.4	57.6	18.1	27.4	3.5	55.1	55.2	87.3	86.7	97.8	96.5	13.7	15.1	99.3	101.4	103.7
46	3#	519	19.4	$1.6 \cdot 10^3$	30.8	3.7	50.8	14.7	26.4	2.0	48.9	50.5	78.8	78.4	93.0	90.8	6.1	11.5	103.2	102.9	105.4
47	3#	545	19.4	$1.6 \cdot 10^3$	38.2	6.7	42.9	12.2	23.1	2.9	44.3	44.1	68.5	68.4	84.7	79.4	5.0	9.8	101.4	105.4	106.6
48	4#	470	8.0	$1.9 \cdot 10^3$	33.0	24.4	27.0	15.6	27.6	1.3	50.2	60.3	76.5	88.7	67.4	82.7	4.6	0.8	96.1	94.6	98.3
49	4#	470	7.6	$0.9 \cdot 10^3$	17.8	21.1	39.0	22.0	14.6	0.5	58.9	60.5	91.0	89.0	80.1	83.0	2.6	0.8	91.0	85.4	93.2
50	4#	493	7.6	$1.9 \cdot 10^3$	26.7	23.5	32.0	17.8	32.1	1.0	52.9	53.0	83.3	78.2	72.5	72.5	0.9	1.4	100.1	97.4	102.3
51	4#	517	7.6	$1.9 \cdot 10^3$	36.2	24.2	25.8	13.8	25.7	1.6	45.2	43.6	70.8	64.5	63.4	59.2	-3.3	2.1	97.7	96.1	102.4
52	4#	542	7.6	$1.9 \cdot 10^3$	42.1	24.1	22.6	11.2	22.0	2.8	37.1	30.9	58.4	46.0	55.2	41.3	-10.9	3.2	99.2	100.7	108.1
53	4#	466	15.2	$1.9 \cdot 10^3$	5.7	13.3	51.9	29.1	35.7	0.8	66.2	66.3	97.8	97.5	90.5	91.0	1.7	0.8	95.4	94.2	97.0
54	4#	491	15.0	$1.9 \cdot 10^3$	11.5	15.7	46.9	25.8	33.3	1.4	63.5	62.5	95.1	92.1	87.4	85.5	0.0	1.5	94.2	92.8	97.8
55	4#	517	15.0	$1.9 \cdot 10^3$	21.0	17.0	40.6	21.4	30.0	1.0	59.3	56.9	89.1	84.0	83.5	77.4	-4.6	2.4	93.0	90.4	96.7
56	4#	542	15.1	$1.9 \cdot 10^3$	30.5	15.7	36.4	17.3	31.7	1.4	54.7	48.6	80.5	72.1	81.2	65.7	-15.7	3.5	99.0	101.1	106.0
57	4#	468	19.4	$1.8 \cdot 10^3$	2.6	10.7	55.9	30.8	34.0	0.6	67.4	67.1	99.1	98.7	92.8	92.2	0.1	0.7	92.4	90.4	94.3
58	4#	495	19.7	$1.8 \cdot 10^3$	8.7	12.2	51.3	27.8	30.5	1.2	65.6	64.8	96.6	95.5	90.9	88.6	-1.4	1.6	88.9	86.5	92.7
59	4#	520	20.5	$1.8 \cdot 10^3$	17.1	13.3	45.2	24.5	33.2	1.2	64.0	60.4	92.3	89.2	88.7	82.2	-1.7	2.7	94.2	95.4	97.8
60	4#	544	19.6	$1.8 \cdot 10^3$	29.2	14.2	38.0	18.6	25.6	2.3	57.5	54.0	82.6	80.0	84.1	72.9	-12.8	3.8	88.5	89.5	97.5

*Org. = Organics
#Corrected $\phi_{v,off}$ due to the presence of methanol vapor in the exit
•All conversions are in %.

Table B.2 Composition of the liquid phase.

No.	Feed	Conditions			Liquid product				Higher alcohols							
		T	P	GHSV	Methanol	H$_2$O	HA*	Total	Ethanol	1-pro-panol	2-pro-panol	2-methyl-1-propanol	1-bu-tanol	2-bu-tanol	2-methyl-1-butanol	1-pen-tanol
(-)	(-)	(K)	(MPa)	(h^{-1})	(wt%)				(wt%)							
1	1	469	7.9	1.0·10^3	68.2	33.0	0.0	101.2	0.00	0.00	0.00	0.00	0.00	0.00	0.00	0.00
2	1	493	8.0	1.0·10^3	71.6	29.2	0.0	100.8	0.00	0.00	0.00	0.00	0.00	0.00	0.00	0.00
3	1	518	8.0	1.0·10^3	69.7	31.4	0.0	101.2	0.01	0.00	0.00	0.00	0.00	0.00	0.00	0.00
4	1	542	8.1	1.0·10^3	63.9	34.1	0.1	98.2	0.08	0.03	0.01	0.01	0.00	0.01	0.00	0.00
5	1	469	15.0	1.5·10^3	70.2	28.6	0.0	98.8	0.00	0.00	0.00	0.00	0.00	0.00	0.00	0.00
6	1	485	15.8	0.5·10^3	72.1	30.2	0.0	102.2	0.00	0.00	0.00	0.00	0.00	0.00	0.00	0.00
7	1	497	15.5	0.5·10^3	71.3	29.2	0.0	100.5	0.02	0.01	0.00	0.00	0.00	0.00	0.00	0.00
8	1	518	15.0	1.5·10^3	70.0	27.9	0.0	97.9	0.01	0.00	0.00	0.00	0.00	0.00	0.00	0.00
9	1	543	15.5	1.5·10^3	68.9	32.3	0.1	101.4	0.05	0.02	0.01	0.01	0.00	0.01	0.00	0.00
10	1	465	20.2	0.5·10^3	71.2	26.9	0.0	98.1	0.01	0.00	0.00	0.00	0.00	0.00	0.00	0.00
11	1	484	20.5	0.5·10^3	68.4	28.5	0.0	96.9	0.00	0.00	0.00	0.00	0.00	0.00	0.00	0.00
12	1	494	20.5	0.6·10^3	67.8	31.4	0.0	99.2	0.00	0.00	0.00	0.00	0.00	0.00	0.00	0.00
13	1	507	20.4	0.8·10^3	68.7	30.4	0.0	99.1	0.00	0.00	0.00	0.00	0.00	0.00	0.00	0.00
14	1	519	20.0	2.0·10^3	68.5	32.0	0.0	100.5	0.00	0.00	0.00	0.00	0.00	0.00	0.00	0.00
15	1	543	20.0	2.0·10^3	68.8	31.9	0.1	100.8	0.03	0.01	0.00	0.00	0.00	0.00	0.00	0.00
16	2#	468	20.7	1.7·10^3	90.3	9.0	0.8	100.0	0.41	0.14	0.02	0.06	0.05	0.08	0.03	0.02
17	2#	469	19.2	1.7·10^3	91.9	8.8	0.7	101.3	0.35	0.11	0.02	0.04	0.04	0.07	0.02	0.02
18	2#	480	20.8	1.6·10^3	89.7	8.3	1.1	99.1	0.53	0.19	0.03	0.09	0.06	0.11	0.04	0.03
19	2#	493	19.7	1.7·10^3	91.4	7.8	1.3	100.5	0.60	0.25	0.03	0.12	0.10	0.12	0.07	0.05
20	2#	520	19.6	1.7·10^3	91.4	6.7	2.2	100.3	0.96	0.43	0.05	0.28	0.13	0.21	0.11	0.07
21	2#	545	19.5	1.7·10^3	91.3	6.1	3.7	101.2	1.46	0.78	0.07	0.59	0.23	0.28	0.22	0.12
22	2	471	7.8	1.3·10^3	96.5	5.0	0.1	101.6	0.05	0.02	0.00	0.01	0.01	0.01	0.00	0.00
23	2	496	7.9	1.3·10^3	95.6	2.8	0.6	99.0	0.32	0.10	0.03	0.02	0.05	0.04	0.01	0.03
24	2	520	8.0	1.3·10^3	93.1	2.9	1.8	97.9	0.98	0.33	0.07	0.07	0.16	0.11	0.05	0.08
25	2	544	7.6	1.3·10^3	90.6	4.2	6.0	100.8	2.88	1.21	0.13	0.52	0.49	0.25	0.28	0.22
26	2	469	15.3	1.1·10^3	94.1	7.1	0.5	101.7	0.27	0.08	0.02	0.03	0.03	0.05	0.02	0.02
27	2	470	15.3	2.2·10^3	93.4	6.5	0.7	100.6	0.39	0.12	0.02	0.05	0.05	0.06	0.03	0.02
28	2	470	15.3	2.2·10^3	95.1	7.1	0.7	102.9	0.37	0.11	0.02	0.04	0.04	0.07	0.02	0.02
29	2	495	14.9	2.2·10^3	95.7	4.5	0.9	101.2	0.46	0.15	0.04	0.05	0.05	0.09	0.03	0.03
30	2	520	15.0	2.2·10^3	97.1	2.6	1.6	101.4	0.77	0.28	0.06	0.12	0.10	0.14	0.06	0.05
31	2	544	15.0	2.2·10^3	93.5	3.5	3.0	100.0	1.39	0.54	0.10	0.29	0.19	0.20	0.13	0.09

*Summation of the concentration of ethanol, 1-propanol, 2-propanol, 2-methyl-1-propanol, 1-butanol, 2-butanol, 2-methyl-1-butanol, 1-pentanol.

#Corrected $\phi_{v,off}$ due to the presence of methanol vapor in the exit.

Continuation of Table B.2.

No.	Feed	Conditions T (K)	P (MPa)	GHSV (h⁻¹)	Liquid product Methanol (wt%)	H₂O	HA*	Total	Higher alcohols Ethanol (wt%)	1-propanol	2-propanol	2-methyl-1-propanol	1-butanol	2-butanol	2-methyl-1-butanol	1-pentanol
32	2	493	20.6	$1.7 \cdot 10^3$	92.4	6.1	1.0	99.4	0.48	0.17	0.03	0.08	0.05	0.10	0.04	0.03
33	2	506	20.5	$1.7 \cdot 10^3$	93.5	5.0	1.2	99.7	0.58	0.21	0.04	0.12	0.07	0.12	0.05	0.03
34	2	519	20.9	$1.7 \cdot 10^3$	93.4	5.2	2.0	100.6	0.88	0.39	0.05	0.23	0.12	0.19	0.10	0.06
35	3#	470	7.8	$1.7 \cdot 10^3$	-	-	-	-	-	-	-	-	-	-	-	-
36	3#	493	7.9	$1.7 \cdot 10^3$	90.6	9.9	0.1	100.6	0.05	0.02	0.01	0.01	0.01	0.02	0.00	0.01
37	3#	517	8.0	$1.7 \cdot 10^3$	-	-	-	-	-	-	-	-	-	-	-	-
38	3#	540	7.9	$1.7 \cdot 10^3$	-	-	-	-	-	-	-	-	-	-	-	-
39	3#	470	14.7	$1.7 \cdot 10^3$	92.2	5.2	0.1	97.5	0.05	0.03	0.00	0.02	0.01	0.01	0.01	0.01
40	3#	493	14.9	$0.8 \cdot 10^3$	93.4	6.6	0.2	100.2	0.09	0.04	0.01	0.02	0.02	0.02	0.01	0.01
41	3#	492	14.8	$1.6 \cdot 10^3$	93.4	7.1	0.2	100.7	0.07	0.03	0.01	0.01	0.01	0.02	0.01	0.01
42	3#	519	14.9	$1.6 \cdot 10^3$	74.8	24.6	1.1	100.5	0.42	0.22	0.04	0.10	0.08	0.15	0.05	0.05
43	3#	544	14.9	$1.6 \cdot 10^3$	76.8	20.5	2.5	99.8	0.85	0.54	0.07	0.30	0.19	0.25	0.15	0.13
44	3#	468	19.4	$1.6 \cdot 10^3$	79.0	21.4	0.2	100.6	0.06	0.03	0.01	0.01	0.01	0.03	0.01	0.01
45	3#	494	19.5	$1.6 \cdot 10^3$	88.6	12.9	0.2	101.7	0.09	0.04	0.01	0.02	0.01	0.05	0.01	0.01
46	3#	519	19.4	$1.6 \cdot 10^3$	91.1	8.5	0.5	100.1	0.20	0.09	0.03	0.04	0.03	0.08	0.02	0.02
47	3#	545	19.4	$1.6 \cdot 10^3$	83.4	15.4	1.7	100.6	0.60	0.37	0.06	0.20	0.12	0.21	0.09	0.08
48	4#	470	8.0	$1.9 \cdot 10^3$	95.7	5.4	0.5	101.6	0.18	0.10	0.01	0.04	0.05	0.02	0.03	0.03
49	4#	470	7.6	$0.9 \cdot 10^3$	93.9	3.8	0.1	97.8	0.05	0.02	0.01	0.00	0.01	0.04	0.00	0.01
50	4#	493	7.6	$1.9 \cdot 10^3$	96.8	3.6	1.2	101.6	0.56	0.23	0.07	0.04	0.12	0.07	0.03	0.07
51	4#	517	7.6	$1.9 \cdot 10^3$	86.7	8.5	5.2	100.4	2.23	1.16	0.08	0.29	0.59	0.32	0.20	0.33
52	4#	542	7.6	$1.9 \cdot 10^3$	60.3	19.8	13.9	93.9	4.87	3.17	0.14	1.75	1.51	0.59	1.07	0.77
53	4#	466	15.2	$1.9 \cdot 10^3$	94.6	2.2	1.3	98.0	0.55	0.24	0.08	0.10	0.10	0.10	0.06	0.05
54	4#	491	15.0	$1.9 \cdot 10^3$	95.2	4.4	1.5	101.0	0.60	0.26	0.14	0.10	0.11	0.12	0.06	0.06
55	4#	517	15.0	$1.9 \cdot 10^3$	93.1	3.5	3.6	100.2	1.58	0.72	0.17	0.26	0.32	0.19	0.15	0.19
56	4#	542	15.1	$1.9 \cdot 10^3$	86.2	5.1	7.5	98.8	3.05	1.67	0.16	0.82	0.68	0.34	0.43	0.39
57	4#	468	19.4	$1.8 \cdot 10^3$	97.4	1.8	1.0	100.2	0.44	0.18	0.09	0.07	0.07	0.10	0.04	0.04
58	4#	495	19.7	$1.8 \cdot 10^3$	95.0	3.8	1.6	100.4	0.63	0.29	0.12	0.13	0.11	0.15	0.07	0.06
59	4#	520	20.5	$1.8 \cdot 10^3$	93.5	4.0	3.2	100.7	1.36	0.63	0.17	0.23	0.27	0.21	0.13	0.16
60	4#	544	19.6	$1.8 \cdot 10^3$	79.4	9.8	8.6	97.7	3.29	1.99	0.12	0.94	0.82	0.45	0.52	0.49

*Summation of the concentration of ethanol, 1-propanol, 2-propanol, 2-methyl-1-propanol, 1-butanol, 2-butanol, 2-methyl-1-butanol, 1-pentanol.

#Corrected $\phi_{v,off}$ due to the presence of methanol vapor in the exit.

Appendix C
Kinetics of high pressure methanol synthesis

Abstract

The reaction rates in high pressure methanol synthesis from CO, CO_2, and H_2 were studied in a continuous spinning basket reactor. The experiments were conducted at pressures between 17.5 and 22.5 MPa and a temperature of 483 K. The experimental data for methanol and water were modeled using a power law kinetic model extended with an adsorption term for methanol. The hydrogenation of CO and CO_2 were taken into account. The kinetic model was derived using a least squares method. The average error was 15% in the predicted methanol production rate and 44% in the predicted water production rate. The kinetic model is the first in its sort for high pressure methanol synthesis over Cu based catalysts from syngases containing CO, CO_2, and H_2.

C.1 Introduction

The methanol synthesis process was originally developed by BASF as a high pressure process (15 – 25 MPa) at moderate temperatures (553 – 623 K) [1, 2]. When improved syngas purification techniques in combination with more active Cu based catalyst were applied, the majority of the high pressure processes was converted to the low pressure process (5 – 10 MPa, 500 – 570 K) [2].

From a thermodynamic point of view high pressure and low temperatures are the most favorable conditions for methanol synthesis (Fig. C.1). However, syngas compression to these high pressures is very energy intensive. High pressure methanol synthesis becomes interesting when the syngas compression step can be omitted due to the availability of syngas at high pressure. This is the case when the syngas is produced by reforming in supercritical water (RSCW), which is a process suitable to convert wet (preferably liquid) biomass to gas at high pressure (> 22.1 MPa) [3]. The high pressure in the latter process is obtained by pumping a liquid instead of gas compression. The envisaged process conditions for this appendix on high pressure methanol synthesis are pressures between 20 to 25 MPa and a temperature of 483 K (see Fig. C.1).
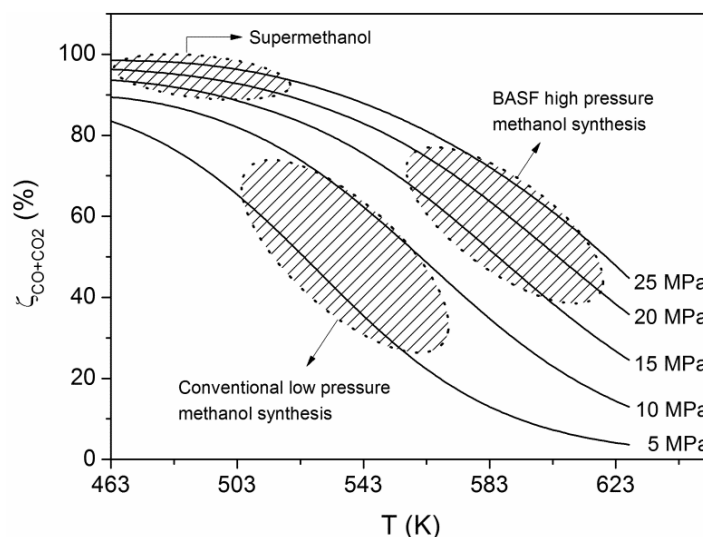

Fig. C.1 Equilibria in methanol synthesis for different pressures ($H_2/CO/CO_2/CH_4$ = 67/24/4/5 vol%). The condition ranges for conventional methanol synthesis, BASF's high pressure methanol synthesis process and the range envisaged in this study are roughly indicated.

Cu based catalysts are commonly applied in industrial methanol synthesis [4]. However, kinetic equations for these catalysts are available in the open literature for the low pressure process only. Kinetics were measured for different catalyst compositions, reactors, syngas compositions, and process conditions [4-16]. The variation in process conditions is indicated in Fig. C.2. Two studies were conducted at $P \leq 1$ MPa, while the majority was conducted at 460 K $\leq T \leq$ 573 K

and 1.5 MPa $\leq P \leq$ 10 MPa. The difference between the kinetic models are considerable due to the use of different methanol synthesis mechanisms, rate determining steps (RDS), types and numbers of active sites, and additional assumptions.

To the authors knowledge kinetic equations for high pressure conditions and low temperatures have not been reported to date (Fig. C.2). Natta published kinetic data for methanol synthesis at 30 MPa, but for a Cu/ZnO catalyst on a Cr_2O_3 support [17], and using gas mixtures composed of solely H_2 and CO at temperatures exceeding 573 K.

In this appendix a kinetic study on high pressure methanol reaction rates is described. The experiments were conducted in a continuous spinning basket reactor using a state of the art Cs doped Cu/ZnO/Al$_2$O$_3$ catalyst. The measurements were conducted at 17.5 – 22.5 MPa and a temperature of 483 K. Kinetic rate equations were obtained by fitting experimental reaction rates to modified power law kinetic equations. Methanol synthesis from CO and CO_2, and the water-gas-shift (WGS) reaction are considered.
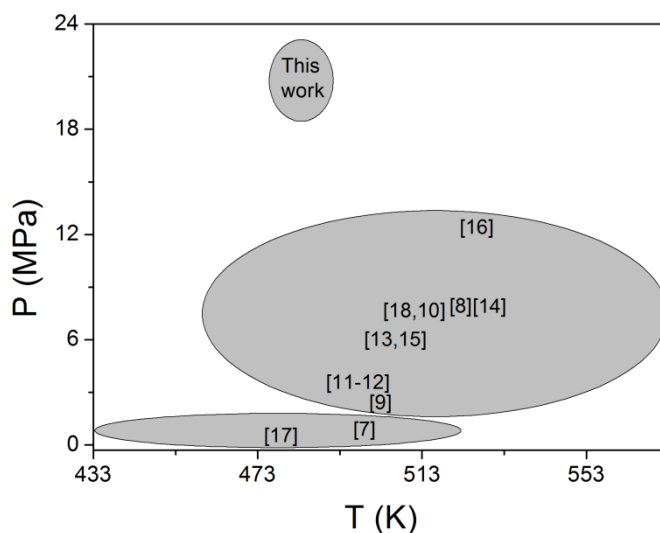

Fig. C.2 Conditions for kinetic studies on methanol synthesis from mixtures of H_2, CO, and CO_2 over Cu based catalysts. The conditions for the study conducted by Kuznetsov *et al.* [15] are taken from reference [4], because they were published in Russian. The locations of the references refer to the average measurement conditions of the respective study.

C.2 Theory

C.2.1 Reactions and kinetic expressions

The synthesis reaction of methanol from syngas involves the hydrogenation of CO (Eq. 1.1), the (reverse) WGS reaction (Eq. 1.2) and the hydrogenation of CO_2 (Eq. 1.3). Depending on reaction conditions and catalysts applied, some of the reactions are very slow and may be ignored.

$$r_1 = CO + 2\ H_2 \ \rightleftharpoons \ CH_3OH \qquad\qquad \Delta_r H^0_{298} = \text{-90.64 kJ/mol} \qquad\qquad \text{(Eq. 1.1)}$$

$$r_2 = CO_2 + H_2 \ \rightleftharpoons \ CO + H_2O \qquad\qquad \Delta_r H^0_{298} = \text{+41.17 kJ/mol} \qquad\qquad \text{(Eq. 1.2)}$$

$$r_3 = CO_2 + 3\ H_2 \ \rightleftharpoons \ CH_3OH + H_2O \qquad\qquad \Delta_r H^0_{298} = \text{-49.47 kJ/mol} \qquad\qquad \text{(Eq. 1.3)}$$

Kinetic models published in the literature are often based on Langmuir-Hinshelwood-Hougen-Watson (LHHW) mechanisms, which include adsorption terms of reactants and reaction products [6, 7, 13, 14]. Due to the limited size of the experimental data set, we have initially explored the use of power law models including an adsorption term for the reaction products to describe the experimental production rates. For each reaction (Eqs. 1.1 − 1.3) the following basic kinetic equations were applied:

$$r_1^{'} = \frac{k_1}{f_{CO}^{n_{CO,1}} f_{H_2}^{n_{H_2,1}}} \frac{\left(f_{CO} f_{H_2}^2 - \dfrac{f_{CH_3OH}}{K_{P_1^o}} \right)}{\left(1 + K_{CH_3OH} f_{CH_3OH} + K_{H_2O} f_{H_2O} \right)} \qquad\qquad \text{(Eq. C.1)}$$

$$r_2^{'} = \frac{k_2}{f_{CO_2}^{n_{CO_2,2}} f_{H_2}^{n_{H_2,2}}} \frac{\left(f_{CO_2} f_{H_2} - \dfrac{f_{CO} f_{H_2O}}{K_{P_2^o}} \right)}{\left(1 + K_{CH_3OH} f_{CH_3OH} + K_{H_2O} f_{H_2O} \right)} \qquad\qquad \text{(Eq. C.2)}$$

$$r_3^{'} = \frac{k_3}{f_{CO_2}^{n_{CO_2,3}} f_{H_2}^{n_{H_2,3}}} \frac{\left(f_{CO_2} f_{H_2}^3 - \dfrac{f_{CH_3OH} f_{H_2O}}{K_{P_3^o}} \right)}{\left(1 + K_{CH_3OH} f_{CH_3OH} + K_{H_2O} f_{H_2O} \right)} \qquad\qquad \text{(Eq. C.3)}$$

The term between brackets is the driving force of the equation. The denominator of the equation contains the fugacity of the reactants to the power 'n' and is part of the power law model. Because the form of the adsorption term is unclear a simplified term to describe the adsorption behavior is used in the denominator. The equilibrium constants, $K_{P_j^o}$, derived by Graaf *et al.* [7, 18], also given in Chapter 5, are used. The reaction rate constant, k_j, is a lumped parameter consisting of several contributions including among others, the activation energy and the number of active sites at the catalyst surface.

C.2.2 Parameter estimation

The kinetic model given in Eqs. C.1 − C.3 contains 11 parameters (e.g. k_1, $n_{CO,1}$, $n_{H2,1}$, K_{CH3OH}, K_{H2O} for Eq. C.1). These parameters need to be estimated from experimental data. The data set obtained for each experiment is composed of the following variables:

$$R_{CH_3OH}^{'}, R_{H_2O}^{'}, T, P, y_{CO}, y_{CO_2}, y_{CH_3OH}, y_{H_2}, y_{H_2O}, \phi_{v,off}^o$$

The pressure, temperature, feed flow, and composition of the feed gas (not given above) are the independent variables, while the methanol and water production rates, volumetric flow rate of the exit gas and gas composition of the exit gas are the dependent variables.

The fugacity of each component was calculated from the temperature, pressure, and composition of the mixture. A modification of the Soave-Redlich-Kwong equation of state for polar components was used [19, 20]. Some of the binary interaction coefficients were fitted to experimental data close to the operating conditions and the procedure is given in Chapter 5. The other binary interaction parameters were taken from the Aspen Hysys database and are provided in Appendix A. The predicted production rates for methanol and water, $\hat{R}'_{CH_3OH}, \hat{R}'_{H_2O}$, were calculated from the kinetic model by supplying the model with the fugacities of the components in combination with the estimated values for the 11 parameters using the following equations:

$$\hat{R}'_{CH_3OH} = \hat{r}'_1 + \hat{r}'_3 \qquad \text{(Eq. C.4)}$$

$$\hat{R}'_{H_2O} = \hat{r}'_2 + \hat{r}'_3 \qquad \text{(Eq. C.5)}$$

The parameters were obtained by minimizing the sum of squared residuals, (SSR), defined as:

$$SSR = F_{obj} = \sum_{l=1}^{N} \left(\left(\hat{R}'_{CH_3OH} - R'_{CH_3OH} \right)^2_l + WF \left(\hat{R}'_{H_2O} - R'_{H_2O} \right)^2_l \right) \qquad \text{(Eq. C.6)}$$

where, N is the number of experiments and WF is a weighing factor. If WF is equal to 1 the 'weight' of the term concerning the reaction rate of water is equal to the methanol term. If WF is equal to 0 the reaction rate of water is not taken into account during the fitting procedure. A direct search algorithm 'lsqcurvefit' was used for parameter estimation. This function uses the 'trust-region-reflective' algorithm to minimize the objective function (Eq. C.6). When a set of optimal parameters was found the variances for the methanol and water production rate are calculated using:

$$s_i^2 = \frac{1}{N-m} \sum_{l=1}^{N} \left(\hat{R}'_i - R'_i \right)^2_l \qquad \text{(Eq. C.7)}$$

The values of the variances are composed of lack of fit of the model proposed and experimental errors. The average absolute errors in the experiments are calculated using Eq. C.8.

$$\Delta R'_i = \frac{1}{N} \sum_{i=1}^{N} \left| \frac{\hat{R}'_i - R'_i}{R'_i} \right| \cdot 100\% \qquad \text{(Eq. C.8)}$$

The values for the k_j's and $n_{i,j}$'s should be greater than 0 to have physical meaning. Boundary conditions were used to obtain positive values for all parameters to be estimated (see Table C.1). The residuals should be normally distributed with zero mean. Furthermore there should be no trending effect of any of the experimental parameters. Matlab version 2008b was used for the fitting procedure.

Table C.1 Boundary conditions for parameter estimation of the 11 parameters. Index j represents the reaction (Eqs. 1.1 – 1.3) , index i represent the components (CO, CO_2, CH_3OH, H_2, H_2O), Inf. = infinite.

Boundary	k_j	$n_{i,j}$	K_i
Lower	0	0	0
Upper	Inf.	10	Inf.

C.3   Experimental section

C.3.1   Materials

A commercial Cs doped $Cu/ZnO/Al_2O_3$ methanol synthesis catalyst was used for all experiments. Pure gases (CO > 99.955 vol%, CO_2 > 99.7 vol%, H_2 > 99.999 vol%) were supplied by Linde Gas Benelux, The Netherlands. Gas mixtures with predetermined compositions were tailor made in the setup (see Fig. C.3) using a gas mixing station. The relative deviation in the gas composition is approximately 3%. The concentration of N_2 was in any case below 0.5 vol% and is neglected. The average gas compositions for the kinetic experiments are shown in Table C.2.

Table C.2 Average gas compositions used for the kinetic experiments.

Gas	H_2 (vol%)	CO (vol%)	CO_2 (vol%)	P (MPa)	T (K)	$\phi_{v,in}$ (NL/h)
1	68.8	27.9	3.3	17.5 – 22.5	483	25 – 65
2	63.7	22.9	13.4	17.5 – 22.5	483	25 – 65
3	74.1	19.2	6.7	17.5 – 22.5	483	25 – 65
4	79.7	10.4	9.9	17.5 – 22.5	483	25 – 65
5	89.3	5.3	5.4	17.5 – 22.5	483	25 – 65
6	84.4	13.0	2.6	17.5 – 22.5	483	25 – 65
7	86.1	1.2	12.7	17.5 – 22.5	483	25 – 65
8	88.5	0	11.5	2.5 & 20.0	486	25 – 65

C.3.1   Experimental setup

The setup including the gas mixing station used for the kinetic experiments is depicted in Fig. C.3. Pure gases are connected to the gas-mixing station and by adjusting the respective gas flows with mass flow controllers (MFC, Brooks) a mixture with the desired composition is obtained. The gas mixture is collected in a gas storage vessel (V = 0.5 L) before it is pressurized in a gas booster (Resato) to 30 MPa and stored in a gas storage bomb (V = 1 L). The feed flow to

the spinning basket reactor from the gas storage bomb can be adjusted by an additional MFC (Brooks). During operation new syngas is prepared constantly with the gas mixing system to maintain a constant feed flow to the reactor.

The spinning basket reactor is electrically heated and the temperature is controlled by a thermocouple located close to the spinning basket. It contains a small basket filled with catalyst (0.1 – 0.3 g). The rotating speed of the spinning basket can be adjusted from 0 to 2000 rpm. The shaft holding the basket is also equipped with a propeller to increase mixing of the system. The propeller blades at the bottom are slightly tilted to force the gas flow upwards. Gas is fed from the top of the reactor, forced top-down through the spinning basket containing the catalyst and removed from the bottom through a dip tube. The diameter of the spinning basket is 4 mm smaller than the diameter of the reactor. An inert stainless steel block is placed at the bottom of the reactor to minimize the dead volume. The gas mixture leaving the reactor can be depressurized through either back-pressure controller (BPC) 1 or 2. When BPC 1 is used the gas mixture is cooled in a condenser to trap all condensables (V = 0.5 L, T = 258 K). The liquid can be tapped and the remaining gas can be quantified and analyzed using a gas chromatograph (GC). The other option is that the gas mixture is depressurized through BPC-2. The composition of the gas flow is then directly analyzed in a GC and quantified. The tubing to the GC is traced and maintained at 373 K at the minimum to avoid condensation. The latter method is used during the kinetic experiments. In blank runs without catalyst at elevated temperatures the composition of the feed was equal to the composition of the off gas confirming the inertness of the system without catalyst.
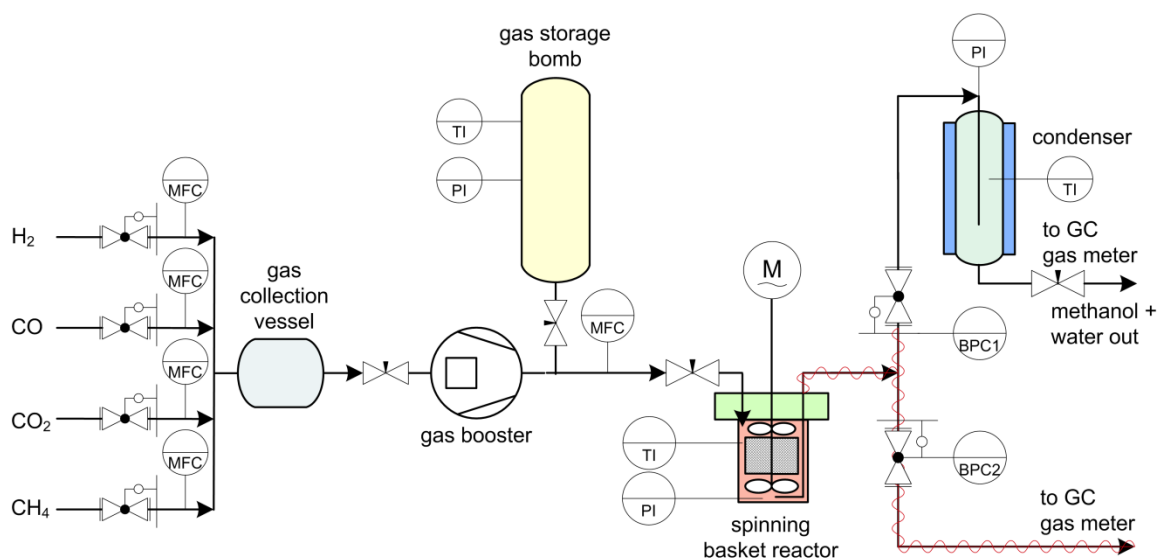

Fig. C.3 Schematic representation of the spinning basket setup including the gas mixing station.

C.3.2 Analyses

The gas mixture was analyzed using a Compact GC (Interscience) with thermal conductivity detectors. Helium was used as carrier gas. H_2, CH_4, and CO were analyzed on a molecular sieves 5 Å column (L = 5 m), while CO_2, H_2O, and CH_3OH, were analyze on a Porabond Q column (L = 10 m). The GC was calibrated for H_2O and CH_3OH by saturating a N_2 stream with these components. This was done by flowing a N_2 feed through wash bottles filled with H_2O or CH_3OH.

C.3.3 Measurements

For a typical measurement approximately 0.1 − 0.3 g of catalyst was used. The catalyst was activated according to the following program (2 h at 443 K, 2 h at 473 K, 2 h at 493 K, 3 Nm^3/kg cat./h, 0.2 MPa). Every day a fresh batch of catalyst was used. The maximum operating time of one batch of catalyst was 12 h.

Element balances (C, H, and O) were calculated for all experiments. The maximum deviation for any element was 3%. The temperature was measured in the spinning basket as close as possible to the basket. Temperature fluctuations during operation were below 0.6 K. The gas composition was measured online every 90 s. When 15 consecutive stable measurements were conducted an experiment was considered to be at steady state.

C.3.4 Measurements of the production rates

The experiments were conducted at steady state conditions and the spinning basket reactor is assumed to behave as a perfectly mixed CISTR. The reaction rates for methanol and water were calculated from material balances over the reactor.

$$R'_{CH_3OH} = y_{CH_3OH} \frac{\phi_{v,off}}{w} \frac{P}{RT} \qquad \text{(mol/kg cat./s)} \qquad \text{(Eq. C.9)}$$

$$R'_{H_2O} = y_{H_2O} \frac{\phi_{v,off}}{w} \frac{P}{RT} \qquad \text{(mol/kg cat./s)} \qquad \text{(Eq. C.10)}$$

where R'_i is the production rate of methanol or water, y_i the methanol or water mole fraction, $\phi_{v,off}$ the volumetric flow rate of the exit gas, w the weight of catalyst, R the universal gas constant, P the pressure of the exit gas flow, and T the temperature of the exit gas flow. The production rates in mol/kg cat./s can easily be converted to g/g cat./h which is a more common unit and used in the results section.

C.4 Results and discussion

C.4.1 General results

Before the kinetic experiments were conducted the presence or absence of external mass and heat transfer limitations, and the influence of catalyst deactivation were experimentally

checked. These checks were conducted at 498 – 523 K, which is higher than for the actual experiments (483 K). If no limitations are observed at these conditions, it is justified to assume that they can also be ignored for the experiments at lower temperatures.

External mass transfer limitations can be neglected because no changes in methanol synthesis rates were observed by varying the rotating speed of the stirrer above values of 800 rpm (syngas 1 at 523 K for all flow rates). At these conditions the highest production rates for methanol were observed. The presence of internal mass transfer limitations was checked by varying the particle size of the catalyst. Besides a pellet (D = 5 mm), three sieve fractions of crushed catalysts were used: 0.25 – 0.43 mm, 0.8 – 1.0 mm, and 2.5 – 2.8 mm.

In each of these experiments 0.2 g of catalyst was used. The experiments were conducted at 523 K for syngas 1 and an exit flow rate of 130 NL/g cat./h. The production rate of methanol was > 13 g/g cat./h, while the highest production rate at 483 K was 7.7 g/g cat./h. The results are shown in Fig. C.4. With decreasing particle size the methanol concentration in the outlet goes up, but remains more or less equal for the three smaller particle sizes (the value of the illustrative straight line). It is assumed that internal mass transfer limitations for these particle sizes are absent and the smallest particle size (0.25 – 0.43 mm) was selected for the kinetic study.
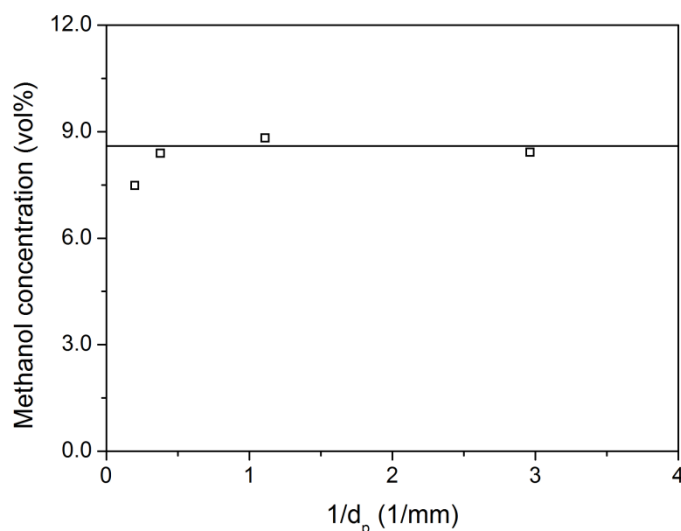

Fig. C.4 Methanol concentration in the outlet as a function of the particle size. P = 20 MPa, T = 523 K, $\phi_{v,off}$ = ± 130 NL/g cat./h, syngas 1: $H_2/CO/CO_2$ = 68.8/27.9/3.3 vol%. Symbols: experimental data point, line: horizontal line for illustrative purposes.

In the literature, initial deactivation of methanol synthesis catalysts in the first 0 – 100 h of operation is reported [21]. In packed bed experiments, the (initial) deactivation as a function of the operating time was confirmed (see Appendix D). To check whether catalyst deactivation took place during the kinetic experiments in the spinning basket, an experiment of 12 h (the maximum operating time of 1 batch of catalyst) was conducted for syngas 1 at 498 K, 19.7 MPa,

and an exit flow rate 130 NL/g cat./h after reduction of the catalyst. The methanol concentration in the outlet is given in Fig. C.5.
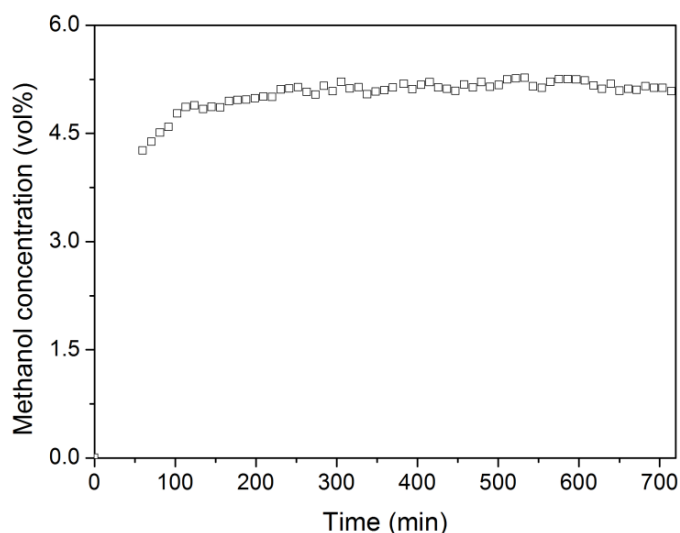

Fig. C.5 Methanol concentration in the outlet as a function of the time on stream. P = 20 MPa, T = 498 K, $\phi_{v,off}$ = 130 NL/g cat./h, syngas: $H_2/CO/CO_2$ = 68.3/27.6/4.1 vol%. Symbols: experimental data point.

At t = 0 the system was at 498 K and feeding started. The pressure was slowly increased to 20.0 MPa. After 180 min the methanol concentration in the exit became stable and remained stable for the remainder of the operating time, indicating that catalyst deactivation for a 12 h run time is negligible.

A total of 70 experiments were conducted. All results are tabulated in Section C.8 at the end of this appendix. In Fig. C.6, some typical results are shown for syngas 5. Here, the production rate of methanol and water are plotted as a function of the pressure. In the pressure range 17.5 – 22.5 MPa the influence of the pressure on the production rates seems marginal and for some data points, the pressure even has a negative influence on the production rates which could point to strong adsorption of one of the components. Similar trends were observed for the other syngas mixtures.
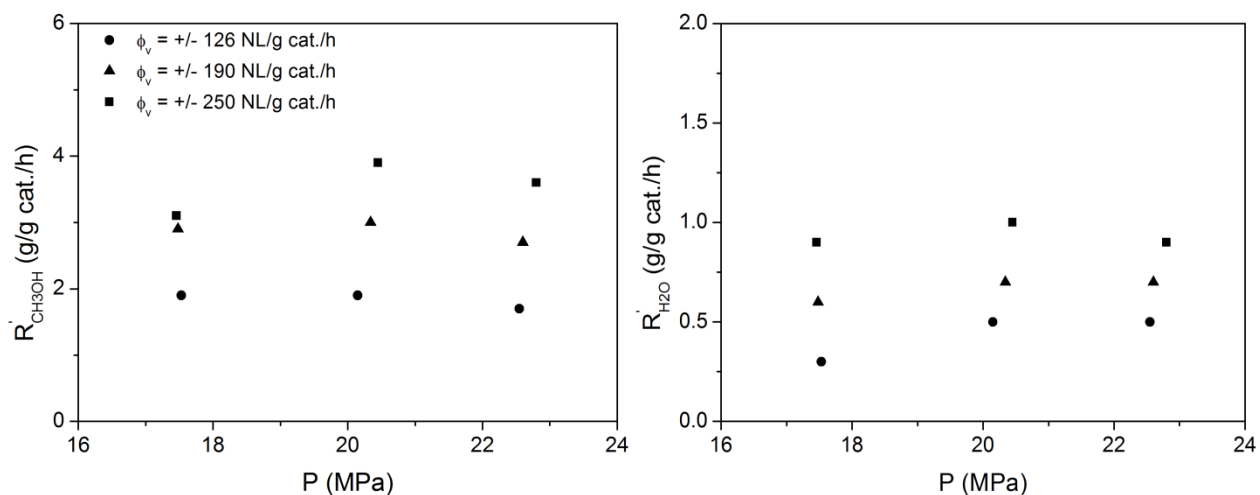
Fig. C.6 Production rates for methanol and water. T = 483 K, syngas 5: $H_2/CO/CO_2$ = 89.3/5.3/5.4 vol%. Symbols: experimental data point.

C.4.2 Parameter estimation

The experimental data was used as input for the kinetic model. The fitting procedure was conducted as described in Section C.2.2. Initial guess values for the parameters were based on the model developed by Graaf *et al.* [7]. Other initial guess values were also tested to check the convergence of the model and the presence of local minima. The convergence of the 'lsqcurvefit' appeared to be satisfactory as guess values for all parameters of 1 resulted in similar values of the sum of the residuals. After the first parameter estimation all experiments with errors below 40% in methanol production rate were retained. Finally, 60 measurements were used in the parameter estimation.

In the parameter estimation it was found that the K_{H2O} could be excluded from the model. In the fit, the reaction rate for the WGS reaction was very small and was omitted. In the kinetic model derived by Graaf *et al.* with a similar catalyst, the reaction rate of the WGS reaction was also very small compared to the CO and CO_2 hydrogenation reaction rates. The final model contained 7 fit parameters and their values are given in Table C.3. The model contains an adsorption term for methanol. The kinetic model derived by Natta for high pressure methanol synthesis kinetics, also contains a methanol adsorption term with a large contribution [17].

The residuals $\left(\hat{R}'_{CH_3OH} - R'_{CH_3OH} \right)$ and $\left(\hat{R}'_{H_2O} - R'_{H_2O} \right)$ were checked and no trending effects were observed. The residuals were normally distributed as a function of all parameters.

Finally, a kinetic model was applied without the adsorption term in the denominator. However, this model was not used as trending effects were observed in the residuals distribution as a function of the $\phi_{v,off}$.

**Table C.3** Values for the fitted parameters of the kinetic model.

Parameter	Value
k_1	$4.26 \cdot 10^{-3}$
k_3	$8.77 \cdot 10^{-6}$
$n_{CO,1}$	1.02
$n_{H2,1}$	1.59
$n_{CO2,3}$	0.67
$n_{H2,3}$	1.40
K_{CH3OH}	1.14

By filling up the parameters given in Table C.3 in the kinetic equations the following set of equations is obtained.

$$r'_{CH_3OH,1} = \frac{4.3 \cdot 10^{-3}}{f_{CO}^{1.0} f_{H_2}^{1.6}} \frac{\left(f_{CO} f_{H_2}^2 - \dfrac{f_{CH_3OH}}{K_{P_1^o}} \right)}{\left(1 + 1.1 f_{CH_3OH} \right)}$$ (Eq. C.11)

$$r'_{CH_3OH,3} = r'_{H_2O,3} = \frac{8.8 \cdot 10^{-6}}{f_{CO_2}^{0.7} f_{H_2}^{1.4}} \frac{\left(f_{CO_2} f_{H_2}^3 - \dfrac{f_{CH_3OH} f_{H_2O}}{K_{P_3^o}} \right)}{\left(1 + 1.1 f_{CH_3OH} \right)}$$ (Eq. C.12)

A parity plot of the calculated methanol production rates vs. the predicted production rates according to Eqs. C.11 and C.12 is given in Fig. C.7.
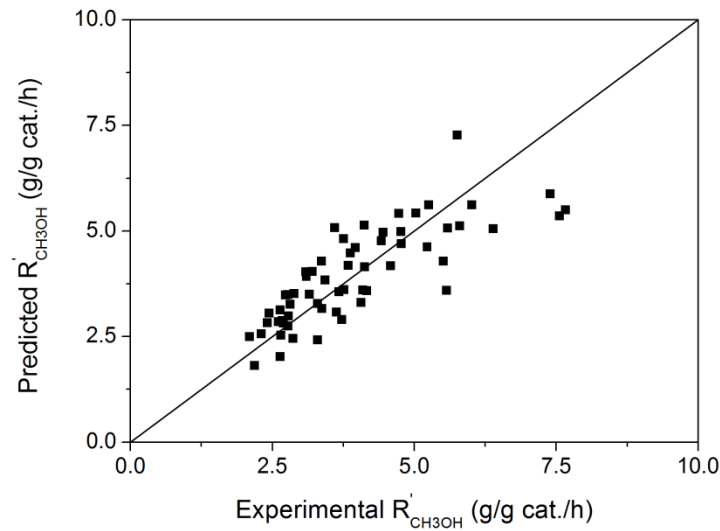
Fig. C.7 Predicted vs. the experimental production rates for methanol in the kinetic experiments.

The average relative error in the model is 15% for the prediction of the methanol synthesis rate. The relative error in the water concentration is larger (44%). Large errors in water concentration are common in modelling kinetics for methanol synthesis. This may be caused by difficulties in the analysis of water and possibly condensation of water after the reactor or in the GC. Graaf *et al.* reported the errors for the production rate of methanol and water for their model and compared these with kinetic models from the literature, see Table C.4 for details. Apparently all models predict the methanol production rate rather good although different catalysts were used.

Table C.4 Errors for methanol and water production rates for various kinetic models. All experimental data, except for the data from this study, were modeled with the model from Graaf *et al.* [7].

Kinetic model from	$\Delta R'_{CH_3OH}$ (%)	$\Delta R'_{H_2O}$ (%)
Seyfert and Luft [14]	10.8	100
Villa *et al.* [13]	12.3	100
Klier *et al.* [8]	10.0	57
Dybkjaer [6]	14.7	167
Graaf *et al.* [7]	6.4	24
This study	15.4	44

The prediction of the production rates of methanol is in general satisfactorily, while the water prediction rates are less accurately predicted. A comparison of experimental and modeled production rates for some selected experiments with syngas 3 is shown in Fig. C.8. A good fit for methanol is observed, whereas the fit for water is less satisfactorily.
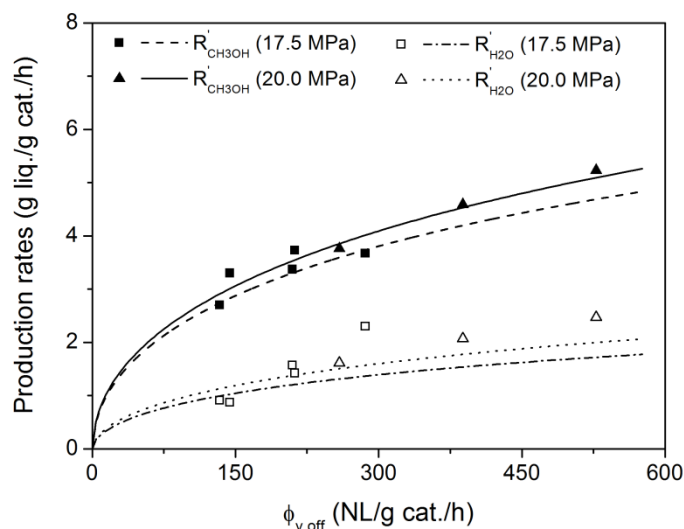

Fig. C.8 Production rates for methanol and water for syngas 3 ($H_2/CO/CO_2$ = 74.1/19.2/6.7 vol%) at different pressures. The symbols represent the experimental data points. The curves are the calculated values.

The experimental methanol production rates measured in this study are high compared to the production rates from the kinetic model developed by Graaf *et al*. [7], see Fig. C.9 for details. The reaction rates from the kinetic model from Graaf *et al*. need to be multiplied with a factor 3 – 10, depending on the gas composition and process conditions, to obtain comparable reaction rates. This may be due to differences in catalyst composition and process conditions. Three measurements were conducted with the catalyst used in this study at a pressure of 2.5 MPa, which was a typical pressure in the study by Graaf *et al*. The results are given in Fig. C.9. The catalyst used in our study is far more active than the earlier version used by Graaf *et al.* in the 1980s. However, when comparing the lower pressure experimental data (2.5 MPa) and the modeled data at the high pressure (20 MPa), it is clear that the methanol production rates within the pressure range of this work are a factor of 2 higher than for 2.5 MPa. Thus, high pressure methanol synthesis is not only advantageous from a thermodynamic point of view but also has clear kinetic advantages.
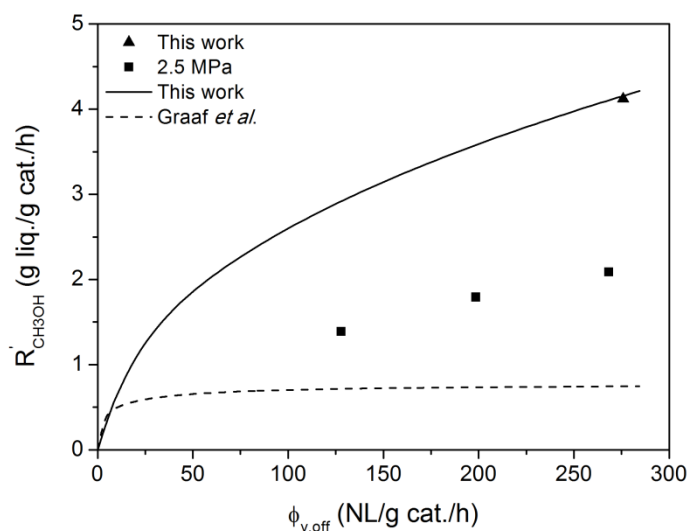

Fig. C.9 Comparison in production rates between the kinetic model proposed here and the model from Graaf *et al*. P = 20.0 MPa, T = 483 K. Catalyst sieve fraction 0.8 – 1.0 mm.

C.5 Discussion

The average error in the methanol and water production rate of respectively 15 and 44% is larger than for the low pressure models (Table C.4). Possibly these errors can be attributed to the selection of the kinetic model and experimental error, but other phenomena might play a role. Some additional experiments were conducted at higher temperatures (498 K and 513 K). Strange phenomena were observed, as depicted in Fig. C.10, where the methanol concentration in the gas is presented versus the gas flow. For the lower temperatures an expected decrease in the methanol concentration is measured, that can be correlated to the reciprocal of the gas flow indicating a rather constant methanol production rate. However, for the higher

temperature the concentration in the outlet increases significantly with temperature. The observations from Fig. C.10 cannot be explained at the moment emphasizing the complexity of the system.
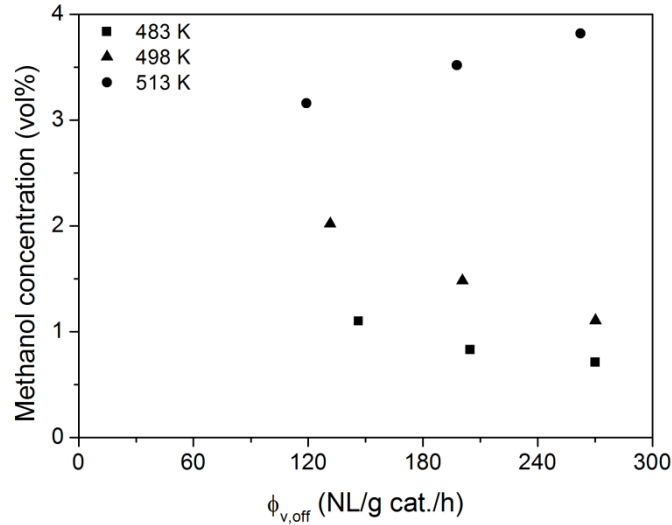

Fig. C.10 Methanol concentration as a function of the exit flow for syngas 1. $H_2/CO/CO_2$ = 68.8/27.9/3.3 vol%. Catalyst sieve fraction $0.25 - 0.43$ mm.

Although mass transfer limitations were not found in experimental tests, a theoretical estimation was carried out. This appeared to be rather difficult as diffusion coefficients of gas mixtures at high pressure are not known and difficult to estimate. Due to the lack of reliable data, only few estimation methods exist to correlate high and low pressure diffusion coefficients [22]. Nevertheless, we made an attempt to conclude whether mass transfer could theoretically play a role in these experiments. The intraparticle profiles were calculated by modeling a packed bed reactor on macroscopic scale as well as the scale of the catalyst. Kinetics, heat transfer, mass transfer, and diffusion coefficients were taken into account. Conditions were selected close to the experimental conditions applied in this study. Diffusion coefficients were estimated using the Fuller equation from ref. [22] corrected by the high pressure correction from Riazi and Whitson also given in ref. [22] and given below:

$$\frac{\rho D_{AB}}{\left(\rho D_{AB}\right)^0} = 1.07\left(\frac{\mu}{\mu^0}\right)^{-0.27-0.28\varpi-\frac{P}{P_c}\left(-0.05-0.1\varpi\right)} \qquad \text{(Eq. C.13)}$$

With ρ the density, D_{AB} the diffusion coefficient, μ the viscosity, ω the accentric factor, P the pressure, and P_c the critical pressure. Two extreme situations were considered, viz. using diffusion coefficients a factor 5 lower and diffusion coefficients a factor 5 higher than those calculated. The intraparticle concentration profiles are shown in Fig C.11.
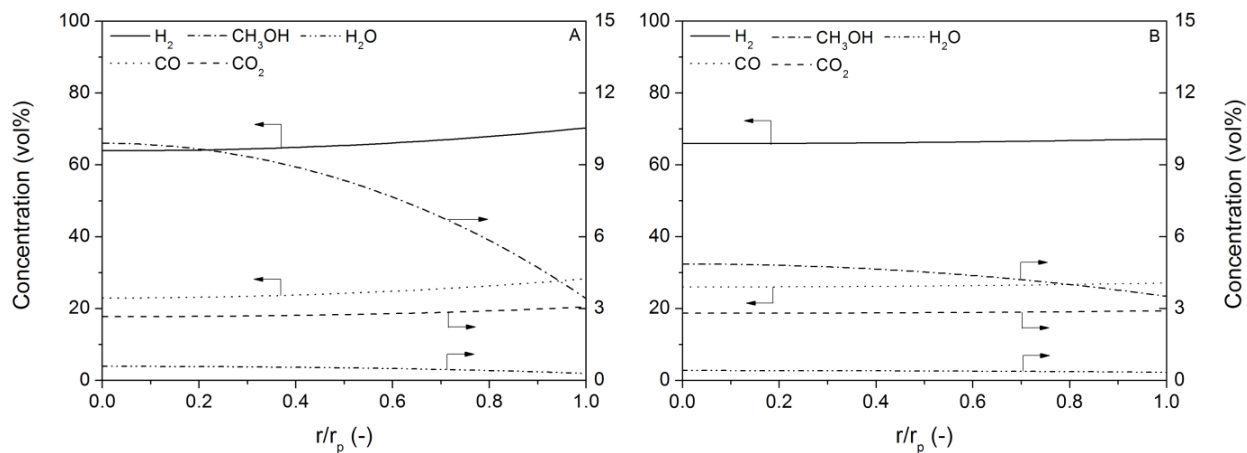
Fig. C.11 Intraparticle concentration profiles as a function of the normalized radius for two diffusion coefficients, 1/5 (A) and 5 (B) times the diffusion coefficient by the Fuller equation (corrected by the Riazi-Whitson relation) [22]. Syngas 1, $H_2/CO/CO_2 = 68.8/27.9/3.3$ vol%, $d_p = 0.4$ mm, $T = 483$ K.

Taking the lowest diffusion coefficients (Fig C.11A), a strong concentration gradient for methanol is calculated, while the concentration gradient almost disappears when the higher diffusion coefficients are taken (Fig. C.11B). The overall effectiveness factor is defined by:

$$\eta_{overall,i} = \frac{3}{r_p} \frac{k_{g,i}\left(C_{i,r_p} - C_{i,g}\right)}{R_{i(C_{i,g},T_g)}} \qquad \text{(Eq. C.14)}$$

With η, the effectiveness factor, $k_{g,i}$ the mass transfer coefficient, C the concentration at the particle surface (C_{i,r_p}) and the bulk ($C_{i,g}$), and $R_{i(C_{i,g},T_g)}$ the production rate based on the gas bulk. The effectiveness factors for the various gaseous components are tabulated in Table C.5. The effectiveness factors and concentration profiles indicate that intraparticle limitations may be present. Their actual presence depends on the 'real' diffusion coefficient.

Table C.5 Overall effectiveness factors for the different components for three situations.

Component	Effectiveness (1/5 * D_{AB})	Effectiveness (D_{AB} as calculated)	Effectiveness (5 * D_{AB})
CO	0.92	0.98	1.00
CO_2	0.71	0.91	0.98
CH_3OH	0.90	0.97	0.99
H_2	0.89	0.97	0.99
H_2O	0.71	0.91	0.98

In addition condensation of methanol and/or water inside the catalyst particle (at perhaps high local concentrations) cannot be fully neglected.

In conclusion, the kinetics derived in this appendix are a good starting point in exploring reaction rates in high pressure methanol synthesis. However, more experimental work is required to fully understand all the phenomena taking place and to be able to derive a more accurate and extended kinetic model for high pressure methanol synthesis.

C.6 Conclusion

The reaction rates for high pressure methanol synthesis from CO, CO_2, and H_2 were studied in a continuous spinning basket reactor. The experiments were conducted at pressures between 17.5 and 22.5 MPa and a temperature of 483 K. The data were modeled using a power law model with an adsorption term for methanol. The fit for the methanol production rates is relatively good, but the deviations for water are larger. An extension of the model to higher temperatures will be very useful and will be the subject of further studies. These kinetic equations are the first for high pressure methanol synthesis over Cu based catalysts from syngases containing CO, CO_2, and H_2 and a good starting point, but more understanding of the system is required to measure and derive more accurate rate equations.

High pressure methanol synthesis has become promising again as the production rates for methanol and water measured in this study are higher than expected based on low-pressure kinetic models extrapolated to high pressures. When a reactor design is made for high pressure methanol synthesis the reactor volumes can be reduced significantly if heat removal is appropriate.

C.7 Nomenclature

C	Concentration (mol/m^3)
D_{AB}	Diffusion coefficient (m^2/s)
f	Partial fugacity (Pa)
F_{obj}	Objective function
k	Reaction rate constant
k_g	Mass transfer constant (m/s)
K	Chemical equilibrium constant
l	Experiment index
m	Number of parameters to be estimated
N	Number of measurements
P	Pressure (Pa)
r	Radius (m)
r	Reaction
r'	Reaction rate (mol/kg cat./s)
R	Universal gas constant (J/mol/K)
R_i'	Production rate (mol/kg cat./s) or (g/g cat./h)
R_i	Production rate (mol/m^3 cat./s)
s^2	Variance
T	Temperature (K)
SSR	Sum of squared residuals
w	Weight catalyst (g or kg)
WF	Weight factor
y_i	Mole fraction

Greek symbols

Δ	Relative error
ΔH_r	Reaction enthalpy at standard conditions (kJ/mol)
η	Effectiveness factor
ϕ	Gas flow (NL/h or NL/g cat./h or m^3/s)
μ	Viscosity (Pa·s)
ρ	Density (kg/m^3)
Σ	Sum

Superscripts

^	Indicates calculated value
0	Indicates standard pressure (0.1 MPa)
n	Fit parameter

Subscripts

c	Critical
i	Component indicator (CO, CO$_2$, CH$_3$OH, H$_2$, H$_2$O)
in	Indicates gas flow in
j	Indicates reaction j (1,2,3)
g	Gas bulk
off	Indicates exit gas flow
p	Particle
P	Indicates based on partial pressures
v	Indicates volumetric

Abbreviations

$cat.$	Catalyst
$liq.$	Liquid

C.8 Kinetic data

Table C.6 Experimental data used for the derivation of the kinetic model.

Syngas - exp.	Conditions		Exit							
	P	T	$\phi_{v,off}$	H_2	CO	CO_2	CH_3OH	H_2O	R'_{CH_3OH}	R'_{H_2O}
	(MPa)	(K)	(NL/g cat./h)	(vol%)	(vol%)	(vol%)	(vol%)	(vol%)	(g/g cat./h)	(g/g cat./h)
1 - 1	17.2	483.6	116.7	66.48	26.48	4.24	1.58	0.72	2.64	0.67
1 - 2	17.1	483.5	172.8	66.96	27.10	3.75	1.16	0.80	2.87	1.12
1 - 3	17.5	483.5	229.3	67.58	27.45	3.32	0.85	0.65	2.78	1.20
1 - 4	19.9	483.8	146.3	67.53	28.22	2.15	1.10	0.52	2.30	0.61
1 - 5	19.9	483.6	204.7	64.70	31.18	2.57	0.83	0.47	2.44	0.77
1 - 6	20.0	483.7	270.2	67.12	29.04	2.50	0.71	0.47	2.73	1.02
1 - 7	22.6	483.7	141.2	67.26	27.72	2.80	1.20	0.61	2.42	0.70
1 - 8	22.6	483.7	214.7	67.43	27.69	3.18	0.92	0.58	2.78	0.97
1 - 9	22.6	483.7	288.9	67.71	27.75	3.11	0.76	0.53	3.10	1.20
2 - 1	17.8	483.6	93.7	61.80	22.58	13.28	1.57	0.53	2.10	0.40
2 - 2	17.9	483.6	141.1	61.48	23.18	13.35	1.29	0.56	2.61	0.64
2 - 3	17.7	483.6	189.2	61.88	23.30	13.08	1.04	0.62	2.81	0.94
2 - 4	20.2	483.7	120.3	61.68	22.32	13.59	1.61	0.46	2.78	0.44
2 - 5	20.0	483.7	183.5	61.96	21.98	13.88	1.39	0.61	3.63	0.91
2 - 6	20.1	483.7	268.5	61.68	23.18	13.24	1.09	0.71	4.16	1.53
2 - 7	22.8	483.7	253.4	62.42	22.99	12.99	0.94	0.26	3.39	0.53
2 - 8	22.7	483.7	376.9	62.23	22.98	13.35	0.89	0.29	4.77	0.89
2 - 9	22.8	483.7	495.6	62.36	23.06	13.29	0.79	0.32	5.59	1.26
3 - 1	17.3	483.6	144.2	73.00	17.79	6.54	1.60	0.75	3.30	0.87
3 - 2	17.4	483.6	212.2	72.83	18.63	6.35	1.23	0.84	3.73	1.42
3 - 3	17.6	483.7	133.5	71.98	16.93	8.42	1.41	0.85	2.70	0.91
3 - 4	17.6	483.6	209.8	72.16	18.52	6.94	1.12	0.93	3.37	1.57
3 - 5	17.7	483.7	286.1	72.69	19.21	6.05	0.90	1.00	3.67	2.30
3 - 6	19.9	484.0	258.9	72.83	19.47	5.61	1.02	0.77	3.76	1.61
3 - 7	20.0	483.9	388.4	72.91	19.44	5.92	0.83	0.66	4.59	2.07
3 - 8	20.0	484.0	527.9	73.30	19.56	5.73	0.69	0.58	5.23	2.47
3 - 9	22.5	483.9	275.0	72.56	19.56	5.85	0.98	0.79	3.84	1.75
3 - 10	22.5	483.8	408.1	72.96	19.48	5.95	0.76	0.67	4.45	2.18
3 - 11	22.5	483.8	537.1	73.35	19.54	5.76	0.66	0.57	5.03	2.48
4 - 1	17.6	483.5	90.4	78.75	10.32	8.96	1.41	0.45	1.82	0.33
4 - 2	17.7	483.6	181.6	78.76	10.45	9.03	1.22	0.49	3.16	0.72
4 - 3	17.6	483.5	247.3	78.83	10.48	8.95	1.16	0.54	4.10	1.06
4 - 4	20.3	483.6	189.7	77.29	11.42	9.60	1.18	0.47	3.21	0.72
4 - 5	20.4	483.6	251.6	78.18	10.86	9.30	1.15	0.48	4.13	0.98
4 - 6	20.3	483.5	213.9	78.35	10.50	9.35	1.10	0.54	3.37	0.92
4 - 7	20.5	483.5	323.9	78.48	10.48	9.45	0.96	0.56	4.42	1.45
4 - 8	20.5	483.6	471.2	78.67	10.45	9.37	0.86	0.59	5.80	2.22
4 - 9	22.5	483.6	121.9	78.78	10.68	9.01	1.09	0.42	1.89	0.41

Continuation of Table C.6.

Syngas - exp.	Conditions		Exit							
	P	T	$\phi_{v,off}$	H_2	CO	CO_2	CH_3OH	H_2O	R'_{CH_3OH}	R'_{H_2O}
	(MPa)	(K)	(NL/g cat./h)	(vol%)	(vol%)	(vol%)	(vol%)	(vol%)	(g/g cat./h)	(g/g cat./h)
4 - 10	22.4	483.6	183.5	78.78	10.58	9.07	1.13	0.42	2.96	0.61
4 - 11	22.4	483.6	244.3	78.89	10.53	8.98	1.14	0.45	3.96	0.87
5 - 1	17.5	483.4	114.3	87.44	5.19	5.25	1.18	0.31	1.93	0.28
5 - 2	17.5	483.4	172.8	87.64	5.20	5.20	1.17	0.40	2.89	0.56
5 - 3	17.5	483.4	232.8	88.41	5.23	4.80	0.93	0.46	3.09	0.86
5 - 4	20.2	483.8	130.6	88.10	5.23	4.77	1.02	0.47	1.90	0.49
5 - 5	20.3	483.7	202.1	87.91	5.21	5.10	1.03	0.45	2.98	0.73
5 - 6	20.5	483.7	272.3	88.12	5.21	4.98	1.00	0.47	3.88	1.02
5 - 7	22.6	483.8	132.8	88.47	5.23	4.74	0.92	0.47	1.74	0.50
5 - 8	22.6	483.8	195.3	88.64	5.27	4.58	0.96	0.45	2.69	0.71
5 - 9	22.8	483.8	264.6	88.49	5.22	4.68	0.95	0.45	3.60	0.95
6 - 1	17.8	483.6	77.3	83.42	12.15	1.67	1.98	0.66	2.19	0.41
6 - 2	17.8	483.6	144.5	83.24	12.77	1.83	1.28	0.82	2.65	0.95
6 - 3	17.8	483.6	195.1	83.58	12.88	1.88	0.95	0.68	2.64	1.06
6 - 4	20.0	483.8	144.3	83.07	12.44	2.35	1.30	0.74	2.68	0.86
6 - 5	19.9	483.7	220.8	83.10	12.76	2.18	1.04	0.86	3.30	1.52
6 - 6	20.0	483.7	296.8	83.41	12.94	2.01	0.81	0.79	3.43	1.89
6 - 7	22.2	483.7	262.0	83.25	13.27	1.69	1.08	0.68	4.06	1.42
6 - 8	22.0	483.7	399.7	83.26	13.22	1.83	0.97	0.70	5.57	2.23
6 - 9	21.9	483.7	527.7	83.68	13.29	1.71	0.73	0.57	5.52	2.41
7 - 1	17.3	483.6	137.1	84.81	1.32	11.67	1.15	0.94	2.26	1.04
7 - 2	17.9	483.5	201.8	84.08	1.34	12.53	0.97	1.05	2.80	1.69
7 - 3	17.9	483.5	270.3	84.66	1.26	12.04	0.97	1.05	3.76	2.27
7 - 4	20.0	483.6	310.2	86.12	1.24	10.65	1.07	0.89	4.77	2.22
7 - 5	20.0	483.6	417.4	85.00	1.24	11.80	1.07	0.88	6.39	2.96
7 - 6	20.0	483.6	537.8	85.04	1.19	11.86	0.98	0.91	7.56	3.95
7 - 7	22.3	483.6	288.7	84.60	1.27	12.12	1.15	0.76	4.73	1.76
7 - 8	22.2	483.6	390.1	84.88	1.23	11.95	1.08	0.81	6.01	2.53
7 - 9	22.2	483.6	510.0	84.88	1.20	11.99	1.01	0.88	7.40	3.62
8 - 1	19.9	486.5	275.9	87.13	0.18	10.84	1.05	0.80	4.12	1.78
8 - 2	20.0	486.4	401.9	87.61	0.15	10.52	0.91	0.81	5.26	2.62
8 - 3	19.9	486.5	571.1	87.80	0.19	10.26	0.94	0.81	7.67	3.73

C.9 References

1   A. Mittasch, K. Winkler, M. Pier, Verfahren zur Gewinnung organischer Verbindungen durch katalytische Gasreaktionen, German patent 441433, (1923).

2   E. Supp, How to produce methanol from coal, Springer-Verlag, Berlin, (1990).

3   J.G. van Bennekom, J. Vos, R.H. Venderbosch, M.A.P. Torres, V.A. Kirilov, H.J. Heeres, Z. Knez, M. Bork, J.M.L. Penninger, Supermethanol: Reforming of crude glycerine in supercritical water to produce methanol for re-use in biodiesel plants, in: 17th European Biomass Conference and Exhibition, Hamburg, (2009) 899-902.

4   J. Skrzypek, J. Stoczynski, S. Ledakowicz, Methanol synthesis, Polish Scientific Publishers PWN, Warsaw, (1994).

5   A. Coteron, A.N. Hayhurst, Kinetics of the synthesis of methanol from $CO + H_2$ and $CO + CO_2 + H_2$ over copper-based amorphous catalysts Chem. Eng. Sci., 49 (1993) 209-221.

6   I.B. Dybkjaer, Design of ammonia and methanol synthesis reactions, in: NATO conference on chemical reactor design and technology, Canada, (1985) 795-819.

7   G.H. Graaf, E.J. Stamhuis, A.A.C.M. Beenackers, Kinetics of low-pressure methanol synthesis, Chem. Eng. Sci., 43 (1988) 3185-3195.

8   K. Klier, V. Chatikavanij, R.G. Herman, G.W. Simmons, Catalytic synthesis of methanol from CO/H_2. IV. The effects of carbon dioxide J. Catal., 74 (1982) 343-360.

9   M.A. McNeil, C.J. Shack, R.G. Rinker, Methanol synthesis from hydrogen, carbon monoxide and carbon dioxide over a $CuO/ZnO/Al_2O_3$ catalyst: II. Development of a phenomenological rate expression, Appl. Catal., 50 (1989) 265-285.

10   C.J. Shack, M.A. McNeil, R.G. Rinker, Methanol synthesis from hydrogen, carbon monoxide, and carbon dioxide over a $CuO/ZnO/Al_2O_3$ catalyst: I. Steady-state kinetics experiments, Appl. Catal., 50 (1989) 247-263.

11   J. Skrzypek, M. Lachowska, H. Moroz, Kinetics of methanol synthesis over commercial copper/zinc oxide/alumina catalysts, Chem. Eng. Sci., 46 (1991) 2809-2813.

12   M. Takagawa, M. Ohsugi, Study on reaction rates for methanol synthesis from carbon monoxide, carbon dioxide, and hydrogen J. Catal., 107 (1987) 161-172.

13   P. Villa, P. Forzatti, G. Buzzo-Ferraris, G. Garone, I. Pasquon, Synthesis of alcohols from carbon oxides and hydrogen. 1. Kinetics of the low-pressure methanol synthesis, Ind. Eng. Chem. Process Des. Dev., 24 (1985) 12-19.

14   W. Seyfert, G. Luft, Untersuchungen zur Methanol-synthese in Mitteldruckbereich, Chem. Ing. Techn., 57 (1985) 482-483.

15   U.D. Kuznetsov, F.S. Shub, M.I. Temkin, Kinetics of methanol synthesis and hydrolysis on copper containing catalysts. 1. Experimental data., Kinet. Catal., 25 (1984) 606-613 (in Russian).

16   O.A. Malinovskaya, A.Y. Rozovskii, I.A. Zdotarskii, Y.V. Lender, Y.S. Matros, G.I. Lin, G.V. Dubovich, N.A. Popova, N.V. Savostina, Synthesis of methanol on Cu-based catalyst: Kinetic model, React. Kinet. Catal. Lett., 34 (1987) 87-92.

17   G. Natta, Synthesis of methanol, in: P.H. Emmett (Ed.) Catalysis: Hydrogenation and dehydrogenation, Rheinhold, New York, (1955) 349-411.

18   G.H. Graaf, P.J.J.M. Sijtsema, E.J. Stamhuis, G.E.H. Joosten, Chemical equilibria in methanol synthesis, Chem. Eng. Sci., 41 (1986) 2883-2890.

19   P.M. Mathias, A versatile equilibrium equation of state, Ind. Eng. Chem. Process Des. Dev., 22 (1983) 385-391.

20   G. Soave, Equilibrium constants from a modified Redlich-Kwong equation of state, Chem. Eng. Sci., 27 (1972) 1197-1203.

21   H.H. Kung, Deactivation of methanol synthesis catalysts - A review, Catal. Today, 11 (1992) 443-453.

22   B.E. Poling, J.M. Prausnitz, J.P. O'Connel, The properties of gases and liquids, 5 ed., McGraw-Hill, Singapore, (2007).

Appendix D
Average methanol production rates in a nonisothermal packed bed

Abstract

Methanol synthesis was investigated in a nonisothermal packed bed reactor at different temperatures (473 < T < 573 K), pressures (7 < P < 20 MPa), gas hourly space velocities ($18 \cdot 10^3$ < $GHSV$ < $39 \cdot 10^3$ m^3 syngas/m^3 cat./h), and using gases with different CO/CO$_2$ ratios varying from 0.3 to 5.8. The average methanol production rates increased with increasing pressure, temperature, and decreasing CO/CO$_2$ ratio, provided that the gas composition was far from equilibrium. When equilibrium was achieved the production rate decreased with increasing temperature. Catalyst deactivation appeared to play a major role and complicated the interpretation of the results. The deactivation seemed to level off after 75 h of operating.

D.1 Introduction

High pressure methanol synthesis is attractive from a thermodynamic and kinetic point of view. At high pressure the equilibria are on the methanol side [1]. In methanol synthesis in general, the reaction rates increase with pressure as kinetic equation comprise fugacities of the reacting component, see e.g. ref. [2]. Experimental data on high pressure methanol synthesis are scarce. To the authors knowledge, Natta is the only author who derived kinetic equations for high pressure ($20 < P < 30$ MPa) methanol synthesis for a $Cu/ZnO/Cr_2O_3$ catalyst [3]. Danes *et al.* derived an equilibrium model based on Russian results for methanol synthesis at high pressure ($10 - 35$ MPa, $573 - 623$ K) from stoichiometric gas mixtures of H_2 and CO slightly impurified with CO_2 and H_2O.

Reaction rates for syngas comprising solely H_2 and CO were measured by Brown and Bennet at 20.7 MPa for temperatures between 573 and 673 K [4]. Methanol synthesis was conducted in an internally recycled reactor using a commercial ZnO/Cr_2O_3 catalyst. High pressure data over $Cu/ZnO/Al_2O_3$ based catalysts were, to the authors knowledge, only obtained by Kotowski [5]. The experiments for a system containing H_2, CO, CO_2, and H_2O were conducted at 25 MPa, $493 - 573$ K. The results are rather inconclusive as only CO conversions are given. The present authors investigated high pressure methanol synthesis focusing on equilibrium conversions in the framework of the Supermethanol project [6].

In this appendix a preliminary research study in a nonisothermal packed bed reactor is conducted to compare methanol synthesis rates at different pressures, temperatures, gas hourly space velocities (*GHSV*), and gas composition.

D.2 Experimental

The model gases used were supplied by Westfalen-AG, Germany. The composition of the model gases is given in Table D.1. The relative deviation in the gas components is 2%. A commercial methanol synthesis catalyst (Cs doped $Cu/ZnO/Al_2O_3$) was used. The catalyst was activated according to the following program: 2 h at 443 K, 2 h at 473 K, 2 h at 493 K, 10 vol% H_2 in N_2, 3 Nm^3/kg cat./h, 0.2 MPa.

Table D.1 Gas composition of the different syngases.

Syngas	H_2	CO	CO_2	CH_4	N_2	S_N[a]	CO/CO_2
	(vol%)	(vol%)	(vol%)	(vol%)	(vol%)	(-)	(-)
1	70	5	20	-	5	2.0	0.3
2	69	13	13	5	-	2.2	1.0
3	68	23	4	5	-	2.5	5.8

[a]S_N (stoichiometric number) is defined in Eq. 1.4.

The setup used here is similar to the setup described extensively in Chapter 5 and 6. However, instead of 2 packed bed reactors, only 1 packed bed was used. The reactor was heated by a

heating medium which was flown through a heating jacket surrounding the packed bed. A schematic representation of the reactor (without the heating jacket) is shown in Fig. D.1.

The catalyst bed was preceded by 10 cm of grid to improve the heating up of the syngas. The grid particles are approximately 0.5 mm wide and 1 mm long and composed of mainly Si and Cr. The grid appeared to be inert as no methanol or other products were obtained in blank runs. The catalyst is mixed with grid with a volumetric ratio of 1:1 to increase heat transfer. The length of the catalyst bed was approximately 10 cm. In each experiment 4 g of catalyst was used. A thermowell was positioned in the center of the catalyst bed (see the grayish rod in Fig. D.1). The temperature was measured at 4 locations at 0.5 cm (T_1) before the catalyst bed, and at 3 (T_2), 6 (T_3), and 9.5 cm (T_4) inside the catalyst bed. During the experiment, the temperature increased along the length of the catalyst bed, often reaching a maximum at T_2 or T_3. The temperature increase could be up to 15 K for syngas 1, 50 K for syngas 2, and 80 K for syngas 3. The temperature of the heating medium was chosen as the temperature to compare the methanol production rates, while the temperature of T_4 (see Fig. D.1) was chosen as the temperature for the comparison with equilibrium conversions. The particle size of the catalyst was between 1 and 3 mm. The experiments were performed at: $7 < P < 20$ MPa, $473 < T < 573$ K, $18 \cdot 10^3 < GHSV < 39 \cdot 10^3$ Nm^3 syngas/m^3 cat./h).
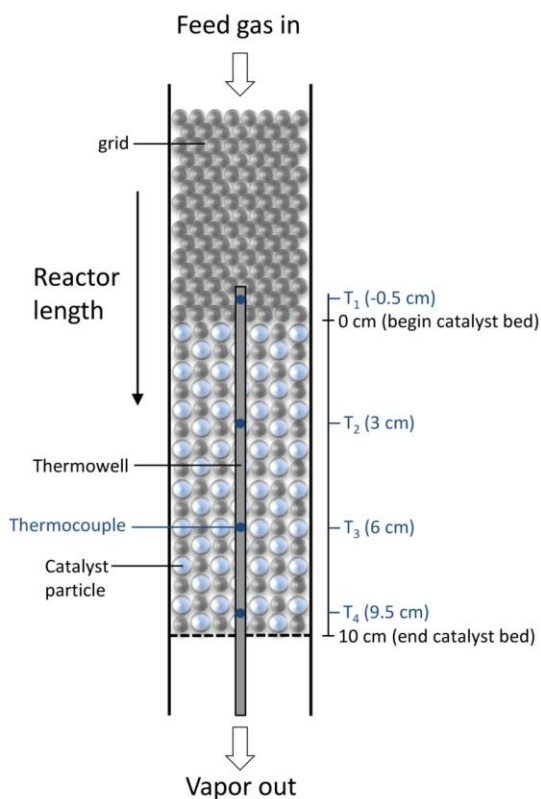
Fig. D.1 Schematic representation of the reactor. The grey rod in the center of the bed is a thermowell.

The dry gas composition was analyzed using an online dual-column GC (GC 955, Syntech Spectras) equipped with thermal conductivity detectors. CO was analyzed over a molecular sieves 5 Å column (L = 1.6 m) with helium as carrier gas. CO_2 was analyzed on a Chromosorb 102 column (L = 1.6 m) with helium as carrier gas. H_2 was analyzed on the molecular sieves column using argon as carrier gas. The water content of the methanol was determined by Karl Fischer-titration.

The measured average production rate (APR_M, g/g cat./h) of methanol is determined with the following equation:

$$APR_M = \frac{\eta_{CH_3OH}}{w \cdot t}$$

(Eq. D.1)

With, η_{CH_3OH} ; the methanol yield in g, w; the weight of catalyst in g, t; time in h. The calculated average production rate (APR_C, g/g cat./h) of methanol is determined with Eq. D.2.

$$APR_C = \frac{\left(\dfrac{\phi_{v,in}\left(y_{CO,in} + y_{CO_2,in}\right)}{V_{m,in}} - \dfrac{\phi_{v,off}\left(y_{CO,off} + y_{CO_2,off}\right)}{V_{m,off}} \right)}{w} \cdot 32.04$$

(Eq. D.2)

With, ϕ_v; the flow rate in m^3/h, y; the mole fraction, V_m; molar volume (m^3/mol) of gas flow in or gas flow off.

D.3 Results and discussion

A total of 72 experiments were conducted. Average methanol production rates were measured directly by collecting the liquid produced and determining the methanol content (Eq. D.1), or calculated indirectly from the CO+CO_2 conversion (Eq. D.2). A comparison of the two methods of determining the average production rate is plotted in Fig. D.2. The APR_C's are structurally higher than the APR_M's due to some evaporation of methanol from the collection vessel and build-up of methanol in dead volumes. The average deviation between the measured and calculated production results is more or less constant implying that the relative error in the experiments decreases at higher production rates.
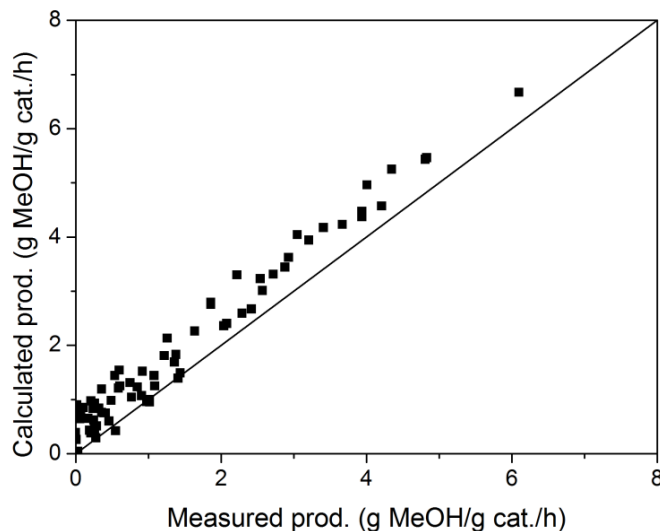
Fig. D.2 Calculated average methanol production rates vs. measured average production rates.

The APR_m's and the ζ_{CO+CO2} as a function of the temperature for syngas 1 are shown in Fig. D.3. Equilibrium conversions were calculated using the model from Chapter 5. The production rates increase with increasing temperature and pressure. Equilibrium is achieved at the highest temperature. The measurements at temperatures around 497 K for 7.5 and 15 MPa deviate from the trend due to deactivation which will be discussed later on.
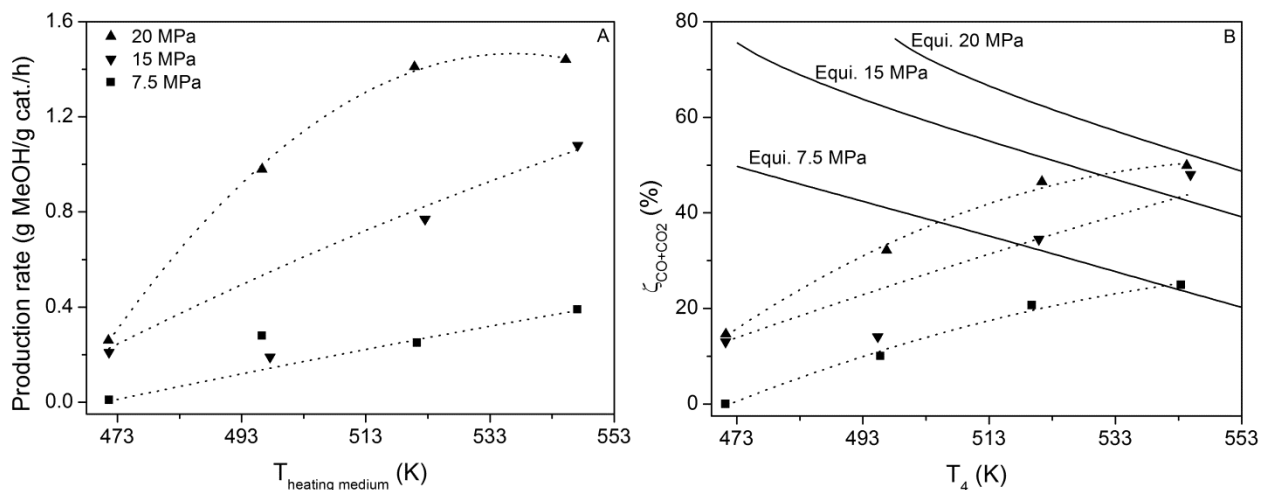
Fig. D.3 Measured average methanol production rates (A) and ζ_{CO+CO2} (B) as a function of the temperature for syngas 1. $GHSV = 19 \cdot 10^3$ Nm^3 syngas/m^3 cat./h. The symbols are experimental data points, the dotted lines are trend lines and for indicative purposes only.

In Fig. D.4 the methanol production rates for syngas 1 are plotted as a function of the pressure. Generally, the production rate increases with increasing pressure. For the highest temperatures there seems to be a linear trend between the production rate and the pressure. The trends at

the lower pressures are less clear. As the kinetics derived by Graaf *et al.* [2] predict more or less linear trends, linear trend lines were drawn.
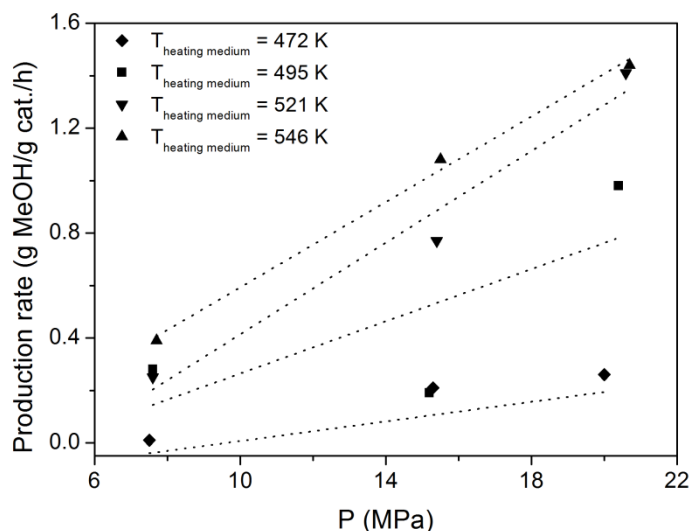
Fig. D.4 Average methanol production rates as a function of the pressure for syngas 1. *GHSV* = $19 \cdot 10^3$ Nm^3 syngas/m^3 cat./h. The symbols are experimental data points, the dotted lines are trend lines and for indicative purposes only.

The production rates as a function of the temperature are compared for two different flows for syngas 2 and shown in Fig. D.5.
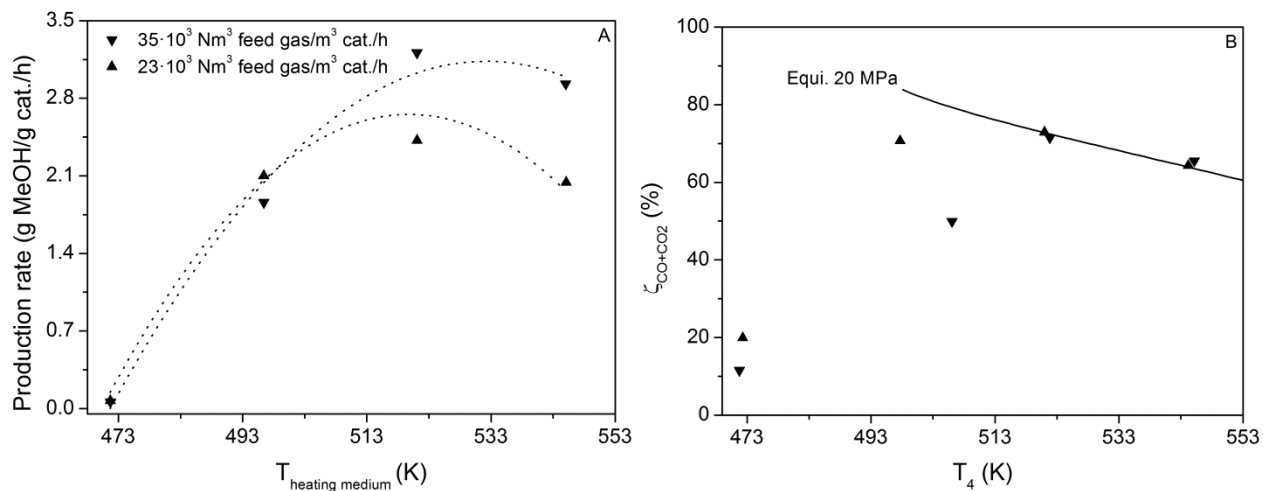
Fig. D.5 Average methanol production rates as a function of the temperature for syngas 2. *P* = 20 MPa. The symbols are experimental data points, the dotted lines are trend lines and for indicative purposes only.

The production rate increases with increasing temperature, till at 523 K equilibrium is reached for both gas flows. A further increase in the temperatures leads to a decrease in the production

rate and conversion. At equilibrium, the exit gas composition is independent of the space velocity, leading to a higher production rate at the highest space velocity. At the lower temperatures the production rates at both space velocities are closer, but as a consequence the conversion in case of the lower space velocity should be lower, which is shown in Fig. D.5B.

The methanol production rates and the conversion for syngas 3 as a function of the pressure are shown in Fig. D.6. The production rate initially increases with temperature, but already at a temperature of the heating medium of 497 K equilibrium is reached. At the lowest temperature the reaction rate increases with increasing pressure as expected. At the higher temperatures, both the conversion and the production rate decrease according to thermodynamics. The equilibrium predictions coincide nicely with the decreasing conversions of the experimental data points. For this gas the trend is different as for gas 1 (see Fig. D.3) as equilibrium is reached at much lower temperatures (497 K vs. 546 K).
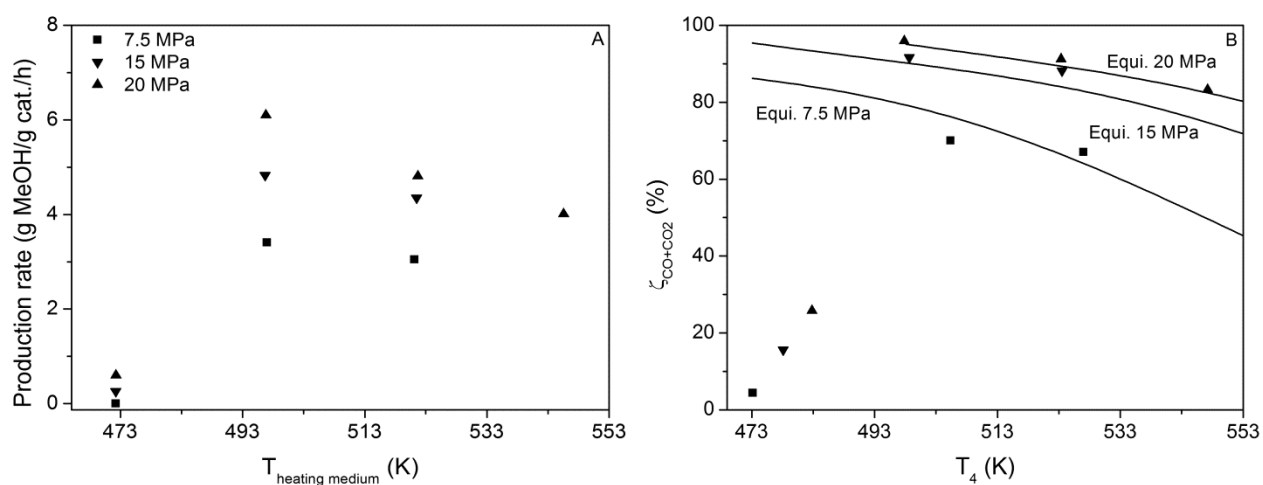
Fig. D.6 Average methanol production rates (A) and ζ_{CO+CO2} (B) as a function of the temperature for syngas 3. *GHSV* = 37·10^3 – 39·10^3 Nm^3 syngas/m^3 cat./h The symbols are experimental data points, the dotted lines are trend lines and for indicative purposes only.

The three syngases under investigation have a similar H_2 and carbon oxides concentration. However, the ratio of CO/CO_2 varies from 0.3 to 5.8. The reaction rate appears to be a strong function of this ratio. The methanol production rates at a temperature of 497 K of the heating medium are given in Fig. D.7 and they increase strongly with an increasing CO/CO_2 ratio. It should be taken into account that in case of the data point for syngas 3 (CO/CO_2 = 5.75), equilibrium is reached in the catalyst bed, but also the highest gas hourly space velocity was used. Probably even higher production rates per gram of catalyst can be obtained when less catalyst would have been used. Nevertheless the trend of the figure is clear.
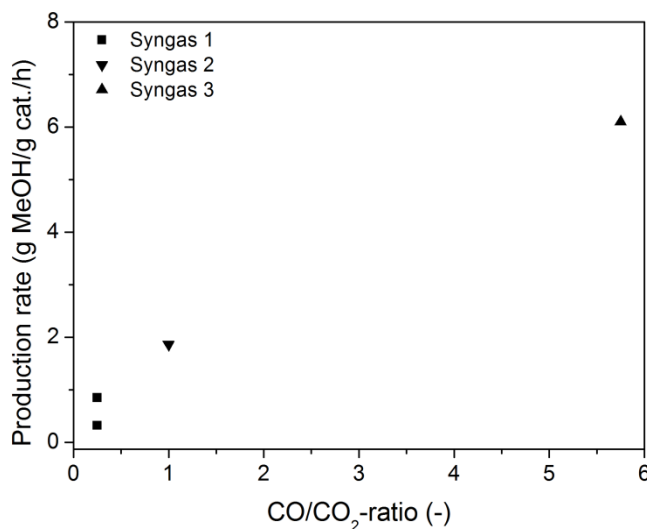
Fig. D.7 Average methanol production rates (A) and ζ_{CO+CO2} conversions (B) as a function of the CO/CO$_2$ ratio. $T_{heating\ medium}$ = 497 K, P = 20 MPa. Syngas 1, $GHSV$ = 28·10^3 Nm^3 syngas/m^3 cat./h; Syngas 2, $GHSV$ = 35·10^3 Nm^3 syngas/m^3 cat./h; Syngas 3, $GHSV$ = 39·10^3 Nm^3 syngas/m^3 cat./h.

For syngas 1 (CO/CO$_2$ = 0.3), two data points are given in Fig. D.7. The data point with the highest production rate was obtained after 13 h of operation, while the other data point was obtained after 75 h of operation. Deactivation was observed for all gas mixtures and was quantified for syngas 1 by repeating a reference experiment (P = 20 MPa, $T_{heating\ medium}$ = 497 K) five times. The production rate of methanol as a function of the operating time decreases significantly and levels off at longer operating times as can be seen in Fig. D.8.
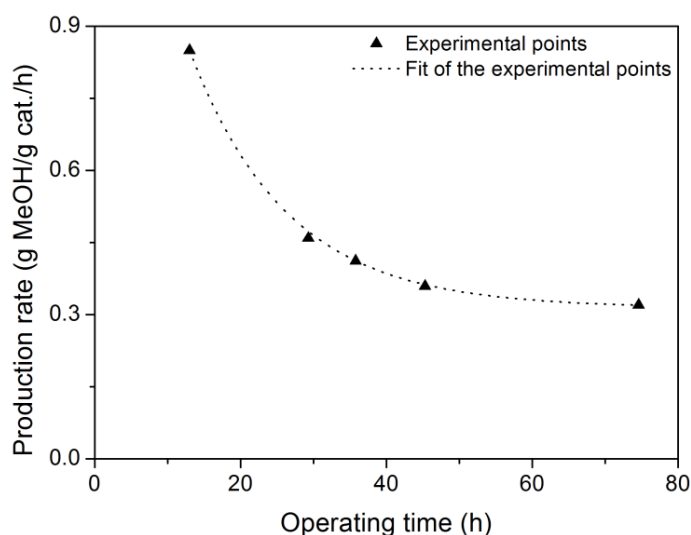
Fig. D.8 Catalyst deactivation for syngas 1. Operating conditions: $T_{heating\ medium}$ = 497 K, P = 20 MPa, $GHSV$ = 28·10^3 Nm^3 syngas/m^3 cat./h.

The methanol production rate after 13 h of operating is almost a factor 3 higher than at 75 h. In the kinetic study (Appendix C) no deactivation for this catalyst was observed during the first 12 h of operation at 498 K. Initial deactivation is a common phenomenon for these kind of catalysts as Bos *et al*. found stable catalyst activity after 72 h of operation [7]. In Kung's extensive review on deactivation, initial deactivation is attributed to loss in active surface area, but no other detectable changes were reported [8]. In the experiments conducted in this study, the BET surface area was measured (see Table D.2). The catalyst was used for approximately 70 h with syngas 2 and 3. For batch 1 of the spent catalyst the BET surface area was substantial lower than the surface area of the fresh catalyst. The BET surface area of batch 2 hardly declined although deactivation was observed during operation. Due to the limited data on catalyst analysis no conclusion can be drawn on the influence of operating time and syngas composition on the loss in active surface area.

Table D.2 Surface area of fresh and spent catalyst.

Catalyst	Time on stream (h)	Syngas	BET area (m^2/g)
Fresh (unreduced)	-	-	91.3
Spent (batch 1)	± 70	2/3	39.7
Spent (batch 2)	± 30	1	87.9

The liquid product of some of the experiments was analyzed on metal content except for Cs (see Table D.3). The liquid product contained a low concentration of the catalyst materials, which was not visual in the liquid. No Cr was detected (grid material) in the effluent. Cu seems to be the most prone to leaching but is also present in the highest amount. Part of the deactivation of the catalyst can be explained by this leaching. Probably the leaching is enhanced by condensation in the reactor which is expected for some of the experiments.

Table D.3 Metal content of the liquid products.

Sample	Time on stream (h)	Syngas	Cu (mg/L)	Zn (mg/L)	Al (mg/L)
1	± 3	2	53	27	2
2	± 10	3	29	11	2
3	± 20	3	27	5	2
4	± 20	1	14	27	1

Cs content of the liquid product was not analyzed.

The deactivation partly explains the deviations from the trend lines for some data points in Figs. D.3 and D.4. The deactivation complicated the interpretation of the results presented in Figs. D.3 – D.7 and makes a quantitative interpretation precarious, however, qualitative trends can be derived. To prevent the influence of deactivation on the measurements either fresh catalyst

should be used for every experiment or the activity should be stabilized by operating at least 75 h before the actual measurements start [9].

D.4 Conclusion

Average methanol production rates were measured focusing on high pressures in a nonisothermal packed bed reactor. The production rate was a strong function of the pressure, temperature, and gas composition. When operating far from equilibrium, the production rate increased with increasing temperature, pressure, and CO/CO_2 ratio. When equilibrium was achieved the production rate decreased with a further increase in temperature. The data points at equilibrium coincided nicely with the theoretical equilibria. Deactivation, however, appeared to play a major role complicating the interpretation and the quantitative analysis of the results. Deactivation leveled off after 75 h of operation.

D.5 References

1   J.G. van Bennekom, J.G.M. Winkelman, R.H. Venderbosch, S.D.G.B. Nieland, H.J. Heeres, Modeling and experimental studies on phase and chemical equilibria in high-pressure methanol synthesis, Ind. Eng. Chem. Res., 51 (2012) 12233-12243.

2   G.H. Graaf, E.J. Stamhuis, A.A.C.M. Beenackers, Kinetics of low-pressure methanol synthesis, Chem. Eng. Sci., 43 (1988) 3185-3195.

3   G. Natta, Synthesis of methanol, in: P.H. Emmett (Ed.) Catalysis: Hydrogenation and dehydrogenation, Rheinhold, New York, (1955) 349-411.

4   C.E. Brown, C.O. Bennet, Methanol synthesis catalysis in an internally recycled reactor, AIChE J., 16 (1970) 817-823.

5   W. Kotowski, The yield of methanol synthesis from various $CO+CO_2+H_2$ mixtures, Przem. Chem., 44 (1965) 66-71.

6   J.G. van Bennekom, J. Vos, R.H. Venderbosch, M.A.P. Torres, V.A. Kirilov, H.J. Heeres, Z. Knez, M. Bork, J.M.L. Penninger, Supermethanol: Reforming of crude glycerine in supercritical water to produce methanol for re-use in biodiesel plants, in: 17th European Biomass Conference and Exhibition, Hamburg (2009) 899-902.

7   A.N.R. Bos, P.C. Borman, M. Kuczynski, K.R. Westerterp, The kinetics of the methanol synthesis on a copper catalyst: An experimental study, Chem. Eng. Sci., 44 (1989) 2435-2449.

8   H.H. Kung, Deactivation of methanol synthesis catalysts - A review, Catal. Today, 11 (1992) 443-453.

9   M. Kuczynski, W.I. Browne, H.J. Fontein, K.R. Westerterp, Reaction kinetics for synthesis of methanol from CO and H_2 on a copper catalyst, Chem. Eng. Process., 21 (1987) 179-191.

Summary

Biodiesel production has grown exponentially in the first decade of the 21th century. During the production process about 10 kg of glycerol is formed for every 100 kg of biodiesel. As a consequence, the development of alternative product outlets for glycerol is high on the research agenda of companies and research institutes. One of the attractive opportunities is the production of green methanol from glycerol, which can be reused in the biodiesel production process. This option has been actively explored within the European Supermethanol project. The goal of this project is to develop a blueprint for a process to convert glycerol into methanol which can be implemented and integrated in an existing biodiesel plant. In this dissertation, the research activities on methanol production from glycerol within the scope of the Supermethanol project are described.

The envisaged Glycerol-to-Methanol (GtM) process consists of a glycerol reforming step in supercritical water to syngas with subsequent methanol synthesis (**Chapter 1**). In the reforming step in supercritical water, a syngas at high pressure (> 20 MPa) is obtained. High pressures are attractive with respect to the chemical equilibria in methanol synthesis. In combination with a relatively low temperature (473 − 523 K), high equilibrium conversions are attainable. The research described in this dissertation focuses on optimizing the reforming of glycerol in supercritical water and high pressure methanol synthesis addressing among others the influence of process conditions. Finally, the two processes are integrated for a unique experimental demonstration of the GtM-process aiming at high methanol yields.

Glycerol reforming in supercritical water, produces a gas mixture containing H_2, CO, CO_2, CH_4, and higher hydrocarbons (C_2H_4, C_2H_6, C_3H_6, and C_3H_8). The gas composition is a strong function of the operating conditions and the presence of a catalyst (**Chapter 2**). For noncatalytic reforming and reforming in the presence of alkali salts, the gas composition is a function of the glycerol conversion and, besides initial glycerol decomposition reactions, the water-gas shift reaction plays a major role. H_2, CO, CH_4, and at least the olefins are primary gas phase products, while the other components are formed in subsequent gas phase reactions. Complete conversion of 1 mole glycerol yields roughly 2 moles of carbon oxide (CO and CO_2) and 1 mole of hydrocarbon.

Unfortunately, this gas composition is not very attractive for methanol synthesis as the hydrocarbon content is rather high (max. ±20 vol%). To reduce the hydrocarbon content, catalytic reforming with dedicated catalysts was investigated (**Chapter 3**). Five different catalysts were tested, with different active metals. All catalysts were found to promote the water-gas shift reaction over the complete temperature range, and for four out of five catalysts almost all CO was converted to CO_2. Catalysts containing Ni demonstrated both beneficial and adverse properties. All higher hydrocarbons were reformed, but the CH_4 concentration approached equilibrium for temperatures exceeding 750 K. Low CH_4 concentrations could only be obtained by the combination of high temperature and low feed concentrations.

In preliminary methanol synthesis experiments, the *in situ* formation of liquid methanol was demonstrated visually in a high pressure view cell reactor (**Chapter 4**). *In situ* condensation of liquid has never before been demonstrated directly, and this phenomenon has very important consequences for the equilibria in methanol synthesis. As the products (methanol and water) are partly withdrawn from the gas phase, the limitations imposed by the chemical equilibria are almost completely eliminated. To obtain insight into the (positive) influences of condensation on the equilibria, an equilibrium model was developed accounting for the formation of a liquid phase (**Chapter 5**). The experimental data showed excellent correlation with the model predictions, in particular at the lower temperatures (468 – 523 K). At operating temperatures around 473 K and a pressure of 20 MPa, unprecedented experimental conversions up to 99.5% of the limiting components were obtained in a packed bed reactor. Operation at these high conversion levels has major benefits for methanol synthesis, and for instance eliminates the syngas recycle stream, which is typically used in conventional methanol synthesis.

High pressure methanol synthesis has been investigated experimentally for several syngas compositions ranging from gases typically used in commercial methanol synthesis to gases obtained in the reforming of glycerol in supercritical water (**Chapter 6**). For all types of gas, high conversions were observed when using a conventional methanol synthesis catalyst (Cs doped $Cu/ZnO/Al_2O_3$). When CO_2 is the major carbon oxide in the gas, the purity of the organic fraction exceeded 99.9%. Gases with higher CO content lead to the formation of substantial amounts of higher alcohols (max. 13 vol%). Furthermore, methanol production rates have been measured in a stirred basket reactor. The experimental data were modeled using a standard kinetic expression for heterogeneous catalysts, and a kinetic equation (the first in its sort) for methanol synthesis at high pressure and low temperature was derived (**Appendix C**).

Finally, the GtM-process was demonstrated experimentally in a dedicated continuous bench scale unit with 1 kg/h aqueous feed (**Chapter 7**). Glycerol reforming and methanol synthesis were integrated and experiments were performed to maximize the conversion of carbon in glycerol to carbon in methanol. The best results were obtained when glycerol was reformed at 998 K using a methanation catalyst (Ni as active metal) in the reforming section. The gas consisted of mainly H_2 and CO_2 while CH_4 levels remained below 2.4 vol%. Subsequently, the gas was converted to methanol in three packed bed reactors in series with a decreasing operating temperature (513 – 481 K). The maximum methanol yield was 0.62 kg methanol/kg glycerol. This is no less than 76% of the maximum theoretical yield of 0.81 kg methanol/kg glycerol.

A conceptual design was prepared by Uhde, Germany for a commercial GtM-process. In the current situation (2012), subsidies for renewable methanol are required to make this process profitable (**Chapter 8**).

The work performed has been of great value in quantifying the potential for the conversion of glycerol by reforming in supercritical water, combined with high pressure methanol synthesis. It identifies key phenomena, experimental results, and conclusions which may provide a firm basis, or simply inspiration for others who are drawn to this field of investigation.

Samenvatting

De productie van biodiesel is flink toegenomen in het eerste decennium van de 21ste eeuw. Bij de productie van 100 kg biodiesel komt ongeveer 10 kg aan glycerol vrij, wat heeft geleid tot een sterk gestegen glycerol aanbod. Als gevolg daarvan wordt er veel onderzoek verricht naar het vinden van alternatieve toepassingen voor glycerol. Een aantrekkelijke mogelijkheid is het omzetten van glycerol naar groene methanol, die hergebruikt kan worden in de productie van biodiesel. Deze mogelijkheid is in detail onderzocht in het Europese Supermethanolproject. Het doel van het project was het ontwerpen van een blauwdruk voor een proces waarin glycerol omgezet wordt naar methanol. In een vervolgstap zou dit proces dan geïntegreerd kunnen worden in een bestaande biodieselfabriek. In dit proefschrift wordt het onderzoek naar de productie van methanol uit glycerol beschreven, uitgevoerd in het kader van het Supermethanolproject.

Het 'Glycerol-to-Methanol' (GtM) proces bestaat uit een vergassingsstap van glycerol in superkritisch water naar synthesegas gevolgd door methanolsynthese (**Hoofdstuk 1**). Tijdens het vergassingsproces wordt een gas op hoge druk (> 20 MPa) geproduceerd. Deze hoge druk is voordelig voor de methanolsynthese, omdat bij deze condities hoge evenwichtsconversies gehaald kunnen worden. Het onderzoek heeft zich op zowel de optimalisatie van het vergassen van glycerol in superkritisch water als de methanolsynthese op hoge druk gericht. De invloed van de procesomstandigheden op de performance van beide individuele processen is uitgebreid bestudeerd. In een tweede fase zijn beide processen geïntegreerd en gedemonstreerd op continue schaal.

Bij de vergassing van glycerol wordt een gasmengsel geproduceerd dat bestaat uit: H_2, CO, CO_2, CH_4 en hogere koolwaterstoffen (C_2H_4, C_2H_6, C_3H_6 en C_3H_8). De gassamenstelling is een functie van de procescondities en de aanwezigheid van een katalysator (**Hoofdstuk 2**). Als geen katalysator wordt gebruikt, is de gassamenstelling voornamelijk een functie van de glycerolconversie. De ontledingsreacties van glycerol en de water-gas-shift-reactie zijn dan de belangrijkste reacties die plaatsvinden. H_2, CO, CH_4 en de olefinen zijn primaire gasproducten. De andere componenten worden in verdere gasfasereacties gevormd. Bij volledige conversie eindigt ongeveer 2 molen koolstof uit glycerol als een koolstofoxide (CO en CO_2) en 1 mol als een koolwaterstof.

De gassamenstelling na de ongekatalyseerde glycerolvergassing in superkritisch water is niet erg gunstig voor de methanolsynthese vanwege de hoge concentratie koolwaterstoffen in het gasmengsel (max. ± 20 vol%). Met behulp van katalysatoren is geprobeerd om de gassamenstelling te beïnvloeden en om met name de vorming van koolwaterstoffen te vermijden (**Hoofdstuk 3**). Vijf verschillende katalysatoren zijn onderzocht met verschillende actieve metalen. Alle katalysatoren stimuleerden de water-gas-shift-reactie voor het complete temperatuurinterval en door vier van de vijf katalysatoren werd vrijwel alle CO omgezet in CO_2. De Ni-katalysatoren bezitten positieve en negatieve eigenschappen. Het gebruik van deze katalysatoren resulteerde in een scherpe reductie van de hoeveelheid hogere koolwaterstoffen

en tevens benaderde de CH_4-concentratie de evenwichtswaarden bij temperaturen boven de 750 K. Reductie van de CH_4-concentratie is mogelijk door te werken bij hoge temperaturen en lage glycerolconcentraties in de voeding.

In de eerste methanolsynthese-experimenten werd de *in situ* vorming van een vloeistof visueel waargenomen in een kijkcelreactor (**Hoofdstuk 4**). *In situ* condensatie is nooit eerder direct gevisualiseerd en heeft grote gevolgen voor de evenwichtsligging in methanolsynthese. De limitaties van het chemisch evenwicht kunnen door condensatie bijna volledig teniet gedaan worden, omdat de producten (methanol en water) gedeeltelijk aan de gasfase onttrokken worden.

Een evenwichtsmodel, waarin rekening wordt gehouden met condensatie, is ontwikkeld om inzicht te krijgen in de (positieve) gevolgen van condensatie op de evenwichtsliggingen van de methanolsynthese (**Hoofdstuk 5**). Met name bij lagere temperaturen (468 – 523 K) komen de berekende evenwichten uitstekend overeen met de experimenteel gemeten waarden. Bij een temperatuur van 473 K en een druk van 20 MPa werd een experimentele conversie van maar liefst 99.5% van de limiterende component gemeten. Door deze hoge conversies kunnen recyclestromen, die in conventionele methanolsynthese gebruikt worden en hoge kosten met zich meebrengen, vermeden worden.

Methanolsynthese op hoge druk is verder systematisch onderzocht voor verschillende gassamenstellingen, variërend van gassen die in commerciële methanolsynthese gebruikt worden tot gassen die verkregen worden door middel van glycerolvergassing (**Hoofdstuk 6**). Voor alle gassen werden hoge conversies gemeten. De zuiverheid van de gevormde methanol is een functie van de synthesegassamenstelling. Bij CO_2-rijke gassen is de productzuiverheid hoog en zijn er waarden hoger dan 99.9% gemeten. Daarentegen werden in geval van CO-rijke gassen substantiële hoeveelheden hogere alcoholen (max. 13 vol%.) gevormd. Verder zijn er productiesnelheden van methanol gemeten op hoge druk in een geroerde continue reactor. De experimentele data is gemodelleerd met behulp van een standaard kinetiekuitdrukking en is de eerste in zijn soort voor methanolsynthese in het hoge-druk-lage-temperatuur-regime (**Appendix C**).

Uiteindelijk is het overall-concept van glycerol naar methanol gedemonstreerd in een speciaal daarvoor ontwikkelde continue opstelling (**Hoofdstuk 7**) met een doorzet van 1 kg/uur van een water-glycerolmengsel. De vergassing van glycerol en methanolsynthese zijn geïntegreerd en verschillende experimenten zijn uitgevoerd om een zo hoog mogelijke koolstofconversie te bereiken. De meest succesvolle configuratie bestond uit glycerolvergassing op 998 K in combinatie met een methaniseringskatalysator (Ni als actief metaal). Het gas dat op deze manier verkregen werd, bevatte voornamelijk H_2 en CO_2 met slechts 2.4 vol% CH_4. Dit gas werd vervolgens omgezet naar methanol in een reactorconfiguratie bestaande uit drie gepakte bedden met aflopende temperaturen (513 – 481 K). De maximale methanolopbrengst was 0.62 kg methanol/kg glycerol. Dit is maar liefst 76% van het theoretisch maximum van 0.81 kg methanol/kg glycerol.

Een conceptontwerp van het GtM-proces is ontwikkeld door Uhde, Duitsland. Op dit moment (2012) zijn er subsidies nodig om het proces rendabel uit te voeren (**Hoofdstuk 8**). Desalniettemin heeft de productie van hernieuwbare methanol uit biomassa potentie voor de toekomst en heeft het onderzoek, beschreven in dit proefschrift, geleid tot betere inzichten in het vergassen van glycerol in superkritisch water. Daarnaast zijn unieke methanolsynthese-experimenten bij hogere drukken uitgevoerd en is de procesconfiguratie voor een geïntegreerd concept geoptimaliseerd.

Word of gratitude

The last 4 years I've been working with full dedication on my PhD dissertation, which at the end became a piece of work involving a lot of people. Here, I have an (extra) opportunity to express my gratitude.

I want to start with thanking Erik Heeres, my promotor, for giving me the opportunity to embark on this PhD research. Although my work location was about 150 km from your office, we met regularly and discussed relevant (cycling, skating, sports in general) and very relevant (work) issues. I want to thank you for your insight, advices, sharp analyses, critical notes, and your boundless enthusiasm even when the articles-to-be-read were piling up.

This PhD project would not have been possible without copromotor Robbie Venderbosch, Daan Assink, Erwin Wilbers, and BTG. I had a flying start as Robbie and Daan were already experts in the field of reforming in supercritical water and Erwin made life and research easy for me in Groningen. At BTG, I came to share an office with Robbie whom I could bother all the time with smart and less smart questions. Robbie, thank you very much for your critical input, sharing your visions, directing the research, improving my writing skills, and always having time for me. I was very lucky for the situation you created and it was a great pleasure having you as daily supervisor and Tour de France-watch-buddy.

I would also like to thank the members of the reading committee: Prof. dr. A.A. Broekhuis, prof. dr. ir. J.A.M. Kuipers, prof. dr. F. Vogel for spending a lot of time on reading the complete manuscript. Frédéric, thank you for showing me and Robbie around at your facilities.

Daan, thanks to you I got the PhD position. You were acquainted with my ambitions and the vacancies at BTG/RuG. After your interference and a brief conversation with Robbie I knew that this should become my new job. Now, I had to convince Erik to appoint me and locate me at BTG in Enschede for most of the time. Fortunately, Bert van de Beld and René Venendaal, the directors of BTG, also agreed and I was on my way. I owe BTG a lot for giving me this opportunity. Daan, I already mentioned you as the initiator. I want to thank you for your enormous contribution in keeping the setups online, your expertise, proofreading my articles, good ideas, joint trainings, and coaching me to several good performances in athletics competitions. Furthermore, we had a great time during the project meetings and brief holiday in Siberia.

Bert, thank you for your help and critical remarks during the course of the research and proof reading my articles. John, thank you for organizing all the project trips, your company, and the proof reading of several articles and deliverables.

Jan Florijn, Richard Hölscher, and Erik Klein Bleumink thanks for fixing my stuff when it broke down. Marja Bakker and Modesta de Vos thank you for the administration and helping me in arranging trips and visas. René thanks for allowing me to organize and join the lustrum trip.

Furthermore, I'd like to thank the rest of my colleagues at BTG, including Koen Lemmens, Hans Heeres, Evert Leijenhorst, Elmar Holle, and William Wolters for helping me out when

necessary. I'm very thankful I could conduct my work at BTG. I enjoyed working there, the atmosphere, the discussions during breaks in particular on Friday, the snacks every Friday, being a member of the almost unbeatable BTG indoor soccer team, and last but not least the trip to Estonia in the summer of 2012. I want to thank all the colleagues at BTG for the wonderful time I had there.

My work was facilitated by several students: Koen, Ria Abdilla, Sebastiaan Nieland, Cheral Theussing, Hielke van den Berg, and Karin Kuipers. You all did a great job and enabled me to do much more work than would have been possible without you. Koen, thank you very much for assisting and helping me after you got employed by BTG, for the 24h shifts we did together, and improving my soccer skills. Sebastiaan, Karin, and Hielke thank you for conducting so many methanol synthesis experiments in a relatively short period. Ria thanks for the work on glycerol oxidation and Cheral for the biodiesel synthesis.

Although most work was carried out at BTG, I travelled regularly to Groningen to do part of the work. I liked working there very much and couldn't have finished the dissertation without the help of Erwin and Jos Winkelman. Erwin, you were indispensable and kept constant track of my experimental work in Groningen. You changed, modified, and improved the setup far more often than I was in Groningen and kept it running and made it possible that the work went on in my absence. You even spent a free Saturday on operating the set-up for taking the pictures that became part of the cover of the dissertation. I enjoyed it very much being your roommate, although it was for only one day a week. In particular, I enjoyed the wampexes and drampexes with some others from the department.

Jos, I want to thank you for helping me a great deal with everything concerning methanol synthesis, thermodynamics, and modeling. Your first designs and descriptions made my modeling life much easier and your patience in answering all my questions is appreciated very much. Agnes Borgesius, thank you very much for proof reading some chapters and the pleasant company in St. Petersburg. Peter Bezant your check on the summary is very much appreciated.

Léon Rohrbach, Jan Henk Marsman, Dagmar Taribuka, Hans van der Velde, and Theodora Tiemersma you were very helpful in finding and performing the right analysis techniques. Ignacio Melián-Cabrera and Valeriya Zarubina, thanks for the conduction of some catalyst characterizations and discussing the results with me. Marcel de Vries and Anne Appeldoorn thank you very much for keeping the setups running and your creative way of finding solutions. Jeffrey Bos, thank you very much for making the pictures and movies of methanol condensation. Henk van de Bovenkamp, Arjan Kloekhorst, and C.B. Rasrendra thank you for helping me out with some analysis techniques. Marya van der Duin, I appreciate your help with the administration and all kinds of declarations. I'd like to thank the rest of the people working at the department of chemical technology for giving me a good time, creating a pleasant work atmosphere, and cozy breaks.

I also want to acknowledge the EU for funding this project and the other project partners involved in the project: Jo Penninger (Sparqle), Michael Bork (Uhde), Valeriy Kirillov, Pavel Snytnikov, Vladimir Belyayev (BIC), Miguel Angel Paris Torres, Rocio Fernandez Flores, Maria del